

# **DESIGN OF NOVEL TRANSITION METAL COMPLEXES: STUDY OF CATALYTIC, ION RECOGNITION AND BIOLOGICAL PROPERTIES**

THESIS SUBMITTED TO **AcSIR** FOR THE AWARD OF  
THE DEGREE OF  
**DOCTOR OF PHILOSOPHY IN CHEMISTRY**  
UNDER THE FACULTY OF SCIENCE



*By*

**VIJI M.**

**Registration No: 10CC12J39002**

UNDER THE GUIDANCE OF

**Dr. D. RAMAIAH**



**PHOTOSCIENCES AND PHOTONICS  
CHEMICAL SCIENCES AND TECHNOLOGY DIVISION  
CSIR-NATIONAL INSTITUTE FOR INTERDISCIPLINARY  
SCIENCE AND TECHNOLOGY (CSIR-NIIST)  
THIRUVANANTHAPURAM - 695 019, KERALA**

**JANUARY, 2017**

## **DECLARATION**

I hereby declare that the Ph. D. thesis entitled: “**DESIGN OF NOVEL TRANSITION METAL COMPLEXES: STUDY OF CATALYTIC, ION RECOGNITION AND BIOLOGICAL PROPERTIES**”, is an independent work carried out by me at the Photosciences and Photonics Section, Chemical Sciences and Technology Division of the CSIR-National Institute for Interdisciplinary Science and Technology (CSIR-NIIST), Trivandrum, under the supervision of Dr. D. Ramaiah and the same has not been submitted elsewhere for other degree, diploma or title.

**(Viji M.)**

January 5, 2017

## CERTIFICATE

This is to certify that the work incorporated in this Ph.D. thesis entitled **“DESIGN OF NOVEL TRANSITION METAL COMPLEXES: STUDY OF CATALYTIC, ION RECOGNITION AND BIOLOGICAL PROPERTIES”** submitted by Ms. Viji M. to the Academy of Scientific and Innovative Research (AcSIR), in partial fulfillment of the requirements for the award of the degree of **Doctor of Philosophy in Chemical Sciences**, embodies original research work under my supervision. I further certify that this work has not been submitted to any other University or Institution in part or full for the award of any degree or diploma. Research material obtained from other sources has been duly acknowledged in the thesis. Any text, illustration, table etc., used in the thesis from other sources, have been duly cited and acknowledged.

(Viji M.)

(D. Ramaiah)

Thesis Supervisor

*Formerly, Head of the Chemical Sciences & Technology Division of the CSIR-National Institute for Interdisciplinary Science and Technology (CSIR-NIIST), Thiruvananthapuram*

## ACKNOWLEDGEMENTS

*I have great pleasure in placing on record my deep sense of gratitude to Dr. D. Ramaiah, my thesis supervisor, for suggesting the research problem and for his guidance, support and encouragement, leading to the successful completion of this work.*

*I would like to express my sincere thanks to Professor M. V. George for his support during the tenure of this work.*

*I wish to thank Dr. A. Ajayaghosh, Dr. Suresh Das, and Dr. Gangan Pratap, present and former Directors of the CSIR-National Institute for Interdisciplinary Science and Technology (CSIR-NIIST), Thiruvananthapuram, for providing me the necessary facilities for carrying out the work.*

*I sincerely thank Dr. K. R. Gopidas, Dr. Joshy Joseph, Dr. N. Unni, Dr. K. Yoosaf, Dr. C. Vijayakumar, Dr. B. P. Deb and Dr. V. Karunakaran, Scientists of the Photosciences and Photonics, Chemical Sciences and Technology Division, for all the help and support extended to me.*

*I thank all the members of the Photosciences and Photonics and in particular, Dr. Akhil, Dr. Suneesh, Dr. Sanju, Dr. Dhanya, Dr. Adarsh, Dr. Betsy, Dr. Albish, Dr. Harishankar, Mr. Shanmugasundaram, Mr. Shameel, Dr. Nidhi, Dr. Lavanya, Ms. Rahi and Mr. Aswin, for their help and cooperation. I also thank members of other Divisions of CSIR-NIIST for their support. I would like to thank Mr. Robert Philip and Mr. Kiran Mohan for their help and support. I also thank Mrs. Saumini, Mr. Saran, Mr. Gokul, Mrs. Viji, and Ms. Athira for NMR and Mass spectral analysis.*

*Words are inadequate to express my gratitude to my parents, sister, and other family members for their endless love and support. I am also indebted and grateful to all my friends, especially Ms. Jubi Jacob, who constantly stood as a source of encouragement and confidence. I would also like to extend my thanks and appreciation to all my teachers for their help and blessings.*

*I sincerely thank Council of Scientific and Industrial Research (CSIR), and DST, Government of India for financial assistance.*

**Viji M.**

## CONTENTS

	Page
<b>Statement</b>	<b>i</b>
<b>Certificate</b>	<b>ii</b>
<b>Acknowledgements</b>	<b>iii</b>
<b>Contents</b>	<b>iv</b>
<b>Preface</b>	<b>vii</b>
<b>List of Figures</b>	<b>xii</b>
<b>List of Tables</b>	<b>xiv</b>
<b>List of Schemes</b>	<b>xv</b>
<b>List of Charts</b>	<b>xvi</b>
<b>List of Abbreviations</b>	<b>xvii</b>
<b>Chapter 1</b>	<b>Transition Metal Complexes: An Overview of Catalytic and Molecular Recognition Properties</b>
<b>1.1</b>	Introduction <b>1</b>
<b>1.2</b>	Transition Metal Complexes as Catalysts <b>3</b>
<b>1.3</b>	Transfer Hydrogenation Reactions <b>4</b>
<b>1.3.1</b>	Iridium-Based Catalysts <b>9</b>
<b>1.3.2</b>	Rhodium-Based Catalysts <b>11</b>
<b>1.3.3</b>	Ruthenium-Based Catalysts <b>15</b>
<b>1.4</b>	Transition Metal Complexes as Molecular Probes <b>20</b>
<b>1.5</b>	Transition Metal Complexes in Biology <b>24</b>
<b>1.6</b>	Objectives of the Present Investigation <b>29</b>
<b>1.7</b>	References <b>30</b>

<b>Chapter 2</b>	<b>Design of Ruthenium(II) Complexes: Investigation of their Photophysical and Catalytic Properties</b>	
2.1	Abstract	38
2.2	Introduction	40
2.3	Results and Discussion	42
2.3.1	Synthesis and Characterization of Ruthenium Complexes	42
2.3.2	Single Crystal X-ray Analysis of the Complexes 3-6	47
2.3.3	Photophysical Properties of the Complexes	53
2.3.4	Catalytic Properties of the Complexes	56
2.4	Conclusions	67
2.5	Experimental Section	68
2.6	References	76
<b>Chapter 3</b>	<b>Design of Silver(I)-NHC Complexes: Study of their Photophysical and Anion Recognition Properties</b>	
3.1	Abstract	81
3.2	Introduction	82
3.3	Results and Discussion	84
3.3.1	Synthesis of the Complexes	84
3.3.2	Photophysical Properties of the Complexes	87
3.3.3	Anion Recognition Properties of the Complexes	89
3.3.4	Selectivity of Detection of Cyanide Ions	92
3.3.5	Mechanism of Cyanide Recognition	98
3.4	Conclusions	101
3.5	Experimental Section	102
3.6	References	106

<b>Chapter 4</b>	<b>Design of Iron(III) and Copper(II) Complexes: Study of their Photophysical and Biological Properties</b>	
4.1	Abstract	111
4.2	Introduction	112
4.3	Results and Discussion	115
4.3.1	Synthesis and Characterization of the Complexes	115
4.3.2	Single Crystal X-ray Analysis of the Ligand and Complex 2	117
4.3.3	Photophysical Properties of the Complexes	124
4.3.4	DNA Binding Studies	127
4.3.5	Protein Interaction Studies	133
4.3.6	<i>In Vitro</i> Cytotoxicity and Fluorescent Staining Studies	138
4.3.7	Mechanism of Biological Activity	144
4.4	Conclusions	145
4.5	Experimental Section	146
4.6	References	155
	<b>List of Publications</b>	<b>161</b>

## PREFACE

Design of functionalized metal complexes with favorable chemical and optical properties is an important area of research because such effective systems can have immense impact on chemical and pharmaceutical industry and also in medicinal, supramolecular chemistry. Among these, the transition metal ion based complexes have attracted much attention for their application in the design of molecular architectures, as catalysts, organic synthesis, sensing and biological applications. With an objective to develop novel efficient catalysts as well as molecular probes, we have synthesized a series of Ru(II), Ag(I), Fe(III) and Cu(II) complexes having different ligands and have investigated their photophysical, biophysical, catalytic and ion recognition aspects. The present thesis has been divided into four chapters and of which the Chapter 1 gives a brief introduction to the applications of the transition metal complexes, especially in the area of catalysis, ion sensing and biological properties. The effect of various ligands on the catalytic efficacy of the metal ion complexes for the transfer hydrogenation reactions of the aromatic ketones was given a special emphasis in this chapter. In addition, the specific objectives of the present thesis were also briefly described at the end of this chapter.

The Chapter 2 of the thesis describes the design of neutral and cationic ruthenium complexes (**1-8**) and investigation of their photophysical, electrochemical and catalytic properties under different conditions. These systems were synthesized in good yields and were characterized based on analytical and spectral evidences. In addition, the structure of the representative examples, such as the complexes **3-6** were also established unambiguously through single crystal X-ray analysis. These derivatives showed absorption



in the range 300-400 nm, along with bathochromic shifted metal to ligand charge transfer transition in the range 400-650 nm and have exhibited good solubility in common organic solvents. Among these systems, the complexes **1** and **2** showed emission in the range of 380-700 nm and exhibited the fluorescence quantum yields ( $\phi_F$ ) of *ca.* 0.03 and 0.39, respectively. The electrochemical properties of the derivatives were investigated which confirmed the presence of ruthenium in these complexes.

The efficacy of these complexes as catalysts for the transfer hydrogenation reaction was evaluated under different conditions including the effect of various substituents on the catalytic efficacy and substrate selectivity. Of these systems, the ruthenium- $\pi$  complexes **1** and **2** were found to act as efficient catalysts for the *ca.* 100% conversion of the aromatic ketones to their corresponding alcohols at a catalyst loading of 2 mol% in isopropanol and reaction time of 5 h. On the other hand, the neutral ruthenium-*NHC* complexes **3** and **4** showed better catalytic efficiency and required only 2 h to observe *ca.* 100% conversion under similar conditions. The increased catalytic activity of the complexes **3** and **4** when compared to **1** and **2** can be attributed to the stability of the complexes due to the existence of strong sigma binding affinity of *N*-heterocyclic carbene (*NHC*) ligand. Furthermore, much better efficacy was observed with the cationic ruthenium-*NHC* complexes **5-8**, which required only 1 h for the reaction and loading of the catalyst was as low as only 0.5 mol%. The observed high efficacy of the cationic ruthenium complexes when compared to the ruthenium- $\pi$  and neutral complexes can be attributed to the strong binding of both *NHC* and pyridine substituents with the metal ion centre, and such interactions significantly improved not only their catalytic properties but also their air and moisture stability.

The synthesis of novel *N*-heterocyclic carbene linked silver complexes, **2** and **4** and the investigation of their photophysical as well as anion recognition properties forms the subject matter of Chapter 3. These complexes have been synthesized in good yields and were characterized on the basis of analytical and spectral evidences. They showed good solubility in the aqueous medium and exhibited characteristic anthracene chromophore absorption (300-400 nm) along with a broad absorption up to 500 nm. The fluorescence spectra of the complexes **2** and **4** exhibited peaks in the range 380–500 nm and quantum yield values are found to be *ca.*  $0.37 \pm 0.01$  and  $0.34 \pm 0.01$ , respectively. As these complexes showed favourable fluorescence quantum yields and good solubility in aqueous medium, we have studied the interaction of the complexes with biologically important various mono and divalent anions such as I<sup>-</sup>, Br<sup>-</sup>, Cl<sup>-</sup>, F<sup>-</sup>, ClO<sub>4</sub><sup>-</sup>, HSO<sub>4</sub><sup>-</sup>, OH<sup>-</sup>, C<sub>6</sub>H<sub>5</sub>COO<sup>-</sup>, S<sup>2-</sup>, SCN<sup>-</sup> and N<sub>3</sub><sup>-</sup> ions. For example, with the addition of cyanide ions to an aqueous solution of the complex **2**, we observed a gradual increase in the fluorescence intensity at 416 nm and which reached saturation upon addition of 20 μM of CN<sup>-</sup> ions. However, the absorption spectrum of the complex **2** showed negligible changes under similar conditions. In contrast, negligible changes were observed in the absorption and emission spectra of the complex **2** with the addition of other anions. Similarly, significant fluorescence changes were also observed in the case of the probe **4** with the addition of CN<sup>-</sup> ions as in the case of the complex **2**, under identical conditions.

These complexes exhibited excellent selectivity for the cyanide ions, when compared to all other anions and the sensitivity of detection was found to be *ca.* 49 and 50 ppb, respectively, for the complexes **1** and **2**. Moreover, negligible interactions were observed

for the imidazolium precursors such as **1** and **3** upon addition of cyanide ions. The nature of interactions has been studied through NMR and fluorescence lifetime measurements, which confirmed that, even though the metal-carbon bond is quite strong, the highly nucleophilic cyanide ions could easily cull the silver ions from the complex through the formation of highly fluorescent imidazolium precursors. These results demonstrate that the *N*-heterocyclic carbene based mono and di-nuclear silver complexes **2** and **4** have potential use as probes for the selective detection of cyanide ions, when compared to all other biologically relevant anions and signal the event through visible “Turn On” in fluorescence intensity.

We report the design and synthesis of two novel biomimetic mononuclear Fe(III) and Cu(II) complexes **1** and **2**, respectively, based on naphthalimide appended tripodal tetradentate ligand **3** and results of their photophysical, electrochemical and biomolecular recognition aspects in the fourth Chapter of the thesis. These systems synthesized good yields and were characterized by various spectral and analytical techniques including single crystal X-ray structure analysis. Uniquely, the coordination with a metal ion modified the ligand scaffold to interact efficiently with ct-DNA (groove binding) and protein (hydrophobic and/or electrostatic interactions). We have determined their affinity for DNA and BSA protein and the values are found to be in the range,  $K_{DNA} = 0.34-1.01 \times 10^4 \text{ M}^{-1}$  and  $K_{BSA} = 4.1-5.0 \times 10^5 \text{ M}^{-1}$ . Furthermore, the fluorescence quenching of BSA with the complexes **1** and **2** occurs through a static mechanism and which found to affect the conformation of BSA around the tryptophan residues.

The *in vitro* biological studies of these systems employing HeLa cell lines indicated that both these complexes exhibited enhanced cytotoxicity and the IC<sub>50</sub> values are found to be *ca.* 32 ± 0.19 and 10 ± 0.21 μM, for the complexes **1** and **2**, respectively, when compared to the free ligand (IC<sub>50</sub> = 150 μM). Interestingly, both the complexes **1** and **2** were found to be non-toxic to normal H9c2 cell lines. The mechanism of *in vitro* biological activity of these complexes has been evaluated through a variety of techniques: acridine orange/ethidium bromide, DAPI staining studies, annexin V-FITC/PI and poly(ADPribose)-polymerase (PARP) cleavage, which confirmed the apoptotic mediated cell death. Our results demonstrate the importance of the complexation of the naphthalimide ligand as well as the potential of these biomimetic metal complexes as cytotoxic and anticancer agents.

In a nutshell, we designed novel transition metal complexes and have investigated their photophysical, biophysical, electrochemical, catalytic and ion recognition properties. Results of our investigations demonstrate that these systems show good air and moisture stability and exhibited favorable photophysical properties. Furthermore, the catalytic reactions of the Ru(II) complexes have revealed that all the synthesized derivatives exhibited high activity and efficacy towards the transfer hydrogenation of aromatic ketones. In addition, the *NHC* linked Ag(I) complexes exhibited favorable photophysical properties as well as high selectivity and sensitivity towards CN<sup>-</sup> ions in the aqueous medium. Furthermore, our studies with the biomimetic Fe(III) and Cu(II) complexes appended with naphthalimide chromophore have indicated that these complexes exhibit effective DNA/protein interactions and thereby their potential use as cytotoxic agents.

---

**Note:** The numbers of compounds given here correspond to those given under the respective Chapters.

## List of Figures

		<b>Page</b>
<b>1.</b>	Figure 1.1	<b>21</b>
<b>2.</b>	Figure 1.2	<b>22</b>
<b>3.</b>	Figure 1.3	<b>24</b>
<b>4.</b>	Figure 2.1	<b>46</b>
<b>5.</b>	Figure 2.2	<b>48</b>
<b>6.</b>	Figure 2.3	<b>49</b>
<b>7.</b>	Figure 2.4	<b>51</b>
<b>8.</b>	Figure 2.5	<b>54</b>
<b>9.</b>	Figure 2.6	<b>54</b>
<b>10.</b>	Figure 2.7	<b>55</b>
<b>11.</b>	Figure 3.1	<b>86</b>
<b>12.</b>	Figure 3.2	<b>87</b>
<b>13.</b>	Figure 3.3	<b>88</b>
<b>14.</b>	Figure 3.4	<b>88</b>
<b>15.</b>	Figure 3.5	<b>90</b>
<b>16.</b>	Figure 3.6	<b>90</b>
<b>17.</b>	Figure 3.7	<b>91</b>
<b>18.</b>	Figure 3.8	<b>92</b>
<b>19.</b>	Figure 3.9	<b>93</b>

<b>20.</b>	Figure 3.10	<b>93</b>
<b>21.</b>	Figure 3.11	<b>94</b>
<b>22.</b>	Figure 3.12	<b>95</b>
<b>23.</b>	Figure 3.13	<b>96</b>
<b>24.</b>	Figure 3.14	<b>97</b>
<b>25.</b>	Figure 3.15	<b>98</b>
<b>26.</b>	Figure 3.16	<b>100</b>
<b>27.</b>	Figure 4.1	<b>117</b>
<b>28.</b>	Figure 4.2	<b>118</b>
<b>29.</b>	Figure 4.3	<b>119</b>
<b>30.</b>	Figure 4.4	<b>120</b>
<b>31.</b>	Figure 4.5	<b>121</b>
<b>32.</b>	Figure 4.6	<b>125</b>
<b>33.</b>	Figure 4.7	<b>126</b>
<b>34.</b>	Figure 4.8	<b>127</b>
<b>35.</b>	Figure 4.9	<b>128</b>
<b>36.</b>	Figure 4.10	<b>129</b>
<b>37.</b>	Figure 4.11	<b>130</b>
<b>38.</b>	Figure 4.12	<b>131</b>
<b>39.</b>	Figure 4.13	<b>132</b>
<b>40.</b>	Figure 4.14	<b>134</b>

<b>41.</b>	Figure 4.15	<b>135</b>
<b>42.</b>	Figure 4.16	<b>136</b>
<b>43.</b>	Figure 4.17	<b>138</b>
<b>44.</b>	Figure 4.18	<b>139</b>
<b>45.</b>	Figure 4.19	<b>140</b>
<b>46.</b>	Figure 4.20	<b>141</b>
<b>47.</b>	Figure 4.21	<b>142</b>
<b>48.</b>	Figure 4.22	<b>143</b>
<b>49.</b>	Figure 4.23	<b>143</b>
<b>50.</b>	Figure 4.24	<b>144</b>

### **List of Tables**

<b>1.</b>	Table 2.1	<b>50</b>
<b>2.</b>	Table 2.2	<b>52</b>
<b>3.</b>	Table 2.3	<b>57</b>
<b>4.</b>	Table 2.4	<b>60</b>
<b>5.</b>	Table 2.5	<b>61</b>
<b>6.</b>	Table 2.6	<b>63</b>
<b>7.</b>	Table 2.7	<b>65</b>
<b>8.</b>	Table 4.1	<b>117</b>

<b>9.</b>	Table 4.2	<b>122</b>
<b>10.</b>	Table 4.3	<b>123</b>
<b>11.</b>	Table 4.4	<b>126</b>
<b>12.</b>	Table 4.5	<b>137</b>

### **List of Schemes**

<b>1.</b>	Scheme 1.1	<b>6</b>
<b>2.</b>	Scheme 1.2	<b>23</b>
<b>3.</b>	Scheme 1.3	<b>24</b>
<b>4.</b>	Scheme 2.1	<b>43</b>
<b>5.</b>	Scheme 2.2	<b>44</b>
<b>6.</b>	Scheme 2.3	<b>45</b>
<b>7.</b>	Scheme 2.4	<b>56</b>
<b>8.</b>	Scheme 2.5	<b>66</b>
<b>9.</b>	Scheme 3.1	<b>85</b>
<b>10.</b>	Scheme 3.2	<b>85</b>
<b>11.</b>	Scheme 3.3	<b>101</b>
<b>12.</b>	Scheme 4.1	<b>116</b>



## **List of Charts**

<b>1.</b>	Chart 1.1	<b>7</b>
<b>2.</b>	Chart 1.2	<b>9</b>
<b>3.</b>	Chart 1.3	<b>10</b>
<b>4.</b>	Chart 1.4	<b>11</b>
<b>5.</b>	Chart 1.5	<b>12</b>
<b>6.</b>	Chart 1.6	<b>13</b>
<b>7.</b>	Chart 1.7	<b>14</b>
<b>8.</b>	Chart 1.8	<b>15</b>
<b>9.</b>	Chart 1.9	<b>16</b>
<b>10.</b>	Chart 1.10	<b>16</b>
<b>11.</b>	Chart 1.11	<b>17</b>
<b>12.</b>	Chart 1.12	<b>18</b>
<b>13.</b>	Chart 1.13	<b>19</b>
<b>14.</b>	Chart 1.14	<b>19</b>
<b>15.</b>	Chart 1.15	<b>21</b>
<b>16.</b>	Chart 1.16	<b>26</b>
<b>17.</b>	Chart 1.17	<b>27</b>
<b>18.</b>	Chart 1.18	<b>27</b>
<b>19.</b>	Chart 1.19	<b>28</b>

<b>20.</b>	Chart 2.1	<b>41</b>
<b>21.</b>	Chart 3.1	<b>84</b>
<b>22.</b>	Chart 4.1	<b>114</b>

### **List of Abbreviations**

- 1.** COD- 1,5-Cyclooctadiene
- 2.** DPEN - Diphenylethylenediamine
- 3.** ATH - Asymmetric transfer hydrogenation
- 4.** TH - Transfer hydrogenation
- 5.** *NHC* - N-heterocyclic carbene
- 6.** Et<sub>3</sub>N - Triethylamine
- 7.** KOH – Potassium hydroxide
- 8.** NaOH – Sodium hydroxide
- 9.** Na<sub>2</sub>CO<sub>3</sub> - Sodium carbonate
- 10.** HCOONa - Sodium formate
- 11.** 2-PrOK - Potassium isopropoxide
- 12.** 2-PrONa - Sodium isopropoxide
- 13.** 2-PrOLi - Lithium isopropoxide
- 14.** KO<sup>t</sup>Bu - Potassium tert-butoxide
- 15.** NaO<sup>t</sup>Bu - Sodium tert-butoxide
- 16.** K<sub>3</sub>PO<sub>4</sub> - Tripotassium phosphate
- 17.** Cs<sub>2</sub>CO<sub>3</sub> - Cesium carbonate

18. CsOH - cesium hydroxide
19. NaOAc - Sodium acetate
20. NaOMe - Sodium methoxide
21. Py - Pyridine
22. TON – Turn Over Number
23. TOF – Turn Over Frequency
24. Cp - Cyclopentadienyl
25. Cl - Chlorine
26. Br - Bromine
27. I - Iodine
28. CN - Cyanide
29. Ru - Ruthenium
30. Rh - Rhodium
31. Ir - Iridium
32. ET - Electron Transfer
33. MLCT - Metal-to-Ligand Charge Transfer
34. LMCT - Ligand-to-Metal Charge Transfer
35. Zn - Zinc
36. Fe - Iron
37. Å - Angstrom
38. °C – Degree Celsius
39. *ca.* - *circa*

40.  $\text{CDCl}_3$  - Deuterated chloroform
41.  $\text{CD}_3\text{CN}$  - Deuterated acetonitrile
42.  $\text{CH}_3\text{CN}$  - Acetonitrile
43.  $\text{CH}_3\text{OH}$  - Methanol
44.  $\text{D}_2\text{O}$  - Deuterated water
45. DMF - Dimethyl formamide
46. DMSO - Dimethyl sulphoxide
47. DNA - Deoxyribonucleic acid
48.  $\Delta S$  - Entropy change
49. *et al.* - *Et alii/alia*
50. FAB - Fast atom bombardment
51. ESI-MS - Electrospray Ionisation Mass Spectrometry
52. F - Fluorine
53.  $\Delta G$  - Free energy change
54. GMP - Guanosine 5'-monophosphate
55.  $\text{H}_2\text{O}$  - Water
56. h - Hour
57.  $\Delta H$  - Enthalpy change
58. HBr - Hydrobromic acid
59. I - Intensity
60. K - Kelvin
61.  $K_{\text{ass}}$  - Association constant
62. LOD - Limit of detection

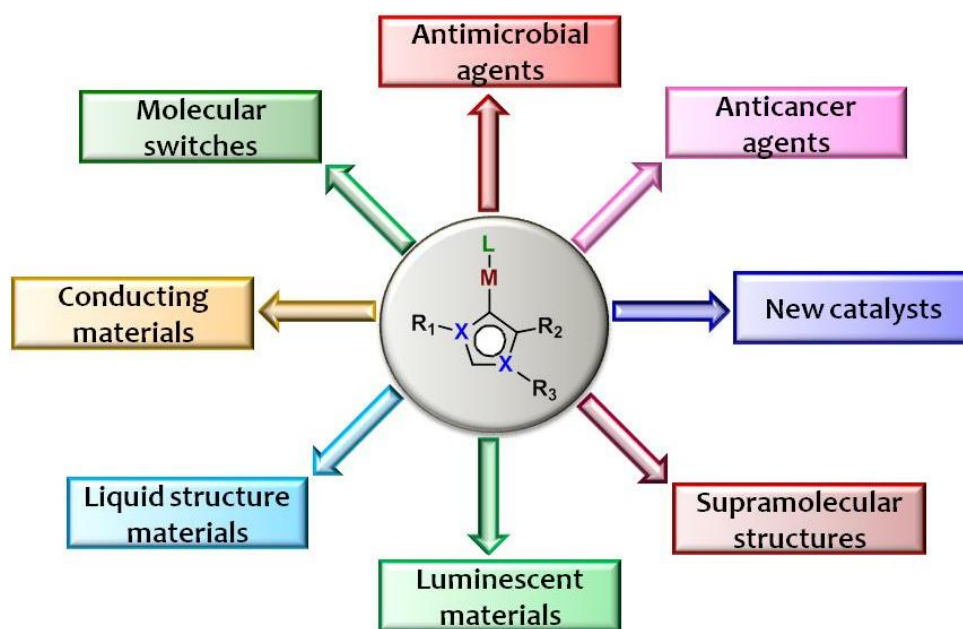
- 63.  $\lambda_{em}$  - Emission wavelength
- 64.  $\lambda_{abs}$  - Absorption wavelength maximum
- 65.  $\lambda_{max}$  - Wavelength maximum
- 66. MALDI- Matrix-assisted laser desorption ionization
- 67. mg - Milligram
- 68. MHz - Megahertz
- 69. mL - Millilitre
- 70.  $\mu\text{M}$  - Micromolar
- 71. mM - Millimolar
- 72. mmol - Millimole
- 73. mp - Melting point
- 74. NIR - Near infrared
- 75. NMR - Nuclear magnetic resonance
- 76. ns - Nanosecond
- 77. N - Nitrogen
- 78.  $\text{O}_2$  - oxygen
- 79. EPA - Environment protection agency
- 80.  $\Phi_F$  - Quantum yield of fluorescence
- 81.  $\tau$ - Relaxation time
- 82. TCSPC - Time-correlated picosecond single photon counting
- 83. T - Temperature
- 84. TMS - Tetramethylsilane

85. THF - Tetrahydrofuran
86. UV - Ultraviolet
87. VIS - Visible
88. Ag<sub>2</sub>O - Silver oxide
89. EDX - Energy-dispersive X-ray
90. AgCl - Silver chloride
91. TGA - Thermogravimetric analysis
92. GC/MS - Gas Chromatography Mass Spectrometry
93. H<sub>2</sub>SO<sub>4</sub> - Sulphuric acid
94. WAXD - Wide-angle X-ray diffraction
95. TBACN - Tetrabutylammonium cyanide
96. BSA - Bovine serum albumin
97. DAPI - (4',6-diamidino-2-phenylindole)
98. BM - Bohr magneton
99. EPR - Electron paramagnetic resonance
100. Cu - Copper
101. EB - Ethidium bromide
102. MTT - [3-(4,5-Dimethylthiazol-2-yl)-2,5-Diphenyltetrazolium Bromide]
103. PI - Propidium iodide
104. kDa - Kilodalton
105. PARP - Poly ADP ribose polymerase

---

## TRANSITION METAL COMPLEXES: AN OVERVIEW OF CATALYTIC AND MOLECULAR RECOGNITION PROPERTIES

---



### 1.1. Introduction

Metal complexes bearing organic ligands constitute a new class of compounds that lie at the interface between the classical organic and inorganic chemistry. Among these complexes, the transition metal ion based systems have provided greater insights into various domains such as molecular architectures, industrial catalysts, sensors, organic synthesis, and biology. Among the various catalysts, the transition metal complexes have been widely used in many organic transformations like hydrogenation, C-C coupling,

olefin metathesis, transfer hydrogenation reactions etc.<sup>1</sup> Many of these catalysts have the potential to high degree of asymmetric induction, which led to the synthesis of enantiomerically pure compounds. One of the strategies to make the processes environmentally green is to achieve atom economy, minimizing both the energy use and chemical waste in industry. In this regard, organometallic catalysis is likely to be one of the key contributors in reducing the waste through recycling of the catalyst.

In other words, a molecular probe is a system that undergoes changes in its physico-chemical properties upon interaction with an analyte or by stimulation with some form of energy. For example, the changes in the fluorescence properties of the probe (either fluorescence quenching or enhancement) in the presence of the analyte can be used efficiently for the recognition of the analyte in solution.<sup>2</sup> In this regard; the development of luminescent transition metal complexes as probes has been an active area of research in recent years. The inherent photophysical properties of the transition metal complexes make them attractive probes for the sensing applications.

Barnett and Rosenberg's serendipitous discovery of *cis*-platin, led to the intensive efforts in development of several tumor inhibiting complexes during the last few decades. The development of alternative drugs to the well-known, *cis*-platin and its derivatives is quite challenging.<sup>3</sup> Despite the tremendous success, the inefficiency against platinum resistant cancers and nephrotoxicity limited the wide use of the *cis*-platin derivatives. Therefore, the organometallic compounds in which the metal ion is covalently bonded to carbon of the supporting ligands have recently been found to be promising anticancer drug candidates.<sup>4</sup> By the rational design of ligands, the organometallic complexes provided good control over the kinetics, lipophilicity and



redox properties of the complexes. Because of these fundamental differences when compared to other compounds, the organometallics offer abundant opportunities in the design and development of novel classes of compounds, potentially with new metal-specific modes of action. The first chapter of this thesis briefly describes the design and development of the transition metal complexes, especially for their applications in the area of catalysis, molecular recognition and biology. The effect of ligands on the catalytic efficacy for the transfer hydrogenation reactions of the aromatic ketones, in particular, was given emphasis in this chapter. In addition, the specific objectives of the present thesis were also briefly described at the end of this Chapter.

## 1.2. Transition Metal Complexes as Catalysts

Catalysis is inevitable in modern synthetic chemistry since *ca.* 90% of the commercial chemicals are obtained by the use of catalysts in at least one step. Even though the history and development of catalysts can be found as far back as the eighteenth century, it is still an active area of research. The catalytic reactions can in principle are environmentally benign, less energy intensive, atom economy is maximum, sustainable and can produce the compounds in *ca.* 100% yields with 100% selectivity. Therefore, the transition-metal complexes as homogenous catalysts have become the most actively studied catalysts and which can activate the substrates and also accelerate the reactions. These systems, by taking advantage of the partially filled d orbitals and by means of coordination, ligand exchange, insertion, elimination, and can lead to the cleavage or formation of H-H, C-H, and C-C bonds. By modifying the ligand scaffold, the activity and selectivity of the transition metal catalysts can be tuned.

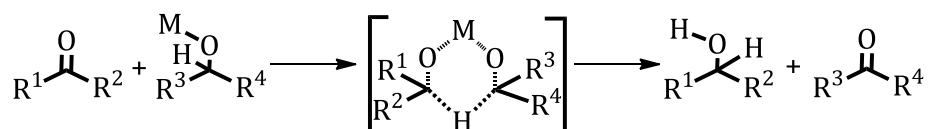
Excellent examples of the transition-metal-catalyzed reactions include asymmetric hydrogenation reactions catalyzed by Rh, Ru, or Ir catalysts having P- or N-containing ligands, olefin metathesis, hydrogenation, transfer hydrogenation, hydrosilylation reactions etc. Among all these reactions, hydrogenation can be considered as one of the core technology in chemical industry. Suitable reaction conditions with well-designed catalysts gave high selectivity to the system. Most excellent catalysts are mainly derived from the existing catalysts and are generated through suitable modification at the core. The applications of organic compounds are enormous and they are the important constituents of many products including plastics, drugs, petrochemicals, food, explosives, and paints. Therefore, the synthesis of the newer compounds with required properties employing catalysts is quite challenging in organic chemistry. In the following sections, we will mainly focus on the transfer hydrogenation reactions catalyzed by the selected transition metal complexes.

### **1.3. Transfer Hydrogenation Reactions**

There are basically two strategies reported for the hydrogenation, which includes the direct hydrogenation using molecular hydrogen and the transfer hydrogenation with the aid of hydrogen donor systems. The transfer hydrogenation (THR) is found to be superior over the conventional hydrogenation process and it has become most popular among hydrogenation reactions in recent years. Some of the advantages of transfer hydrogenation are, i) limited use of hazardous chemicals, ii) mild experimental conditions, iii) ease of availability of sacrificial hydrogen donors, and iv) recycling of catalysts. In 1903, Knoevenagel<sup>5</sup> reported the transfer hydrogenation reaction of

dimethyl 1,4-dihydroterephthalate using palladium black as the catalyst, in which the hydrogen transfer was gained between donor and acceptor units. Braude and Linstead<sup>6</sup> have explained three categories of the hydrogen transfer reactions, which include the hydrogen migration within the molecule, hydrogen disproportionation and lastly the transfer of hydrogen between unlike donors and acceptor groups. The third category is widely known as the transfer hydrogenation reaction, which is divided into several types depending on the nature of the catalyst employed. These include Meerwein-Ponndorf-Verley (MPV) reduction, transition metal-catalyzed reaction, organo-catalytic, enzyme-catalyzed, thermal, base-catalyzed, and un-catalyzed processes.

In 1925, Meerwein and Verley have independently reported the MPV reduction, and it was the first transfer hydrogenation reaction of the carbonyl compounds.<sup>7</sup> MPV reduction involves the use of the aluminium oxide promoter and secondary alcohol solvent for the hydrogenation of the ketones. Followed by the use of aluminium oxide, various metals such as zirconium, lanthanum, cerium, samarium, and ytterbium has been reported for the reduction reactions.<sup>8</sup> The MPV reduction follows a six-membered cyclic transition state wherein both the carbonyl substrate and secondary alcohol are coordinated to the metal center (Scheme 1.1). Furthermore, a number of heterogeneous catalysts based on Lewis acids or bases such as supported aluminum alkoxides, magnesium oxide, hydrotalcites, hydrous zirconia, supported ZrO<sub>2</sub> etc have been utilized for MPV reduction.<sup>9</sup> The MPV reduction has also been extensively applied in the chemical manufacture of flavor agents, but the requirement of large amount of reagents, undesired side reactions and the moisture sensitivity have limited the practical applications of this reaction.<sup>10</sup>



**Scheme 1.1.** Hydrogen transfer in the MPV reduction via a cyclic transition state.

The discovery of late transition-metal catalysts was one of the greatest achievements in the area of transfer hydrogenation reactions.<sup>11</sup> The pioneering work related to this reaction was reported by Henbest, Mitchell, and co-workers during 1960,<sup>12</sup> and have demonstrated the use of the iridium hydride for the hydrogenation of cyclohexanones and  $\alpha$ ,  $\beta$ -unsaturated ketones with isopropanol as the hydrogen donor. In the 1970s, seminal contributions were made by Sasson and Blum<sup>13</sup> by introducing  $\text{RuCl}_2(\text{PPh}_3)_3$  as the catalyst. Almost two decades later, Chowdhury and Backvall<sup>14</sup> have found that by use of catalytic amount of NaOH promoted the catalytic activity of  $[\text{RuCl}_2(\text{PPh}_3)_3]$  to  $10^3$ - $10^4$  times. In the early 1980s, the first examples of the asymmetric transfer hydrogenation reactions (ATHR) using the Ru catalysts have been reported,<sup>15</sup> which received significant attention. The asymmetric hydrogenation (AHR) was widely applied in pharmaceutical industries,<sup>16</sup> and Noyori and Knowles have been awarded the Nobel Prize in 2001 for their important contributions to this area.<sup>17</sup> The development of late transition metal-catalyzed transfer hydrogenation and asymmetric hydrogenation have showed great progress in the recent years, and Ir, Ru, and Rh complexes bearing N, P, O, S, C element based ligands (like metal-*N*-heterocyclic carbenes, half sandwich, multi-dentate metal complexes, and their combinations) and such catalysts have become popular among the scientists working in this area.

*N*-Heterocyclic carbenes (*NHCs*) are the cyclic carbenes having at least one  $\alpha$ -amino substituent. In 1960s Ofele and Wanzlick<sup>18</sup> have independently carried out seminal work on *NHCs*, and were followed by Lappert and coworkers<sup>19</sup> on organometallic compounds. These heterocyclic ligands have received prominence in the area of the coordination chemistry and the organometallic catalysis after the isolation of stable the *NHC* by Arduengo *et al.*, (Chart 1.1) in 1991.<sup>20</sup> The success of *NHCs* is often attributed to their strong  $\sigma$ -electron-donating properties,<sup>21</sup> which allow the formation of very strong *NHC*-metal bonds and prevent decomposition of the catalyst. Furthermore, the potential of *NHCs* as supporting ligands was realized, when they were coordinated with metals such as Ir, Ru, and Rh as the transition metal-catalysts.<sup>22</sup> In the transfer hydrogenation reactions, various sacrificial hydrogen sources such as alcohols (including 2-propanol, MeOH, EtOH, glycerol), formic acid, Hantzsch esters, hydrazine, benzothiazoles, etc were employed and of which 2-propanol and formate are the main reducing agents used in such reactions.

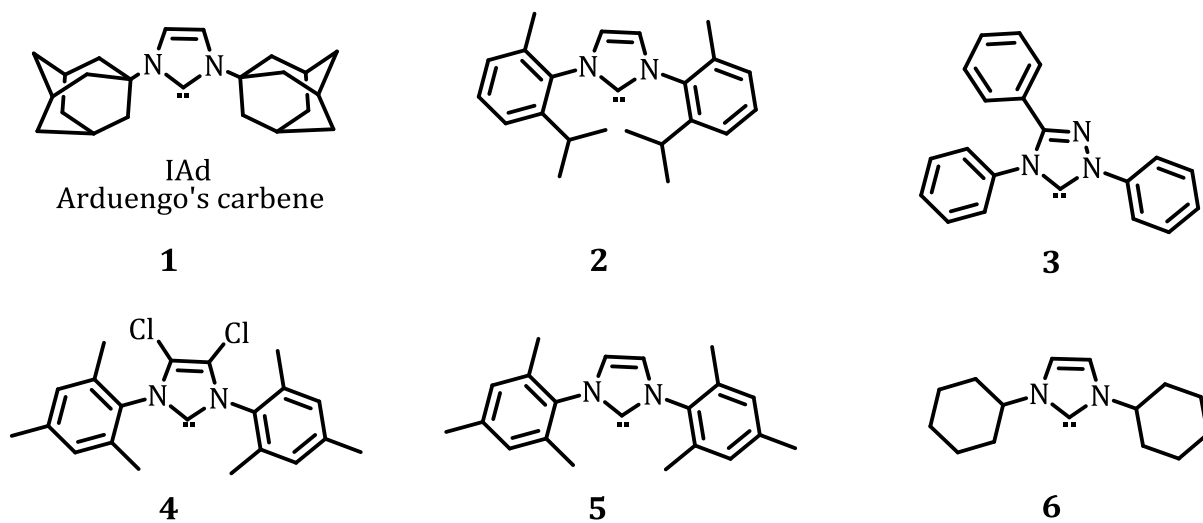


Chart 1.1

A series of organic and inorganic bases such as Et<sub>3</sub>N, KOH, NaOH, Na<sub>2</sub>CO<sub>3</sub>, HCOONa, 2-PrOK, 2-PrONa, 2-PrOLi, KO<sup>t</sup>Bu, NaO<sup>t</sup>Bu, K<sub>3</sub>PO<sub>4</sub>, Cs<sub>2</sub>CO<sub>3</sub>, CsOH, NaOAc, and NaOMe have also been employed in transfer hydrogenation. Of the various substrates, the unsaturated compounds including ketones, aldehydes, imines, nitro compounds, nitriles, oximes, α, β-unsaturated esters, α, β-unsaturated acids, α, β-unsaturated carbonyl compounds, heterocycles, alkenes, and alkynes have been reduced to the corresponding hydrogenated compounds through transfer hydrogenation in the presence of either homogeneous or heterogeneous transition-metal catalysts.

The detailed mechanistic studies have been explored by taking the ketones as the substrates and two mechanisms have been commonly proposed for transfer hydrogenation. These include, an inner sphere mechanism involving the substrate coordination and while the outer sphere mechanism excludes the substrate coordination. The inner-sphere mechanism involves the insertion of the ketone substrate into an M-H bond with a concomitant elimination of acetone molecule. The alkoxide thus formed then gets protonated by the incoming hydrogen source; releasing the alcohol product from the metal.<sup>23</sup> The outer sphere mechanism proposed by Noyori<sup>24</sup> which involves the deprotonation of the alcohol by the nucleophilic nitrogen donor with the simultaneous hydride transfer to the adjacent metal centre via a highly ordered transition state. This simultaneous transfer results in the generation of alcohol product. These two mechanisms are entirely different from those of the MPV reduction in which the ketone interacts with the metal alkoxide.

### 1.3.1. Iridium-Based Catalysts

The pioneering work on the transition-metal catalyzed THR was reported by Nolan *et al.*,<sup>25</sup> based on the iridium-*NHC* complex,  $[\text{Ir}(\text{COD})(\text{Py})(\text{NHC})]\text{PF}_6$ , **7**. Further, these complexes were used for transfer hydrogenation of several unsaturated substrates including ketones, olefins, and nitroarenes with 2-propanol as hydrogen donor. These complexes were found to exhibit high activity toward all the substrates, especially ketones. After the work by Nolan *et al.*, many Ir-*NHC* complexes have been reported. Cp\*-functionalized *NHC* ligands were also designed and coordinated to  $[\text{Ir}(\mu\text{-Cl})(\text{COD})]_2$  by Royo *et al.*,<sup>26</sup> to get the complex **8**. They have employed the catalyst for transfer hydrogenation of various ketones at a low catalyst loading of 0.01 mol% with up to a TON of 9900. The four coordinate iridium complex,  $[\text{IrBr}(\text{COD})(\text{C-NHC})]$ , **9** developed by Hahn and Oro<sup>27</sup> showed transfer hydrogenation of cyclohexanone using 2-propanol as the hydrogen source in presence of catalytic amount of KOH. In 2007, Crabtree and co-workers<sup>28</sup> have demonstrated the use of triazole based iridium complex for the successful transfer hydrogenation of C=O, C=N, and C=C groups in the presence of 1 mol % of **10** with 2-propanol or cyclopentanol as the hydrogen source (Chart 1.2).

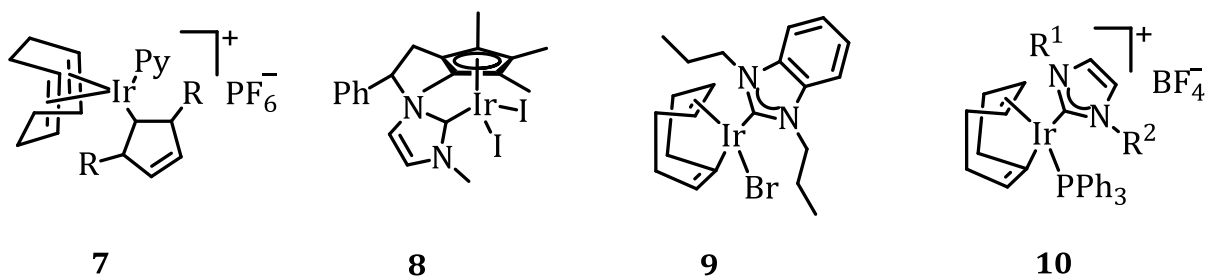


Chart 1.2

Gulcemal's group has developed a series of new iridium-*NHC* complexes through transmetalation reactions from the in situ prepared silver(I)-*NHC* complexes<sup>29</sup> (Chart 1.3). Ester functionalized iridium complexes, **11** showed good results in the reduction of carbonyls in the transfer hydrogenation process with >99% conversion. The transfer hydrogenation of carbonyls catalyzed by the complexes **12** and **13** was completed in very short reaction times down to 2 min, with a TOF of 12000 h<sup>-1</sup>. The complexes **13a-b** were found to show high activity for the transfer hydrogenation of imines, this was attributed to the existence of both flexible and sterically demanding benzyl substituents on the nitrogen atoms of *NHC* ligand. This study brought more attention to the use of alkylated benzyl-functionalized benzimidazole *NHC* ligands in homogeneous catalysis.

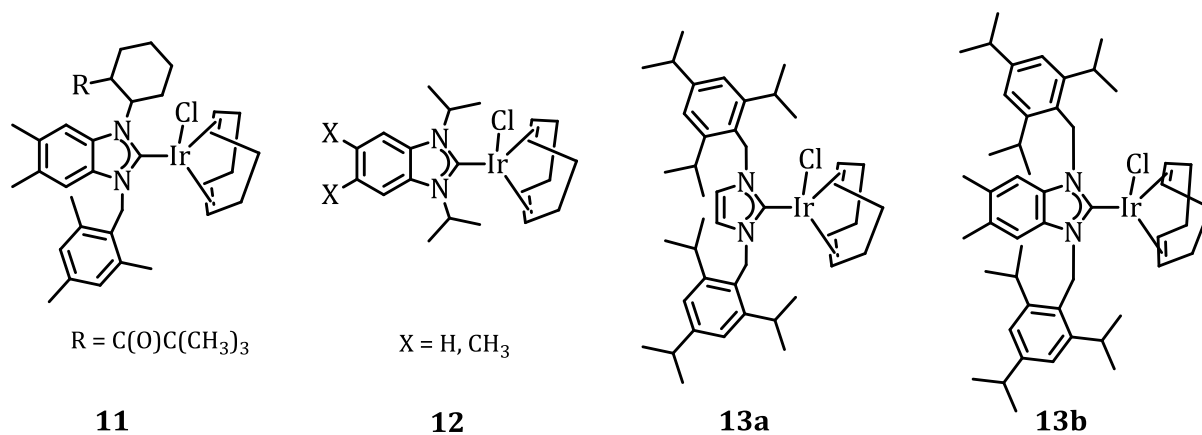


Chart 1.3

Bis-*NHCs* as chelating ligands have also received increasing interest in homogeneous transfer hydrogenation catalysis (Chart 1.4). The complexation of the bis-*NHCs* with iridium gave complexes having various CNC donor ligands. Bis-*NHCs* are supplemented by a hemilabile pyridyl donor in most of the complexes.<sup>30</sup> The catalytic



performance of the complex **14** in the transfer hydrogenation of ketones was tested with various substrates under different conditions. Desired alcohol products were obtained in 30-60 min using a catalytic amount of 0.01-0.3 mol% of the complexes. Half-sandwich complexes of iridium (**16** and **17**) were also an important components in the family of the iridium complexes that were used in the transfer hydrogenation (Chart 1.4).<sup>31</sup> Recent examples showed that half-sandwich iridium catalysts incorporates a variety of coordinating ligands based on N, P, C elements, which were found to be quite efficient for the transfer hydrogenation.

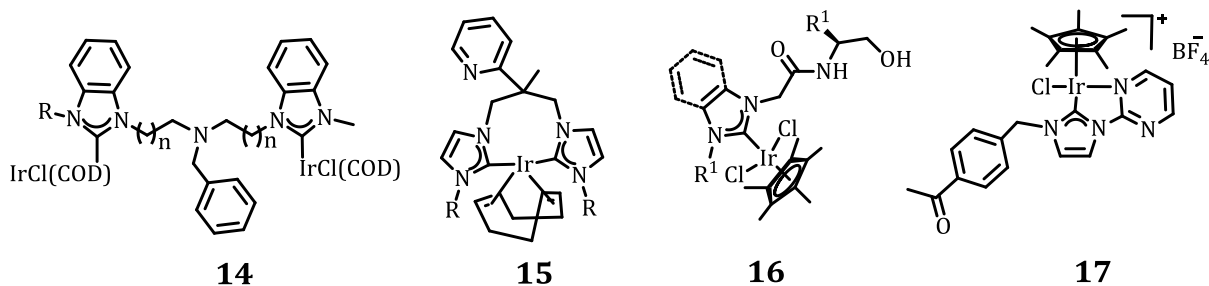
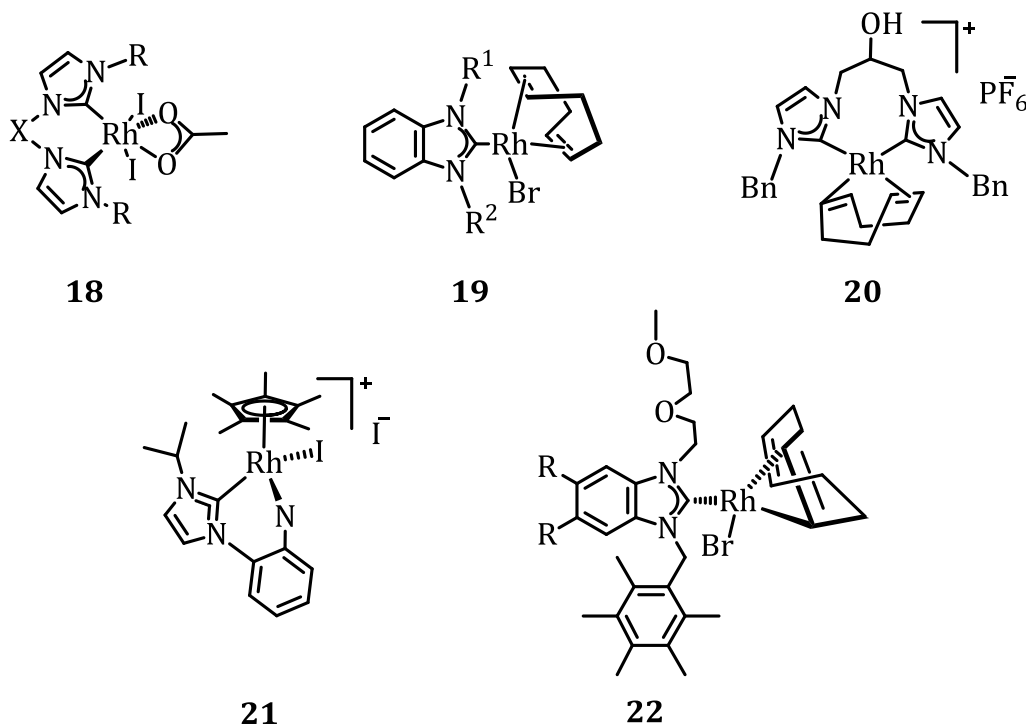


Chart 1.4

### 1.3.2. Rhodium-Based Catalysts

In 2002 Crabtree and Peris have reported the first example of robust and air-stable Rh-NHC catalyst **18** for the transfer hydrogenation reactions. These complexes exhibited good catalytic activity in the transfer hydrogenation with both ketones and imines and were found to be inactive for olefins. After this pioneering report, several seminal studies on the transfer hydrogenation catalyzed by Rh complexes with different NHCs such as benzannulated NHCs **19**, bridged bis-NHC **20**, amine-functionalized NHC

**21**, and diether-functionalized *NHC* **22** were reported (Chart 1.5).<sup>32</sup> For example, Kuhn's group has reported a bis-Rh-*NHC* complex bridged with hydroxyl groups, which was a



**Chart 1.5**

potential anchoring point for the immobilization onto different solid supports providing recyclable metal-*NHC* catalysts. On the basis of their previous studies on the rhodium-*NHC* catalysts,  $[\text{Rh}(\text{NHC})\text{X}(\text{COD})]$ , new types of complexes have been reported for the potential anchoring point for immobilization onto different ketones (Chart 1.6).<sup>33</sup> For example, the catalyst **23** with perimidin-2-ylidene *NHC* ligand exhibited low catalytic activity due to the weak sigma donating property of the ligand, whereas catalyst **24** bearing symmetric mesityl (Mes) substituents efficiently promoted the transfer hydrogenation reaction with high conversion yields within 2 h at a catalyst loading of 0.5 mol%. The comparison of the efficiencies of the catalysts clearly indicated the effect

of substituents, wherein the catalyst **24a** with imidazoline induced a faster reaction than **24b** having imidazole group. The pyridazine-annelated bis-*NHC* cationic rhodium complexes **25** also showed a good activity in transfer hydrogenation of ketones.<sup>34</sup>

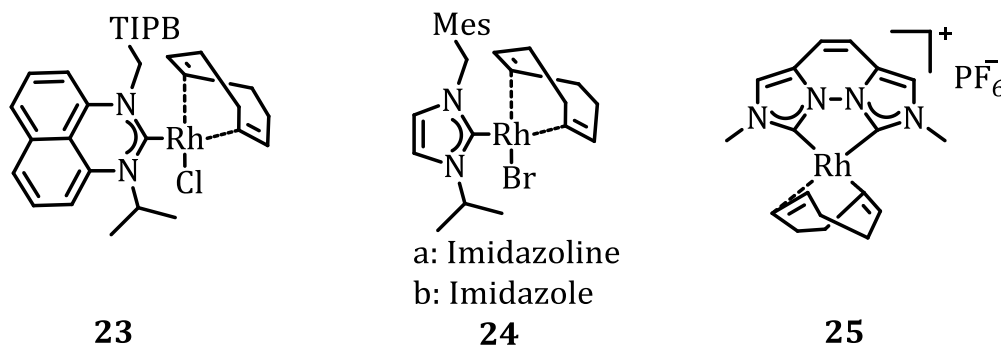


Chart 1.6

Triazolyl ligands were also used in the Rh catalyzed homogeneous transfer hydrogenation reactions (Chart 1.7). A square planar rhodium-cod complex **26** based on *t<sub>z</sub>NHC* and an Arduengo-type *NHC* motif was synthesized, wherein this *t<sub>z</sub>NHC-NHC* ligand possesses stronger electron-donating properties than that of classic di-*NHC* ligands. This complex was successfully used as an efficient catalyst for the transfer hydrogenation of carbonyls, imines, and dienes using 2-propanol as the hydrogen source.<sup>35</sup> More importantly, the *tz-NHC* complex was found to be much more active than its analogue **27** in which the triazolyl moiety coordinates to the metal center through a nitrogen donor. Adolfsson and Singh *et al.*,<sup>36</sup> have synthesized a series of triazole-functionalized amide ligands, which on combination with half-sandwich rhodium precursor [RhCl<sub>2</sub>Cp\*]<sub>2</sub> **28** showed high catalytic efficacy in the asymmetric transfer hydrogenation of ketones.

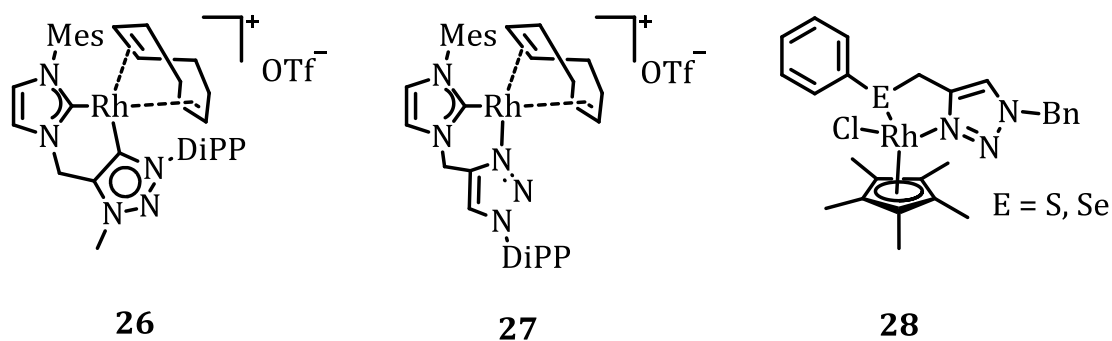


Chart 1.7

The half-sandwich rhodium complexes were extensively used as catalysts for the transfer hydrogenation (Chart 1.8).<sup>37</sup> An easily accessible Rh(III)- $\eta^5$ -Cp\* complex **29** containing a bis(phosphino)amine ligand catalyzed the substituted acetophenones in 2-propanol. Air and moisture-stable complex **30** was prepared and was the first rhodium catalysts of carbonyls in glycerol, where complex **30b** with Se atoms displayed better activity than the S-containing analogue **30a**. The tethered half-sandwich rhodium complex **31** containing TsDPEN and a functionalized Cp\* unit catalyzed asymmetric transfer hydrogenation of ketones with the HCO<sub>2</sub>H/Et<sub>3</sub>N mixture as hydrogen source under mild conditions. Water-soluble rhodium complexes were also exhibit transfer hydrogenation, which proceeded smoothly in water and produced various functional compounds.<sup>38</sup> Deng's group have reported the cationic amphiphilic surfactant-type ligands and the corresponding chiral rhodium-Cp\* for transfer hydrogenation with high enantioselectivity.<sup>39</sup> The high level of enantioselectivity was taken into account by hydrophobic interactions between the alkyl chains of the aliphatic ketones and the catalyst. Employing the rhodium catalysts in the transfer hydrogenation, several functional products such as amines, piperidines etc have been successfully synthesized.

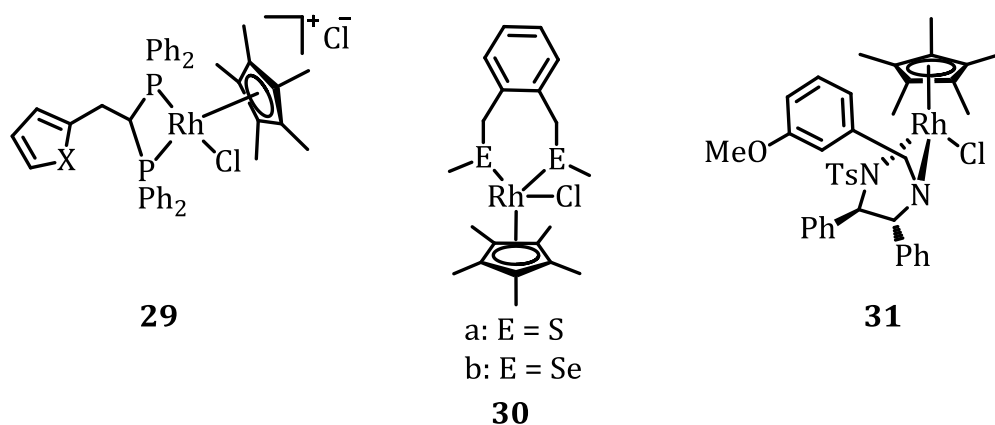


Chart 1.8

### 1.3.3. Ruthenium-Based Catalysts

The catalysts based on Ruthenium are the most widely used catalysts for transfer hydrogenation reactions in the recent years and have found practical applications in pharmaceutical industries. The ligand choice is very crucial towards both selectivity and efficacy of the metal catalysts. Among the various ligands, *NHCs* showed significant role in the synthesis of the homogeneous organometallic catalysts. The Ruthenium *NHC* complexes with a wide structural diversity in its coordination motifs have recently exhibited good activity and selectivity in catalytic transfer hydrogenation.<sup>40</sup> Donor functionalized groups such as pyridine, pyrimidine, indenyl etc. on *NHCs* showed prominent activity in catalysis involving ruthenium metal center. The development of Noyori catalysts (Chart 1.9)<sup>41</sup> showed significant applications in the synthesis of the functional compounds and in the exploration of new routes to tethered ruthenium catalysts. The Noyori catalyst **33** exhibited excellent activities towards hindered ketones, a variety of alcohols were quantitatively prepared with high enantioselectivity through the transfer hydrogenation procedure.

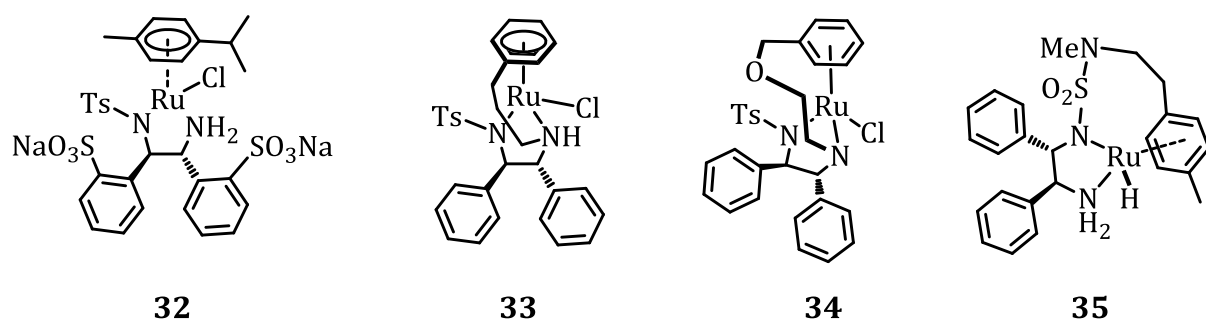


Chart 1.9

These catalysts were also found to be a good for the synthesis of enantioenriched  $\gamma$ -lactones with ee up to 94%. Ikariya and Wills have independently reported the application of ether-tethered half-sandwiched ruthenium complexes (**34** and **35**) (Chart 1.9)<sup>42</sup> for the asymmetric transfer hydrogenation of ketones. Stephan *et al.*,<sup>43</sup> have observed that the ruthenium(II) catalyst **35** was highly active and enantioselective in the transfer hydrogenation of 1-naphthyl ketones to secondary 1-naphthyl alcohols at room temperature in HCO<sub>2</sub>H-Et<sub>3</sub>N. The Ruthenium *NHC* complexes **36** and **37** that contain a pyridine moiety were also showed excellent activity in transfer hydrogenation reactions with a low catalyst loading (Chart 1.10).<sup>44</sup> Olefin-tethered *NHC* ruthenium complex **38** was found to be efficient towards the transfer hydrogenation of olefins to alkanes and alkynes to olefins under various conditions.

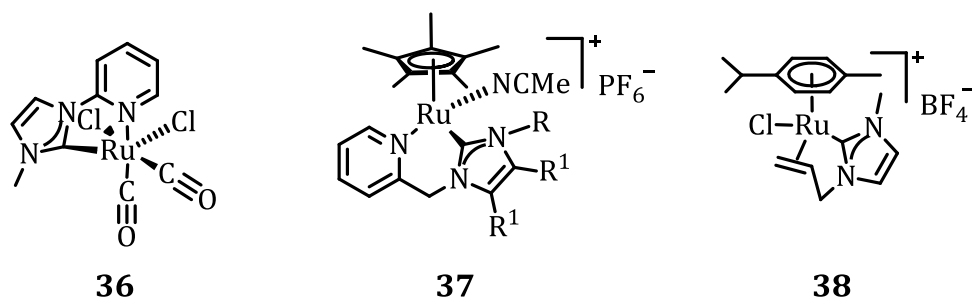


Chart 1.10

The pyridine-based ruthenium catalysts were also used in the transfer hydrogenation of a wide variety of substrates in recent years. Several symmetrical pyridine-based ruthenium complexes were synthesized by Yu and Pizzano (Chart 1.11).<sup>45</sup> The complex **39** with chiral pyridyl-based 1*H*-pyrazolyl-oxazolanyl ligand was found to be robust catalyst for asymmetric transfer hydrogenation of ketones under mild conditions, with good to excellent conversions.<sup>45b</sup> Also, the complex **40** containing both a pybox (2,6-bis(oxazoline)pyridine) and a monodentate phosphite ligand was shown to be highly active in asymmetric transfer hydrogenation of *N*-aryl imines using 2-propanol as hydrogen source.<sup>45c</sup> The 6,6'-dihydroxy terpyridine based ruthenium complex **41** showed good transfer hydrogenation activities for many carbonyls, but the chemoselectivity was not satisfactory when the carbonyl with olefins were tested.<sup>45d</sup>

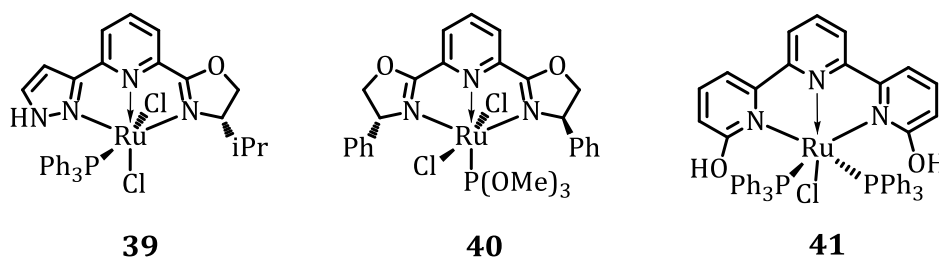
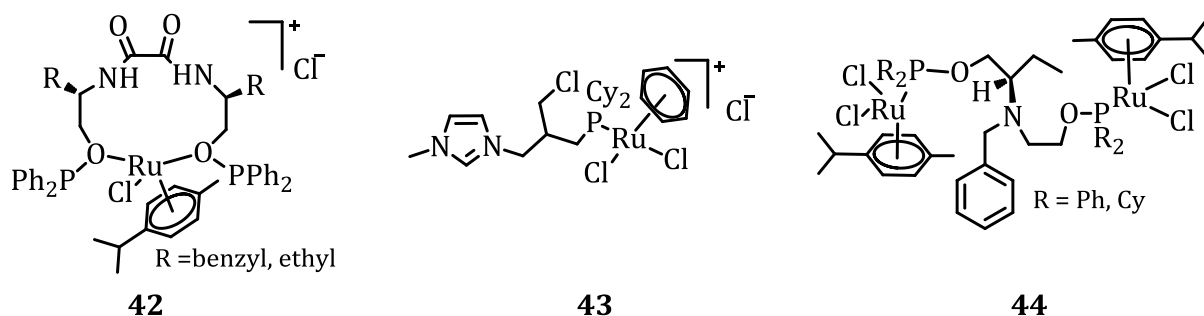


Chart 1.11

A variety of half-sandwich ruthenium complexes containing arene (including benzene, *p*-cymene, and hexamethylbenzene) ligands have been widely explored in the transfer hydrogenation.<sup>46</sup> The discovery of the Noyori catalysts;  $[\text{RuCl}(\text{TsDPEN})(\eta^6\text{-}p\text{-cymene})]$  and  $[\text{RuCl}(\text{TsDPEN})(\eta^6\text{-mesitylene})]$  was one of the breakthroughs in the ruthenium-catalysed transfer hydrogenation reactions.<sup>47</sup> The versatile P-based ligands have also been introduced into half-sandwich ruthenium complexes **42-44** that have

been intensively explored in the transfer hydrogenation of carbonyl compounds (Chart 1.12).<sup>48</sup> The half-sandwich ruthenium complexes with bidentate ligands such as P-N,



**Chart 1.12**

bipyridine,  $\alpha$ -amino-oximes, amino alcohol, Schiff base, thioamide, and 1,3-diamines (**45-48**) have been recently exploited for the transfer hydrogenation reactions (Chart 1.13).<sup>49</sup> Among these, the complexes containing 4,4'-dimethoxy-2,2'-bipyridine **45** showed catalytic activity with the use of HCOONa as the hydrogen donor in the reduction of water-soluble and insoluble ketones. The recent developments have shown that the binuclear and trinuclear ruthenium complexes have been used as a promising class of catalysts for the transfer hydrogenation (Chart 1.14). The Li and Aydemir groups<sup>50a,b</sup> have demonstrated the use of phosphinite-bridged dinuclear ruthenium arene complexes **49** and **50** for the hydrogenation of ketones. A binuclear ruthenium(II) pyridazine complex **51** was also found to be an efficient catalyst for the transfer hydrogenation reactions of the ketones.<sup>50c</sup> Moreover, the tridentate ligands such as aminophosphine-phosphinite and phosphinite ligands have also been used for the



development of trinuclear neutral ruthenium(II) dichloro complex **52**, which exhibited transfer hydrogenation reaction of the ketones in 2-propanol.<sup>50d</sup>

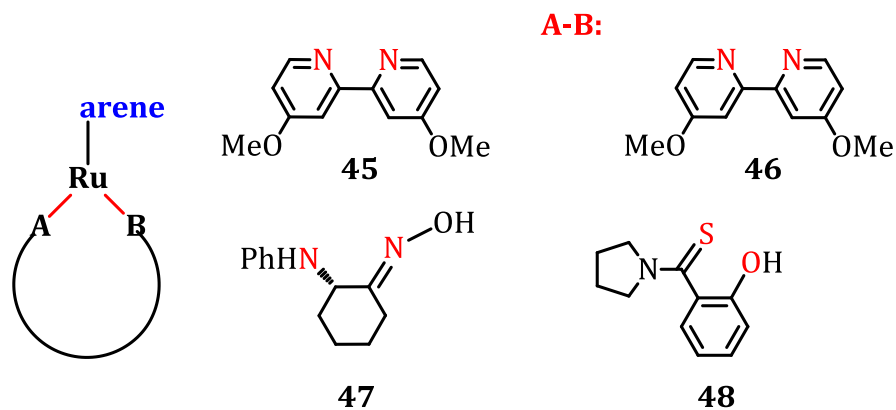


Chart 1.13

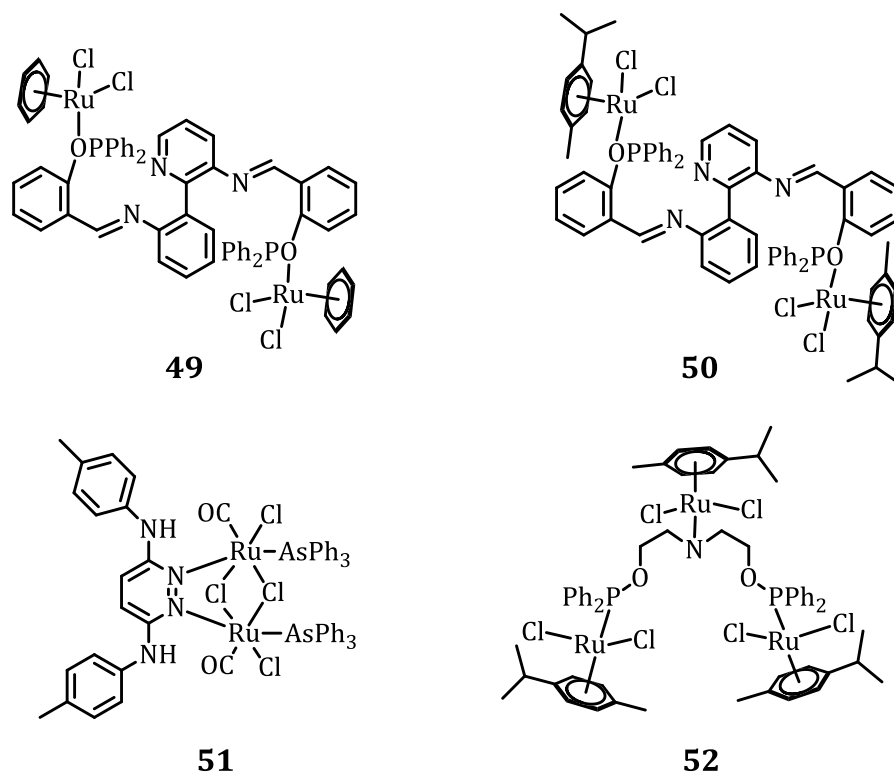
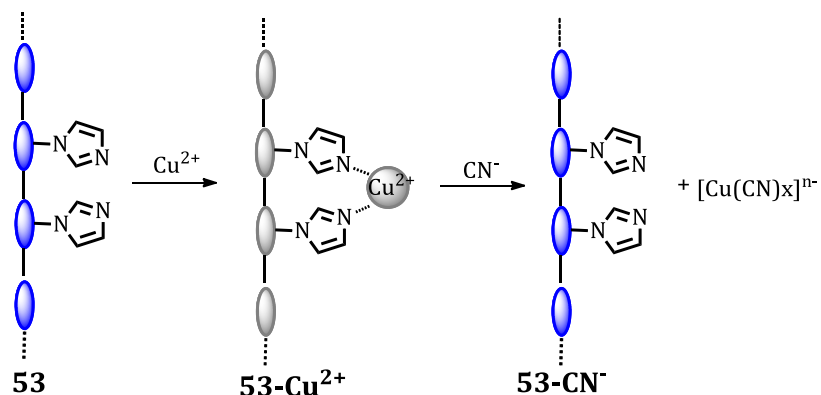


Chart 1.14

## 1.4. Transition Metal Complexes as Molecular probes

Recognition events in chemistry, biology, and materials science are quite important and which led to the development of molecular probes that provide useful information about the molecular interactions.<sup>51</sup> These probes are being used in various fields such as diagnostics, monitoring, and analytical tools in biochemical, medical, and environmental areas as well as in industry. Various types of probes have been reported for the recognition of various analytes such as cations, anions, and biomolecules based on optical or electrochemical techniques. A wide variety of systems have also been reported with macrocyclic and acyclic systems functioning as effective and selective anion receptors. Among these, the metal complexes have played an important role in anion receptor chemistry; the presence of metal ion can induce a range of changes in physico-chemical properties of the receptor. In most of the examples, the metal complex is incorporated as a receptor group, whose photochemical or redox properties are changed upon binding of an anion. The metal complex motif can also be used as structural component in anion receptors, wherein its coordination can change the geometric properties of the receptor. Recently, the molecular probes based on colorimetric and fluorimetric assays have attracted a great deal of attention.<sup>52</sup> Of these, the fluorescence based detection techniques showed advantages over the other methods due to their high sensitivity, rapidness and technical simplicity.<sup>53</sup> In fact, the development of fluorescent probes based on the transition metal complexes is an area that is emerging in the supramolecular chemistry for the design of probes for various anions,<sup>54</sup> cations<sup>55</sup> and also biomolecules.<sup>56</sup>

In 2008, Tang and co-workers, have reported synthesis of a polyacetylene bearing imidazole moieties in the side chain **53** as a sensory polymer to selectively detect the presence of  $\text{Cu}^{2+}$  based on the fluorescence intensity turn-off mechanism.<sup>57</sup>



**Figure 1.1.** Schematic representation of detection of  $\text{Cu}^{2+}$  and  $\text{CN}^-$  ions through fluorescence changes by the functionalized polyacetylene probe **53**.

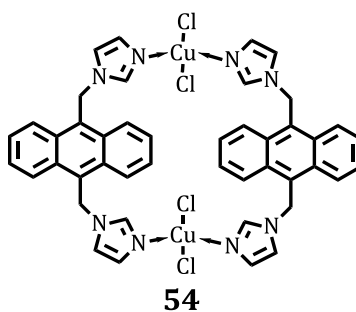


**Chart 1.15**

Subsequently, the quenched luminescence of **53** by  $\text{Cu}^{2+}$  could be turned on after the addition of  $\text{CN}^-$ , making it a very sensitive, and selective probe for the cyanide ions (Figure 1.1). In 2010, our group has reported  $\text{Cu}^{2+}$  ion induced formation of a novel water soluble metallocyclophane **54**, (Chart 1.15), which uniquely exhibited the selective recognition of guanosine 5'-monophosphate (GMP) through changes in fluorescence intensity utilizing the synergistic effects of electrostatic, coordinative and

pi-stacking interactions inside the cavity.<sup>58</sup> In 2011, Sabzi and coworkers,<sup>59</sup> have reported a silver nanoparticle based colorimetric sensor for the selective detection of cyanide ions in aqueous medium. This approach relies on the simple redox reaction between Ag nanoparticles and dissolved oxygen in the presence of  $\text{CN}^-$  ions. The concentration of the cyanide ions can be determined from the absorbance intensity of the SPR band at 394 nm. In 2010, Zhao and coworkers,<sup>60</sup> have reported an OFF-ON red-emitting phosphorescent thiol probe **55** using the  $^3\text{MLCT}$  photophysics of Ru(II) complexes (Figure 1.2). This non-luminescent probe because of the MLCT was altered by the electron transfer from Ru(II) to an intramolecular electron sink (2,4-dinitrobenzenesulfonyl). When the thiol group was cleaved, the electron sink and the MLCT were re-established. Ajayaghosh and coworkers,<sup>61</sup> in 2010 demonstrated the use of a zinc ion specific fluorophore, **56** for the colorimetric and fluorimetric screening of endogenous  $\text{CN}^-$  in bio-relevant samples (Scheme 1.2). The fluorescent  $\text{Zn}^{2+}$  complex, **56-Zn<sup>2+</sup>** upon  $\text{CN}^-$  addition generates a blue fluorescence that allows the detection of the latter and was useful for the screening of natural products with and without endogenous cyanide content.

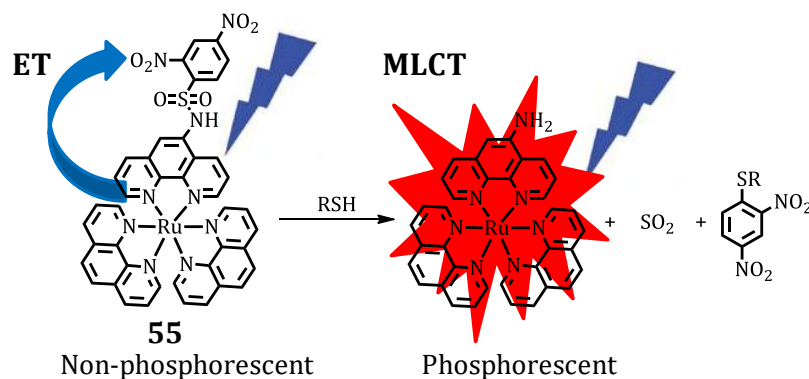
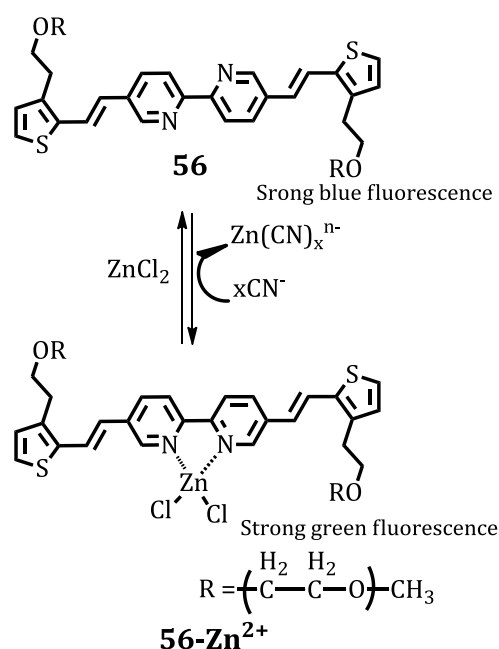


**Figure 1.2.** Representation of thiol detection by the phosphorescent probe **55**.



**Scheme 1.2.** Sensing of CN<sup>-</sup> ions by a Zn<sup>2+</sup> specific molecular probe **56**.

In another report Reddy and coworkers,<sup>62</sup> have described a highly selective probe **57** for the sensing of CN<sup>-</sup> ions in a semi-aqueous environment on the basis of a simple phosphorescent iridium(III) complex with a detection limit of  $2.16 \times 10^{-8}$  M. A unique colorimetric and ratiometric phosphorescence response to the cyanide was realized through interaction of the electron-deficient formyl moiety of the cyclometalated iridium(III) complex with CN<sup>-</sup> through the formation of cyanohydrin adduct **58** (Figure 1.3). In another report, Gopidas and coworkers<sup>63</sup> have demonstrated a highly selective and sensitive Ru-bipyridine based luminescence chemodosimeter **59** (Scheme 1.3) for the detection of Cu<sup>2+</sup> ions. They have used a strategy, which involves oxidation of the aromatic amines by Cu<sup>2+</sup>, thereby providing a “Turn-ON” luminescence chemodosimeter for Cu<sup>2+</sup>, which acts by way of PET inhibition, occurring through a chemical reaction.

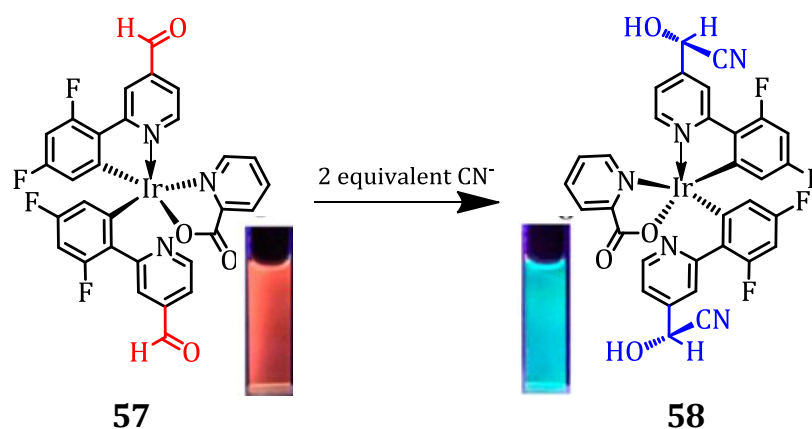
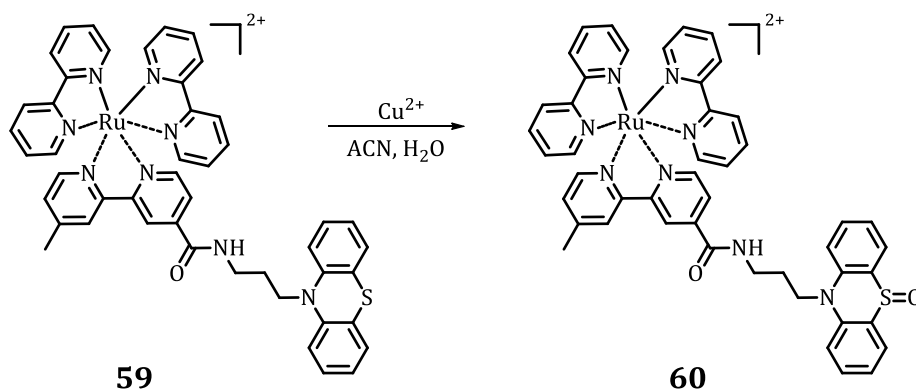


**Figure 1.3.** Sensing of cyanide ions using the probe iridium complex **57**.



**Scheme 1.3.** Sensing of  $\text{Cu}^{2+}$  ions by a ruthenium-bipyridine probe **59**.

## 1.5. Transition Metal Complexes in Biology

The transition complexes have been well explored and some of them play an important role in various biochemical processes.<sup>64</sup> Recent efforts have shown that significant progress in utilization of the transition metal complexes as drugs to treat several human diseases like carcinomas, lymphomas, infection control, anti-inflammatory, diabetes, and neurological disorders.<sup>65</sup> The transition metals exhibit different oxidation states and can interact with a number of negatively charged

molecules. This activity of transition metals has led to the development of metal based drugs with promising pharmacological applications and which may offer unique therapeutic opportunities. The metal ions perform a wide variety of tasks such as carrying oxygen throughout the body and shuttling electrons. Hemoglobin, an iron-containing protein that binds to oxygen through its iron atom, ferries this vital molecule to body tissues.<sup>66</sup> The metal ions such as zinc provide the structural framework for the zinc fingers that regulate the function of genes in the nuclei of cells. Similarly, calcium-containing minerals are the basis of bones, the structural framework of the human body. Zinc is a natural component of insulin, a substance crucial to the regulation of sugar metabolism. The metal ions such as copper, zinc, iron, and manganese are incorporated into catalytic proteins and the metalloenzymes, which facilitate a multitude of chemical reactions needed for life.<sup>67</sup> Other metal ions like gallium, germanium, tin, bismuth, titanium, ruthenium, rhodium, iridium, molybdenum, copper, iron, gold were shown to be effective against various tumors.<sup>67</sup>

Currently, *cis*-platin (**61**), carboplatin (**62**) and oxaliplatin (**63**) (Chart 1.16) are the only metal-based anticancer agents in clinical use. The metal ion complexes used in the tumour therapies displayed a remarkable therapeutic activity for a series of tumours. Severe dose-limiting side effects and drug resistance are the main drawbacks associated with this kind of therapy. Of these platinum complexes, satraplatin (**64**), an octahedral platinum(IV) complex, was the most interesting candidate in an advanced clinical stage. Contrary to the clinically established square-planar platinum(II) complexes, which are administered intravenously, satraplatin can be applied orally due to its kinetic inertness.<sup>68</sup>

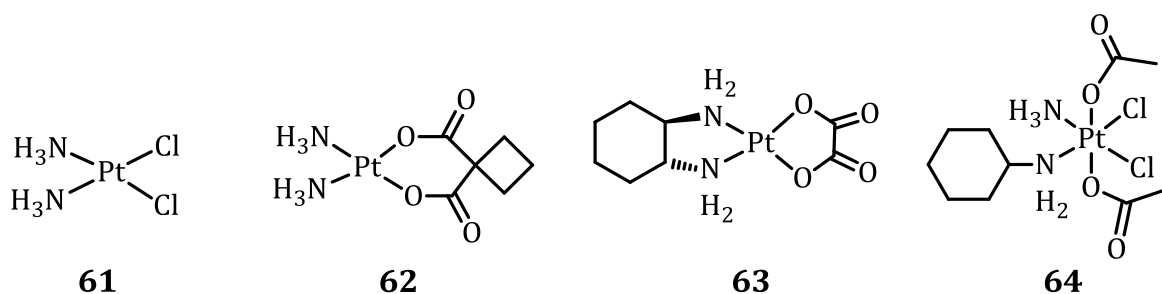


Chart 1.16

Because of the side effects and drug resistance, the chance to find active platinum complexes with a simple set of ligands and better therapeutic properties in comparison to *cis*-platin, carboplatin and oxaliplatin has limited success. Consequently, two main strategies have been adopted, of which one involves the synthesis of platinum complexes containing ligands with the specific function of improving tumour selectivity; and the second one involves the development of non-classical platinum complexes clearly violating the classic structure-activity relationships. While non-classical platinum complexes are increasingly being developed because they do not mimic *cis*-platin in their modes of action, the metal ions other than platinum inherently have more or less ideal properties for such applications. Differences in coordination geometry, binding preferences, electrovalence, redox activity, ligand exchange reactions, or even the simple capacity of replacement of essential metal ions form the chemical basis to develop attractive candidates. In this regard, the growing field of the metal ion complexes with biologically active ligands deserves a special attention and some of the representative examples are shown below.

In 2012, Dyson and coworkers have reported two series of ruthenium(II) arene complexes with pendant naphthalimide moieties,<sup>69</sup> in which the naphthalimide was



connected via the arene unit **65** and imidazole linker **66** (Chart 1.17). In both the series of complexes, the naphthalimide increased the cytotoxicity of the ruthenium(II) arene system. The high selectivity towards cancer cells over model healthy HEK cells was observed for the former series, which were also active against the cis-platin-resistant cells. In another report, Chakravarty and coworkers have reported the carbohydrate appended ternary iron(III) complex **67** (Chart 1.18), which showed significant photocytotoxicity when exposed to red light and exhibited low dark toxicity.<sup>70</sup> These complexes preferentially internalized in the HeLa cells and caused cell death in an apoptotic pathway by the generation of reactive oxygen species (ROS) on irradiation.

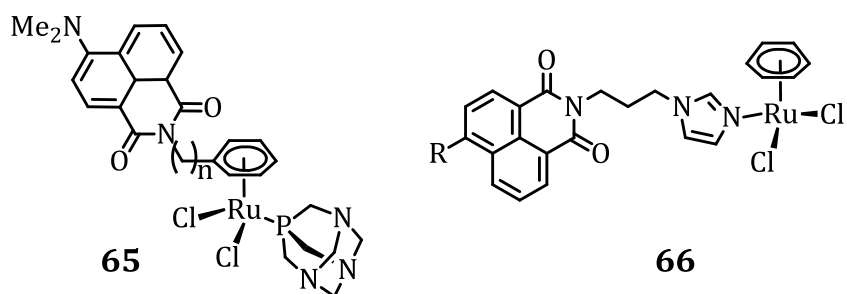


Chart 1.17

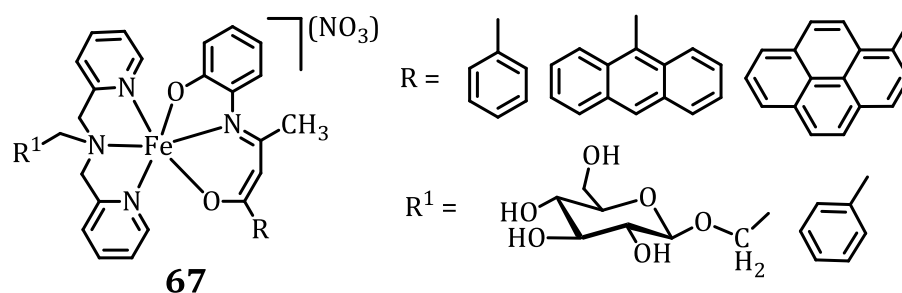


Chart 1.18

In 2013, Alzuet *et al.*, have reported the synthesis of mixed-ligands<sup>71</sup> **68** and **69** (Chart 1.19) based the copper(II)-sulfonamide complexes and have reported their interactions with DNA. The *in vitro* nuclease activity and their ability to damage DNA in yeast cells were also described. These complexes also exhibited higher anticancer activity against colon adenocarcinoma Caco-2 cell lines and leukemia Jurkat T lymphocytes through apoptosis mediated cell death. Sadler and coworkers<sup>72</sup> have synthesized and demonstrated the potential of the half-sandwich cyclopentadienyl Ir(III) pyridine complex **70** (Chart 1.19) for their anticancer activity. All these complexes displayed high potency toward A2780, A549, and MCF-7 human cancer cells, comparable to, and for some complexes even higher than, the clinical anticancer drug *cis*-platin. Importantly, the anticancer efficacy can be fine-tuned by varying the pyridine-based ligands and the presence of electron-donating groups found to significantly improve the anticancer activity of these systems. As described above, the transitional metal based complexes can have wide applications ranging from catalysis to diagnostics to therapeutics and hence are worth for further explorations.

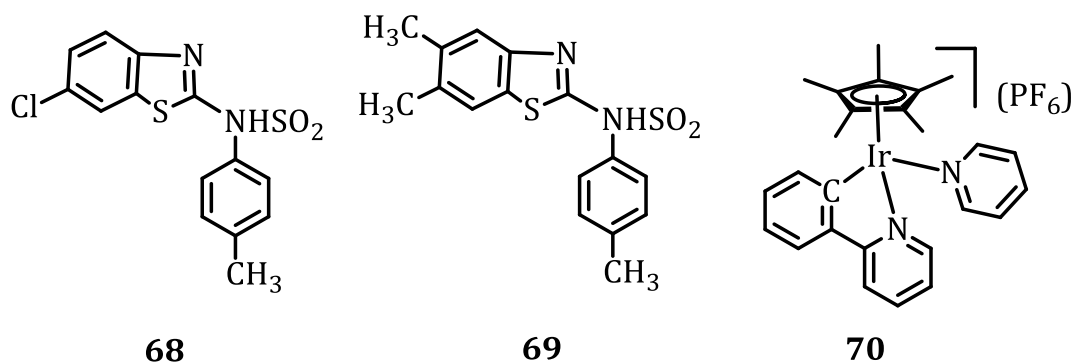


Chart 1.19

## 1.6. Objectives of the Present Investigation

Development of the transition metal complexes with favorable chemical and optical properties is an important area of research because such systems can have immense significance in creating molecular architectures, industrial catalysts, organic synthesis, sensing and biology. In this context, our main objectives have been to design few novel transition metal complexes that can exhibit catalytic activity, selective binding to various ions and also exhibit high biological activity. Another objective is to design few neutral and cationic ruthenium complexes and to investigate their potential as catalysts for the transfer hydrogenation reactions. Yet another objective has been the design of few silver-*NHC* complexes, and to investigate their potential as molecular probes for the selective recognition of important anions. The last objective of the thesis has been the design of two novel biomimetic mononuclear iron and copper complexes based on naphthalimide appended tripodal tetradentate ligands and study of their photophysical, and *in vitro* biological properties.

Our results indicate that the systems synthesized showed excellent solubility in the aqueous medium, favorable optical properties and have exhibited catalytic transfer hydrogenation activity towards aromatic ketones. The study of effect of various substituents on the catalytic transfer hydrogenation reactions of the aromatic ketones have confirmed that the complexes investigated are quite stable to air and moisture and have exhibited excellent activity at a low catalyst loading conditions, thereby demonstrating their use as efficient catalysts for transfer hydrogenation reactions. Furthermore, the silver complexes under investigation were found to be selective in

recognizing the cyanide ions, when compared to the other biologically important anions and signaled the event through changes in the “Turn On” fluorescence intensity. Our detailed studies have confirmed that these systems have favorable photophysical properties and exhibit selective and sensitive interactions with cyanide ions involving the mechanism of displacement approach. The copper and iron derivatives, on the other hand, have exhibited good affinity towards DNA and proteins, as confirmed through photophysical and chiroptical studies. Furthermore, the *invitro* biological properties of these complexes employing HeLa cell lines have indicated that both these complexes show significant cellular growth inhibition when compared to the free ligands. Our results indicate that these systems which showed effective DNA/protein interactions and can have potential use as anticancer agents.

## 1.7. References

1. (a) Duo-Sheng, W.; Qing-An, C.; Sheng-Mei, L.; Yong-Gui, Z. *Chem. Rev.* **2012**, *112*, 2557. (b) Vougioukalakis, G. C.; Grubbs, R. H. *J. Am. Chem. Soc.* **2008**, *130*, 2234. (c) Diez Gonzalez, S.; Marion, N.; Nolan, S.P. *Chem. Rev.* **2009**, *109*, 3612.
2. (a) Zheng, S.; Lynch, P. L. M.; Rice, T. E.; Moody, T. S.; Gunaratne, H. Q. N.; de Silva, A. P. *Photochem. Photobiol. Sci.* **2012**, *11*, 1675. (b) Miyaji, H.; Kim, H. K.; Sim, E. K.; Lee, C. K.; Cho, W. S.; Sessler, J. L.; Lee, C. H. *J. Am. Chem. Soc.* **2005**, *127*, 12510.
3. (a) Jakupec, M. A.; Galanski, M.; Arion, V. B.; Hartinger, C. G.; Keppler, B. K. *Dalton Trans.* **2008**, *2*, 183. (b) Dyson, P. J.; Sava, G. *Dalton Trans.* **2006**, 1929.
4. Gilles, G.; Ingo, O.; Nolte, N. M. *J. Med. Chem.* **2011**, *54*, 3.
5. Knoevenagel, E.; Bergdolt, B. *Chem. Ber.* **1903**, *36*, 2857.

6. Braude, E. A.; Linstead, R. P. *J. Chem. Soc.* **1954**, 3544.
7. (a) Verley, A. *Bull. Soc. Chim. Fr.* **1925**, 37, 537. (b) Meerwein, H.; Schmidt, R. *Liebigs Ann. Chem.* **1925**, 444, 221.
8. Chuah, G. K.; Jaenicke, S.; Zhu, Y. Z.; Liu, S. H. *Curr. Org. Chem.* **2006**, 10, 1639.
9. Figueras, F. *Top. Catal.* **2004**, 29, 189.
10. Campbell, E. J.; Zhou, H.; Nguyen, S. T. *Org. Lett.* **2001**, 3, 2391.
11. Ikariya, T.; Blacker, A. J. *Acc. Chem. Res.* **2007**, 40, 1300.
12. (a) Haddad, Y. M. Y.; Henbest, H. B.; Husbands, J.; Mitchell, T. R. B. *Proc. Chem. Soc. London* **1964**, 361. (b) Trochagr, J.; Henbest, H. B. *Chem. Commun.* **1967**, 544.
13. Sasson, Y.; Blum, J. *Tetrahedron Lett.* **1971**, 12, 2167.
14. Chowdhury, R. L.; Backvall, J.-E. *J. Chem. Soc., Chem. Commun.* **1991**, 1063.
15. (a) Bianchi, M.; Matteol, U.; Menchi, G.; Frediani, P.; Pratesi, U.; Piacenti, F.; Botteghi, C. *J. Organomet. Chem.* **1980**, 198, 73. (b) Matteoli, U.; Frediani, P.; Bianchi, M.; Botteghi, C.; Gladiali, S. *J. Mol. Catal.* **1981**, 12, 265.
16. (a) Pugin, B.; Blaser, H.-U. *Top. Catal.* **2010**, 53, 953. (b) Václavík, J.; Sot, P.; Vilhanova, B.; Pechacek, J.; Kuzma, M.; Kacer, P. *Molecules* **2013**, 18, 6804.
17. (a) Kitamura, M.; Tokunaga, M.; Noyori, R. *J. Am. Chem. Soc.* **1995**, 117, 2931. (b) Fujii, A.; Hashiguchi, S.; Uematsu, N.; Ikariya, T.; Noyori, R. *J. Am. Chem. Soc.* **1996**, 118, 2521. (c) Noyori, R. *Angew. Chem., Int. Ed.* **2002**, 41, 2008.
18. (a) Ofele, K. *J. Organomet. Chem.* **1968**, 12, 42. (b) Wanzlick, H.-W.; Schonherr, H.-J. *Angew. Chem., Int. Ed. Engl.* **1968**, 7, 141.
19. (a) Lappert, M. F. *J. Organomet. Chem.* **1975**, 100, 139. (b) Lappert, M. F. *J. Organomet. Chem.* **1988**, 358, 185.

20. Arduengo, A. J.; Harlow, L. R.; Kline, M. J. *Am. Chem. Soc.* **1991**, *113*, 361.
21. Wu, X.; Xiao, J. *Chem. Commun.* **2007**, 2449.
22. Peris, E.; Crabtree, R. H. *Coord. Chem. Rev.* **2004**, *248*, 2239.
23. Adrian, B. C.; Paul J. D. *Organometallics* **2007**, *26*, 4357.
24. Haack, K.-J.; Hashiguchi, S.; Fujii, A.; Ikariya, T.; Noyori, R. *Angew. Chem., Int. Ed. Engl.* **1997**, *36*, 285.
25. Hillier, A. C.; Lee, H. M.; Stevens, E. D.; Nolan, S. P. *Organometallics* **2001**, *20*, 4246.
26. da Costa, A. P.; Viciano, M.; Sanau, M.; Merino, S.; Tejada, J.; Peris, E.; Royo, B. *Organometallics* **2008**, *27*, 1305.
27. Hahn, F. E.; Holtgrewe, C.; Pape, T.; Martin, M.; Sola, E.; Oro, L. A. *Organometallics* **2005**, *24*, 2203.
28. Gnanamgari, D.; Moores, A.; Rajaseelan, E.; Crabtree, R. H. *Organometallics* **2007**, *26*, 1226.
29. Gulcemal, S.; Gökçeb, A. G.; Çetinkaya, B. *Dalton Trans.* **2013**, *42*, 7305.
30. Yasar, S.; Cavell, K. J.; Ward, B. D.; Kariuki, B. *Appl. Organomet. Chem.* **2011**, *25*, 374.
31. (a) Aydemir, M.; Baysal, A.; Turgut, Y. *Appl. Organomet. Chem.* **2011**, *25*, 270. (b) Betanzos-Lara, S.; Liu, Z.; Habtemariam, A.; Pizarro, A. M.; Qamar, B.; Sadler, P. J. *Angew. Chem. Int. Ed.* **2012**, *51*, 3897. (c) Talwar, D.; Li, H. Y.; Durham, E.; Xiao, J. *Chem.-Eur. J.* **2015**, *21*, 5370.
32. (a) Turkmen, H.; Pape, T.; Hahn, F. E.; Cetinkaya, B. *Eur. J. Inorg. Chem.* **2008**, 5418. (b) Jokic, N. B.; Zhang-Prese, M.; Goh, S. L. M.; Straubinger, C. S.; Bechlars, B.; Herrmann, W. A.; Kühn, F. E. *J. Organomet. Chem.* **2011**, *696*, 3900. (c) Cross, W. B.; Daly, C. G.; Boutadla, Y.; Singh, K. *Dalton Trans.* **2011**, *40*, 9722.

33. (a) Akıncı, P. A.; Gülcemal, S.; Kazheva, O. N.; Alexandrov, G. G.; Dyachenko, O. A.; Cetinkaya, E.; Cetinkaya, B. *J. Organomet. Chem.* **2014**, 765, 23. (b) Gulcemal, S. *Appl. Organometal. Chem.* **2012**, 26, 246.
34. Gierz, V.; Urbanaite, A.; Seyboldt, A.; Kunz, D. *Organometallics* **2012**, 31, 7532.
35. Sluijter, S. N.; Elsevier, C. J. *Organometallics* **2014**, 33, 6389.
36. (a) Timmis, F.; Adolfsson, H. *Org. Biomol. Chem.* **2010**, 8, 4536. (b) Saleem, F.; Rao, G. K.; Kumar, A.; Mukherjee, G.; Singh, A. K. *Organometallics* **2014**, 33, 2341.
37. (a) Nordin, M.; Liao, R.-Z.; Ahlford, K.; Adolfsson, H.; Himo, F. *ChemCatChem* **2012**, 4, 1095. (b) Ok, F.; Aydemir, M.; Durap, F.; Baysal, A. *Appl. Organomet. Chem.* **2014**, 28, 38. (c) Nova, A.; Taylor, D. J.; Blacker, A. J.; Duckett, S. B.; Perutz, R.N.; Eisenstein, O. *Organometallics* **2014**, 33, 3433. (d) Prakash, O.; Sharma, K. N.; Joshi, H.; Gupta, P. L.; Singh, A. K. *Organometallics* **2014**, 33, 2535. (e) Echeverria, P.-G.; Ferard, C.; Phansavath, P.; Ratovelomanana-Vidal, V. *Catal. Commun.* **2015**, 62, 95.
38. (a) Li, J.; Li, X.; Ma, Y.; Wu, J.; Wang, F.; Xiang, J.; Zhu, J.; Wang, Q.; Deng, J. *RSC Adv.* **2013**, 3, 1825. (b) Kang, G.; Lin, S.; Shiwakoti, A.; Ni, B. *Catal. Commun.* **2014**, 57, 111.
39. Li, J.; Tang, Y.; Wang, Q.; Li, X.; Cun, L.; Zhang, X.; Zhu, J.; Li, L.; Deng, J. *J. Am. Chem. Soc.* **2012**, 134, 18522.
40. (a) Monney, A.; Venkatachalam, G.; Albrecht, M. *Dalton Trans.* **2011**, 40, 2716. (b) Yasar, S.; Cekirdek, S.; Ozdemir, I. *J. Coord. Chem.* **2014**, 67, 1236. (c) Wdowik, T.; Samojłowicz, C.; Jawiczuk, M.; Malinska, M.; Wozniak, K.; Grela, K. *Chem. Commun.* **2013**, 49, 674. (d) Yigit, B.; Yigit, M.; Ozdemir, I.; Çetinkaya, E. *Transition Met. Chem.* **2012**, 37, 297. (e) Witt, J.; Pothig, A.; Kuhn, F. E.; Baratta, W. *Organometallics* **2013**,

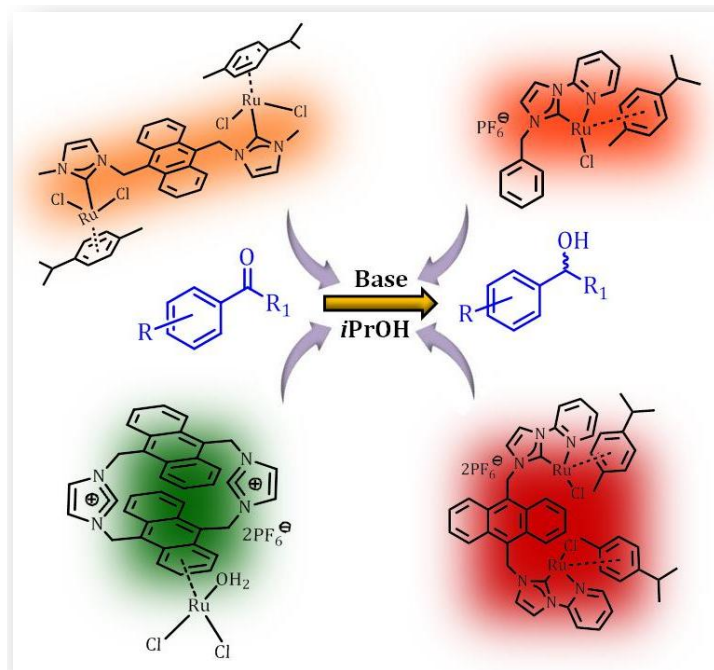
- 32,4042. (e) Aktas, A.; Gok, Y. *Catal. Lett.* **2015**, *145*, 631. (f) Zielinski, G. K.; Samojlowicz, C.; Wdowik, T.; Grela, K. *Org. Biomol. Chem.* **2015**, *13*, 2684.
41. (a) Cheung, F. K.; Clarke, A. J.; Clarkson, G. J.; Fox, D. J.; Graham, M. A.; Lin, C.; Criville, A. L.; Wills, M. *Dalton Trans.* **2010**, *39*, 1395. (b) Ji, Y.; Xue, P.; Ma, D. D.; Li, X. Q.; Gu, P.; Li, R. *Tetrahedron Lett.* **2015**, *56*, 192. (c) Soni, R.; Jolley, K. E.; Clarkson, G. J.; Wills, M. *Org. Lett.* **2013**, *15*, 5110. (d) Soni, R.; Collinson, J.-M.; Clarkson, G. C.; Wills, M. *Org. Lett.* **2011**, *13*, 4304. (e) Su, Y.; Tu, Y.-Q.; Gu, P. *Org. Lett.* **2014**, *16*, 4204.
42. (a) Touge, T.; Hakamata, T.; Nara, H.; Kobayashi, T.; Sayo, N.; Saito, T.; Kayaki, Y.; Ikariya, T. *J. Am. Chem. Soc.* **2011**, *133*, 14960. (b) Parekh, V.; Ramsden, J. A.; Wills, M. *Catal. Sci. Technol.* **2012**, *2*, 406.
43. Kisic, A.; Stephan, M.; Mohar, B. *Org. Lett.* **2013**, *15*, 1614.
44. (a) Li, X.-W.; Wang, G.-F.; Chen, F.; Li, Y.-Z.; Chen, X.-T.; Xue, Z.-L. *Inorg. Chim. Acta* **2011**, *378*, 280. (b) Fernandez, F. E.; Puerta, M. C.; Valerga, P. *Organometallics* **2011**, *30*, 5793. (c) Fernandez, F. E.; Puerta, M. C.; Valerga, P. *Organometallics* **2012**, *31*, 6868.
45. (a) Horn, S.; Albrecht, M. *Chem. Commun.* **2011**, *47*, 8802. (b) Ogweno, A. O.; Ojwach, S. O.; Akerman, M. P. *Dalton Trans.* **2014**, *43*, 1228. (c) Li, K.; Niu, J.-L.; Yang, M.-Z.; Li, Z.; Wu, L.-Y.; Hao, X.-Q.; Song, M.-P. *Organometallics* **2015**, *34*, 1170. (d) Ye, W.; Zhao, M.; Yu, Z. *Chem.-Eur. J.* **2012**, *18*, 10843. (e) Menendez-Pedregal, E.; Vaquero, M.; Lastra, E.; Gamasa, P.; Pizzano, A. *Chem.-Eur. J.* **2015**, *21*, 549.
46. (a) Moore, C. M.; Szymczak, N. K. *Chem. Commun.* **2013**, *49*, 400. (b) Manzini, S.; Fernandez-Salas, J. A.; Nolan, S. P. *Acc. Chem. Res.* **2014**, *47*, 3089.



47. (a) Carrion, M. C.; Ruiz-Castaneda, M.; Espino, G.; Aliende, C.; Santos, L.; Rodríguez, A. M.; Manzano, B. R.; Jalon, F. A.; Lledos, A. *ACS Catal.* **2014**, *4*, 1040. (b) Mercan, D.; Cetinkaya, E.; Sahin, E. *Inorg. Chim. Acta* **2013**, *400*, 74. (c) Dayan, S.; Kayacı, N.; Kalaycioglu, N. O.; Dayan, O.; Oztürk, E. C. *Inorg. Chim. Acta* **2013**, *401*, 107. (d) Gök, L.; Türkmen, H. *Tetrahedron* **2013**, *69*, 10669. (e) Volbeda, J.; Jones, P. G.; Tamm, M. *Inorg. Chim. Acta* **2014**, *422*, 158.
48. (a) Zhang, B.; Wang, H.; Lin, G.-Q.; Xu, M.-H. *Eur. J. Org. Chem.* **2011**, 4205. (b) Soni, R.; Cheung, F. K.; Clarkson, G. C.; Martins, J. E. D.; Graham, M. A.; Wills, M. *Org. Biomol. Chem.* **2011**, *9*, 3290. (c) Lu, C.; Luo, Z.; Huang, L.; Li, X. *Tetrahedron: Asymmetry* **2011**, *22*, 722. (d) Zhou, X.; Wu, X.; Yan, G. B.; Xiao, J. *J. Mol. Catal. A: Chem.* **2012**, *357*, 133. (e) Dayan, S.; Kalaycioglu, N. O.; Daran, J. C.; Labande, A.; Poli, R. *Eur. J. Inorg. Chem.* **2013**, 3224.
49. (a) Kayan, C.; Meriç, N.; Aydemir, M.; Ocağ, Y. S.; Baysal, A.; Temel, H. *Appl. Organomet. Chem.* **2014**, *28*, 127. (b) Facchetti, G.; Gandolfi, R.; Fusè, M.; Zerla, D.; Cesarotti, E.; Pellizzoni, M.; Irimoldi, M. *New J. Chem.* **2015**, *39*, 3792.
50. (a) Fu, Q.; Zhang, L.; Yi, T.; Zou, M.; Wang, X.; Fu, H.; Li, R.; Chen, H. *Inorg. Chem. Commun.* **2013**, *38*, 28. (b) Aydemir, M.; Durap, F.; Baysal, A.; Meric, N.; Buldag, G.; Gumgum, B.; Ozkar, S.; Yıldırım, L. T. *J. Mol. Catal. A: Chem.* **2010**, *326*, 75. (c) Raja, N.; Ramesh, R. *Tetrahedron Lett.* **2012**, *53*, 4770. (d) Meric, N.; Durap, F.; Aydemir, M.; Baysal, A. *Appl. Organomet. Chem.* **2014**, *28*, 803.
51. (a) Lehn, J.-M.; *Angew. Chem. Int. Ed.* **1988**, *27*, 89. (b) Martinez-Manez, R.; Sancenon, F. *Coord. Chem. Rev.* **2006**, *250*, 3081.

52. Martínez-Mañez, R.; Sancenón, F.; Hecht, M.; Biyical, M.; Rurack, K. *Anal. Bioanal. Chem.* **2011**, *399*, 55.
53. (a) Constable, E. C.; Martinez-Manez, R.; Cargill Thompson, A. M. W.; Walker, J. V. J. *J. Chem. Soc., Dalton Trans.* **1994**, 1585. (b) Métivier, R.; Leray, I.; Valeur, B. *Chem.—Eur. J.* **2004**, *10*, 4480
54. (a) Badugu, R.; Lakowicz, J. R.; Geddes, C. D. *J. Am. Chem. Soc.* **2005**, *127*, 3635. (b) Agou, T.; Sekine, M.; Kobayashi, J.; Kawashima, T. *Chem. Eur. J.* **2009**, *15*, 5056. (c) Zelder, F. H. *Inorg. Chem.* **2008**, *47*, 1264. (d) Yang, Y.; Zhao, Q.; Feng, W.; Li, F. *Chem. Rev.* **2013**, *113*, 192.
55. (a) Fabbrizzi, L.; Licchelli, M.; Mancin, F.; Pizzeghello, M.; Rabaioli, G.; Taglietti, A.; Tecilla, P.; Tonellato, U. *Chem.-Eur. J.* **2002**, *8*, 94. (b) Jyothish, K.; Avirah, R. R.; Ramaiah, D. *Org. Lett.* **2006**, *8*, 111. (c) de Silva, A. P.; Uchiyama, S. *Nat. Nanotechnol.* **2007**, *2*, 399.
56. (a) Santos-Figueroa, L. E.; Moragues, M. E.; Climent, E.; Agostini, A.; Martinez-Manez, R.; Sancenon, F. *Chem. Soc. Rev.* **2013**, *42*, 3489. (b) Kuruvila, E.; Joseph, J.; Ramaiah, D. *J. Phys. Chem. B* **2005**, *109*, 21997.
57. Zeng, Q.; Cai, P.; Li, Z.; Qina, J.; Tang, B. Z. *Chem. Commun.* **2008**, 1094.
58. Nair, A. K.; Neelakandan, P. P.; Ramaiah, D. *Chem. Commun.* **2009**, 6352.
59. Hajizadeh, S.; Farhadi, K.; Forough, M.; Sabzi, R. E. *Anal. Methods* **2011**, *3*, 2599.
60. Ji, S.; Guo, H.; Yuan, X.; Li, X.; Ding, H.; Gao, P.; Zhao, C.; Wu, W.; Wu, W.; Zhao, J. *Org. Lett.* **2010**, *12*, 2876.
61. Divya, K. P.; Sreejith, S.; Balakrishna, B.; Jayamurthy, P.; Anees, P.; Ajayaghosh, A. *Chem. Commun.* **2010**, *46*, 6069.

62. Bejoymohandas, K. S.; Kumar, A.; Sreenadh, S.; Varathan, E.; Varughese, S.; Subramanian, V.; Reddy, M. L. P. *Inorg. Chem.* **2016**, *55*, 3448.
63. Ajayakumar, G.; Sreenath K.; Gopidas, K. R. *Dalton Trans.* **2009**, 1180.
64. Katherine, H. T.; Chris, O. *Science*, **2003**, *300*, 936.
65. Helen T. C.; Kim R. D. *Acc. Chem. Res.* **2005**, *38*, 146.
66. Christiana, X. Z.; Lippard, S. J. *Current Opinion in Chemical Biology* **2003**, *7*, 481.
67. Michael J. C.; Fuchun, Z.; Dominic R. F. *Chem. Rev.* **1999**, *99*, 2511.
68. Jakupec, M. A.; Galanski, M.; Arion, Vladimir, B.; Hartinger, C. G.; Keppler, B. K. *Dalton Trans.* **2008**, 183.
69. Kilpin, K. J.; Clavel, C.M.; Edafe, F.; Dyson, P. J. *Organometallics* **2012**, *31*, 7031.
70. Basu, U.; Khan, I.; Hussain, A.; Gole, B.; Kondaiah, P.; Chakravarty, A. R. *Inorg. Chem.* **2014**, *53*, 2152.
71. Gonzalez-Alvarez, M.; Pascual-Alvarez, A.; Agudo, L. C.; Castineiras, A.; Liu-Gonzalez, M.; Borrassa, J.; Alzuet-Pina, G. *Dalton Trans.* **2013**, *42*, 10244.
72. Liu, Z.; Romero-Canelon, I.; Habtemariam, A.; Clarkson, G. J.; Sadler, P. J. *Organometallics* **2014**, *33*, 5324.

**DESIGN OF RUTHENIUM(II) COMPLEXES: INVESTIGATION OF THEIR PHOTOPHYSICAL AND CATALYTIC PROPERTIES****2.1. Abstract**

We designed and synthesized a series of novel neutral and cationic ruthenium complexes **1-8** and have investigated their photophysical and catalytic properties under different conditions. These systems have been synthesized in good yields and were characterized on the basis of analytical and spectral evidences. In addition, the structure of the representative examples, such as complexes **3-6** were characterized through single crystal X-ray analysis. These derivatives showed absorption in the range 300-400

nm, along with bathochromic shifted metal to ligand charge transfer transition in the range 400-650 nm. Among these systems, the complexes **1** and **2** showed emission in the range 380-700 nm and exhibited the fluorescence quantum yields ( $\phi_F$ ) of *ca.* 0.03 and 0.39, respectively. The electrochemical properties of the derivatives have been determined and which confirmed the presence of ruthenium in these complexes.

The efficacy of these complexes as catalysts for transfer hydrogenation reaction was evaluated under different conditions. Of these, the ruthenium- $\pi$  complexes, **1** and **2** were found to act as catalysts for the conversion of the aromatic ketones to their corresponding alcohols with 2 mol% catalyst in 2 mL isopropanol at 5 h of reaction time. On the other hand, the neutral ruthenium-*NHC* complexes **3** and **4** showed catalytic efficiency of *ca.* 100% within 2 h of reaction under similar conditions. The increased catalytic activity of the complexes **3** and **4** when compared to **1** and **2** can be attributed to the stability of the complex through strong sigma binding affinity of *N*-heterocyclic carbene (*NHC*) ligand. Excellent reaction yields were achieved with the cationic ruthenium-*NHC* complexes **5-8**. These systems required just 1 h and the catalyst loading of only *ca.* 0.5 mol% to achieve the similar results. The electronic effects and generality of reaction were also tested by using both electron rich and deficient aromatic ketones. In comparison to the ruthenium- $\pi$ , neutral and the cationic ruthenium complexes showed better catalytic activity, this can be attributed to the strong binding of both *NHC* and pyridine substituents to the metal centre. These complexes are found to be stable to air and moisture and showed excellent catalytic activity at a low catalyst loading conditions, thereby demonstrating their use as efficient catalysts for the transfer hydrogenation reaction of the aromatic ketones.

## 2.2. Introduction

During the past decade, the development of ligands bearing donors other than phosphorus has been an active area of interest in homogeneous catalysis, and organic synthesis. The metal complexes containing nitrogen donor ligands attracted much interest among the various coordinating ligands and are found to be excellent catalysts for various reduction reactions.<sup>1,2</sup> Of the various ligands reported, N-heterocyclic carbenes (*NHCs*) have emerged as a flexible class, when compared to phosphorous containing ligands.<sup>3</sup> Furthermore, *NHCs* bearing transition metal complexes have been well studied for their use as catalysts in C=O, C=C and C=N reduction reactions and also in olefin metathesis.<sup>4,6</sup> Of the reported examples, the metal complexes based on iridium, rhodium, and ruthenium complexes having *NHC* ligands have been found to be excellent pre-catalysts for important reduction reactions such as hydrogenation, transfer hydrogenation (TH), and hydrosilylation.<sup>7,8</sup> Among these examples, the ruthenium complexes bearing *NHCs* have exhibited high catalytic efficacy for the reduction of ketones, aldehydes, imines, nitro aromatics, alkenes, and carbon dioxide.<sup>9,10</sup>

Of the various reduction reactions, the transfer hydrogenation is preferred in the large-scale industry due to the advantages such as the reduced waste generation and energy consumption, and it was found to be an alternative to the classical hydrogenation processes using molecular hydrogen.<sup>11</sup> Recently, Caramori and coworkers have reported a detailed theoretical study on cation- $\pi$  interactions in ruthenophane type of systems.<sup>12</sup> These computational insights provided a new strategy for the development of simple and efficient metal complexes for various applications. Noyori and Baratta and co-

workers have developed Ru(II) and Os(II) complexes as efficient catalysts for the transfer hydrogenation of ketones and imines.<sup>13,14</sup> Though a good number of examples of the metal-NHC-complexes have been reported for the transfer hydrogenation reactions,<sup>15</sup> the development of new catalysts with high stability is quite challenging in recent years. In this context, we have synthesized and unambiguously characterized a

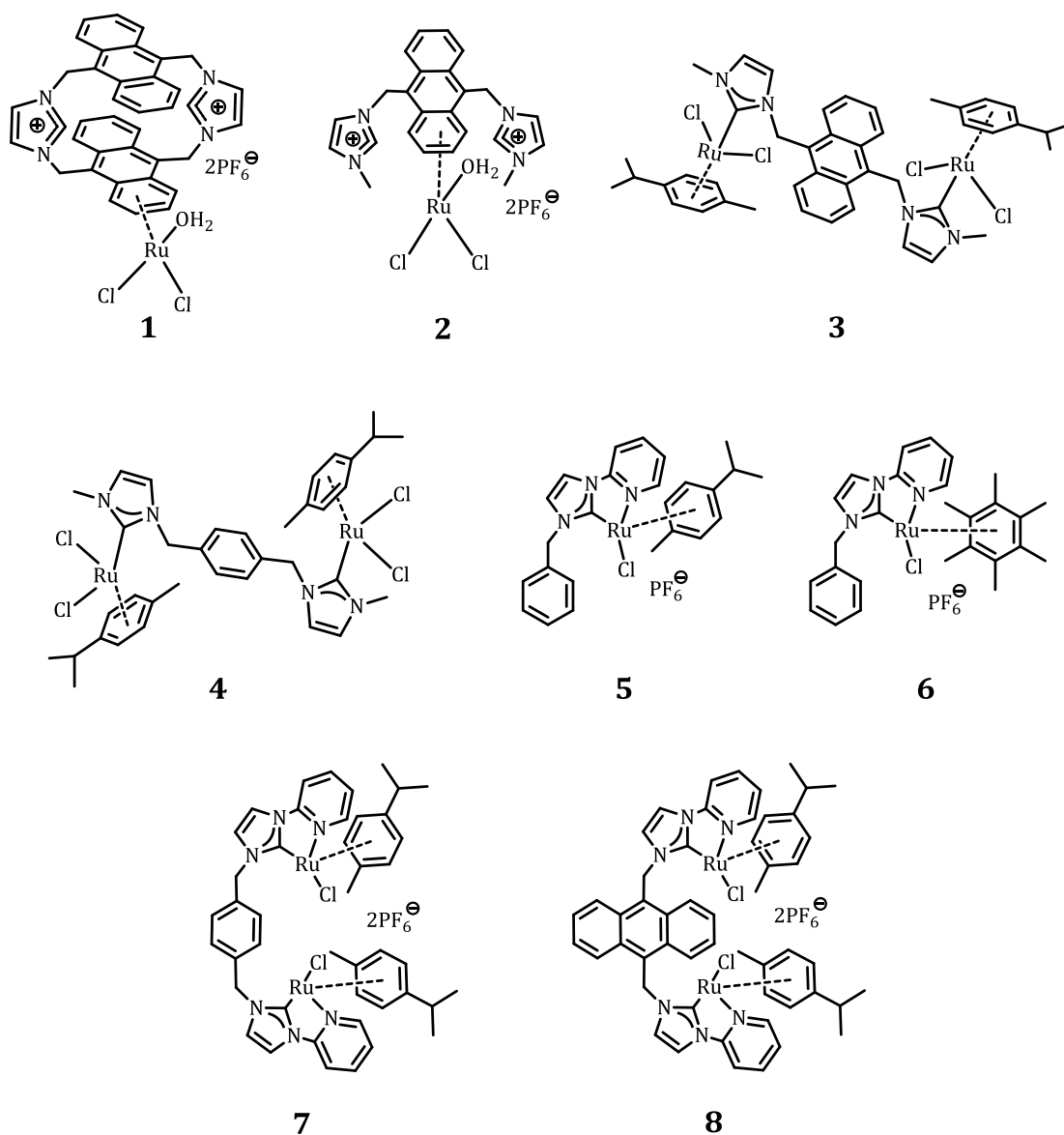


**Chart 2.1.** Structures of the complexes 1-8 under investigation.

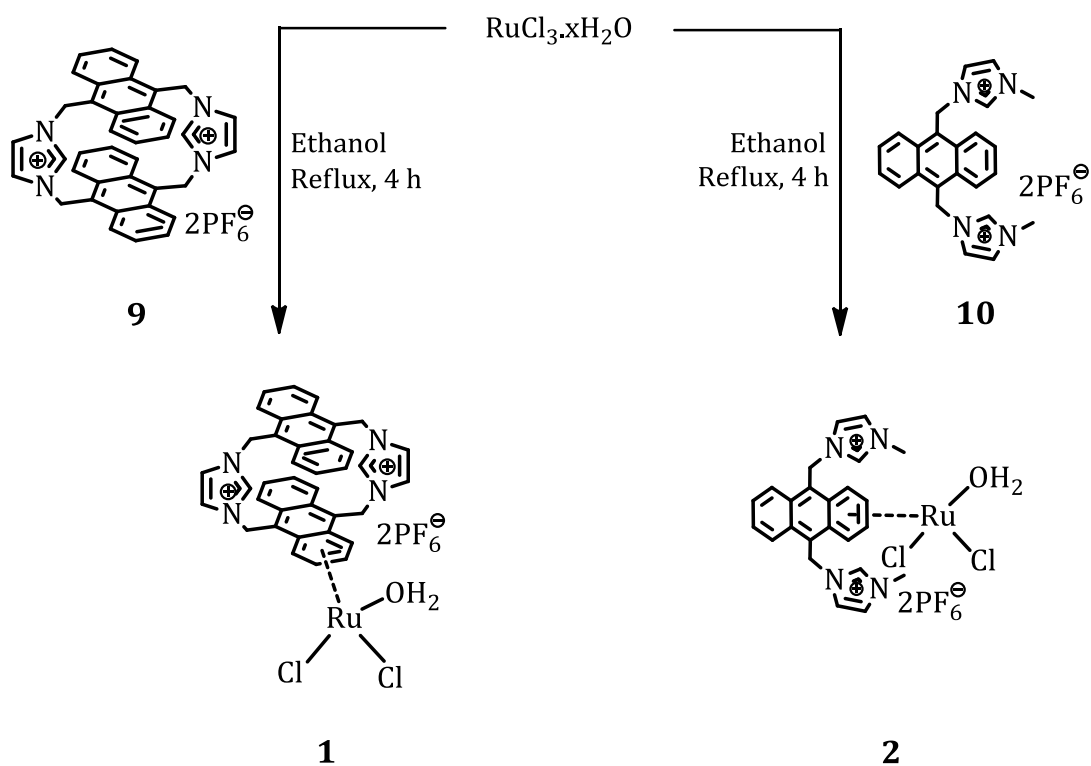
series of novel ruthenium(II) complexes **1-8** (Chart 2.1), and have and investigated their photophysical and electrochemical properties. Uniquely, these complexes exhibited significantly increased air and moisture stability and also showed their use as robust catalysts for the transfer hydrogenation reactions of various aromatic ketones, substituted with electron donor and acceptor functional groups. Our results indicate that, the stability as well as catalytic efficacy of the complexes can be successfully tuned by modifying the ligand scaffold.

## 2.3. Results and Discussion

### 2.3.1. Synthesis and Characterization of the Complexes

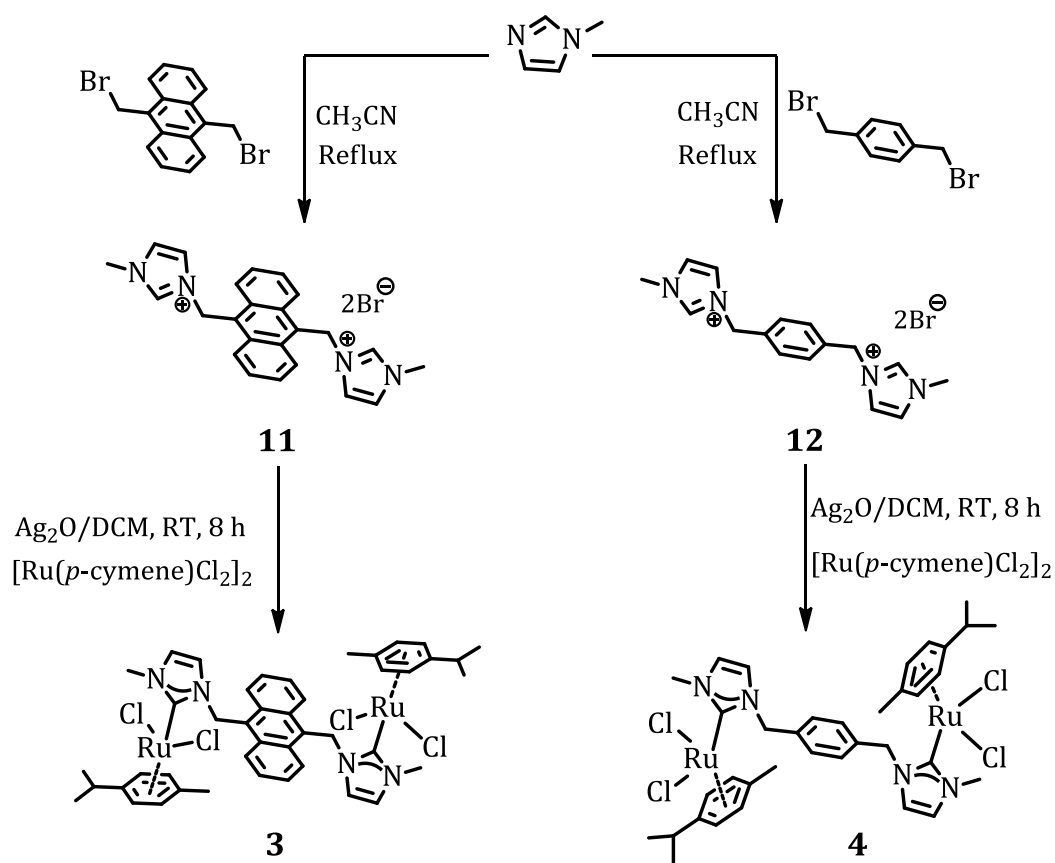
The synthetic strategy adopted for the preparation of the ruthenium complexes **1-8** is shown in Schemes 2.1-2.3. The synthesis of the anthracene substituted ligands **9** and **10** was achieved through the modified literature reported procedure.<sup>16</sup> As shown in Scheme 2.1, the reductive complexation of the ligands **9** and **10** with  $\text{RuCl}_3 \cdot x\text{H}_2\text{O}$  gave the ruthenium- $\pi$  complexes **1** and **2**, respectively, in quantitative yields. Both the ligands **9** and **10** and their metal ion complexes **1** and **2** were characterized by various spectral and analytical evidences. The ligands **11** and **12**, substituted with anthracene and phenyl moieties were prepared as per the reported procedure.<sup>16,17</sup> Subsequent reaction of **11** and **12** with  $\text{Ag}_2\text{O}$  followed by complexation with  $[\text{Ru}(n^6\text{-}p\text{-cymene})\text{Cl}_2]_2$  in dichloromethane resulted in the synthesis of new dinuclear ruthenium complexes **3** and **4** in *ca.* 39 and 40% yields, respectively (Scheme 2.2). The cationic complexes **5-8**, on the other hand, were synthesised in a three-step route starting from the imidazole





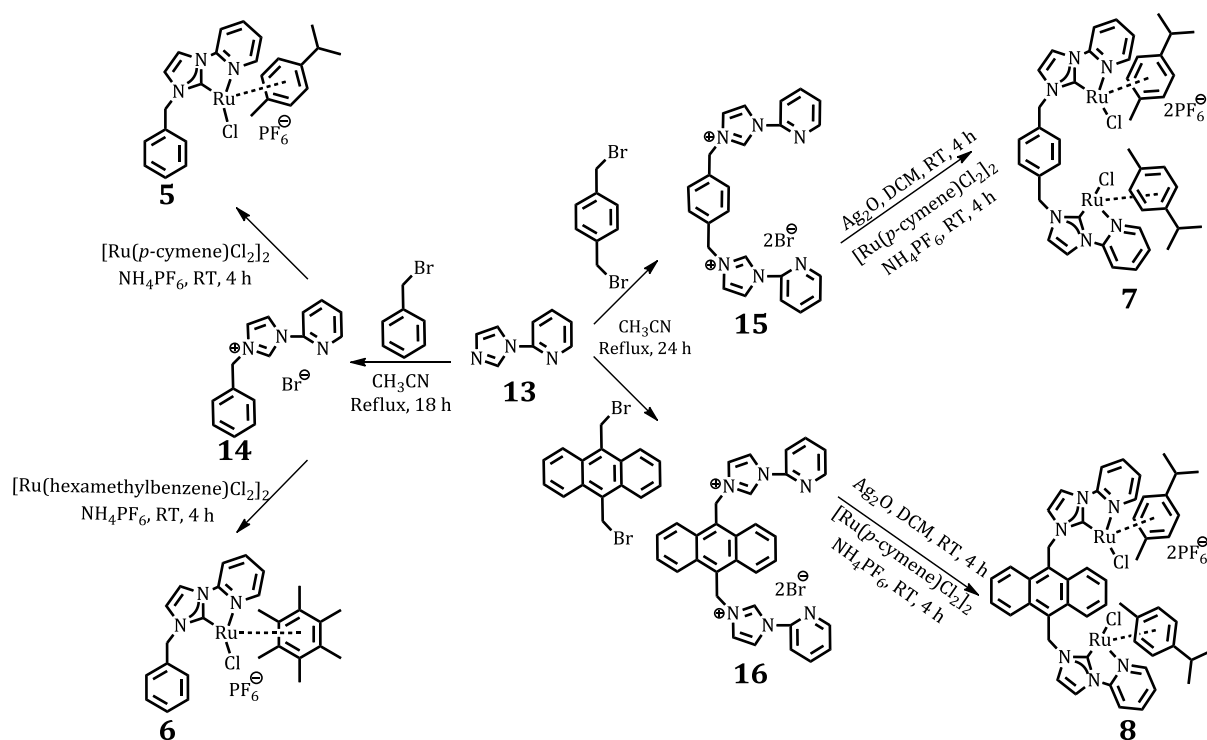
**Scheme 2.1.** Synthesis of the complexes **1** and **2**.

derivative<sup>18</sup> **13** as shown in Scheme 2.3. In the first step, the synthesis of the imidazolium salts **14**, **15** and **16** was achieved by the reaction of 2-(1H-imidazol-1-yl)pyridine with the corresponding aryl halide in acetonitrile. Subsequently, the complexes **5-8** were synthesized by the deprotonation of the ligands with  $\text{Ag}_2\text{O}$  followed by the complexation with ruthenium precursors, such as  $[\text{Ru}(n^6\text{-}p\text{-cymene})\text{Cl}_2]_2$  and  $[\text{Ru}(\text{hexamethylbenzene})\text{Cl}_2]_2$  at 25 °C in  $\text{CH}_2\text{Cl}_2$ . The divalent complexes **5-8** were isolated in moderate yields as their hexafluorophosphate salts after treatment with ammonium hexafluorophosphate and were recrystallized from a mixture (9:1) methanol and chloroform. All the ligands and metal complexes were characterized on the basis of



**Scheme 2.2.** Synthesis of the complexes **3** and **4**.

analytical and spectral evidence. In addition, the structures of representative complexes **3-6** have been unambiguously established through single crystal X-ray analysis. For example, the conversion of ligands to metal complexes was characterized by  $^1\text{H}$  and  $^{13}\text{C}$  NMR spectroscopy. There was a broadening in the  $^1\text{H}$  NMR signals when cyclophanes are converted in to its ruthenophane complexes. The complex **1** showed complete broadening in the aromatic protons, whereas the complex **2** showed significant shift in the imidazolium protons along with the broad aromatic protons. The singlet at  $\delta$  8.87



**Scheme 2.3.** Synthesis of the complexes 5-8.

ppm and 9.26 ppm corresponding to the imidazolium proton in **11** and **12** was disappeared upon the formation of complexes **3** and **4**, and also by the appearance of a new signal due to the C<sub>2</sub> (carbene carbon) of the imidazol-2-ylidene units at  $\delta$  173.16 and 173.97 ppm, respectively in the <sup>13</sup>C NMR spectrum. The azolium precursors were characterized with much downfield signal for the strongly deshielded C<sub>2</sub> proton of imidazolium moiety, which appeared at  $\delta$  9.37, 10.32 and 10.08 ppm for **14**, **15** and **16**, respectively. The ruthenium complexes were characterized by the disappearance of carbenic proton followed by a downfield shift in the carbenic carbon atoms to  $\delta$  186.14, 190.56, 186.22 and 185.88 ppm respectively, for the complexes **5-8**.

To understand the elemental composition of complexes **1** and **2**, we have carried out EDX analysis, where both the complexes showed characteristic peaks corresponds to ruthenium ion<sup>19</sup> which furthermore confirmed the presence of the metal ion in these systems (Figure 2.1). Furthermore, the complexation of the ligands **9** and **10** with metal ion was also confirmed through MALDI-TOF mass spectrometry analysis. We observed a peak at  $m/z$  731.92 ( $M^+ - 2PF_6^-$ ) for the complex **1** while  $m/z$  558.39 ( $M^+ - 2PF_6^-$ ) was observed for the complex **2**, in the mass spectrum, which confirmed the formation of 1:1 complexes between the ligands and metal ion.

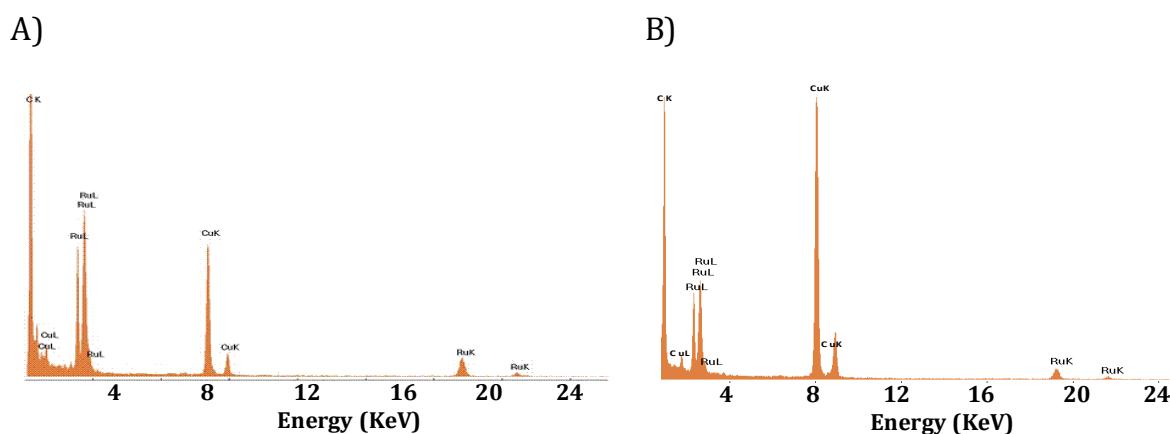


**Figure 2.1.** EDX spectra of A) complex **1** and B) complex **2**.

We have furthermore carried out the powder X-ray diffraction data analysis of the complexes **1** and **2**. The recorded patterns for the complexes **1** and **2** were clearly distinct from those obtained for the ligand molecules. This allowed a quick confirmation of the presence of the ruthenium metal ion in the complexes. Even though the overall pattern reveals low crystallinity, we could observe few broad reflections characteristic to those of the ruthenium ion, centered at 5.9, 9.5, 11.3, 12.3, 16.2° for the complex **1**

and few broad reflections centered at 5.7, 9.4, 11.3, 12.3, 17.1° for the complex **2**, respectively, as reported in the literature for the ruthenium based complexes.<sup>20</sup>

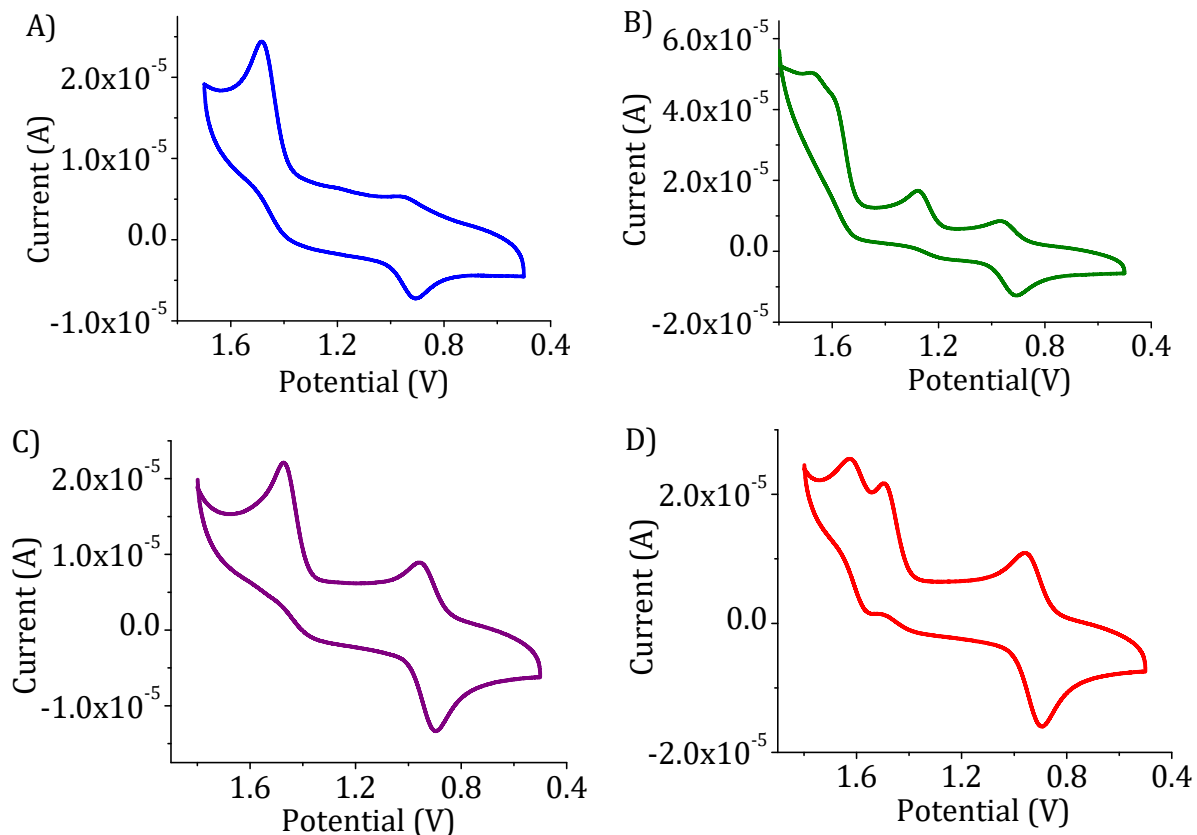


**Figure 2.2.** Cyclic voltammograms of the complexes A) **5** (1 mM), B) **6** (1 mM), C) **7** (1 mM), and D) **8** (1 mM), in acetonitrile at a scan rate of 100 mV/s.

To understand the redox and thermal stability properties, we have carried out cyclic voltammetry, square wave measurements and thermogravimetric analysis (TGA) of the complexes **1-8** under different conditions. The oxidation potentials vs Ag/Ag<sup>+</sup> measured for all complexes, which showed one electron oxidation of the redox couple Ru(II)/Ru(III) as reported in the literature for similar systems.<sup>21</sup> These complexes exhibited quasi-reversible electrochemical wave and the potentials are found to be +1.11, +1.12, +1.13, +1.14, +1.48, +1.28, +1.47, and +1.49 V, respectively (Figure 2.2),

for the complexes **1-8**. In the thermogravimetric analysis of the complexes **1** and **2** we observed three major decomposition phases in the temperature range *ca.* 100-500 °C, with the corresponding weight loss of *ca.* 76% and 70%, respectively. Similarly complexes **3** and **4** showed two step decomposition patterns in the temperature range *ca.* 40-520 °C and 30-425 °C, respectively, with the corresponding weight loss of *ca.* 66 and 59%. The thermograms of the complexes **5-8** in the temperature range of 20-900 °C, showed a weight loss of *ca.* 62, 72, 70, and 85%, respectively. These observations can be attributed to the loss of chloride ions first followed by the decomposition of aromatic moieties present in the complexes.

### 2.3.2. Single Crystal X-ray Analysis of the Complexes 3-6

The structures of complexes **3-6** were unambiguously established by single crystal X-ray structure analysis. The ORTEP views of the complexes with atom numbering scheme are shown in Figures 2.3 and 2.4 and their selected crystallographic data, bond lengths and bond angles are listed in Tables 2.1-2.2. X-ray-quality crystals of complexes **3-6** were grown via slow evaporation of mixture of chloroform and methanol in triclinic and monoclinic fashion. For example, in the case of the complexes (**3** and **4**), Ru(II) atoms were coordinated to all the six carbon atoms of two *p*-cymene rings (C21-C26 in **3**, C10-C15 in **4**), two *NHC* donor atom (C4 in **3** and C1 in **4**) and four chloride ions. Both the complexes have similar structure except in complex **3**, anthracene acts as bridging moiety between two cymene-Ru centers whereas phenyl ring acts as bridging moiety in complex **4**. The coordination geometry around both the Ru(II) centers in complexes was best described as pseudo-octahedral with arene ring having three

coordination sites in a  $\eta^6$ -fashion, carbene and two chloride ions occupying the remaining coordination sites. Both the complexes **3** and **4** showed coordinatively saturated (18e<sup>-</sup>) “three-legged piano-stool” geometry with the  $\pi$ -bonded  $\eta^6$ -arene ring forming the seat and a carbene donor atom of **11/12** and two Cl<sup>-</sup> constituting the legs of the stool with bond angles of C(4)-Ru(1)-Cl(2) (89.46°), Cl(2)-Ru(1)-Cl(3) (83.56°) C(4)-Ru(1)-Cl(3) (88.96°) (for **3**).

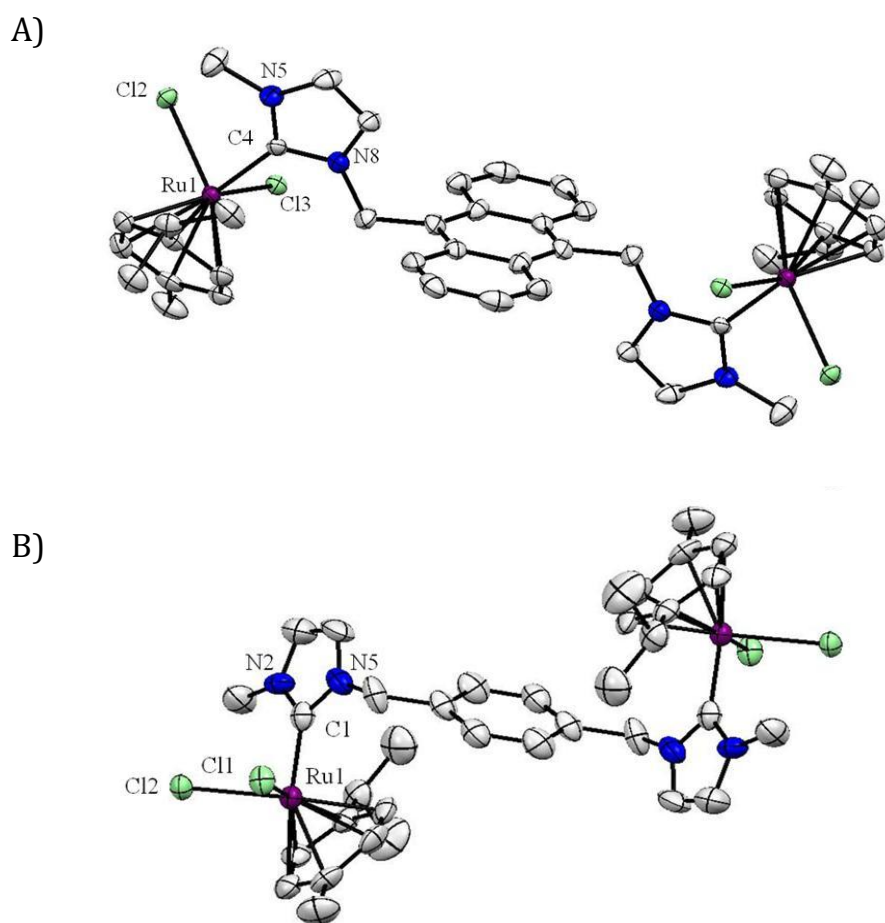


**Figure 2.3.** ORTEP views of the complexes A) **3** and B) **4** at 50% probability level (hydrogen atoms and solvents were removed for clarity).

**Table 2.1.** Crystal data and structure refinement details for the complexes **3-6**.

	Complex <b>3</b>	Complex <b>4</b>	Complex <b>5</b>	Complex <b>6</b>
Crystal system	Triclinic	Monoclinic	Monoclinic	Monoclinic
Space group	<i>P</i> -1	<i>P</i> 21/ <i>c</i>	<i>P</i> 21/ <i>c</i>	<i>C</i> 2/ <i>c</i>
<i>a</i> (Å)	8.201(6)	16.376(11)	13.3979(7)	29.1612(11)
<i>b</i> (Å)	9.946(7)	10.424(7)	10.3168(5)	12.5438(5)
<i>c</i> (Å)	21.325(15)	20.145(10)	19.7429(9)	16.5284(6)
$\alpha$ (°)	81.89(3)	90	90	90
$\gamma$ (°)	87.42(2)	90	90	90
$\beta$ (°)	84.71(2)	127.64(4)	101.468(2)	103.261(2)
<i>V</i> (Å <sup>3</sup> )	1714(2)	2723(3)	2674.45	5884.75
<i>Z</i>	1	2	4	8
Temperature /K	150(2)	150(2)	150(2)	296(2)
$\lambda$ (Å) (Mo- <i>K</i> $\alpha$ )	0.71073	0.71073	0.71073	0.71073
Crystal size (mm)	0.4x0.2x0.1	0.1x0.1x0.1	0.2x0.15x0.1	0.2x0.15x0.1
<i>F</i> (000)	846	1356	1312	2752
Theta range for data collection	3.0-27.4	3.142- 26.347	2.24-28.22	3.001-26.247
Data/restraints/parameters	7351/0/ 354	5531/0/28 1	13667/0/79 9	15656/0/ 1025
GOF on <i>F</i> <sup>2</sup>	1.210	1.226	1.050	0.999
<i>R</i> <sub>1</sub> [ <i>I</i> > 2 $\sigma$ ( <i>I</i> )]	0.1059	0.1477	0.0352	0.0577
w <i>R</i> <sub>2</sub> [ <i>I</i> > 2 $\sigma$ ( <i>I</i> )]	0.2212	0.2229	0.0965	0.1840

The Ru-C (carbene) distances of 2.074(7) Å in **3** and 2.056 Å in **4** were comparable to those in the low-spin Ru(II)-carbene complexes.<sup>22</sup> The *p*-cymene ring in both complexes was almost planar, and ruthenium was displaced by 1.719 Å (Ru-C<sub>arene</sub>) (for **3**) and 1.693 Å (for **4**) from centroid of *p*-cymene ring which was similar to related



Ru(II) arene complexes  $[\text{Ru}(\eta^6\text{-}p\text{-cymene})(\text{en})\text{Cl}](\text{PF}_6)$  (1.669 Å)<sup>23</sup> and  $[\text{Ru}(\eta^6\text{-}p\text{-cymene})\text{Ru}(\text{L}_1)\text{Cl}](\text{PF}_6)$  (1.689 Å).<sup>24</sup> In both the complexes, the coordination of two imidazolyl carbene to Ru(II) centers produces a twisting of imidazolyl moieties and Ru(II) centers adopt a trans position to each other in such a way that each Ru(II) centre was 0.462 Å away from anthracene plane however in case of the complex **4**, Ru(II) centre was 3.297 Å away from the benzene ring.

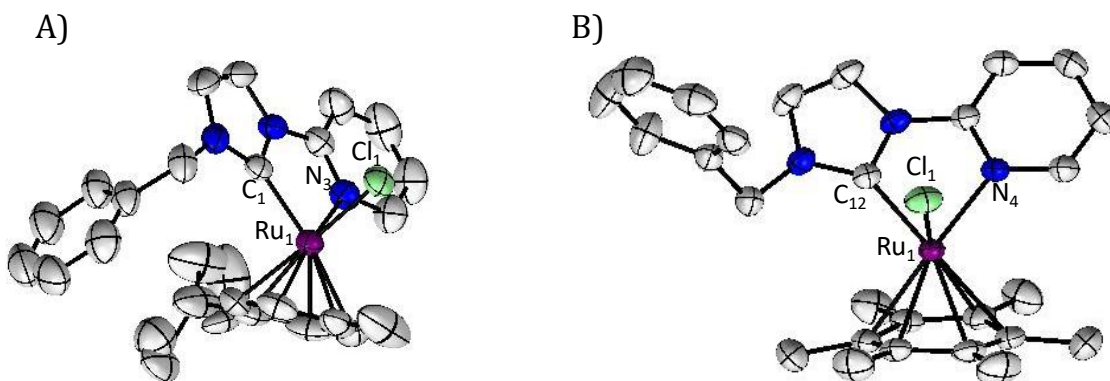


**Figure 2.4.** ORTEP views of the complexes A) **5** and B) **6** at 50% probability level (hydrogen atoms and counter ions were removed for clarity).

Similarly the ruthenium atom in the complexes **5** and **6** was surrounded by the  $\eta^6$ -bonded arene (*p*-cymene ring in the complex **5** and hexamethylbenzene in the complex **6**, respectively), a chelating *NHC* ligand (**14**), the chloride and thus attains a “three legged piano-stool” geometry; which is archetypical of  $[(\eta^6\text{-arene})\text{Ru}(\mathbf{14})\text{Cl}]^+$  half-sandwich arene complexes. The arene ring constitutes a seat, the chloride, pyridine nitrogen ( $\text{N}_{\text{py}}$ ) and carbene ( $\text{C}_{\text{NHC}}$ ), of the *NHC* ligand (**14**), constitute three legs of the piano-stool. In the complexes (**5** and **6**), Ru-Cl and Ru- $\text{N}_{\text{py}}$  bond lengths were

approximately identical 2.4 and 2.1 Å, respectively and analogous to the literature reports.<sup>25</sup>

**Table 2.2.** Selected bond lengths (Å) and bond angles (deg) for the complexes **3-6**.

	Bond Lengths (Å)		Bond Angles (°)	
Complex <b>3</b>	C4-Ru1	2.074(7)	C4-Ru-Cl3	89.0(2)
	Cl2-Ru1	2.457(2)	C4-Ru1-Cl2	89.44(19)
	Cl3-Ru1	2.470(2)	C4-Ru1-Cl3	89.0(2)
	Ru1-C <sub>Ar</sub>	1.719(2)		
Complex <b>4</b>	C1-Ru1	2.056(11)	C1-Ru1-Cl1	90.0(3)
	Cl1-Ru1	2.452(3)	C1-Ru1-Cl2	89.70(3)
	Cl2-Ru1	2.441(2)	Cl2-Ru1-Cl1	83.49(9)
	Ru1-C <sub>Ar</sub>	1.693(2)		
Complex <b>5</b>	C1-Ru1	2.017(3)	Cl1-Ru1-C1	84.11(7)
	N3-Ru1	2.095(2)	N3-Ru1-C1	76.65(11)
	Cl1-Ru1	2.405(7)	Cl1-Ru1-N3	84.14(7)
	Ru1-C <sub>Ar</sub>	1.714(3)		
Complex <b>6</b>	C12-Ru1	2.025(5)	Cl1-Ru1-C12	84.84(14)
	N4-Ru1	2.106(4)	N4-Ru1-C12	76.04(18)
	Cl1-Ru1	2.414(13)	Cl1-Ru1-N4	88.76(12)
	Ru1-C <sub>Ar</sub>	1.740(2)		

The Ru-C<sub>NHC</sub> bond lengths were 2.017 (for the complex **5**) and 2.024 Å (for the complex **6**), typical for Ru-C<sub>NHC</sub> σ-bonds, indicating that the back-donation is negligible for these complexes.<sup>26</sup> In particular, Ru-C<sub>Ar</sub> distances were found to be 1.714(3) (for the complex **5**), 1.740(2) (for the complex **6**), which is comparable to reported literature for

similar “three-leg piano-stool” ruthenium complexes.<sup>27</sup> Bond angles subtended by the ligand forming the legs and the ruthenium atom were deviated from 90° (Cl1-Ru1-C1 = 84.11(7)°, N3-Ru1-C1 = 76.65(11)°, Cl1-Ru1-N3 = 84.14(7)°; for the complex **5** and Cl1-Ru1-C12 = 84.84(14)°, N4-Ru1-C12 = 76.04(18)°, Cl1-Ru1-N4 = 88.76(12)°; for the complex **6**) and attest to a pseudo-octahedral arrangement around ruthenium centre. In both the complexes, ligand (**14**) binds to the ruthenium metal centre via  $C_{NHC}$ , Npy atom forming one five-membered chelate ring with bite angles of C(1)-Ru(1)-N(3): 76.63° (for **5**), which is slightly longer than C(12)-Ru(1)-N(4): 76.05° (for **6**) probably due to the highly sterically demanding situation of the p-cymene ligand. Interestingly, the phenyl arm attached to imidazolyl nitrogen showed flip, when a plane was drawn through *NHC* ligands (**14**), towards the leg of piano-stool geometry in the complex **5**, whereas reverse to the leg of piano-stool geometry was observed for the complex **6**. This flip was probably due to the steric hindrance of hexamethylbenzene ligand.

### 2.3.3. Photophysical Properties of the Complexes

In order to understand the photophysical properties of the complexes, we have recorded the absorption and emission properties of the complexes **1-8** in solution state. The absorption spectra of the ligands and the complexes **1** and **2** in DMSO solution showed characteristics anthracene centered electronic spectral band in the region around 350-400 nm (Figures 2.5 and 2.6). In addition, the complexes **1** and **2** displayed a band at ~ 615 nm ( $\epsilon = 2.42 \times 10^3 \text{ M}^{-1}\text{cm}^{-1}$ ) and ~ 610 nm ( $\epsilon = 0.98 \times 10^3 \text{ M}^{-1}\text{cm}^{-1}$ ) attributed to metal -to- ligand charge transfer (MLCT) transitions, respectively. Both the

ligands and complexes **1** and **2** showed characteristic emission of the anthracene chromophore with *ca.* 70% and 20% quenching in the fluorescence intensity for **1** and **2**, respectively.

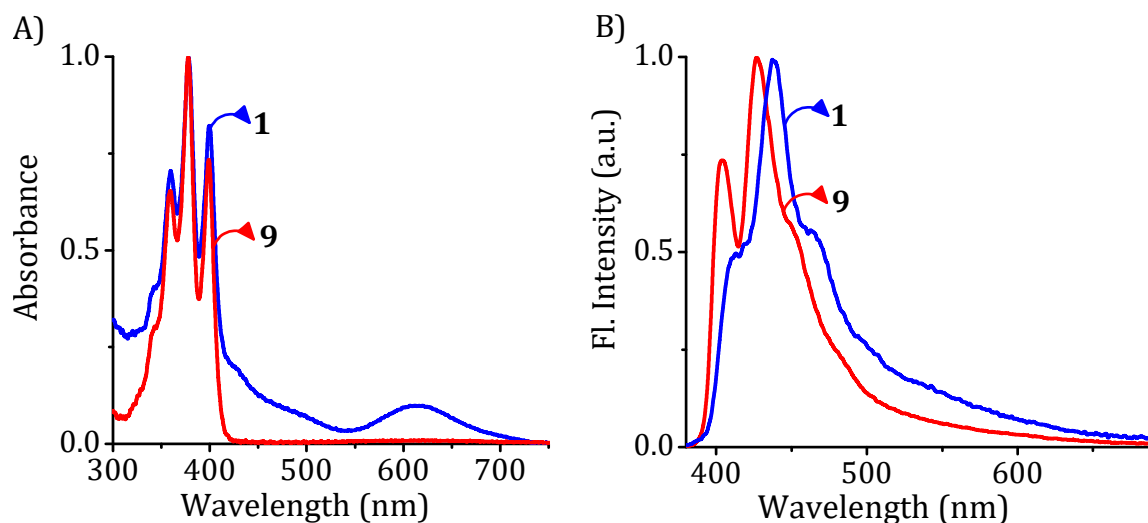


**Figure 2.5.** Normalized A) Absorption and B) emission spectra of the ligand **9** (10  $\mu$ M) and the complex **1** (10  $\mu$ M) in DMSO. Excitation wavelength, 350 nm.

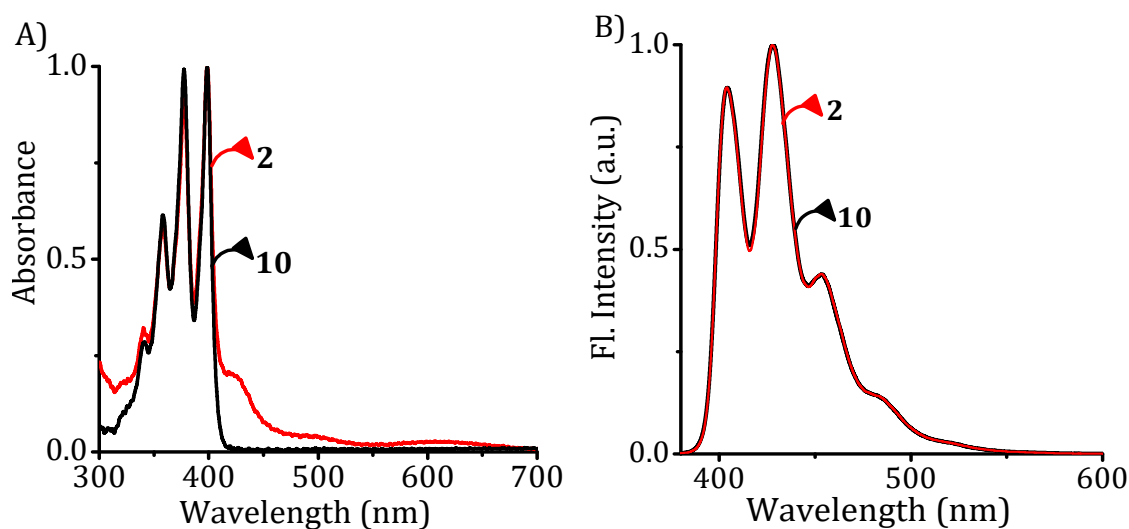


**Figure 2.6.** Normalized A) Absorption and B) emission spectra of the ligand **10** (10  $\mu$ M) and the complex **2** (10  $\mu$ M) in DMSO. Excitation wavelength, 365 nm.

The fluorescence lifetime of the complexes **1** and **2** were subsequently analyzed through picosecond time-resolved fluorescence analysis. The complex **1** showed a double exponential decay with a lifetime of *ca.* 9.3 ns (6%) and *ca.* 28.9 ns (94%), whereas the complex **2** exhibited a mono exponential decay with a lifetime of *ca.* 9.3 ns (100%). The ruthenium-*NHC* complexes **3-8** also showed structured absorption in the region of 250-400 nm along with broad absorptions extending up to 500 nm (Figure 2.7). The structured absorption arises from the  $\pi$ - $\pi^*$  transition of the anthracene and phenyl moiety, whereas the broad absorptions can be attributed to the metal-to-ligand charge transitions (MLCT). All the complexes were found to be non-fluorescent in nature.

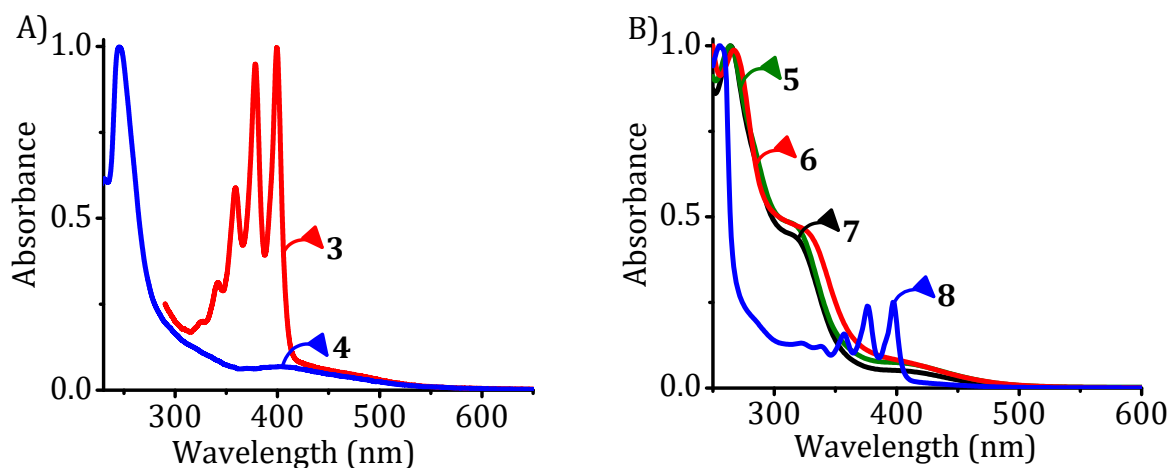


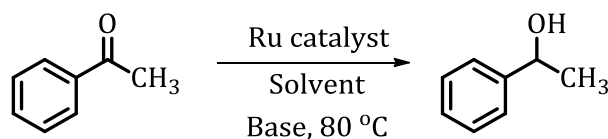
**Figure 2.7.** Normalized absorption spectra A) complexes **3** and **4** (10  $\mu$ M each) in chloroform and B) complexes **5-8** (10  $\mu$ M each) in acetonitrile, respectively.

Geometry optimization for the complexes **3** and **4** were also performed at DFT level. Theoretical calculations of complexes **3** and **4** have been carried out using the density functional theory (DFT) employing the LANL2DZ basis set. TD-DFT calculations

were performed on both the complexes and major transitions along with their orbital contribution were determined. For the complex **3**, two transitions observed at 450 nm which corresponds to HOMO→LUMO transition ( $f = 0.0099$ ) and HOMO-2→LUMO having orbital contribution of 97% and 2%, respectively. Transition near 400 nm was mainly due to HOMO-6→LUMO (56%), HOMO-4→LUMO (37%) transitions.

### 2.3.4. Catalytic Properties of the Complexes

As the complexes **1-8** exhibited good air and moisture stability, we have investigated their use in catalytic transfer hydrogenation reactions of the aromatic ketones. To understand the catalytic activity of the complexes, the transfer hydrogenation of acetophenone was carried out as a representative example (Scheme 2.4) under different conditions. A mixture of the catalyst (any one of the complexes **1-8**) in different solvents in the presence of various bases was heated first at 40 °C for 10 min and then the substrate, acetophenone was added slowly. The reaction mixture temperature was then raised to 80 °C and the reaction was further continued for specified time. The products formed were analyzed through GC-MS and NMR spectroscopic techniques and the results obtained under different conditions are summarized in Table 2.3.



**Scheme 2.4.** Transfer hydrogenation of acetophenone in presence of the complexes **1-8**.

**Table 2.3.** Optimization conditions for transfer hydrogenation of acetophenone in presence of complexes **1-8**.<sup>a</sup>

Entry	Solvent	Base	Conversion (%)								
			<b>1</b>	<b>2</b>	<b>3</b>	Complexes		<b>6</b>	<b>7</b>	<b>8</b>	
1	t-Butanol	NaOH	NC	NC	NC	NC	NC	NC	NC	NC	NC
2	t-Butanol	KOH	NC	NC	NC	NC	NC	NC	NC	NC	NC
3	Glycerol	NaOH	NC	NC	50	48	52	60	62	65	
4	2-propanol	Cs <sub>2</sub> CO <sub>3</sub>	19	5	<10	<10	10	15	10	12	
5	2-propanol	Na <sub>2</sub> CO <sub>3</sub>	35	15	21	15	6	3	15	18	
6	2-propanol	KO <sup>t</sup> Bu	55	49	60	55	40	46	64	75	
7	2-propanol	KOH	86	70	>99	95	>99	>99	100	100	
8	2-propanol	NaOH	>99	96	100	>99	100	100	100	100	
9	2-propanol	NaOH	<sup>b</sup> 52	<sup>b</sup> 46	<sup>b</sup> 62	<sup>b</sup> 58	<sup>c</sup> 45	<sup>c</sup> 48	<sup>c</sup> 58	<sup>c</sup> 60	

<sup>a</sup> Average of three independent experiments and S.D  $\pm$  1% and experimental conditions: acetophenone (0.1 mmol), complexes **1** or **2** (2 mol%, 5 h), complexes **3** or **4** (2 mol%, 2 h), complexes **5-8** (0.5 mol%, 2 h), base (0.05 mmol), solvent (2 mL), temperature (80  $\pm$  2 °C). Yields determined by GC-MS analyses. Catalyst used: <sup>b</sup>1 mol% and <sup>c</sup>0.25 mol%. NC: No conversion.

For example, the hydrogenation of acetophenone (0.1 mmol) in t-butanol (2 mL) and in the presence of all the complexes **1-8** and NaOH/KOH (0.05 mmol) gave negligible conversion and the substrate was isolated as unchanged (entries 1-2). Similarly, negligible conversion of the substrate was observed in presence of complexes **1** and **2** (entry 3), when we employed glycerol as the solvent in presence of the bases

such as NaOH and KOH. In contrast, when we employed complexes **3** and **4** in glycerol under reaction conditions, we observed an increased substrate conversion yield of *ca.* 50 and 48% (entry 3) respectively. The complexes **5-8** also catalyzed the transfer hydrogenation reactions in glycerol with a conversion yield in the range of *ca.* 52-65% (entry 3) using NaOH as the base promoter. However, when we used the solvent 2-propanol and employed Cs<sub>2</sub>CO<sub>3</sub> as the base, we observed a marginal substrate conversion to the desired 1-phenylethanol, of *ca.* 5-19% (entry 4), using the complexes **1-2**, under identical reaction conditions.

To optimize the reaction conditions as well as to understand the effect of base, we have carried out the transfer hydrogenation employing different bases such as Na<sub>2</sub>CO<sub>3</sub>, KOtBu, KOH and NaOH. Of all the bases employed, we observed that NaOH acts as the best promoter with an efficiency of *ca.* 100 and 96% (entry 8) for the conversion of acetophenone to 1-phenylethanol, using the complexes **1** and **2**, respectively, with a turnover frequency (TOF) value of 2500h<sup>-1</sup> for the complex **1** (at 50% conversion). Interestingly, complexes **3** and **4** in the presence of both NaOH and KOH have been proven to catalyze the reduction of acetophenone at a load of 2 mol% in 2-propanol, affording 1-phenylethanol about *ca.* 95-100% (entries 7-8) and achieving a TOF of 5000 h<sup>-1</sup>. Moreover transfer hydrogenation reactions with the complexes **5-8** also exhibited excellent catalytic efficiencies, affording a *ca.* 99-100% (entries 7-8) conversion for the substrate with a high turnover frequency (TOF) of about 11110 h<sup>-1</sup> within 2 h of reaction time. In contrast, when the catalyst loading was decreased the by *ca.* 50%, the complexes **1** and **2** at 1 mol%, showed lower efficiency for the conversion of the substrate (*ca.* 46-52%) (entry 9). Similarly, the complexes **3** and **4** at 1 mol% also

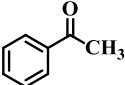
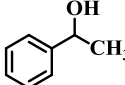
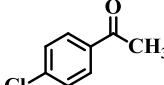
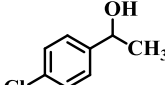
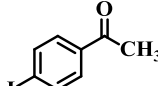
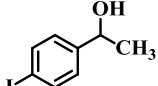
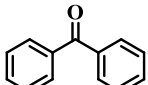
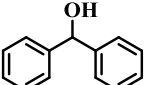
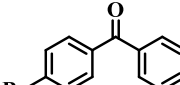
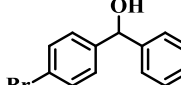
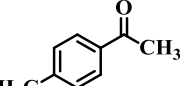
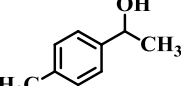
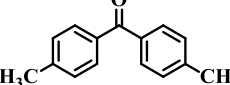
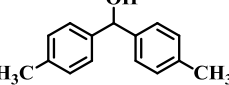
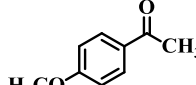
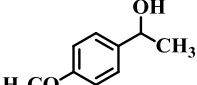


showed decreased substrate conversion yield of *ca.* 62 and 58%, respectively (entry 9). Reduced conversion yields of *ca.* 45-60% were observed with the complexes **5-8** at a loading of 0.25 mol% (entry 9). These results demonstrate that we require a minimum of 0.5 and 2 mol% loading of the catalysts **5-8** and **1-4**, respectively, to achieve a *ca.* 100% transfer hydrogenation of acetophenone under moderate reaction conditions.

To understand the generality of the reaction, we have carried out reactions with the aromatic ketones having different substituents using the complexes **1-4** (Tables 2.4-2.5). For example, the substrates having electronegative substituents like 1-(4-chlorophenyl)ethanone (Table 2.4, entry 2) and 1-(4-iodophenyl)-ethanone (Table 2.4, entry 3) in presence of NaOH in 2-propanol gave *ca.* 100% of 1-(4-chlorophenyl)-ethanol and 1-(4-iodophenyl)ethanol, respectively, for both the complexes **1** and **2**, with a TOF value of *ca.* 2500 h<sup>-1</sup>. In contrast, both these substrates exhibited the efficiency in the range *ca.* 90-97% conversion, when KOH was employed as the base promoter (entries 2 and 3). The substrate 2,2-difluoro-1-phenylethanone (Table 2.5, entry 1) exhibited *ca.* 100% conversion to the product 2, 2-difluoro-1-phenylethanol using the complexes **3** as well as **4** in the presence of both NaOH and KOH as the base promoters in 2-propanol. Similar observations were also made with the chloro- and iodo-substituted acetophenones (Table 2.5, entries 2-3), which have resulted in *ca.* 95-100% yield under identical reaction conditions. When benzophenone (Table 2.4, entry 4) and (4-bromophenyl)(phenyl)methanone (Table 2.4, entry 5) were used as the substrates, we observed the efficient transfer hydrogenation to furnish *ca.* 96% of the desired products, diphenylmethanol and (4-bromophenyl)(phenyl)methanol, respectively, in the presence of the complex **1** and NaOH as the promoter. Similarly complexes **3** and **4** gave

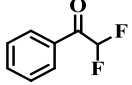
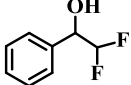
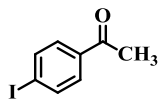
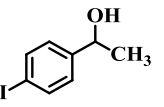
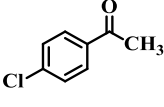
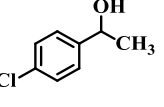
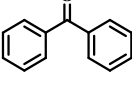
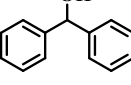
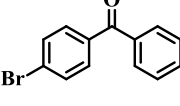
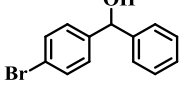
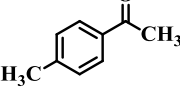
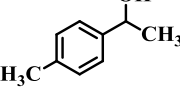
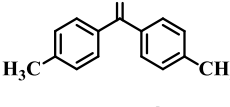
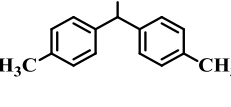
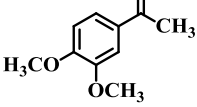
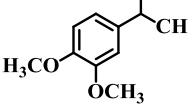
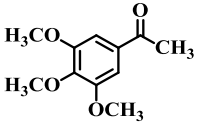
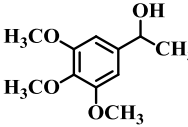
quantitative conversion of the substrates of about *ca.* 90-100% (Table 2.5, entries 4-5) under similar reaction conditions.

**Table 2.4.** Transfer hydrogenation of the aromatic ketones catalyzed by the complexes **1** and **2**.<sup>a</sup>

Entry	Substrate	Product	Conversion (%), TOF (h <sup>-1</sup> )			
			Complex <b>1</b>		Complex <b>2</b>	
			NaOH	KOH	NaOH	KOH
1			100 (2500)	86 (2150)	100 (2500)	80 (2000)
2			100 (2500)	90 (2250)	100 (2500)	97 (2425)
3			100 (2475)	95 (2375)	100 (2500)	94 (2350)
4			96 (2400)	70 (1750)	95 (2375)	60 (1500)
5			96 (2400)	96 (2400)	97 (2425)	90 (2250)
6			94 (2350)	51 (1275)	98 (2450)	52 (1300)
7			79 (1975)	27 (675)	77 (1925)	40 (1000)
8			82 (1650)	36 (900)	66 (2050)	42 (1050)

<sup>a</sup> Average of three independent experiments and S.D  $\pm$  1% and experimental conditions: Substrate (0.1 mmol), the complexes **1** or **2** (2 mol%), base (NaOH/KOH, 0.05 mmol), 2-propanol (2 mL) at  $80 \pm 2$  °C and reaction time 5 h.

**Table 2.5.** Transfer Hydrogenation of aromatic ketones catalyzed by the complexes **3** and **4**.<sup>a</sup>

Entry	Substrate	Product	Complex <b>3</b> Complex <b>4</b> Conversion % (TOF h <sup>-1</sup> )			
			NaOH	KOH	NaOH	KOH
1			100 (5000)	100 (5000)	100 (5000)	100 (5000)
2			>99 (4998)	98 (4900)	100 (5000)	96 (4800)
3			>99 (4990)	99 (4990)	>99 (4995)	95 (4750)
4			97 (4850)	96 (4800)	100 (5000)	>99 (4955)
5			91 (4550)	>99 (4995)	95 (4750)	98 (4900)
6			>99 (4960)	>99 <sup>b</sup> (4975)	98 (4900)	>99 <sup>b</sup> (4952)
7			98 (4900)	95 <sup>b</sup> (4750)	97 (4850)	96 <sup>b</sup> (4800)
8			93 (4650)	97 <sup>b</sup> (4850)	98 (4900)	96 <sup>b</sup> (4800)
9			96 (4800)	96 <sup>b</sup> (4800)	90 (4500)	92 <sup>b</sup> (4600)

<sup>a</sup> Average of three independent experiments and S.D.  $\pm$  1% and experimental conditions: Substrate (0.1 mmol), the complexes **3** or **4** (2 mol%), base (NaOH/KOH, 0.05 mmol), 2-propanol (2 mL) at  $80 \pm 2$  °C and duration of the reaction 2 h. <sup>b</sup> Reaction time extended to 3 h.

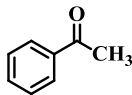
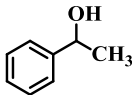
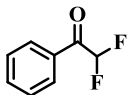
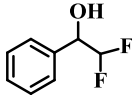
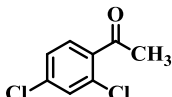
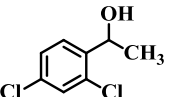
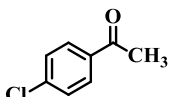
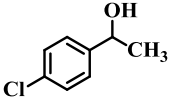
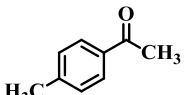
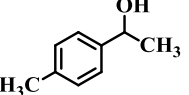
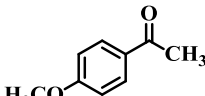
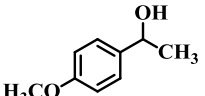
However, when we employed KOH as the promoter, we observed significantly decreased conversion yields (*ca.* 70 and 60%) of diphenylmethanol from benzophenone

for the complexes **1** and **2**, respectively (Table 2.4, entry 4). We have furthermore investigated the transfer hydrogenation reaction of the aromatic ketones bearing electron rich substituents. It was noted that the reaction of 1-(p-tolyl)ethanone (Table 2.4, entry 6) in presence of the complexes **1** and **2** with NaOH resulted in *ca.* 94% and 98% conversion to the corresponding 1-(p-tolyl)ethanol, respectively. However, the substrates such as di-p-tolylmethanone (Table 2.4, entry 7) and 1-(3,4-dimethoxyphenyl)ethanone (Table 2.4, entry 8) showed moderate conversion rates of (*ca.* 79 and 82%) to their corresponding secondary alcohols in the presence of the complex **1**. Similarly, reduced conversion rates (*ca.* 77 and 66%) were observed with the complex **2**. In contrast, when KOH used as the promoter instead of NaOH we observed significantly reduced conversion yields in the range *ca.* 27-51% for complexes **1** and **2** under identical conditions (Table 2.4, entries 6-8). Importantly, our results furthermore confirm that one can selectively achieve the efficient transfer hydrogenation of carbonyl group using the complexes **1** and **2** in the presence of the labile and electronegative groups such as chlorine, bromine and iodine. In contrast, the aromatic ketones having electron rich substituents such as methyl and methoxy groups have an adverse effect on the efficiency of the transfer hydrogenation reaction.

Interestingly, the substrates bearing electron rich substituents exhibited excellent conversion yield to the corresponding alcohols in the range *ca.* 93-99% (Table 2.5, entries 6-9), when we employed NaOH as the base promoter in 2-propano in presence of the complexes **3** and **4**. Interestingly, upon changing the base promoter to KOH, we observed a *ca.* 92-99% conversion of the substrate to the product within 3 h of reaction under identical conditions. From the experiments we observed that, both the neutral

Ru(II)-NHC complexes **3** and **4** afforded nearly same efficiencies in presence of NaOH as well as KOH and also found to be highly efficient towards the transfer hydrogenation of both electron rich and deficient aromatic ketones within very short duration.

**Table 2.6.** Transfer hydrogenation of aromatic ketones catalyzed by the complexes **5-8**.<sup>a</sup>

Entry	Substrate	Product	Conversion (%), (Time, h) (TOF, h <sup>-1</sup> )			
			Complex <b>5</b>	Complex <b>6</b>	Complex <b>7</b>	Complex <b>8</b>
1			> 99 (2) (11110)	99 (2) (10000)	100 (2) (10000)	100 (2) (10000)
2			100 (1) (20000)	100 (1) (20000)	100 (1) (20000)	100 (1) (20000)
3			100 (2) (9090)	100 (2) (8300)	100 (1) (18000)	100 (1) (18180)
4			100 (2) (8700)	100 (2) (9000)	100 (2) (10000)	100 (1) (17850)
5			100 (4) (5000)	> 99 (4) (4900)	97 (3) (3300)	100 (3) (3500)
6			> 99 (5) (4000)	98 (6) (3572)	100 (3) (6666)	> 99 (3) (7142)

<sup>a</sup> Average of three independent experiments and S.D  $\pm$  1% and experimental conditions: Substrate (0.1 mmol), the complexes **5-8** (0.5 mol%), base (NaOH 0.05 mmol), 2-propanol (2 mL) at  $80 \pm 2$  °C.

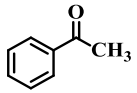
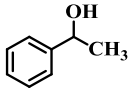
To understand the potential of the cationic complexes **5-8**, we have expanded the transfer hydrogenation reactions towards some of the electron rich and deficient aromatic ketones as shown in Table 2.6. The hydrogenation reactions were performed

by following the optimized conditions at different time scales. With a catalyst loading of *ca.* 0.5 mol%, the complexes **5-8** exhibited excellent catalytic efficiency for the transfer hydrogenation of 2,2-difluoro-1-phenylethanone (entry 2) within 1 h, affording a highest TOF value of *ca.* 20000 h<sup>-1</sup> (at 50% formation of the product). Likewise the reactions occur well with 1-(2,4-dichlorophenyl)ethanone (entry 3) and 1-(4-chlorophenyl)ethanone (entry 4) with a conversion yield of *ca.* 100%. We observed excellent yields within 2 h in the presence of mononuclear complexes **5** and **6**, while the dinuclear complexes **7** and **8** required only 1 h to achieve the same results.

Eventually, we have carried out the reactions using substrates such as 1-(*p*-tolyl)ethanone (entry 5) and 1-(4-methoxyphenyl)ethanone (entry 6) under similar conditions, wherein we observed *ca.* 97-100% substrate conversion at a catalyst loading of only 0.5 mol%. In comparison to the ruthenium- $\pi$  and neutral ruthenium complexes, the cationic ruthenium complexes showed better catalytic activity, this can be attributed to the strong binding of both *NHC* and pyridine substituents to the metal centre. The systems synthesized are stable to air and moisture and showed excellent catalytic activity at a low catalyst loading conditions, thereby demonstrated these systems as efficient catalysts for transfer hydrogenation reactions.

Further, to understand the robustness of the complexes **1-8**, the efficiency of transfer hydrogenation reaction of acetophenone was compared with the ligand precursors and also literature known ruthenium based catalysts (Table 2.7). Interestingly, the ligand precursors (Table 2.7, entries 4-5) as well as the ruthenium precursor, RuCl<sub>3</sub>.xH<sub>2</sub>O showed negligible conversion of the substrate to the desired

**Table 2.7.** Comparative catalytic efficiency of transfer hydrogenation of acetophenone.<sup>a</sup>

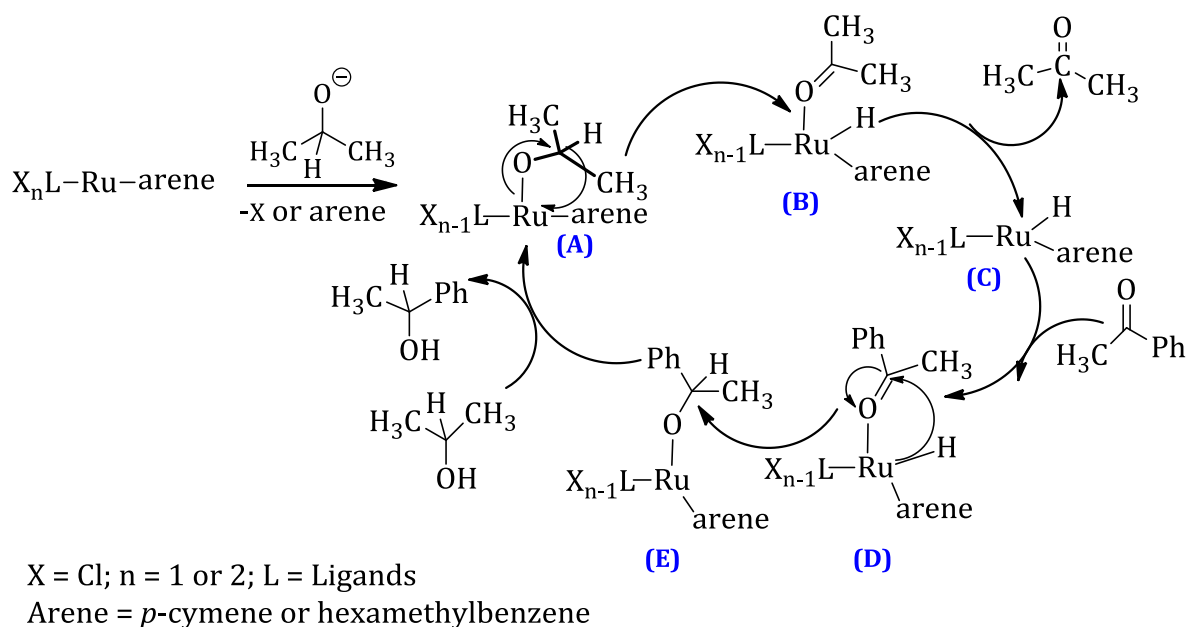
Entry	Substrate	Product	Catalyst	Conversion (%)
1			Complexes <b>1-2</b>	96-100
2	"	"	Complexes <b>3-4</b>	100
3	"	"	Complexes <b>5-8</b>	100
4	"	"	Ligands alone	No conversion
5	"	"	RuCl <sub>3</sub> .xH <sub>2</sub> O	No conversion
6	"	"	[Ru( <i>p</i> -Cymene)Cl <sub>2</sub> ] <sub>2</sub>	47
7	"	"	Hoveyda-Grubbs' 2 <sup>nd</sup>	60

<sup>a</sup> Reaction conditions: acetophenone (0.1 mmol), catalysts entries 1-2, 4-7 (2 mol%) and entry 3 (0.5 mol%), NaOH (0.05 mmol), 2-propanol (2 mL), temperature ((80 ± 2 °C) and reaction time, 2-5 h.

product under similar conditions. In contrast, the reaction with the commercially available ruthenium catalysts such as [Ru(*p*-Cymene)Cl<sub>2</sub>]<sub>2</sub><sup>28</sup> (Table 2.7, entry 6) and the second generation "Hoveyda-Grubbs" catalyst,<sup>29</sup> (Table 2.7, entry 7) furnished only moderate yields of the transfer hydrogenation products under identical catalytic conditions. We also have carried out the transfer hydrogenation reactions of the corresponding aldehydes as the substrates in presence of all the complexes; we observed negligible conversion of the substrate under identical reaction conditions.

The mechanism of transfer hydrogenation of the aromatic ketones to the corresponding aromatic alcohols using the ruthenium complexes is briefly shown in Scheme 2.5, as per the experimental evidence and literature reports.<sup>30</sup> The loss of chloride molecule followed by the addition of 2-propoxide gives an active ruthenium

catalyst species A, which can further undergo  $\beta$ -hydride migration and loss of acetone to give a ruthenium hydride complex C. Subsequently, the formation of the coordinated complex D can be rationalized through the interaction of the intermediate complex C with the substrate, which in turn can undergo hydride transfer to form the intermediate E. The desired aromatic alcohol formation can be postulated through the reaction of the intermediate E with the solvent 2-propanol in the presence of the base promoter and thereby generating the activated ruthenium catalyst species A.



**Scheme 2.5.** Possible mechanism for transfer hydrogenation of acetophenone.

$^1\text{H}$  NMR and GC-MS data of few representative transfer hydrogenation products:

### 1-Phenylethanol

$^1\text{H}$  NMR ( $\text{CD}_3\text{CN}$ , TMS, 500 MHz)  $\delta$  1.36-1.38 (d, 3H), 3.24 (s, 1H), 4.76-4.81 (m, 1H), 7.21-7.22 (t, 1H), 7.30-7.36 (m, 4H);  $m/z$  Calcd for  $\text{C}_8\text{H}_{10}\text{O}$  122.07; Found 122 ( $\text{M}^+$ ).



1-(4-Chlorophenyl)ethanol

$^1\text{H}$  NMR ( $\text{CD}_3\text{CN}$ , TMS, 500 MHz)  $\delta$  1.35-1.36 (d, 3H), 3.28 (s, 1H), 4.76-4.81 (m, 1H), 7.33 (s, 4H); m/z Calcd for  $\text{C}_8\text{H}_9\text{ClO}$  156.03; Found 156 ( $\text{M}^+$ ).

Diphenylmethanol

$^1\text{H}$  NMR ( $\text{CD}_3\text{CN}$ , TMS, 500 MHz)  $\delta$  3.82 (s, 1H), 5.77 (d, 1H), 7.20-7.23 (t, 2H), 7.29-7.32 (t, 4H), 7.36-7.38 (d, 4H); m/z Calcd for  $\text{C}_{13}\text{H}_{12}\text{O}$  184.08; Found 184 ( $\text{M}^+$ ).

(4-Bromophenyl)(phenyl)methanol

$^1\text{H}$  NMR ( $\text{CD}_3\text{CN}$ , TMS, 500 MHz)  $\delta$  3.88 (s, 1H), 5.7 (d, 1H), 7.29-7.36 (m, 7H), 7.46-7.47 (d, 2H); m/z Calcd for  $\text{C}_{13}\text{H}_{11}\text{BrO}$  261.99; Found 262 ( $\text{M}^+$ ).

1-(4-Iodophenyl)ethanol

$^1\text{H}$  NMR ( $\text{CD}_3\text{CN}$ , TMS, 500 MHz)  $\delta$  1.34-1.35 (d, 3H), 3.27 (s, 1H), 4.74-4.76 (m, 1H), 7.14-7.16 (d, 2H), 7.67-7.68 (d, 2H); m/z Calcd for  $\text{C}_8\text{H}_9\text{IO}$  247.97; Found 248 ( $\text{M}^+$ ).

1-(*p*-Tolyl)ethanol

$^1\text{H}$  NMR ( $\text{CD}_3\text{CN}$ , TMS, 500 MHz)  $\delta$  1.34-1.35 (d, 3H), 2.30 (s, 3H), 3.1 (s, 1H), 4.74-4.76 (m, 1H), 7.13-7.14 (d, 2H), 7.22-7.24 (d, 2H); m/z Calcd for  $\text{C}_9\text{H}_{12}\text{O}$  136.08; Found 136 ( $\text{M}^+$ ).

## 2.4. Conclusions

In summary, we designed and synthesized air and moisture stable ruthenium complexes **1-8**, and have demonstrated their use as efficient catalysts. The catalytic activity of these complexes **1-8** was analyzed for the transfer hydrogenation reactions of the aromatic ketones. The electronic effects on catalytic reactions were also studied by

employing both electron rich and electron deficient aromatic ketones. The simple complexes **1** and **2** were found to act as efficient catalysts for *ca.* 100% conversion of the aromatic ketones to their corresponding alcohols with only 2 mol% catalyst loading in 2-propanol at 5 h of reaction time. In particular, these complexes were highly efficient for the aromatic ketones having electron deficient substituents, when compared to the electron rich substrates. On the other hand, the neutral ruthenium-*NHC* complexes **3-4** exhibited high selectivity and activity of *ca.* 100% conversion for the aromatic ketones bearing both electron rich and deficient substituents at a loading of 2 mol% but required only 2 h. In the case of the cationic ruthenium-*NHC* complexes **5-8**, we observed excellent reaction yields of *ca.* 100% conversion within 1 h with a catalyst loading of only 0.5 mol% with a high turnover frequency (TOF) of 20000 h<sup>-1</sup> thereby their use as robust catalysts for the transfer hydrogenation reaction.

## 2.5. Experimental Section

### 2.5.1. General Techniques

The general equipment used and the methodologies followed for calculation of the fluorescence quantum yields were described in our earlier publications.<sup>16a,31</sup> The cyclic voltammetry measurements were carried out using a CV-50W electroanalyzer in acetonitrile using platinum wire as auxiliary electrode, compound coated platinum electrode as working electrode. The potentials were referenced to the standard Ag/AgCl electrode and ferrocene (0.45 V, E<sub>1/2</sub>) was used as an external standard. Thermal stability measurements were performed at a heating rate of 10 °C/min in nitrogen atmosphere using Shimadzu, DTG-60 equipment. EDX analyses of the complexes were

done using with a FEI Tecnai G2-30 Transmission Electron Microscope operating at 120 kV. WAXD measurements were carried out on a XEUSS SAXS/WAXS system using a Genix microsource from Xenocs operated at 50 kV and 0.6 mA. The Cu K $\alpha$  radiation ( $\lambda = 1.54 \text{ \AA}$ ) was collimated with a FOX2D mirror and two pairs of scatterless slits from Xenocs. The 2D patterns were recorded on a Mar345 image plate and processed using Fit2D software. All the measurements were made in the transmission mode. GC-MS spectra were recorded on SHIMADZU Gas Chromatograph Mass Spectrometer-QP 2010 equipment.

## 2.5.2. Materials and Methods

Anthracene, benzyl bromide, 1,4-dibromobenzene, Ag<sub>2</sub>O, RuCl<sub>3</sub>.xH<sub>2</sub>O, [Ru(*n*<sup>6</sup>-*p*-cymene)Cl<sub>2</sub>]<sub>2</sub>, [Ru(hexamethylbenzene)Cl<sub>2</sub>]<sub>2</sub> and the aromatic ketones were purchased from Aldrich and S. D. Fine Chemicals, India and used as received. Ligands **9**, **10**, **11**, **12** and **14** were prepared by reported procedures.<sup>16,19</sup> All the solvents were purified and dried prior to use.

## 2.5.3. Preparation of the Ligand and Complexes

**2.5.3.1. Synthesis of the Complex 1:** To a solution of **9** (50 mg, 0.06 mmol) in distilled ethanol (10 mL) was added RuCl<sub>3</sub>.xH<sub>2</sub>O (12.5 mg, 0.06 mmol) and the reaction mixture was then refluxed for 4 h at 80 °C. The reaction mixture was then filtered and washed thoroughly with ethanol and dried under vacuum to give the complex **1** in 80% yield. Mp > 300 °C; <sup>1</sup>H NMR (500 MHz, DMSO-d<sub>6</sub>, TMS)  $\delta$  5.64 (s, 2H), 6.44 (s, 8H), 7.47-7.48 (d, 8H), 8.06 (d, 8H), 8.32 (s, 4H); <sup>13</sup>C NMR (125 MHz, DMSO-d<sub>6</sub>)  $\delta$  45.6, 123.6, 124.3, 126.4, 127.6, 129.3, 132.5; MALDI-TOF-MS: Calcd for C<sub>38</sub>H<sub>32</sub>Cl<sub>2</sub>N<sub>4</sub>ORu, 732.09;

Found, 731.92 (M<sup>+</sup>); Elemental Anal. Calcd for C<sub>38</sub>H<sub>32</sub>OCl<sub>2</sub>N<sub>4</sub>RuP<sub>2</sub>F<sub>12</sub> (%): C, 44.63; H, 3.15; N, 5.48. Found: C, 44.45; H, 3.42; N, 5.65.

**2.5.3.2. Synthesis of the Complex 2:** To a solution of **10** (50 mg, 0.075 mmol) in distilled ethanol (10 mL) was added RuCl<sub>3</sub>.xH<sub>2</sub>O (15.7 mg, 0.075 mmol) and the reaction mixture was then refluxed for 4 h at 80 °C. The reaction mixture was then filtered and washed thoroughly with ethanol and dried under vacuum to give the complex **2** in 88% yield. Mp > 300 °C; <sup>1</sup>H NMR (500 MHz, DMSO-d<sub>6</sub>, TMS) δ 3.77 (s, 6H), 6.58 (s, 4H), 7.69 (d, 4H), 7.77 (d, 4H), 8.60 (s, 4H), 8.93 (s, 2H); <sup>13</sup>C NMR (125 MHz, DMSO-d<sub>6</sub>) δ 36.3, 45.3, 122.7, 124.0, 124.7, 126.9, 127.7, 130.6, 136.7; MALDI-TOF-MS: Calcd for C<sub>24</sub>H<sub>26</sub>Cl<sub>2</sub>N<sub>4</sub>ORu, 558.46; Found, 558.39 (M<sup>+</sup>); Elemental Anal. Calcd for C<sub>24</sub>H<sub>26</sub>OCl<sub>2</sub>N<sub>4</sub>RuP<sub>2</sub>F<sub>12</sub> (%): C, 33.98; H, 3.09; N, 6.60. Found: C, 34.20; H, 3.30; N, 6.74.

**2.5.3.3. Synthesis of the Complex 3:** To a solution of **11** (50 mg, 0.09 mmol) in dry dichloromethane (20 mL) was added Ag<sub>2</sub>O (22 mg, 0.09 mmol). The reaction mixture was then stirred for 4 h at room temperature followed by the addition of *p*-cymene dimer precursor [Ru(*η*<sup>6</sup>-*p*-cymene)Cl<sub>2</sub>]<sub>2</sub> (55 mg, 0.09) and further stirred for 4 h. The reaction mixture was then passed through celite column and the solvents were evaporated to dryness. The orange solid was obtained by precipitation in diethyl ether, yielded the complex **3** in 39% yield. The single crystals were obtained by recrystallization from a mixture (10:1) of chloroform and methanol. Mp > 300 °C; <sup>1</sup>H NMR (500 MHz, CDCl<sub>3</sub>, TMS) δ 1.36-1.37 (d, 12H), 1.58 (s, 6H), 2.31 (s, 6H), 3.04-3.10 (quint, 2H), 4.10 (s, 4H), 5.43 (s, 4H), 5.63 (s, 4H), 6.13 (s, 2H), 6.74 (s, 2H), 7.59 (m, 4H), 8.38 (m, 4H); <sup>13</sup>C NMR (125 MHz, DMSO-d<sub>6</sub>); δ 20.9, 23.9, 30.6, 32.9, 47.1, 117.7, 123.9,

125.5, 126.0, 126.6, 127.9, 128.7, 131.2, 163.9, 173.1 ppm; Elemental Anal. Calcd for  $C_{44}H_{50}Cl_4N_4Ru_2$  (%): C, 53.88; H, 5.34; N, 5.71. Found: C, 53.65; H, 5.64; N, 5.88.

**2.5.3.4. Synthesis of the Complex 4:** To a solution of **12** (50 mg, 0.11 mmol) in dry dichloromethane (20 mL) was added  $Ag_2O$  (27 mg, 0.11 mmol). The reaction mixture was then stirred for 4 h at room temperature followed by the addition of *p*-cymene dimer precursor  $[Ru(\eta^6\text{-}p\text{-cymene})Cl_2]_2$  (67 mg, 0.11 mmol) and further stirred for 4 h. The reaction mixture was then passed through celite column and the solvents were evaporated to dryness. The orange solid was obtained by precipitation in diethyl ether, yielded the complex **4** in 40% yield. The single crystals were obtained by recrystallization from a mixture (10:1) of chloroform and methanol. Mp > 300 °C ;  $^1H$  NMR (500 MHz,  $CDCl_3$ , TMS)  $\delta$  1.26-1.27 (d, 12H), 1.58 (s, 6H), 2.07 (s, 6H), 2.91-2.97 (quint, 2H), 4.05 (s, 4H), 5.08 (s, 4H), 5.39 (s, 4H), 6.78 (s, 2H), 6.98 (s, 2H), 7.32 (s, 4H);  $^{13}C$  NMR (125 MHz,  $DMSO-d_6$ )  $\delta$  21.4, 23.9, 30.3, 31.5, 117.2, 125.0, 126.1, 127.4, 127.7, 128.4, 137.1, 165.4, 173.9 ppm; Elemental Anal. Calcd for  $C_{36}H_{46}Cl_4N_4Ru_2$  (%): C, 49.09; H, 5.49; N, 6.36. Found: C, 48.99; H, 5.42; N, 6.30.

**2.5.3.5. Synthesis of the Complex 5:** To a solution of **14** (50 mg, 0.15 mmol) in dry dichloromethane (15mL) was added  $Ag_2O$  (19 mg, 0.079 mmol). The reaction mixture was then stirred for 4 h at room temperature followed by the addition of metal precursor  $[Ru(\eta^6\text{-}p\text{-cymene})Cl_2]_2$  (48 mg, 0.079 mmol) and further stirred for next 2 h. The reaction mixture was then passed through celite column and the solvents were evaporated to dryness. The solid obtained was again dissolved in water and 1.5 equivalent of ammonium hexafluorophosphate in water was added. The solid obtained

by precipitation was dried and further recrystallized from diethyl ether, yielded the complex **5** in 50% yield. The single crystals were obtained by recrystallization from a mixture (10:1) of methanol and chloroform. Mp > 300 °C; <sup>1</sup>H NMR (500 MHz, CD<sub>3</sub>CN, TMS) δ 0.88-0.91 (d, 6H), 2.14 (s, 3H), 2.35-2.41 (quint, 1H), 5.49-5.50 (dd, 1H), 5.54-5.57 (d, 1H), 5.72-5.75 (d, 1H), 5.86-5.88 (t, 1H), 5.97-5.98 (t, 1H), 6.09-6.11 (d, 1H), 7.25 (s, 1H), 7.26 (s, 1H), 7.45 (s, 5H), 7.78-7.80 (d, 1H), 7.88-7.89 (d, 1H), 8.11-8.15 (m, 1H), 9.16-9.17 (t, 1H); <sup>13</sup>C NMR (125 MHz, CD<sub>3</sub>CN) δ 19.2, 22.3, 24.3, 31.8, 55.8, 83.2, 87.9, 91.0, 92.1, 101.0, 106.3, 109.6, 113.6, 124.2, 125.5, 127.2, 129.3, 130.1, 136.5, 142.5, 152.7, 156.5, 186.1 ppm; ESI-MS: m/z Calcd for C<sub>25</sub>H<sub>27</sub>N<sub>3</sub>ClRu, 506.0937; Found, 506.0949 (M<sup>+</sup>); Elemental Anal. Calcd for C<sub>25</sub>H<sub>27</sub>N<sub>3</sub>ClPF<sub>6</sub>Ru (%): C, 46.05; H, 4.33; N, 6.44. Found: C, 46.26; H, 4.28; N, 6.46.

**2.5.3.6. Synthesis of the Complex 6:** To a solution of **14** (50 mg, 0.15 mmol) in dry dichloromethane (20 mL) was added Ag<sub>2</sub>O (19 mg, 0.079 mmol). The reaction mixture was then stirred for 4 h at room temperature followed by the addition of metal precursor [Ru(hexamethylbenzene)Cl<sub>2</sub>]<sub>2</sub> (53 mg, 0.079 mmol) and further stirred for next 2 h. The reaction mixture was then passed through celite column and the solvents were evaporated to dryness. The solid obtained was again dissolved in water and 1.5 equivalent of ammonium hexafluorophosphate in water was added. The solid obtained by precipitation was dried and further recrystallized from diethyl ether, yielded the complex **6** in 60% yield. The single crystals were obtained by recrystallization from a mixture (10:1) of methanol and chloroform. Mp > 300 °C; <sup>1</sup>H NMR (500 MHz, CD<sub>3</sub>CN, TMS) δ 2.19 (s, 18H), 5.44-5.52 (q, 2H), 7.09-7.10 (d, 1H), 7.35-7.38 (m, 3H), 7.46-7.50

(m, 3H), 7.71-7.73 (d, 1H), 7.80-7.81 (d, 1H), 8.06-8.09 (m, 1H), 8.70-8.71 (m, 1H);  $^{13}\text{C}$  NMR (125 MHz,  $\text{CD}_3\text{CN}$ )  $\delta$  16.5, 55.6, 99.9, 113.0, 124.1, 125.2, 130.3, 136.3, 141.9, 153.1, 153.7, 190.6 ppm; ESI-MS:  $m/z$  Calcd for  $\text{C}_{25}\text{H}_{27}\text{N}_3\text{ClRu}$ , 534.1250; Found, 534.1263 ( $\text{M}^+$ ); Elemental Anal. Calcd for  $\text{C}_{27}\text{H}_{31}\text{ClN}_3\text{PF}_6\text{Ru}$  (%): C, 47.69; H, 4.74; N 6.18. Found: C, 47.65; H, 4.79; N, 6.14.

**2.5.3.7. Synthesis of the Ligand 15:** To a mixture of 2-(1H-imidazol-1-yl)pyridine (200 mg, 1.37 mmol) in dry acetonitrile (10 mL) was added 1,4-bis(bromomethyl)benzene (182 mg, 0.69 mmol). The reaction mixture was refluxed for 36 h at 100 °C in a pressure tube and the product obtained was then filtered and washed thoroughly with acetonitrile and dried under vacuum. The product was further purified by recrystallization from acetonitrile to give precursor **15** in 80% yield. Mp > 200 °C;  $^1\text{H}$  NMR (500 MHz,  $\text{DMSO-d}_6$ , TMS)  $\delta$  5.58 (s, 4H), 7.62 (s, 4H), 7.64-7.67 (m, 2H), 8.03-8.05 (m, 4H), 8.20-8.24 (m, 2H), 8.55-8.56 (t, 2H), 8.65-8.66 (m, 2H), 10.32 (s, 2H);  $^{13}\text{C}$  NMR (125 MHz,  $\text{DMSO-d}_6$ )  $\delta$  52.0, 114.2, 119.7, 123.4, 125.2, 129.1, 135.1, 140.5, 146.3, 149.1 ppm; ESI-MS: Calcd for  $\text{C}_{24}\text{H}_{22}\text{N}_6$ , 394.1895; Found, 393.1836 ( $\text{M}^+-1$ ).

**2.5.3.8. Synthesis of the Ligand 16:** To a mixture of 2-(1H-imidazol-1-yl)pyridine (200 mg, 1.37 mmol) in dry acetonitrile (10 mL) was added 9,10-dibromomethylantracene (251 mg, 0.69 mmol). The reaction mixture was refluxed for 36 h at 100 °C in a pressure tube and the product obtained was then filtered and washed thoroughly with acetonitrile and dried under vacuum. The product was further purified by recrystallization from acetonitrile to give precursor **16** in 75% yield. Mp > 240 °C;  $^1\text{H}$  NMR (500 MHz,  $\text{DMSO-d}_6$ , TMS)  $\delta$  6.72 (s, 4H), 7.59-7.60 (t, 2H), 7.63-7.66 (m, 2H), 7.79-

7.81 (m, 4H), 8.00-8.02 (d, 2H), 8.17-8.20 (m, 2H), 8.48-8.49 (d, 2H), 8.63-8.69 (d, 6H), 10.08 (s, 2H);  $^{13}\text{C}$  NMR (125 MHz, DMSO- $d_6$ )  $\delta$  45.6, 114.5, 119.4, 123.2, 124.6, 125.3, 126.3, 127.7, 130.8, 134.6, 140.5, 146.2, 149.2 ppm; ESI-MS: Calcd for  $\text{C}_{32}\text{H}_{26}\text{N}_6$ , 494.2208; Found, 493.2213 ( $\text{M}^+-1$ ).

**2.5.3.9. Synthesis of the Complex 7:** To a solution of **15** (50 mg, 0.09 mmol) in dry dichloromethane (20 mL) was added  $\text{Ag}_2\text{O}$  (21 mg, 0.09 mmol). The reaction mixture was then stirred for 4 h at room temperature followed by the addition of metal precursor  $[\text{Ru}(n^6\text{-}p\text{-cymene})\text{Cl}_2]_2$  (55 mg, 0.09 mmol) and further stirred for next 4 h. The reaction mixture was then passed through celite column and the solvents were evaporated to dryness. The solid obtained was again dissolved in water and 2.5 equivalent of ammonium hexafluorophosphate in water was added. The solid obtained by precipitation was dried and further recrystallized from diethyl ether, yielded the complex **7** in 40% yield. Mp > 300 °C;  $^1\text{H}$  NMR (500 MHz,  $\text{CD}_3\text{CN}$ , TMS)  $\delta$  0.86-0.91 (m, 12H), 2.25 (s, 6H), 2.3-2.4 (quint, 2H), 5.48-5.49 (d, 2H), 5.55-5.58 (d, 2H), 5.74-5.77 (d, 2H), 5.85-5.88 (t, 2H), 5.99-6.02 (m, 2H), 6.10-6.12 (m, 2H), 7.25-7.26 (d, 2H), 7.43-7.48 (m, 6H), 7.77-7.86 (m, 2H), 7.87-7.88 (t, 2H), 8.11-8.12 (d, 2H), 9.15-9.16 (d, 2H);  $^{13}\text{C}$  NMR (125 MHz,  $\text{CD}_3\text{CN}$ )  $\delta$  19.2, 22.5, 24.3, 31.8, 55.4, 83.3, 88.0, 91.0, 92.1, 100.9, 106.4, 109.8, 113.6, 124.2, 125.4, 127.2, 130.0, 137.0, 142.5, 152.6, 156.5, 186.2 ppm; Elemental Anal. Calcd for  $\text{C}_{44}\text{H}_{48}\text{Cl}_2\text{N}_6\text{P}_2\text{F}_{12}\text{Ru}_2$  (%): C, 43.11; H, 4.11; N, 6.86. Found: C, 43.09; H, 4.23; N, 6.79.

**2.5.3.10. Synthesis of the Complex 8:** To a solution of **16** (50 mg, 0.076 mmol) in dry dichloromethane (20 mL) was added  $\text{Ag}_2\text{O}$  (18 mg, 0.076 mmol). The reaction mixture was then stirred for 4 h at room temperature followed by the addition of metal



precursor  $[\text{Ru}(\eta^6\text{-}p\text{-cymene})\text{Cl}_2]_2$  (47 mg, 0.076 mmol) and further stirred for next 4 h. The reaction mixture was then passed through celite column and the solvents were evaporated to dryness. The solid obtained was again dissolved in water and 2.5 equivalent of ammonium hexafluorophosphate in water was added. The solid obtained by precipitation was dried and further recrystallized from diethyl ether, yielded the complex **8** in 45% yield. Mp > 300 °C;  $^1\text{H}$  NMR (500 MHz,  $\text{CD}_3\text{CN}$ , TMS)  $\delta$  1.01-1.06 (m, 12H), 2.27 (s, 6H) 2.57-2.65 (q, 2H), 5.89-5.90 (d, 2H), 6.13-6.14 (d, 2H), 6.34-6.35 (d, 2H), 6.44-6.45 (d, 2H), 6.61-6.68 (m, 4H), 6.77-6.81 (m, 2H), 7.48-7.51 (m, 2H), 7.68-7.69 (d, 2H), 7.73-7.76 (m, 8H), 8.12-8.16 (m, 2H), 8.66 (s, 2H), 9.25-9.27 (d, 2H);  $^{13}\text{C}$  NMR (125 MHz,  $\text{CD}_3\text{CN}$ );  $\delta$  19.3, 22.5, 32.1, 49.3, 84.3, 87.7, 91.7, 92.8, 100.9, 107.1, 108.7, 113.6, 117.8, 124.3, 126.1, 128.7, 129.9, 132.1, 142.6, 152.5, 156.6, 185.8 ppm; Elemental Anal. Calcd for  $\text{C}_{52}\text{H}_{52}\text{Cl}_2\text{N}_6\text{P}_2\text{F}_{12}\text{Ru}_2$  (%): C, 47.10; H, 4.10; N, 6.34. Found: C, 47.32; H, 4.13; N, 6.28.

**2.5.3.11. General Procedure for Transfer Hydrogenation:** An oven-dried Schlenk-tube was charged with 2-propanol (2 mL). The solvent was degassed by means of three cycles under  $\text{N}_2$ . The catalyst (0.5-2 mol%) was added and dissolved by using ultrasound (10 min). Base (0.05 mmol) was added and the mixture then preheated in a sealed tube at 80 °C for 10 min. Substrate (0.1 mmol) was added with a syringe and further allowed to react for the specified time. Aliquots were taken at fixed intervals and analyzed by GCMS. After the reaction time, the mixture was passed through silica column in hexane and the solvent was evaporated to dryness. The catalytic reactions were carried out in duplicates to confirm the reproducibility of the results.

### 2.5.4. X-ray Crystallography

Single crystals of the complexes **3** and **4** were obtained from a mixture (9:1) of CHCl<sub>3</sub>-CH<sub>3</sub>OH. The data sets for the single-crystal X-ray studies for **3**.3CHCl<sub>3</sub> and **4**.2CHCl<sub>3</sub> were collected with Mo K $\alpha$  ( $\lambda$  = 0.71073 Å) radiation on a RIGAKU diffractometer. The complexes **5** and **6** were collected on Bruker APEX2 diffractometer. All the structure calculations were performed using SHELXTL.

### 2.5.5. DFT Calculations

The DFT calculations for the complexes **3** and **4** were carried out using Gaussian 09 program package.<sup>32a</sup> The Becke's three parameters hybrid exchange functional with the Lee-Yang-Parr (LYP) non-local correlation functional was used throughout the computational study.<sup>32b,c</sup> A LANL2DZ basis set was used in the calculation. The Gauss View-5 program was used for pictorial representation of frontier molecular orbitals.

## 2.6. References

1. (a) Suleyman, G.; Aytac, G. G.; Bekir, C. *Inorg. Chem.* **2013**, *52*, 10601. (b) Verena, G.; Aurelija, U.; Alexander, S.; Doris, K. *Organometallics* **2012**, *31*, 7532. (c) Lindsay, J. H.; Michael, J. F.; Martin, C. *Organometallics* **2011**, *30*, 4108.
2. (a) Guidone, S.; Songis, O.; Falivene, L.; Nahra, F.; Slawin, A. M. Z.; Jacobsen, H.; Cavallo, L.; Cazin, C. S. J. *ACS Catal.* **2015**, *5*, 3932. (b) Bokka, A.; Hua, Y.; Berlin, A. S.; Jeon, J. *ACS Catal.* **2015**, *5*, 3189. (c) Kumar, A.; Bheeter, L. P.; Gangwar, M. K.; Sortais, J. B.; Darcel, C.; Ghosh, P. *J. Organomet. Chem.* **2015**, *786*, 63. (d) Pastva, J.; Skowerski, K.; Czarnocki, S. J.; Zilkova, N.; Cejka, J.; Bastl, Z.; Balcar, H. *ACS Catal.*

- 2014**, 4, 3227. (e) Mingshuo, Z.; Le, L.; Seth, B. H. *J. Am. Chem. Soc.* **2014**, 136, 7058.
- (f) Huff, C. A.; Sanford, M. S. *ACS Catal.* **2013**, 3, 2412. (g) Masato, I.; Akira, W.; Yuji, S.; Takao, I. *Organometallics* **2010**, 29, 4584.
3. (a) Diez-Gonzalez, S.; Nolan, S. P.; *Coord. Chem. Rev.* **2007**, 251, 874. (b) Mataa, J. A.; Poyatos, M.; Peris, E. *Coord. Chem. Rev.* **2007**, 251, 841. (c) Farrell, J. M.; Posaratnanathan, R. T.; Stephan, D. W. *Chem. Sci.* **2015**, 6, 2010.
4. (a) Cabrero-Antonino, J. R.; Alberico, E.; Junge, K.; Junge, H.; Beller, M. *Chem. Sci.* **2016**, 7, 3432. (b) Marion, N.; Navarro, O.; Mei, J.; Stevens, E. D.; Scott, N. M.; Nolan, S. P. *J. Am. Chem. Soc.* **2006**, 128, 4101. (c) Wang, D.; Bi, Q.; Yin, G.; Zhao, W.; Huang, F.; Xieac, X.; Jiang, M. *Chem. Commun.* **2016**, 52, 14226.
5. (a) Zhu, K.; Shaver, M. P.; Thomas, S. P. *Chem. Sci.* **2016**, 7, 3031. (b) Jin, T.; He, D.; Li, W.; Stanton, C. J.; Pantovich, S. A.; Majetich, G. F.; Schaefer, H. F.; Agarwal, J.; Wang, D.; Li, G. *Chem. Commun.* **2016**, 52, 14258.
6. (a) Quigley, B. L.; Grubbs, R. H. *Chem. Sci.* **2014**, 5, 501. (b) Hu, X. *Chem. Sci.* **2011**, 2, 1867. (c) Louie, J.; Bielawski, C. W.; Grubbs, R. H. *J. Am. Chem. Soc.* **2001**, 123, 11312. (d) Vougioukalakis, G. C.; Grubbs, R. H. *J. Am. Chem. Soc.* **2008**, 130, 2234. (e) Chen, J. R.; Li, C. F.; An, X. L.; Zhang, J. J.; Zhu, X. Y.; Xiao, W. J. *Angew. Chem. Int. Ed.* **2008**, 47, 2489. (f) Nagarkar, A. A.; Kilbinger, A. F. M. *Chem. Sci.* **2014**, 5, 4687. (g) Debleds, O.; Campagne, J.-M. *J. Am. Chem. Soc.* **2008**, 130, 1562.
7. (a) Yang, C.; Mehmood, F.; Lam, T. L.; Chan, S. L. F.; Wu, Y.; Yeung, C. S.; Guan, X.; Li, K.; Chung, C. Y. S.; Zhou, C. Y.; Zoua, T.; Che, C. M. *Chem. Sci.* **2016**, 7, 3123. (b)

- Praetorius, J. M.; Crudden, C. M. *Dalton Trans.* **2008**, 4079. (c) Sergio, S.; Miriam B.; Peris, E. *Organometallics* **2010**, *29*, 275. (d) Jeong, J.; Park, S.; Chang, S. *Chem. Sci.* **2016**, *7*, 5362.
8. (a) Baratta, W.; Paolo, D. R.; Alessandro, D. Z.; Alessandra, S.; Ennio, Z.; Pierluigi, R. *Angew. Chem. Int. Ed.* **2004**, *43*, 3584. (b) Vuong, K. Q.; Timerbulatova, M. G.; Peterson, M. B.; Bhadbhade, M.; Messerle, B. A. *Dalton Trans.* **2013**, *42*, 14298. (c) Alexandre, A. M.; Robert, H. M. *Inorg. Chem.* **2010**, *49*, 11039.
9. (a) Kumar, S.; Saleem, F.; Singh, A. K. *Dalton Trans.* **2016**, *45*, 11445. (b) Yigit, M.; Yigit, B.; Ozdemir, I.; Cetinkaya, E.; Cetinkaya, B. *Appl. Organomet. Chem.* **2006**, *20*, 322. (c) Horn, S.; Albrecht, M. *Chem. Commun.* **2011**, *47*, 8802. (d) Poyatos, M.; Maise-Francois, A.; Bellemin-Laponnaz, S.; Peris, E.; Gade, L. H. *J. Organomet. Chem.* **2006**, *691*, 2713. (e) Sanz, S.; Azua, A.; Peris, E. *Dalton Trans.* **2010**, *39*, 6339.
10. (a) Chao-Yu, W.; Ching-Feng, F.; Yi-Hong, L.; Shei-Ming P.; Shiuh-Tzung, L. *Inorg. Chem.* **2007**, *46*, 5779. (b) Yanyun, L.; Shenluan, Y.; Xiaofeng, W.; Jianliang, X.; Weiyi, S.; Zhenrong, D.; Jingxing, G. *J. Am. Chem. Soc.* **2014**, *136*, 4031.
11. (a) Arturo, A.; Jose, A. M.; Eduardo, P.; Frederic, L.; Jean, M.; Evelina, C. *Organometallics* **2012**, *31*, 3911. (b) Yawen, W.; Dong, X.; Qian, L.; Chao, W.; Jianliang, X. *Green Chem.* **2013**, *15*, 629. (c) Om, P.; Kamal, N. S.; Hemant, J.; Pancham, L. G.; Ajai, K. S. *Organometallics* **2014**, *33*, 2535.
12. Caramori, G. F.; Garcia, L. C.; Andrada, D. M.; Frenking, G. *Organometallics* **2014**, *33*, 2301.

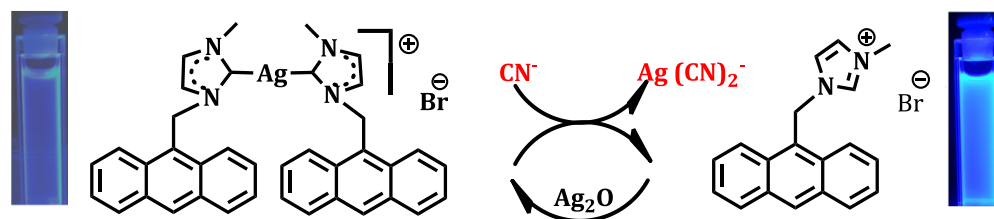
13. Takeshi, O.; Noriyuki, U.; Kunihiko, T.; Kunihiko, M.; Christian, S.; Noyori, R. *J. Am. Chem. Soc.* **2006**, *128*, 8724.
14. Baratta, W.; Chelucci, G.; Herdtweck, E.; Magnolia, S.; Siega, K.; Rigo, P. *Angew. Chem. Int. Ed.* **2007**, *46*, 7651.
15. Diez Gonzalez, S.; Marion, N.; Nolan, S. P. *Chem. Rev.* **2009**, *109*, 3612.
16. (a) Viji, M.; Nair, A. K.; Nandajan, P. C.; Ramaiah, D. *RSC Adv.* **2014**, *4*, 47982. (b) Neelakandan, P. P.; Ramaiah, D. *Angew. Chem. Int. Ed.* **2008**, *47*, 8407.
17. Ganesan, K.; Alias, Y. *Int. J. Mol. Sci.* **2008**, *9*, 1207.
18. (a) Verma, A. K.; Singh, J.; Kasi Sankar, V.; Chaudhary, R.; Chandra, R. *Tetrahedron Lett.* **2007**, *48*, 4207. (b) Barbante, G. J.; Francis, P. S.; Hogan, C. F.; Kheradmand, P. R.; Wilson, D. J. D.; Barnard, P. J. *Inorg. Chem.* **2013**, *52*, 7448.
19. Dinesh, K. M.; Aasif, A. D.; Jin-Soo, H. *J. Mol. Catal. A: Chem.* **2013**, *376*, 63.
20. (a) Gonell, S.; Peris, E. *ACS Catal.* **2014**, *4*, 2811. (b) Mahn-Jong, K.; Rama, K.; Hongwei, Y.; Frederick, M. M.; Fausto, P.; Scolastica, S.; Sebastiano, C. Tina, H.; Gary, K.; Krishnan, R. *Inorg. Chem.* **2002**, *41*, 2471.
21. (a) Ramasamy, R.; Christian, K.; Fritz, S. *Electrochem. Commun.* **2000**, *2*, 190. (b) Mahn-Jong, K.; Rama, K.; Hongwei, Y.; Frederick, M. M.; Fausto, P.; Scolastica, S.; Sebastiano, C.; Tina, H.; Gary, K.; Krishnan, R. *Inorg. Chem.* **2002**, *41*, 2471.
22. (a) Joseph, D.; Mukesh, K.; Matthias, Z.; Elizabeth, T. P. *Organometallics* **2013**, *32*, 966. (b) Julia, W.; Alexander, P.; Fritz, E. K.; Baratta, W. *Organometallics* **2013**, *32*, 4042.

23. Robert, E. M.; Rhona, E. A.; Piedad del Socorro, M.; Haimei, C.; Jeff, C.; Nathan, D. H.; Simon, P.; Andrew, P.; Gary, B.; Duncan, I. J.; Peter, J. S.; *J. Med. Chem.* **2001**, *44*, 3616.
24. Mani, G.; Rangasamy, L.; Suresh, E.; Anvarbatcha, R.; Mohammad, A. A.; Mallayan, P. *Dalton Trans.* **2014**, *43*, 1203.
25. Zirngast, M.; Pump, E.; Leitgeb, A.; Albering, J. H.; Slugovc, C. *Chem. Commun.* **2011**, *47*, 2261.
26. Gnanamgari, D.; Sauer, E. L. O.; Schley, N. D.; Butler, C.; Incarvito, C. D.; Crabtree, R. H. *Organometallics* **2009**, *28*, 321.
27. Pandiarajan, D.; Ramesh, R. *J. Organomet. Chem.* **2013**, *723*, 26.
28. Lundberg, H.; Adolfsson, H. *Tetrahedron Lett.* **2011**, *52*, 2754.
29. Louie, J.; Bielawski, C. W.; Grubbs, R. H. *J. Am. Chem. Soc.* **2001**, *123*, 11312.
30. Alonso, D. A.; Brandt, P.; Nordin, S. J. M.; Andersson, P. G. *J. Am. Chem. Soc.* **1999**, *121*, 9580.
31. (a) Kuruvilla, E.; Ramaiah, D. *J. Phys. Chem. B* **2007**, *111*, 6549. (b) Nair, A. K.; Neelakandan, P. P.; Ramaiah, D. *Chem. Commun.* **2009**, 6352.
32. (a) Frisch, M. J.; Trucks, G. W.; Schlegel, H. B. *et al.* Gaussian 09, Revision D.01, Gaussian, Inc., Wallingford CT, **2009**. (b) Lee, C.; Yang, W.; Parr, R. G. *Phys. Rev. B* **1988**, *37*, 785. (c) Becke, A. D. *Phys. Rev. A* **1988**, *38*, 3098.

---

**DESIGN OF SILVER(I)-NHC COMPLEXES: STUDY OF THEIR  
PHOTOPHYSICAL AND ANION RECOGNITION PROPERTIES**

---



### 3.1. Abstract

With an objective of developing molecular probes, we have synthesized novel N-heterocyclic carbene linked silver complexes **2** and **4** and its imidazolium precursors **1** and **3**, and have investigated their photophysical as well as anion recognition properties. All the compounds showed good solubility in aqueous medium and favourable photophysical properties. The stability of the complexes was further studied by monitoring the <sup>1</sup>H NMR spectrum after the addition of trifluoroacetic acid. When studied the interaction of the complexes **2** and **4** with various anions, these systems showed significant changes in the emission spectra with the addition of cyanide ions, whereas absorption spectra showed negligible changes. Moreover, negligible interactions were observed for the imidazolium precursors **1** and **3** upon addition of cyanide ions. These systems showed selective interaction with cyanide ions, when

compared to other biologically relevant anions and the sensitivity of detection was found to be *ca.* 49 and 50 ppb, respectively, for the complexes **2** and **4**. Both the complexes showed similar kind of spectral changes on interaction with 2 to 4 equivalents of cyanide ions. The effect of pH on the recognition event was also studied by varying the pH of the solution from 2 to 12, wherein the complexes showed similar changes in the emission spectra as observed in the aqueous medium. The nature of interactions has been studied through <sup>1</sup>H NMR and emission lifetime measurements, which confirmed that, even though the metal-carbon bond is quite strong, the highly nucleophilic cyanide ions could easily cull the silver ion from the complex through the formation of a highly fluorescent imidazolium precursor **1** and the stable soluble Ag(CN)<sub>2</sub><sup>-</sup> salt. Similar observation was made in the case of the complex **4**. Our results demonstrate that the N-heterocyclic carbene based mono and di-nuclear silver complexes **2** and **4** have potential use as probes for the detection of cyanide ions, when compared to all other biologically relevant anions and signal the event through visible enhancement in the fluorescence intensity.

### 3.2. Introduction

The development of fluorescent sensors for various analytes, especially anions has been one of the prominent areas of research in recent years.<sup>1,2</sup> Among the various anions, cyanide is considered as one of the most poisonous target to living organisms. These ions are extremely toxic and lethal to mammals due to their high affinity towards the heme unit <sup>3</sup> as well as the active site of cytochrome a<sub>3</sub>.<sup>4</sup> Such interactions cause decrease in oxygen concentration in the tissue, especially of the central nervous (CNS)



and cardiovascular (CVS) tissues, thereby resulting in hypoxia.<sup>5</sup> Of the various sources, hydrogen cyanide gas and the crystalline metal cyanides are the main causes of the cyanide poisoning and the United States of Environmental Protection Agency (US-EPA) has set their maximum contaminant levels in drinking water at 0.2 mg/L, which is equivalent to 200 parts per billion (ppb).<sup>6</sup> Cyanide ions are also ingredients in the preparation of a wide variety of products such as dyes, pharmaceuticals, plastics etc.<sup>7</sup> Due to this extensive usage, cyanide ion poisoning has become a major concern because of the hazardous impact on physiological and environmental conditions, leading to the high toxicity and inhibition of the activity of many biologically important enzymes.<sup>8</sup>

A variety of probes based on optical and electrochemical techniques have been reported for the detection of biologically relevant anions.<sup>9-12</sup> Of which, the optical probes, especially based on fluorescence have gained great importance because of their easy handling, fast response and high sensitivity.<sup>12</sup> Among the various fluorescent probes for the cyanide ions, recently the reaction based probes have attracted immense attention due to their high selectivity and sensitivity towards the analytes.<sup>13-19</sup> Most of these fluorescent probes are based on the reactions such as complexation/decomplexation,<sup>20</sup> nucleophilic addition,<sup>21</sup> and benzyl cyanide reaction.<sup>22</sup> Especially, the probes involving the displacement approach utilize the affinity of the cyanide ions towards various metal ions to form stable  $[M(CN)_x]^{n-}$  complexes.<sup>23</sup> In this context, we have designed and synthesized two N-heterocyclic carbene based mono- and dinuclear silver complexes **2** and **4** (Chart 3.1) and have investigated their anion recognition

properties. Uniquely, these probes act as chemodosimeters for cyanide ions with a sensitivity of *ca.* 50 ppb and signalled the event through turn on fluorescence intensity.

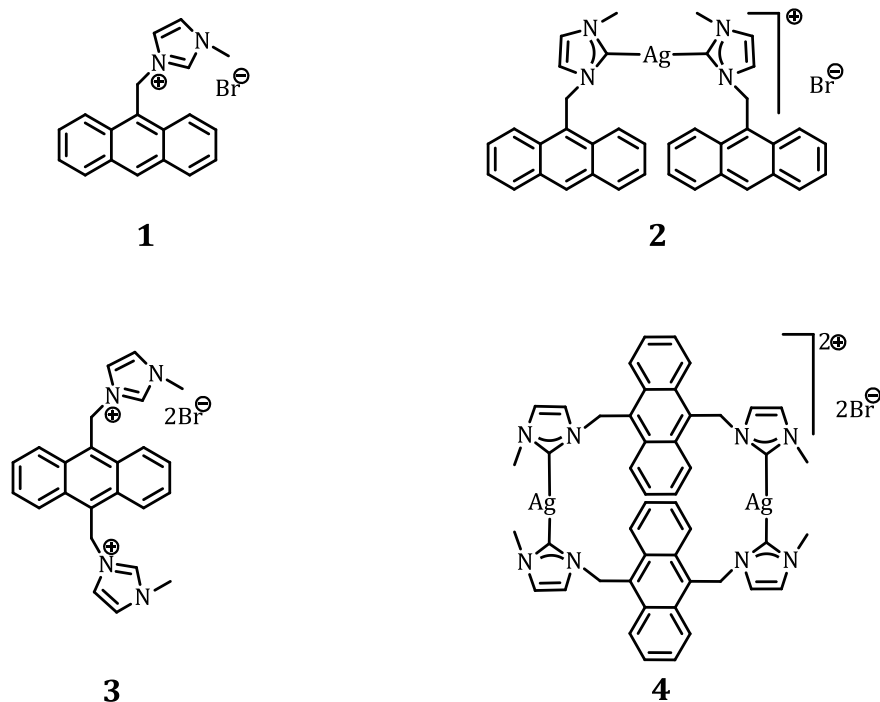


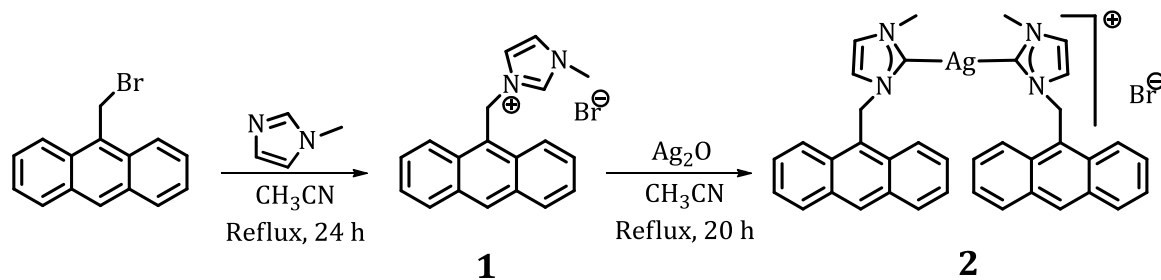
Chart 3.1. Structures of the compounds **1-4** investigated.

### 3.3. Results and Discussion

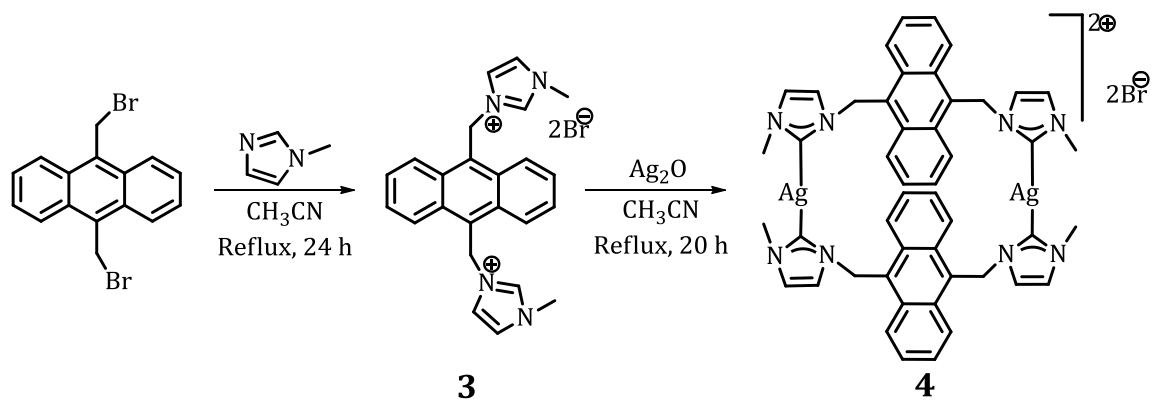
#### 3.3.1. Synthesis of the Complexes

Synthesis of the *NHC* complexes **2** and **4** was achieved in *ca.* 70% and 69%, respectively, through refluxing their corresponding imidazolium precursors **1** and **3** with silver oxide (Schemes 3.1-3.2) in dry acetonitrile for 20 h. In this reaction, Ag<sub>2</sub>O not only generates carbene intermediate through deprotonation of the imidazolium moiety but also acts as the metal center, which generally adopts a linear coordination in the dinuclear complexes.<sup>24</sup> The products, thus obtained were unambiguously characterized by

spectroscopic and analytical evidence such as UV-Vis,  $^1\text{H}$  and  $^{13}\text{C}$  NMR, MALDI-TOF MS and CHN analysis.



**Scheme 3.1.** Synthesis of silver-NHC complex **2**.



**Scheme 3.2.** Synthesis of silver-NHC complex **4**.

The formation of the metal carbon (Ag-C) bond in the complexes **2** and **4** can be easily evidenced through the  $^1\text{H}$  and  $^{13}\text{C}$  NMR analysis. The  $^1\text{H}$  NMR spectra of the precursors **1** and **3** in  $\text{CD}_3\text{CN}$  showed the peaks corresponding to the proton ( $\text{H}_2$ ) attached to carbon-2 of the imidazolium moiety as singlets at  $\delta$  8.79 and 8.13 ppm respectively, which disappeared upon complexation with  $\text{Ag}^+$  ions. We have recorded  $^1\text{H}$  NMR spectra of the complexes in  $\text{D}_2\text{O}$ , wherein the singlets at  $\delta$  8.82 and 8.14 ppm, corresponding to carbene proton of **1** and **3**, respectively, were disappeared upon complexation with  $\text{Ag}^+$  ions. Similarly, the singlets at  $\delta$  7.37 and 7.46 ppm for **1** and  $\delta$  7.32 and 7.35 ppm for **3**, corresponding to the imidazolium protons showed downfield

shift upon metal ion complexation (Figures 3.1 and 3.2). Similarly, in the  $^{13}\text{C}$  NMR spectra, we observed a downfield shift for the carbene carbons from  $\delta$  135.7 and 135.5 ppm to  $\delta$  179.5 and 179.9 ppm, when **1** and **3** were converted to the NHC complexes **2** and **4**, respectively. The binding stoichiometry of the complexes was determined from the MALDI-TOF MS analysis. In the case of the complex **2**, we got a 1 : 2 metal to ligand ratio, while a 1 : 1 ratio was observed for the complex **4**. For a better understanding of the stability of the complexes under low pH conditions, we have checked the  $^1\text{H}$  NMR spectra of both the complexes after the addition of trifluoroacetic acid (TFA). The spectra were found to be intact, indicating thereby that these complexes are quite stable even at low pH conditions in the aqueous medium.

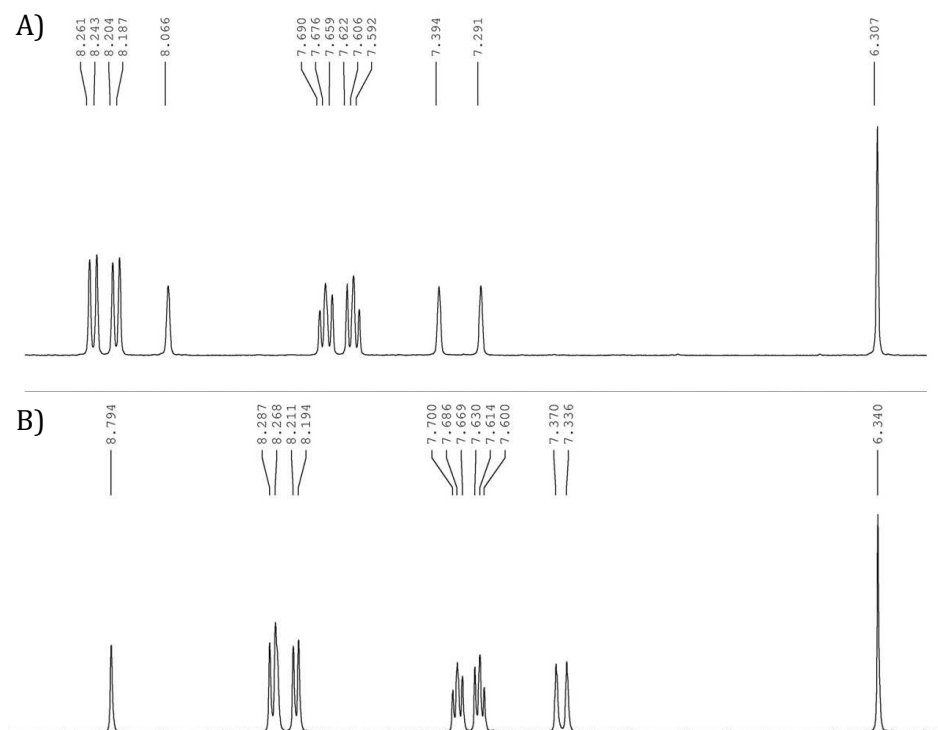


**Figure 3.1.**  $^1\text{H}$  NMR spectra of A) the complex **2** and B) imidazolium precursor **1** in  $\text{CD}_3\text{CN}$ .

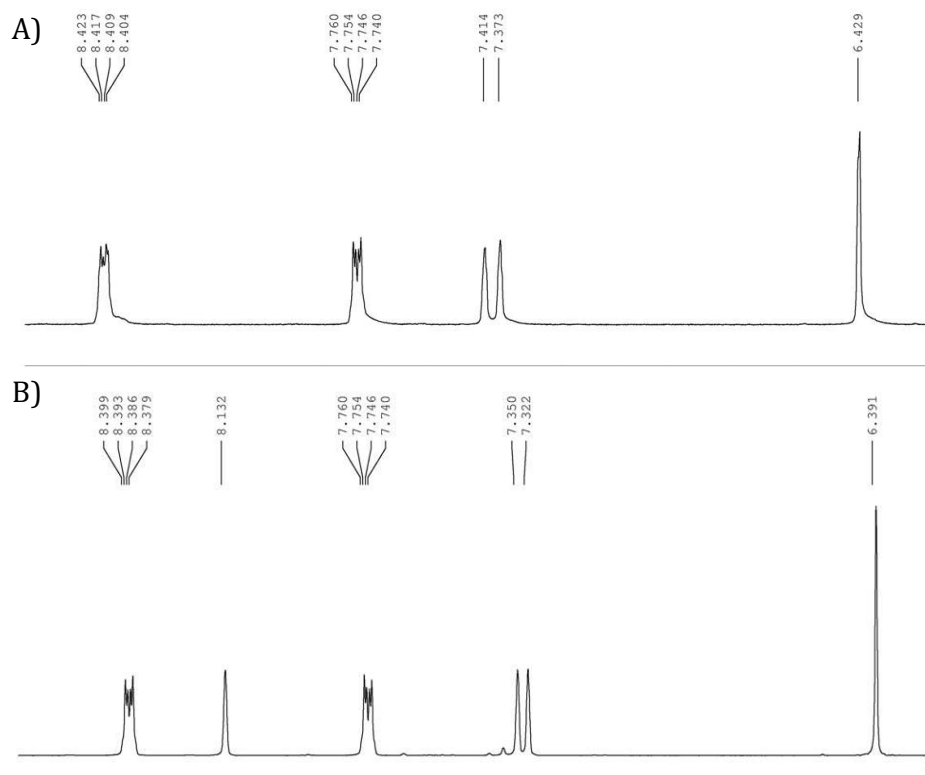


**Figure 3.2.** <sup>1</sup>H NMR spectra of A) the complex **4** and B) imidazolium precursor **3** in CD<sub>3</sub>CN.

### 3.3.2. Photophysical Properties of the Complexes

The photophysical properties of the complexes were carried out in aqueous medium. The complex **2** showed an absorption spectrum with a maximum at 394 nm ( $\epsilon = 2.3 \times 10^4 \text{ M}^{-1}\text{cm}^{-1}$ ), along with a broad absorption tailing up to 500 nm (Figure 3.3). While the fluorescence spectra exhibited characteristic peaks corresponding to the anthracene chromophore in the range 380–500 nm having maximum at 416 nm. The imidazolium precursor **1** also showed similar type of absorption and emission characteristics. The fluorescence quantum yields of the complex **2** and its imidazolium

precursor **1** were determined and these values are found to be *ca.*  $0.37 \pm 0.01$  and  $0.70 \pm 0.01$ , respectively ( $\lambda_{\text{ex}} = 365 \text{ nm}$ ).

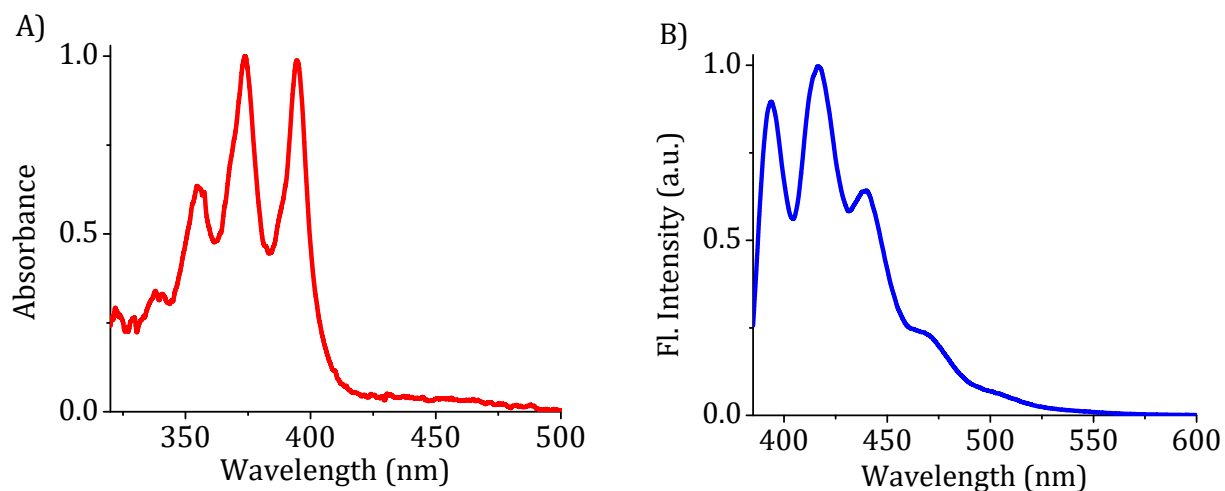


**Figure 3.3.** A) Normalized absorption and B) emission spectra of the complex **2** ( $5 \mu\text{M}$ ) in water. Excitation wavelength, 365 nm.

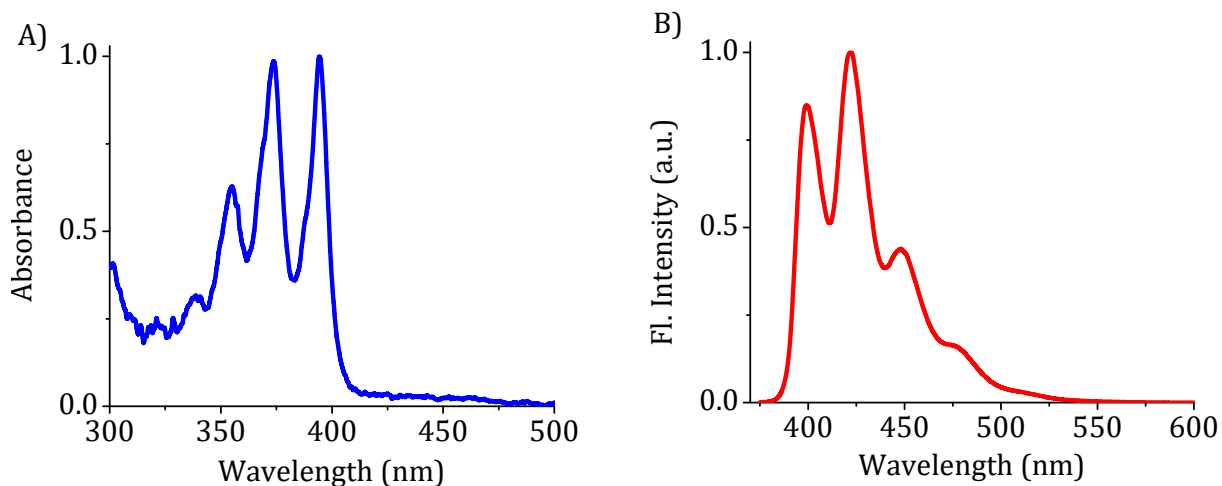


**Figure 3.4.** A) Normalized absorption and B) emission spectra of the complex **4** ( $5 \mu\text{M}$ ) in water. Excitation wavelength, 365 nm.

Further the radiative and non-radiative decay constants for the systems have been calculated from the fluorescence quantum yields and lifetime values. The complex **2** exhibited a radiative decay constant of  $0.053 \text{ ns}^{-1}$  (kr) and non-radiative decay constant of  $0.090 \text{ ns}^{-1}$  (knr), whereas the corresponding imidazolium precursor **1** showed  $0.087 \text{ ns}^{-1}$  (kr) and  $0.037 \text{ ns}^{-1}$  (knr), respectively, which supports the changes in the fluorescence quantum yields observed for these systems. The NHC complex **4** also exhibited absorption maximum at 394 nm with a broad absorption which extended up to 500 nm and characteristic emission peaks in the range 380–500 nm (Figure 3.4). The fluorescence quantum yields of the complex **4** and its imidazolium precursor **3** were determined and these values are found to be *ca.*  $0.34 \pm 0.01$  and  $0.54 \pm 0.03$  ( $\lambda_{\text{ex}} = 365 \text{ nm}$ ), respectively. The complex **4** exhibited a radiative decay constant of  $0.042 \text{ ns}^{-1}$  (kr) and non-radiative decay constant of  $0.082 \text{ ns}^{-1}$  (knr) and the precursor **3** (kr =  $0.066 \text{ ns}^{-1}$ , knr =  $0.056 \text{ ns}^{-1}$ ) also behaved similarly with respect to their emission profiles.

### 3.3.3. Anion Recognition Properties of the Complexes

As the NHC complexes **2** and **4** exhibited favourable fluorescence quantum yields and good solubility in the aqueous medium, we evaluated their potential as probes for various biologically relevant anions. Addition of tetrabutylammonium cyanide (TBACN) to an aqueous solution of the probe **2** ( $5 \mu\text{M}$ ), we observed negligible changes in its absorption properties (Figure 3.5A). However, in the emission spectrum ( $\lambda_{\text{ex}} = 365 \text{ nm}$ ), we observed a gradual increase in the fluorescence intensity at 416 nm and reached saturation upon addition of  $20 \mu\text{M}$  of cyanide ions (Figure 3.5B). The probe **4** also showed similar changes in the absorption

and emission profiles upon the addition of 4 equivalents of cyanide ions under identical conditions (Figure 3.6). These observations clearly indicated that both the complexes serve as probes for the recognition of cyanide ions.

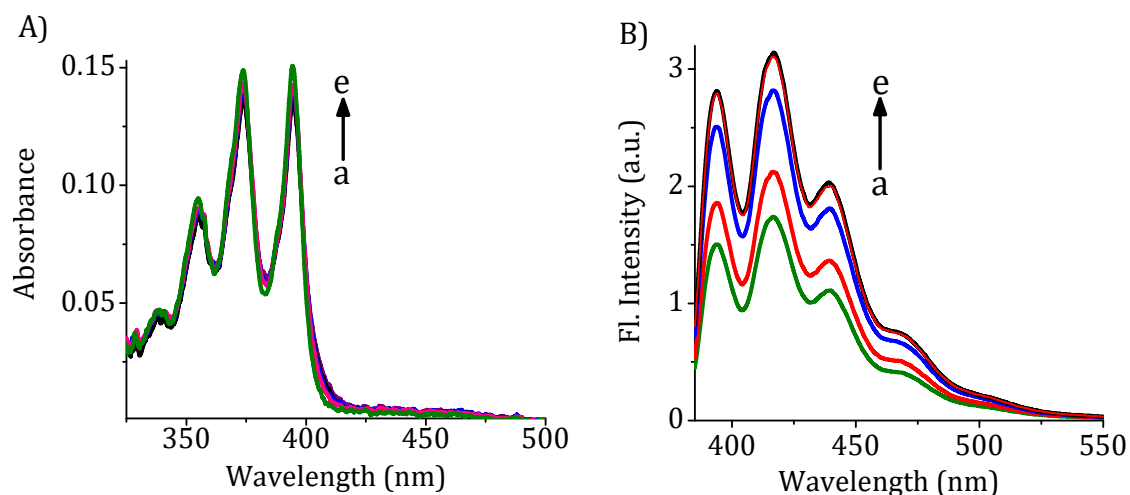


**Figure 3.5.** Changes in the A) absorption and B) fluorescence spectra of the probe 2 (5 μM) with the addition of CN<sup>-</sup> ions in the aqueous medium. [CN<sup>-</sup>] a) 0, and e) 20 μM. Excitation wavelength, 365 nm.

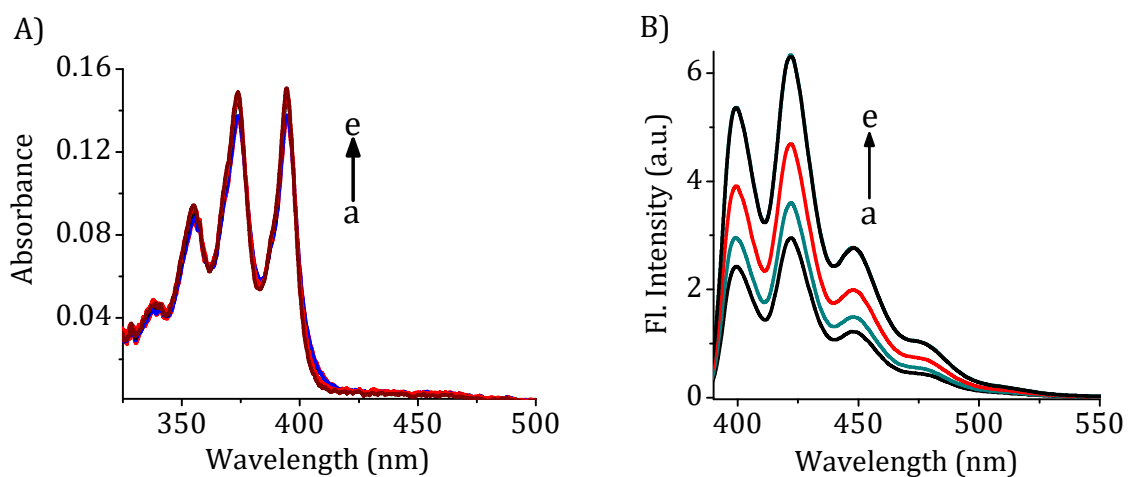


**Figure 3.6.** Changes in the A) absorption and B) emission spectra of the probe 4 (5 μM) with the addition of CN<sup>-</sup> ions in aqueous medium. [CN<sup>-</sup>] a) 0, and e) 20 μM. Excitation wavelength, 365 nm.



To understand the effect of pH on the recognition event, we have carried out the pH dependent interaction studies by varying the pH of the phosphate buffer from 2 to 12. When we monitored the absorption and emission changes of the complexes upon the addition of cyanide ions, it was found that the absorption spectra of both the complexes **2** and **4** showed negligible changes, whereas the emission spectra showed *ca.* 2–3 fold enhancement in the fluorescence intensity (Figures 3.7 and 3.8). The emission spectrum of the complexes exhibited similar changes in the pH range 2–12 as observed earlier in the aqueous medium, which clearly indicated that these complexes are stable under all pH conditions and has negligible effect on the interaction of the complexes **2** and **4** with the cyanide ions.

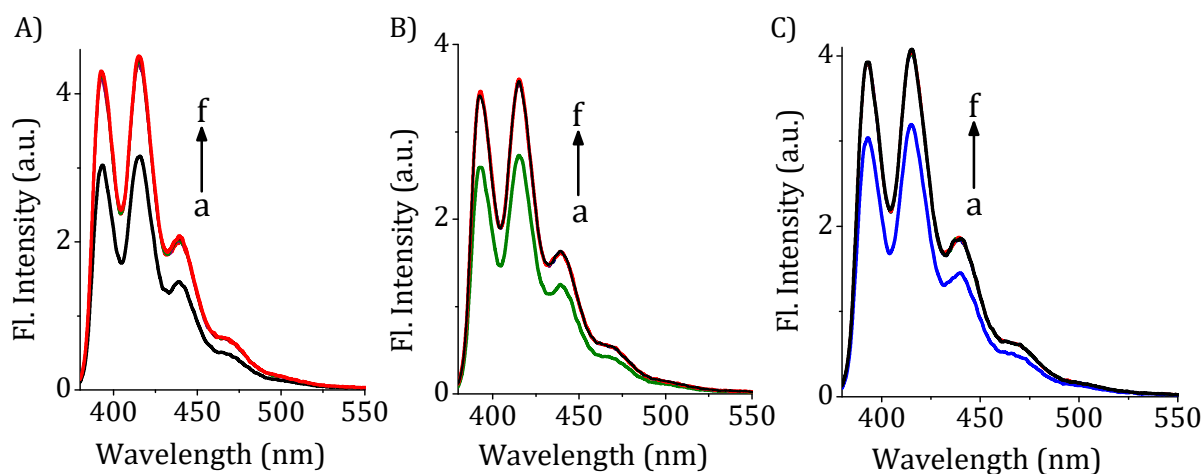


**Figure 3.7.** Changes in the fluorescence spectra of the probe **2** ( $5 \mu\text{M}$ ) at different pH A) pH 2, B) pH 7 and C) pH 12 with the addition of the cyanide ions.  $[\text{CN}^-]$  a) 0, and f)  $50 \mu\text{M}$ . Excitation wavelength, 365 nm.

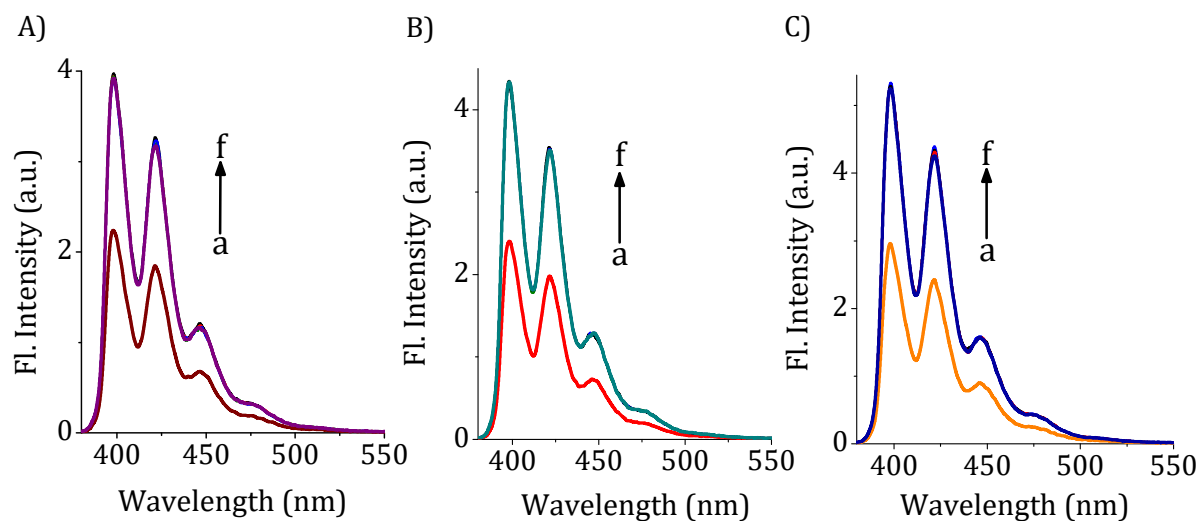


**Figure 3.8.** Changes in the fluorescence spectra of the probe **4** (5 μM) at different pH A) pH 2, B) pH 7, C) pH 12 with the addition of cyanide ions. [CN<sup>-</sup>] a) 0, and f) 50 μM. Excitation wavelength, 365 nm.

### 3.3.4. Selectivity of Detection of Cyanide Ions

To investigate the selectivity of the probes **2** and **4** towards cyanide ions, we have studied their interactions with the biologically relevant anions such as I<sup>-</sup>, Br<sup>-</sup>, Cl<sup>-</sup>, F<sup>-</sup>, ClO<sub>4</sub><sup>-</sup>, HSO<sub>4</sub><sup>-</sup>, OH<sup>-</sup>, C<sub>6</sub>H<sub>5</sub>COO<sup>-</sup>, S<sup>2-</sup>, SCN<sup>-</sup> and N<sub>3</sub><sup>-</sup> ions. The absorption and emission changes of the probes were monitored by the addition of all these competing anions. The addition of *ca.* 100-fold higher concentrations all these anions showed negligible changes in absorption and emission spectra of the complexes. These observations clearly indicate that the complexes **2** and **4** are highly selective towards cyanide ions even in the presence of other competing anions (Figures 3.9 and 3.10).

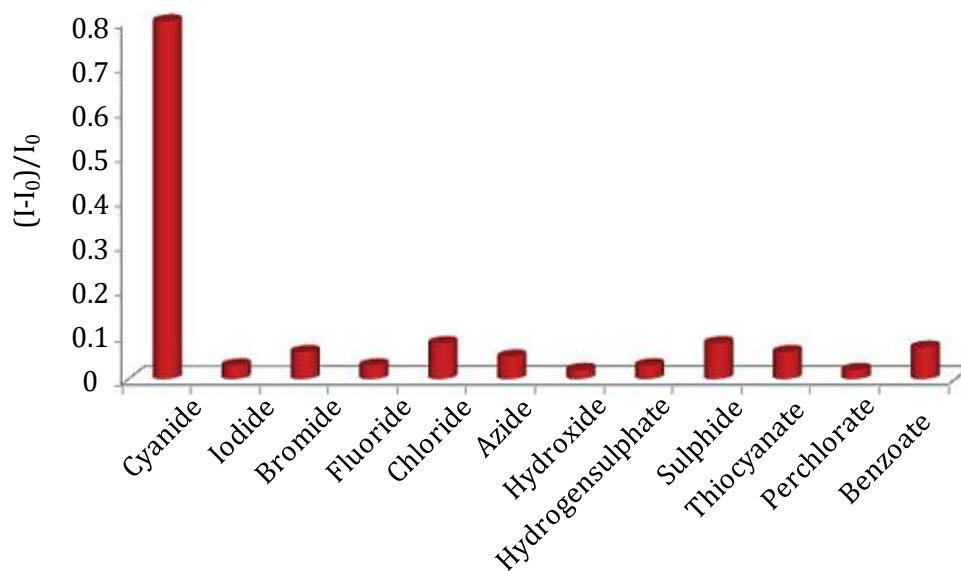


**Figure 3.9.** Selectivity plot showing the changes in the fluorescence intensity  $(I-I_0)/I_0$  of the complex **2** ( $5 \mu\text{M}$ ) with the addition of different anions. Excitation wavelength, 365 nm.

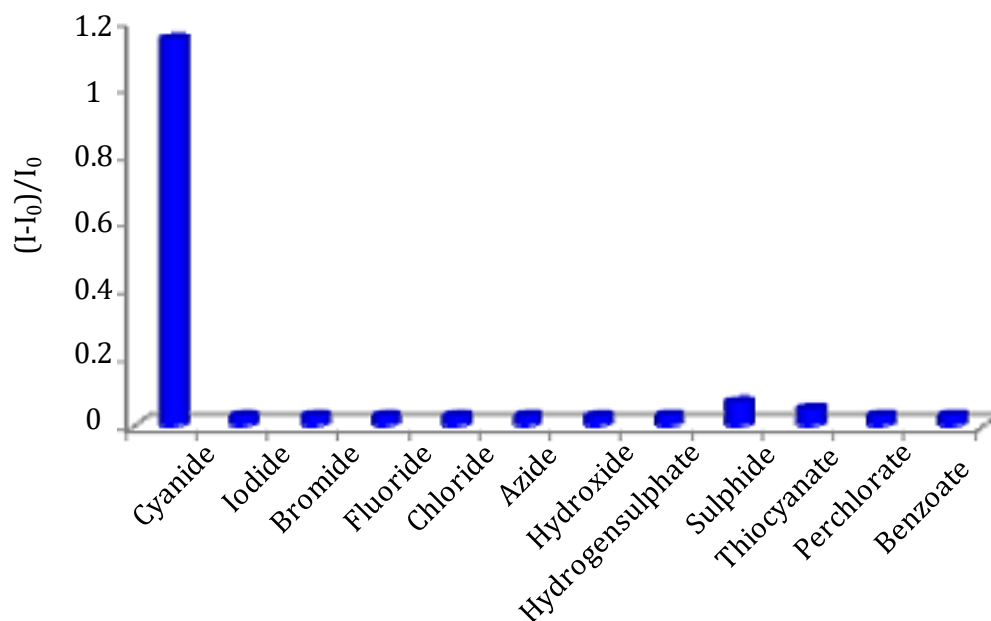


**Figure 3.10.** Selectivity plot showing the changes in the fluorescence intensity  $(I-I_0)/I_0$  of the complex **4** ( $5 \mu\text{M}$ ) with the addition of different anions. Excitation wavelength, 365 nm.

To understand the uniqueness of the probes **2** and **4**, we have investigated the interactions of the precursors **1** and **3**, which lack silver ions with various anions. Both these precursors showed negligible changes in their absorption and fluorescence spectra in the presence of all anions including  $\text{CN}^-$  ions (Figures 3.11 and 3.12).

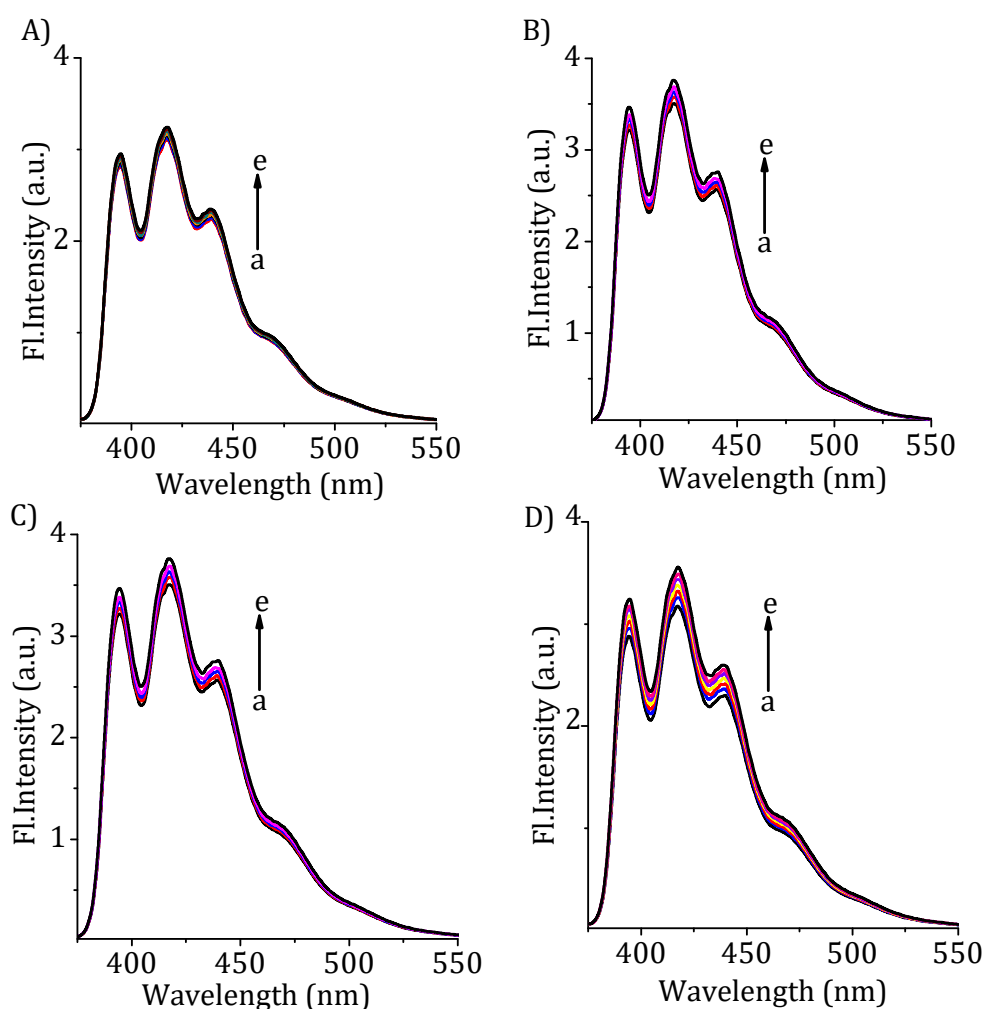


**Figure 3.11.** Emission spectral changes showing the interaction of the precursor **1** (5 μM) with the addition of various competing anions a) 0; e) 2 mM; A) cyanide ( $\text{CN}^-$ ), B) azide ( $\text{N}_3^-$ ), C) sulphide ( $\text{S}_2^-$ ) and D) thiocyanate ( $\text{SCN}^-$ ) ions. Excitation wavelength, 365 nm.

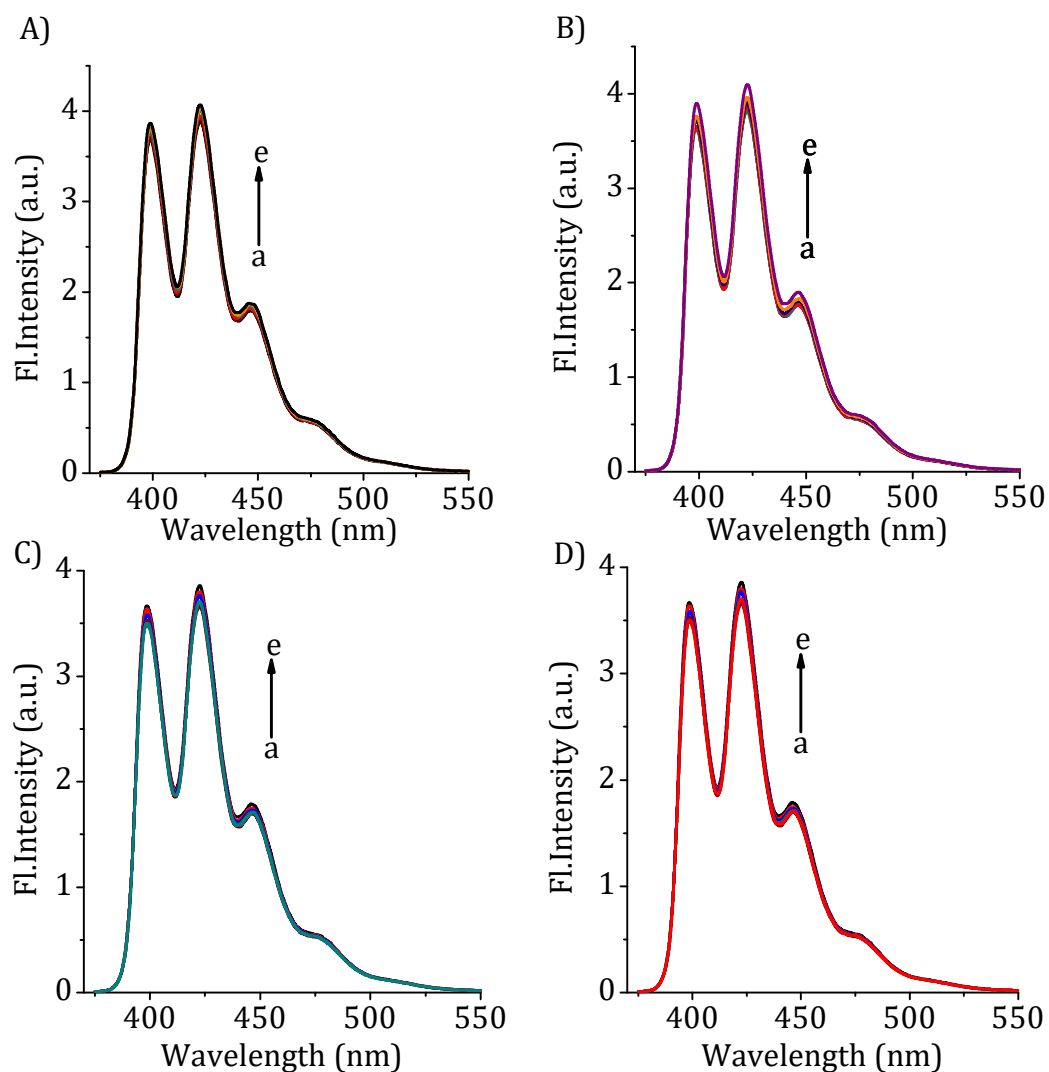


**Figure 3.12.** Emission spectral changes showing the interaction of the precursor **3** (5  $\mu\text{M}$ ) with the addition of various competing anions a) 0; e) 2 mM; A) Cyanide ( $\text{CN}^-$ ), B) sulphide ( $\text{S}_2^{2-}$ ), C) thiocyanate ( $\text{SCN}^-$ ) and D) azide ( $\text{N}_3^-$ ) ions. Excitation wavelength, 365 nm.

Furthermore to understand the interaction of the imidazolium precursor **1** with the cyanide ions, we have carried out the  $^1\text{H}$  NMR titration experiments in the presence of the cyanide ions. The negligible changes in the NMR spectra with the addition of excess cyanide ions confirm the negligible interaction between the

precursor **1** and the cyanide ions. These observations demonstrate that the *NHC* complexes **2** and **4** show selective interactions with the cyanide ions and the mechanism of the recognition is through displacement of the silver ions from the complexes. To estimate the effect of halides as competing anions, we have investigated the interactions of both the complexes with the chloride ions by  $^1\text{H}$  NMR spectroscopy. Expectedly, we observed negligible changes, which further confirm the selectivity of the cyanide ions over chloride ions.

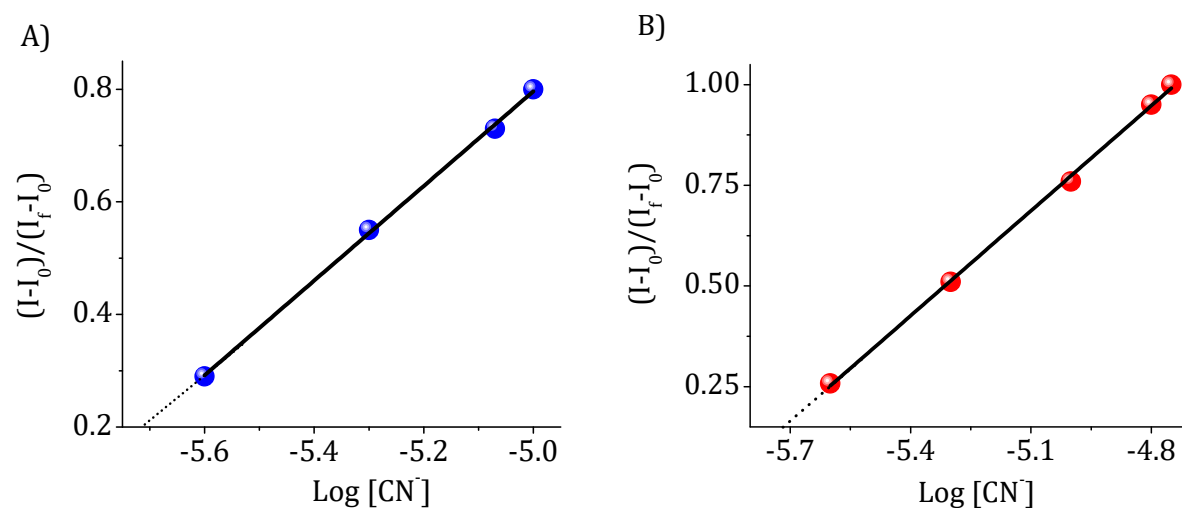


**Figure 3.13.** Calibration curve  $(I-I_0)/(I_f-I_0)$  for A) the probe **2** ( $5 \mu\text{M}$ ) and B) the probe **4** ( $5 \mu\text{M}$ ) as a function of  $[\text{CN}^-]$ , in  $\mu\text{M}$ . Excitation wavelength, 365 nm, respectively.

To determine the sensitivity of the detection, the fluorescence changes of the *NHC* complexes **2** and **4** were recorded by the addition of various concentrations of the cyanide ions. With gradual increase in the concentration of the cyanide ions, we observed a regular enhancement in the fluorescence intensity of the probes **2** and **4**.

Figure 3.13 shows the linear plots of the relative changes in fluorescence intensity vs. concentration of the cyanide ions. The limit of detection of the cyanide ions was found to be 49 (1.89  $\mu\text{M}$ ) and 50 ppb (1.94  $\mu\text{M}$ ), respectively, for **2** and **4**.

To understand the ability of these complexes in determining the concentration of the cyanide ions in an unknown sample, the concentration of the complex **2** was maintained at 5  $\mu\text{M}$ , whilst the  $\text{CN}^-$  ions concentration was varied from 0-20  $\mu\text{M}$ . The fluorescence spectra were monitored at 416 nm and the changes in the fluorescence intensity was plotted against the concentration resulting in a linear relationship (Figure 3.14). From this plot, we have determined the unknown concentration of the cyanide ions by measuring its fluorescence intensity in the aqueous medium and also in the presence of other anions.

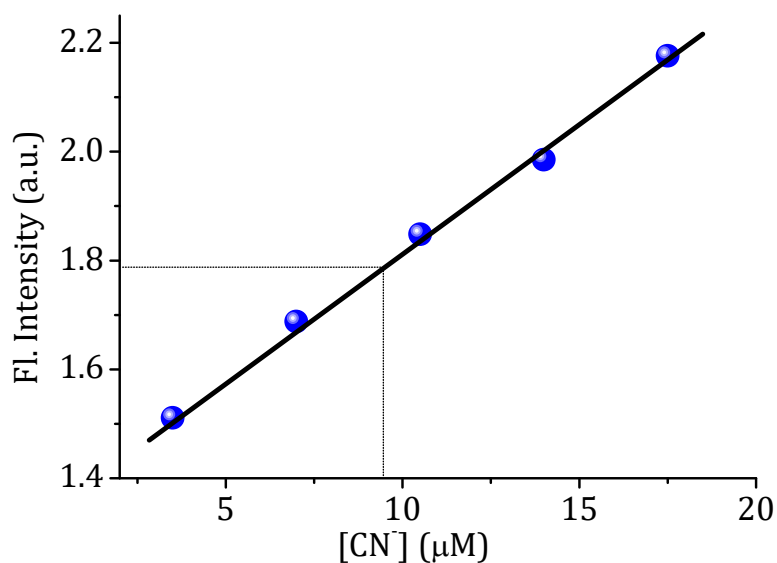


**Figure 3.14.** Linear plot between the changes in the fluorescence emission of the probe **2** (5  $\mu\text{M}$ ) at 416 nm vs cyanide ions for the quantitative estimation of the cyanide ions in water.

### 3.3.5. Mechanism of Cyanide Recognition

To gain a better understanding of the nature of interactions, we have monitored the changes in the  $^1\text{H}$  NMR spectra of the silver complexes **2** and **4** with the addition of tetrabutylammonium cyanide solution. As shown in Figure 3.15, upon addition of  $\text{CN}^-$  ions in  $\text{CD}_3\text{CN}$  at  $25^\circ\text{C}$ , we observed prominent changes in the  $^1\text{H}$  NMR spectrum of the probe **2**. On gradual addition of the cyanide ions to the probe **2**, we observed the appearance of a peak corresponding to the carbene proton ( $\text{H}_2$ ) at 8.7 ppm. Similar changes were observed in the case of the complex **4** with *ca.* 4 equivalents of  $\text{CN}^-$  ions.

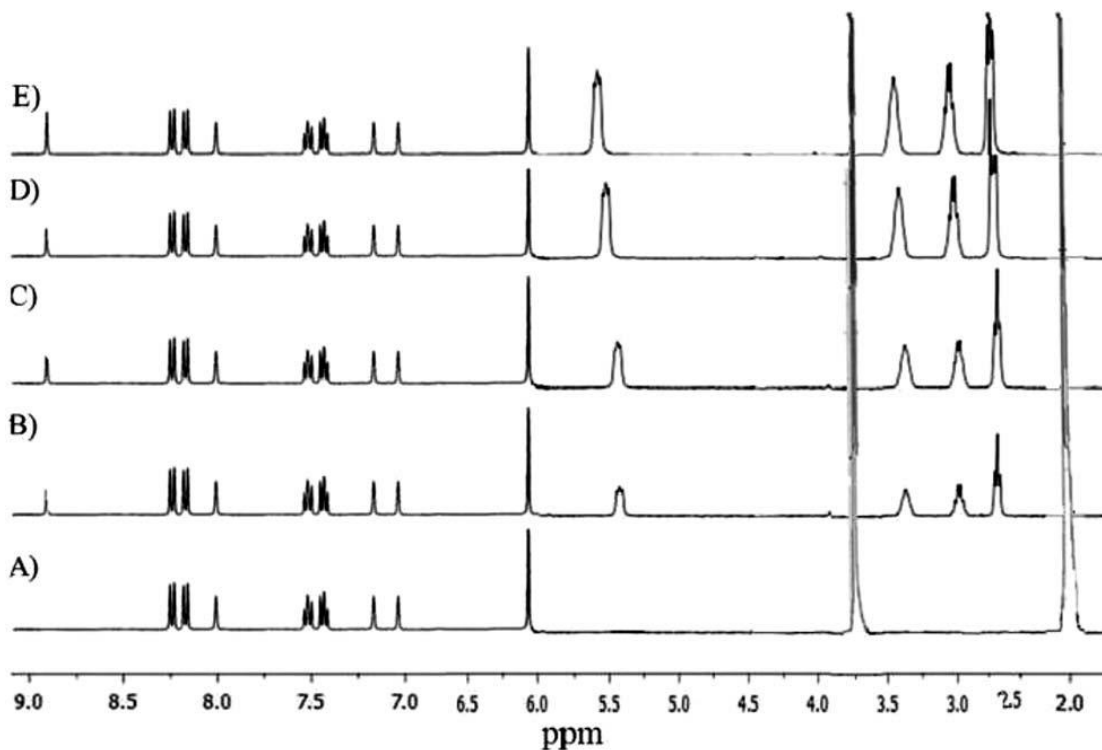


**Figure 3.15.**  $^1\text{H}$  NMR spectra of A) the probe **2** alone and (B-E) with the addition of different concentrations of tetrabutylammoniumcyanide solution in  $\text{CD}_3\text{CN}$ .



The authenticity of the reaction was also confirmed by isolating the product, after the addition of the excess  $\text{CN}^-$  ions to the complexes **2** and **4**. The  $^1\text{H}$  NMR spectra of the isolated products were found to be essentially identical to those of the precursors **1** and **3**. These results clearly indicate that the imidazolium precursors **1** and **3** were regenerated due to the decomplexation of the complexes **2** and **4**, respectively, upon reaction with the cyanide ions. The observation of enhanced fluorescence intensity upon addition of  $\text{CN}^-$  ions furthermore confirms the decomplexation of the silver complexes **2** and **4** in the presence of the strong nucleophilic cyanide ions.

The interaction between the silver *NHC* complexes **2** and **4** with the cyanide ions was subsequently analyzed through picosecond time-resolved fluorescence analysis. The complex **2** exhibited a mono-exponential decay with an excited state lifetime of  $7.1 \pm 0.05$  ns in the aqueous medium. Upon addition of saturated amount of tetrabutylammonium cyanide solution ( $20 \mu\text{M}$ ) to this complex resulted in a new species with an increase in the excited state lifetime of  $8.07 \pm 0.01$  ns. To check the nature of the new species that was formed after the reaction, we have recorded the lifetime of the corresponding imidazolium precursor **1**. The precursor **1** showed a mono-exponential decay with an excited state lifetime of  $8.08 \pm 0.01$  ns, which is identical to the species obtained after the addition of the cyanide ions to the complex **2** (Figure 3.16A). Similar experiments were carried out in the case of the complex **4**. Interestingly, the complex **4** showed a mono-exponential decay with an excited state lifetime of  $8.11 \pm 0.03$  ns. After addition of the cyanide ions, the fluorescence lifetime

of the complex was changed to  $8.19 \pm 0.03$  ns and which correspond to the imidazolium precursor **3** ( $8.21 \pm 0.01$  ns) (Figure 3.16B). These results also confirm the formation of the imidazolium precursors **1** and **3** after the decomplexation of the NHC complexes **2** and **4**, respectively, upon interaction with the cyanide ions.

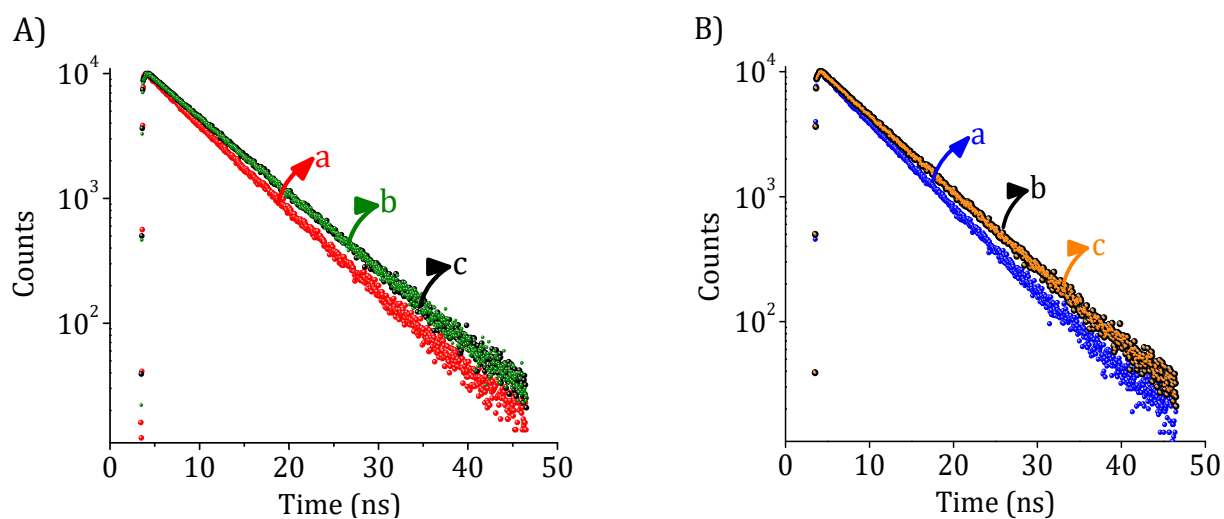
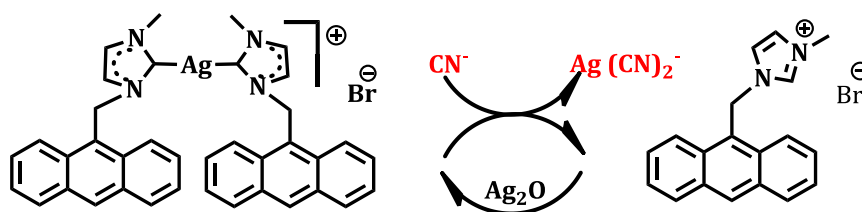


**Figure 3.16.** Lifetime profiles monitored at 416 nm A) the complex **2** ( $5 \mu\text{M}$ ): a) alone, b) after the addition of cyanide ions and c) the imidazolium precursor **1** ( $5 \mu\text{M}$ ) and B) the complex **4** ( $5 \mu\text{M}$ ): a) alone, b) after the addition of cyanide ions and c) the imidazolium precursor **3** ( $5 \mu\text{M}$ ), respectively, in the aqueous medium.

Scheme 3.3 shows the proposed mechanism of the decomplexation of the probe **2** by the addition of the cyanide ions. Even though the metal-carbon bond is quite strong, the highly nucleophilic cyanide ions could easily cull the silver ion from the complex through the formation of the highly fluorescent imidazolium precursor **1** and the stable soluble  $\text{Ag}(\text{CN})_2^-$  salt. The plot between the relative changes in the fluorescence intensity versus concentration of the cyanide ions for the complex **4**

showed a sigmoidal nature, which may be due to the stepwise cleavage of the Ag–C bond in the sensing mechanism.<sup>25</sup> These results, thus demonstrate that the strong binding affinity of the silver ions towards the CN<sup>-</sup> ions make the probes **2** and **4** as efficient chemodosimeters for the recognition of the cyanide ions.

#### Mechanism of Cyanide detection



**Scheme 3.3.** Possible mechanism for the detection of CN<sup>-</sup> ions using the probe **2**.

### 3.4. Conclusions

In conclusion, we have developed two novel silver N-heterocyclic carbene based complexes that possess the anthracene chromophore as the optically active unit. These probes exhibited good solubility in the aqueous medium and high selectivity towards the cyanide ions, when compared to other biologically relevant anions in the aqueous medium. Uniquely these probes act as chemodosimeters for the cyanide ions with a sensitivity as low as *ca.* 50 ppb (LOD = 50 ppb) and signal the event through the visible enhancement in the fluorescence intensity.

## 3.5. Experimental Section

### 3.5.1. General Techniques

The melting points were determined on a Mel-Temp II melting point apparatus and details of various equipments were published elsewhere. The IR spectra were recorded on a Perkin Elmer Model 882 infrared spectrometer. The electronic absorption spectra were recorded on a Shimadzu UV-3101 or 2401 PC UV-VIS-NIR scanning spectrophotometer.<sup>26</sup> The fluorescence spectra were recorded on a SPEX-Fluorolog F112X spectrofluorimeter. <sup>1</sup>H and <sup>13</sup>C NMR were recorded on a 500 MHz Bruker advanced DPX spectrometer. MALDI-TOF MS analysis was performed with a Shimadzu Biotech Axima CFR plus instrument equipped with a nitrogen laser in the linear mode. All the solvents used were purified and distilled before use. Quantum yields of fluorescence were measured by the relative methods using optically dilute solutions. The quantum yields of fluorescence were calculated using quinine sulphate ( $\Phi_F = 0.54$ ; in 0.1 N H<sub>2</sub>SO<sub>4</sub>) as the standard and as per the equation 3.1,

$$\Phi_u = \frac{A_s F_u n_u^2}{A_u F_s n_s^2} \Phi_s \quad \text{----- (eq 3.1)}$$

wherein,  $A_s$  and  $A_u$  are the absorbance of the standard and unknown, respectively.  $F_s$  and  $F_u$  are the areas of fluorescence peaks of the standard and unknown and  $n_s$  and  $n_u$  are the refractive indices of the solvents used for the standard and unknown, respectively.  $\Phi_s$  and  $\Phi_u$  are the fluorescence quantum yields of the standard and unknown. The fluorescence lifetimes were measured using IBH picoseconds time correlated single

photon counting system. The fluorescence decay profiles were deconvoluted using IBH datastation software V2.1 and minimizing the  $\chi^2$  values of the fit to  $1 \pm 0.1$ . Doubly distilled water was used for all the studies and all experiments were carried out at room temperature ( $25 \pm 1$  °C), unless otherwise mentioned.

### 3.5.2. Materials and Methods

Anthracene, N-methylimidazole, HBr in acetic acid, paraformaldehyde, anthracenemethanol, phosphorous tribromide, silveroxide, tetrabutylammonium cyanide, tetrabutylammonium chloride, tetrabutylammonium iodide, sodium sulphide, ammonium thiocyanate, tetrabutylammonium bromide, tetrabutylammonium azide, tetrabutylammonium hydroxide, tetrabutylammonium hydrogensulphate, tetrabutylammonium benzoate, tetrabutylammonium perchlorate, and tetrabutylammonium fluoride were purchased from Aldrich and S. D. Fine Chemicals, India and used as received.

### 3.5.3. Synthesis of the Compounds 1-4

**3.5.3.1. Synthesis of the Imidazolium Precursor 1.** To a mixture of N-methylimidazole (90 mg, 1.102 mmol) in dry acetonitrile (30 mL) was added 9-bromomethylantracene (200 mg, 0.735 mmol) and the reaction mixture was then refluxed for 24 h at 80 °C. The reaction mixture was then filtered and washed thoroughly with acetonitrile and dried. The product was further purified by recrystallization from acetonitrile to give 190 mg (61%) of the precursor **1**. Mp 245-269 °C;  $^1\text{H}$  NMR (500 MHz,  $\text{D}_2\text{O}$ , TMS)  $\delta$  3.67 (s, 3H), 6.31 (s, 2H), 7.37 (s, 1H), 7.46 (s, 1H), 7.64-7.62 (t, 2H,  $J = 15$

Hz), 7.69-7.67 (t, 2H, J = 15 Hz), 8.23-8.22 (d, 2H, J = 8.5 Hz), 8.28-8.26 (d, 2H, J = 9 Hz), 8.82 (s, 1H);  $^{13}\text{C}$  NMR (125 MHz,  $\text{CD}_3\text{CN}$ )  $\delta$  35.5, 45.2, 120.4, 122.5, 123.4, 125.3, 128.1, 129.2, 130.6, 135.3; HRMS (FAB): Calcd for  $\text{C}_{19}\text{H}_{17}\text{N}_2$ , 273.139; Found, 273.138 ( $\text{M}^+$ ).

**3.5.3.2. Synthesis of the NHC Probe 2.** To a solution of imidazolium precursor **1** (100 mg, 0.239 mmol) in dry acetonitrile (20 mL) was added  $\text{Ag}_2\text{O}$  (27.7 mg, 0.119 mmol). The reaction mixture was then refluxed under argon atmosphere at 80 °C for 20 h. The reaction mixture was then passed through celite and the solution was concentrated and dried. The complex was then subjected to counter ion exchange with silver hexafluorophosphate followed by tetrabutylammonium bromide to yield the NHC complex **2** in 70% yield. Mp > 300 °C;  $^1\text{H}$  NMR (500 MHz,  $\text{D}_2\text{O}$ , TMS)  $\delta$  3.71 (s, 3H), 6.45 (s, 2H), 7.40 (s, 1H), 7.49 (s, 1H), 7.67-7.64 (t, 2H, J = 8 Hz), 7.73-7.70 (t, 2H, J = 8.5 Hz), 8.27-8.15 (d, 2H, J = 7.5 Hz), 8.31-8.29 (d, 2H, J = 9 Hz),  $^{13}\text{C}$  NMR (125 MHz,  $\text{CD}_3\text{CN}$ )  $\delta$  38.2, 45.9, 120.4, 122.5, 123.4, 125.3, 128.1, 129.2, 130.6, 179.5; MALDI-TOF MS: Calcd for  $\text{C}_{38}\text{H}_{32}\text{N}_4\text{AgBr}$ , 732.09; Found, 732.00 ( $\text{M}^+$ ). Elemental Anal. Calcd for  $\text{C}_{38}\text{H}_{32}\text{AgBrN}_4$  (%): C, 62.14; H, 4.67; N, 7.63. Found: C, 62.04; H, 4.62; N, 7.59.

**3.5.3.3. Synthesis of the Imidazolium Precursor 3.** To a mixture of N-methylimidazole (112 mg, 1.37 mmol) in dry acetonitrile (30 mL) was added 9,10-dibromomethylantracene (200 mg, 0.549 mmol). The reaction mixture was refluxed for 24 h at 80 °C and then filtered and washed thoroughly with acetonitrile and dried. The product was further purified by recrystallization from acetonitrile to give 230 mg (63%) of the precursor **3**. Mp 255-282 °C;  $^1\text{H}$  NMR (300 MHz,  $\text{D}_2\text{O}$ , TMS)  $\delta$  3.69 (s, 3H), 6.39 (s, 2H), 7.32 (s, 1H), 7.35 (s, 1H), 7.76-7.73 (m, 2H), 8.14 (s, 1H), 8.40-8.37 (m, 2H);  $^{13}\text{C}$  NMR

(125 MHz, CD<sub>3</sub>CN)  $\delta$  35.9, 45.6, 122.3, 124, 126.1, 128.0, 131.0, 135.9; HRMS (FAB): Calcd for C<sub>24</sub>H<sub>24</sub>N<sub>4</sub>Br, 447.118; Found, 447.117 (M<sup>++</sup>Br).

**3.5.3.4. Synthesis of the NHC Probe 4.** To a solution of the imidazolium precursor **3** (100 mg, 0.151 mmol) in dry acetonitrile (30 mL) was added Ag<sub>2</sub>O (70.7 mg, 0.303 mmol). The reaction mixture was then refluxed under argon at 80 °C for 20 h. The reaction mixture was then passed through celite and the solution was concentrated and dried. The complex was then subjected to counter ion exchange with silver hexafluorophosphate followed by tetrabutylammonium bromide to yield the NHC complex **4** in 69% yield. Mp > 330 °C; <sup>1</sup>H NMR (500 MHz, D<sub>2</sub>O, TMS)  $\delta$  3.69 (s, 3H), 6.32 (s, 2H), 7.37 (s, 1H), 7.42 (s, 1H), 7.75-7.73 (m, 2H), 8.34-8.32 (m, 2H); <sup>13</sup>C NMR (125 MHz, CD<sub>3</sub>CN)  $\delta$  38.6, 45.6, 122.2, 124.6, 126.7, 127.5, 128.8, 130.8, 179.9; MALDI-TOF-MS: Calcd for C<sub>48</sub>H<sub>46</sub>N<sub>8</sub>Ag<sub>2</sub>, 950.19; Found, 951.53 (M<sup>++1</sup>). Elemental Anal. Calcd for C<sub>48</sub>H<sub>44</sub>Ag<sub>2</sub>Br<sub>2</sub>N<sub>8</sub> (%): C, 51.82; H, 4.35; N, 10.07. Found: C, 51.79; H, 4.33; N, 10.04.

**3.5.3.5. Calculation of Limit of Detection (LOD).** To determine the sensitivity of the detection, the fluorescence changes of the NHC complexes were recorded by the addition of various concentrations of the cyanide ions. The limit of detection (LOD) was calculated by plotting a graph between  $(I-I_0)/(I_f-I_0)$  versus the log [CN<sup>-</sup>], wherein 'I<sub>0</sub>' represents the fluorescence intensity of the complex alone, 'I' is the fluorescence intensity at each addition of the cyanide ions and 'I<sub>f</sub>' is the fluorescence intensity at the final addition of the cyanide ions. By extrapolating, the straight line plot to the X-axis gave the logarithmic value of LOD, from which, the value of LOD was determined.

### 3.6. References

1. (a) Beer, P. D.; Gale, P. A. *Angew. Chem. Int. Ed.* **2001**, *40*, 486. (b) Martínez-Máñez, R.; Sancenón, F. *Chem. Rev.* **2003**, *103*, 4419. (c) Amendola, V.; Esteban-Gómez, D.; Fabbrizzi, L.; Licchelli, M. *Acc. Chem. Res.* **2006**, *39*, 343.
2. (a) Duke, R. M.; Gunnlaugsson, T. *Tetrahedron Lett.* **2010**, *51*, 5402. (b) Park, J.; Kim, H.; Choi, Y.; Kim, Y. *Analyst* **2013**, *138*, 3368. (c) Wu, M.-Y.; He, T.; Li, K.; Wu, M.-B.; Huang, Z.; Yu, X.-Qi. *Analyst* **2013**, *138*, 3018. (d) Ramaiah, D.; Neelakandan, P. P.; Nair, A. K.; Avirah, R. R. *Chem. Soc. Rev.* **2010**, *39*, 4158.
3. (a) Badugu, R.; Lakowicz, J. R.; Geddes, C. D. *J. Am. Chem. Soc.* **2005**, *127*, 3635. (b) Croise, C. M.; Zelder, F. *ACS Appl. Mater. Interfaces* **2012**, *4*, 725. (c) Dai, Z.; Boon, E. M. *J. Am. Chem. Soc.* **2010**, *132*, 11496. (d) Croise, C. M.; Zelder, F. *Inorg. Chem.* **2009**, *48*, 1272.
4. (a) Gotor, R.; Costero, A. M.; Gil, S.; Parra, M.; Manez, R. M.; Sancenon, F.; Gavina, P. *Chem. Commun.* **2013**, *49*, 5669. (b) Blackledge, W. C.; Blackledge, C. W.; Griesel, A.; Mahon, S. B.; Brenner, M.; Pilz, R. B.; Boss, G. R. *Anal. Chem.* **2010**, *82*, 4216. (c) Panda, C.; Dhar, B. B.; Malvi, B.; Bhattacharjee, Y.; Gupta, S. S. *Chem. Commun.* **2013**, *49*, 2216.
5. (a) Lou, X.; Ou, D.; Li, Q.; Li, Z. *Chem. Commun.* **2012**, *48*, 8462. (b) Lou, X.; Qin, J.; Li, Z. *Analyst* **2009**, *134*, 2071. (c) Cambal, L. K.; Swanson, M. R.; Yuan, Q.; Weitz, A. C.; Li, H. H.; Pitt, B. R.; Pearce, L. L.; Peterson, J. *Chem. Res. Toxicol.* **2011**, *24*, 1104.



6. (a) Guidelines for Water Reuse, U.S. Environmental Protection Agency, EPA/625/R-04/108-2004., Washington, DC. (b) Radhakumary, C.; Sreenivasan, K. *Analyst* **2012**, *137*, 5387. (c) Qian, G.; Li, X.; Wang, Z. Y. *J. Mater. Chem.* **2009**, *19*, 522. (d) Gee, H. C.; Lee, C. H.; Jeong, Y. H.; Dong, W. *Chem. Commun.* **2011**, *47*, 11963.
7. (a) Young, C.; Tidwell, L.; Anderson, C. in *Cyanide: Social, Industrial, and Economic Aspects*, Minerals, Metals, and Materials Society, Warrendale, **2001**. (b) Palomares, E.; Martinez-Diaz, M. V.; Torres, T.; Coronado, E. *Adv. Funct. Mater.* **2006**, *16*, 1166.
8. Xu, Z.; Chen, X.; Kim, H. N.; Yoon, J. *Chem. Soc. Rev.* **2010**, *39*, 127.
9. (a) Jo, J.; Lee, D. *J. Am. Chem. Soc.* **2009**, *131*, 16283. (b) Kim, Y.; Zhao, H.; Gabbi, F. *Angew. Chem., Int. Ed.* **2009**, *48*, 4957. (c) Shankar, B. H.; Ramaiah, D. *J. Phys. Chem. B* **2011**, *115*, 13292. (d) Divya, K. P.; Sreejith, S.; Balakrishna, B.; Jayamurthy, P.; Anees, P. *Chem. Commun.* **2010**, *46*, 6069.
10. (a) Avirah, R. R.; Jyothish, K.; Ramaiah, D. *Org. Lett.* **2007**, *9*, 121. (b) Iashin, V.; Koso, T. V.; Stranius, K.; Muuronen, M.; Heikkinen, S.; Kavakka, J.; Tkachenko, N. V.; Helaja, J. *RSC Adv.* **2013**, *3*, 11485. (c) Chang, J.; Lu, Y.; He, S.; Liu, C.; Zhao, L.; Zeng, X. *Chem. Commun.* **2013**, *49*, 6259.
11. (a) Ghosh, A.; Joy, A.; Schuster, G. B.; Douki, T.; Cadet, J. *Org. Biomol. Chem.* **2008**, *6*, 916. (b) Lee, J. H.; Jeong, A. R.; Shin, I. S.; Kim, H. J.; Hong, J. I. *Org. Lett.* **2010**, *12*, 764. (c) Zheng, S.; Lynch, P. L. M.; Rice, T. E.; Moody, T. S.; Gunaratne, H. Q. N.; de Silva, A. P. *Photochem. Photobiol. Sci.* **2012**, *11*, 1675. (d) Miyaji, H.; Kim, H. K.; Sim,

- E. K.; Lee, C. K.; Cho, W. S.; Sessler, J. L.; Lee, C. H. *J. Am. Chem. Soc.* **2005**, *127*, 12510. (e) Shang, L.; Jin, L.; Dong, S. *Chem. Commun.* **2009**, 3077.
12. (a) Kuruvilla, E.; Nandajan, P. C.; Schuster, G. B.; Ramaiah, D. *Org. Lett.* **2008**, *10*, 4295. (b) Jin, J.; Zhang, J.; Zou, L.; Tian, H. *Analyst* **2013**, *138*, 1641. (c) Nair, A. K.; Neelakandan, P. P.; Ramaiah, D. *Chem. Commun.* **2009**, 6352.
13. (a) de Silva, A. P.; Gunaratne, H. Q. N.; Gunnlaugsson T.; Huxley, A. J. M.; McCoy, C. P.; Rademacher, J. T.; Rice, T. E. *Chem. Rev.* **1997**, *97*, 1515. (b) Liu, X.-L.; Duan, X.-Y.; Du, X.-J.; Song, Q.-H. *Chem. Asian J.* **2012**, *7*, 2696. (c) Shankar, B. H.; Ramaiah, D. *J. Phys. Chem B* **2011**, *115*, 13292. (d) Jisha, V. S.; Arun, K. T.; Hariharan, M.; Ramaiah, D. *J. Am. Chem. Soc.* **2006**, *128*, 6024. (e) Nandajan, P. C.; Neelakandan, P. P.; Ramaiah, D. *RSC Adv.* **2013**, *3*, 5624. (f) Wang, C.; Xu, L.; Wang, Y.; Zhang, D.; Shi, X.; Dong, F.; Yu, K.; Lin, Q.; Yang, B. *Chem. Asian J.* **2012**, *7*, 1652.
14. (a) Figueroa, L. E. S.; Moragues, M. E.; Climent, E.; Agostini, A.; Manez, R. M.; Sancenon, F. *Chem. Soc. Rev.* **2013**, *42*, 3489. (b) Jun, M. E.; Roy, B.; Ahn, K. H. *Chem. Commun.* **2011**, 47, 7583.
15. (a) Neelakandan, P. P.; Ramaiah, D. *Angew. Chem., Int. Ed.* **2008**, *47*, 8407. (b) Kuruvilla, E.; Ramaiah, D. *J. Phys. Chem. B* **2007**, *111*, 6549. (c) Song, K. C.; Kim, J. S.; Park, S. M.; Chung, K. C.; Ahn, S.; Chang, S. K. *Org. Lett.* **2006**, *8*, 3413.
16. (a) Han, M. S.; Kim, D. H. *Angew. Chem.* **2002**, *114*, 3963. (b) Jose, D. A.; Mishra, S.; Ghosh, A.; Shrivastav, A.; Mishra S. K.; Das, A. *Org. Lett.* **2007**, 1979. (c) Niu, H. T.; Su, D.; Jiang, X.; Yin, Y. Z.; He, J.; Cheng, J. P. *Org. Biomol. Chem.* **2008**, *6*, 3038. (d)

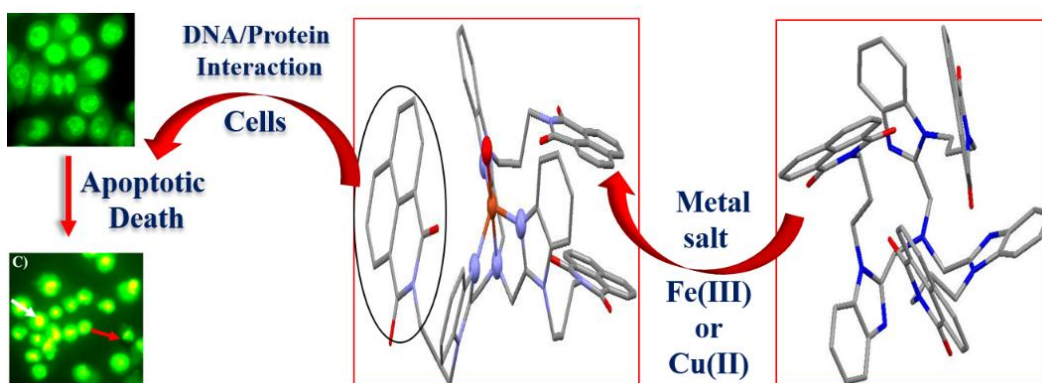
- Quinlan, E.; Matthews, S. E.; Gunnlaugsson, T. *J. Org. Chem.* **2007**, *72*, 7497. (e) Cho, E. J.; J. Ryu, B.; Lee, Y. J.; Nam, K. C. *Org. Lett.* **2005**, *7*, 2607.
17. (a) Gunnlaugsson, T.; Kruger, P. E.; Lee, T. C.; Parkesh R.; Pfeffera, F. M.; Husseya, G. M. *Tetrahedron Lett.* **2003**, *44*, 6575. (b) Liu, Y.; Li, Z.; Zhang, H. Y.; Wang, H.; Li, C. J. *J. Supramol. Chem.* **2008**, *20*, 419. (c) Comes, M.; Marcos, M. D.; Manez, R. M.; Sancenon, F.; Soto, J.; Villaescusa L. A.; Amoros, P. *Chem. Commun.* **2008**, 3639.
18. (a) Wang, L.; He, X.; Guo, Y.; Xua, J.; Shao, S. *Org. Biomol. Chem.* **2011**, *9*, 752. (b) Lin, Y. D.; Pen, Y. S.; Su, W.; Liau, K. L.; Wen, Y. S.; Tu, C. H.; Sun C. H.; Chow, T. *Chem.–Asian J.* **2012**, *7*, 2864. (c) Adarsh, N.; Avirah R. R.; Ramaiah, D. *Org. Lett.* **2010**, *12*, 5720.
19. (a) Du, J.; Hu, M.; Fan, J. Peng, X. *Chem. Soc. Rev.* **2012**, *41*, 4511. (b) Chan, J.; Dodani, S. C.; Chang, C. J. *Nat. Chem.* **2012**, *4*, 973.
20. (a) Hajizadeh, S.; Farhadi, K.; Forough, M.; Sabzi, R. E. *Anal. Methods* **2011**, *3*, 2599. (b) Jamkratoke, M.; Ruangpornvisuti, V.; Tumcharern, G.; Tuntulani; T. Tomapatanaget, B. *J. Org. Chem.* **2009**, *74*, 3919.
21. (a) Lee, K. S.; Kim, H. J.; Kim, G. H.; Shin, I.; Hong, J. I. *Org. Lett.* **2008**, *10*, 49. (b) Yuan, L.; Lin, W.; Yang, Y.; Song, J.; Wang, J. *Org. Lett.* **2011**, *13*, 3730.
22. (a) Cho, D. G.; Kim, J. H.; Sessler, J. L. *J. Am. Chem. Soc.* **2008**, *130*, 12163. (b) Sessler J. L.; Cho, D. G. *Org. Lett.* **2008**, *10*, 73.

23. (a) Jung, H. S.; Han, J. H.; Kim, Z. H.; Kang, C.; Kim, J. S. *Org. Lett.* **2011**, *13*, 5056. (b) Guliyev, R.; Buyukcakil, O.; Sozmen, F.; Bozdemir, O. A., *Tetrahedron Lett.* **2009**, *50*, 5139.
24. (a) Vougioukalakis, G. C.; Grubbs, R. H. *Chem. Rev.* **2010**, *110*, 1746. (b) Wan, X.; Xu, F.; Zhang, Z.; Song, H. Z. *Anorg. Allg. Chem.* **2011**, *637*, 34. (c) Jyothish, K.; Avirah, R. R.; Ramaiah, D. *Org. Lett.* **2006**, *8*, 111.
25. Snehadrinarayan, K.; Debabrata, S.; Jan, W. B.; Michael, S. *Inorg. Chem.* **2012**, *51*, 7075.
26. (a) Jisha, V. S.; Thomas, A. J.; Ramaiah, D. *J. Org. Chem.* **2009**, *74*, 6667. (b) Nair, A. K.; Neelakandan, P. P.; Ramaiah, D. *Chem. Commun.* **2009**, 6352.

---

**DESIGN OF IRON(III) AND COPPER(II) COMPLEXES : STUDY OF THEIR PHOTOPHYSICAL AND BIOLOGICAL PROPERTIES**

---



### 4.1. Abstract

We synthesized two novel biomimetic mononuclear complexes,  $[\text{Fe}(\mathbf{3})\text{Cl}_2]^+$  (**1**) and  $[\text{Cu}(\mathbf{3})(\text{H}_2\text{O})]^{2+}$  (**2**) based on naphthalimide appended tripodal tetradentate ligand (**3**) and have investigated their photophysical and biological properties. The structures of the complexes were established on the basis of analytical and spectroscopic evidences. In addition, structures of the ligand **3** and complex **2** were established unambiguously through single crystal X-ray analysis. Uniquely, the coordination with a metal ion enhanced the ligand scaffold to interact efficiently with biopolymers such as ct-DNA (groove binding) as well as protein (hydrophobic and/or electrostatic interactions). We have determined the affinity of these complexes for DNA/protein and the values are found to be in the range,  $K_{DNA} = 0.34\text{-}1.01 \times 10^4 \text{ M}^{-1}$  and  $K_{BSA} = 4.1\text{-}5.0 \times 10^5 \text{ M}^{-1}$ .

Furthermore, the fluorescence quenching of BSA with complexes **1** and **2** occurs through a static mechanism and affects the conformation of BSA around the tryptophan residues. The *in vitro* biological studies of these systems employing HeLa cell lines indicated that both these complexes exhibited enhanced cytotoxicity ( $IC_{50} = 32 \pm 0.19$  and  $10 \pm 0.21$   $\mu\text{M}$  for complexes **1** and **2**, respectively), when compared to the ligand **3** ( $IC_{50} = 150$   $\mu\text{M}$ ). Interestingly, both the complexes **1** and **2** were found to be non-toxic to normal H9c2 cell lines. The mechanism of *in vitro* biological activity of these complexes has been evaluated through a variety of techniques: acridine orange/ethidium bromide, DAPI staining studies, annexin V-FITC/PI and poly(ADPribose)- polymerase (PARP) cleavage, which confirmed the apoptotic mediated cell death. Our results demonstrate the importance of complexation of the naphthalimide ligand **3** as well as the potential of these biomimetic metal complexes as cytotoxic and anticancer agents.

## 4.2. Introduction

Recently, considerable attention has been devoted to develop metallo-drugs that can interact with molecular targets such as DNA and proteins, because of their applications as anticancer agents.<sup>1</sup> The majority of DNA targeted anticancer drugs bind through covalent and/or non-covalent modes (electrostatic, groove and intercalation).<sup>2</sup> Of these, cisplatin and its analogues, which are in clinical use interact through a dual DNA binding mode (intercalation and crosslinks).<sup>3</sup> However, their use is limited by dose-limiting side-effects such as neuro-, oto-, hepato- and nephrotoxicity due to the presence of heavy metal ions. The drawbacks associated with the platinum based drugs have prompted the search for more effective, less noxious and target specific anticancer drugs

derived from transition-metal ions. In this context, the development of biomimetic-metal complexes with versatile properties and potential to bind DNA and proteins through a multitude of interactions as anticancer drugs has been an active area of research.

In our quest to design potent anticancer agents, we have synthesized a tripodal tetradentate ligand having benzimidazole nitrogen donors.<sup>4</sup> To enhance the efficiency of the benzimidazole based ligand, we tethered it with biologically active naphthalimide units. The naphthalimide derivatives are an important class of DNA intercalating drugs, which are known to exhibit high anticancer activity.<sup>5</sup> For example, the naphthalimide based amonafide (Quinamed®) and mitonafide have entered into phase II clinical trials and both these drugs efficiently bind to DNA via intercalation and inhibit topoisomerase II activity.<sup>5</sup> Among the various systems developed, the use of mixed-ligand metal complexes as well as coordinating the ligand with biologically active units have acquired much attention in recent years. For example, Gunnlaugsson *et al.*, have reported the first examples of monomeric mixed ligand platinum and ruthenium complexes having a naphthalimide chromophore.<sup>6</sup> These systems exhibited high binding affinity for DNA and displayed cytotoxicity through apoptosis in MCF-7 and HeLa cell lines. Also the transition metal based scorpionates having a naphthalimide chromophore (as an intercalator) showed high binding affinity towards ct-DNA ( $K_{DNA} = 10^5 \text{ M}^{-1}$ ).<sup>6</sup> A similar approach was adopted by Dyson *et al.*, for ruthenium(II) arene complexes, where the intercalating moiety (naphthalimide) along with the binding ability of ruthenium(II) arene moiety with proteins led to their enhanced cytotoxicity.<sup>6</sup>

Several reports were also available on metal complexes, wherein the biologically active molecule was covalently linked to the coordinating ligands.<sup>6</sup> Apart from DNA, proteins are also prime molecular targets to improve the effectiveness of the anticancer metallo-drugs and to understand overall drug distribution, excretion, activity and toxicity.<sup>7</sup> Serum albumin, the major constituent of blood plasma is the major transport protein, which helps in the translocation of several compounds to specific targets. BSA has 80% structural homology to serum albumin and the molecular interaction of compounds with BSA is effected through the binding sites in the hydrophobic cavities. This interaction helps to deliver the drugs to the designated area during therapy.<sup>7</sup> Herein, we report the synthesis of two novel biomimetic metal complexes **1** and **2** coordinated to a tripodal tetradentate ligand **3**, appended with three naphthalimide moieties (Chart 4.1) and have investigated their interactions with DNA/proteins and *in vitro* biological activity. Uniquely, the metal coordination modified the ligand scaffold to interact efficiently with other chromophores present as well as with DNA and proteins and induced cell death through the apoptotic pathway.

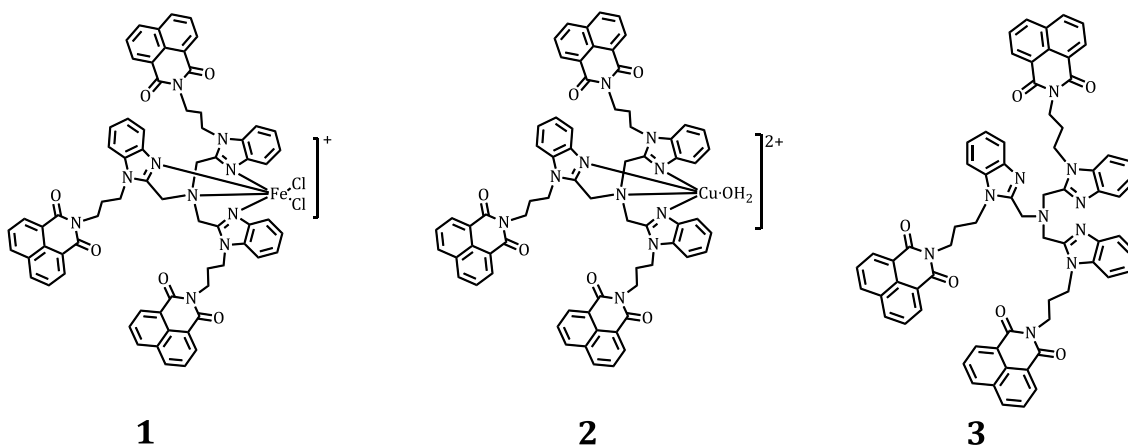


**Chart 4.1.** Structures of the compounds **1-3** investigated.



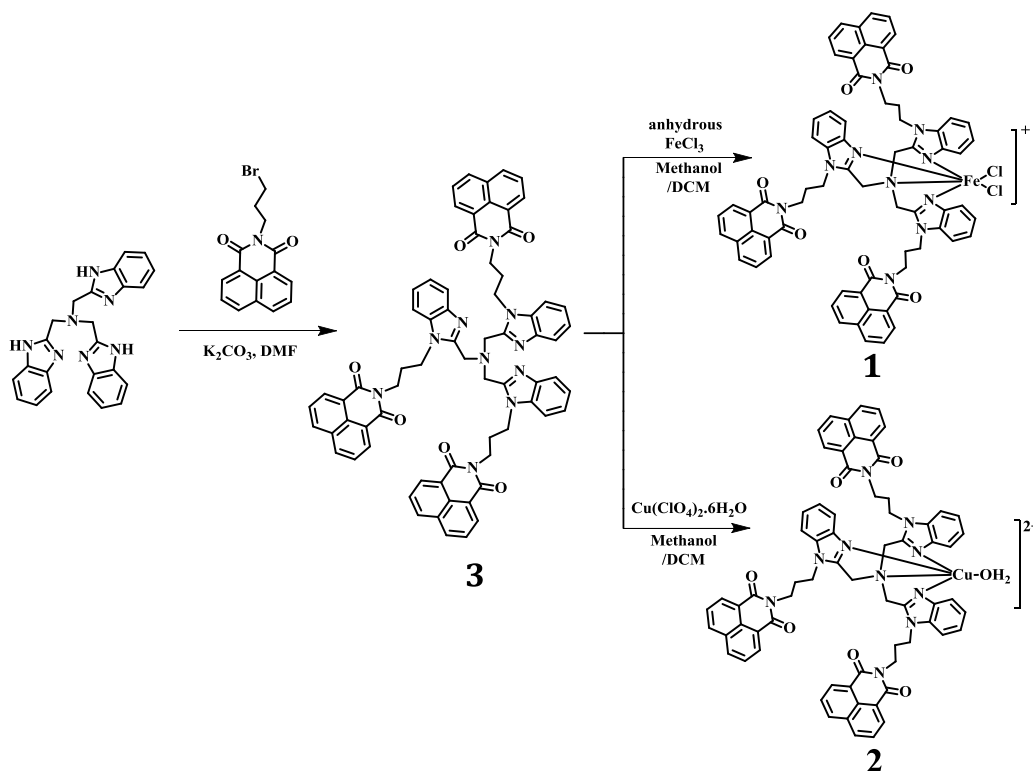
## 4.3. Results and Discussion

### 4.3.1. Synthesis and Characterization of the Complexes

The synthesis of the naphthalimide substituted tripodal ligand **3** and its Fe(III) and Cu(II) complexes, **1** and **2**, has been achieved as shown in Scheme 4.1. The tripodal ligand **3** was synthesized by the reaction of tris(2-benzimidazolyl- methyl)amine with 2-(3-bromopropyl)-benzo[de]isoquinoline-1,3-dione<sup>8</sup> in dry dimethylformamide. The synthesis of monomeric Fe(III) (**1**) and Cu(II) (**2**) complexes was achieved by the reaction of the ligand (**3**) with anhydrous FeCl<sub>3</sub> and Cu(ClO<sub>4</sub>)<sub>2</sub>·6H<sub>2</sub>O in quantitative yields. The structures of the ligand as well as complexes **1** and **2** have been characterized by various spectral and analytical techniques. The coordination of benzimidazole nitrogen to the metal center in **1** and **2** was characterized by FTIR analysis, wherein we observed a shift of  $\nu$  C=N from 1590 cm<sup>-1</sup> of free ligand to around 1580 cm<sup>-1</sup> for both these complexes. In addition, the complex **2** displayed characteristic bands at 1100 and 623 cm<sup>-1</sup> of the uncoordinated perchlorate ions. The MALDI-TOF spectra showed a peak at  $m/z = 1210$  and  $1183$  for  $[M^{+}-2Cl]^{+}$  and  $[M^{+}-H_2O]^{2+}$ , respectively, for the complexes **1** and **2**.

The molar conductivity values for the complexes **1** and **2** were determined as 58 and 130  $\Omega^{-1}\text{cm}^2\text{mol}^{-1}$ , which are characteristics of uni-univalent and uni-bivalent electrolytic behavior, respectively.<sup>9</sup> The room temperature magnetic moments of the complexes in the solid state were determined and the values are found to be 5.88 and 1.71 BM for **1** and **2**, respectively, indicating the discrete paramagnetic mononuclear behavior of these complexes. A solution magnetic moment of 6.13 BM (for **1**) and 1.98

(for **2**) were also measured by the Evans method<sup>10</sup> and this value is consistent with (high-spin)  $d^5$  (for **1**) and  $d^9$  (for **2**) systems, respectively.



**Scheme 4.1.** Synthesis of the ligand and the complexes **1** and **2**.

The electrochemical properties of complexes **1** and **2** exhibited a quasi-reversible wave at  $E_{1/2} = 311$  mV, for **1** and 11 mV, for **2** ( $\Delta E_p = 278$  (**1**) and 168 mV (**2**) vs. Ag/AgCl), which are assignable to the  $Fe^{III}/Fe^{II}$  and  $Cu^{II}/Cu^I$  redox couple, respectively (Figure 4.1 and Table 4.1), with ferrocene as an internal standard. The X-band EPR spectrum of the copper complex, **2** in DMSO at room temperature was recorded and  $g$  values (2.18–2.05) observed were consistent with the reported literature.<sup>11</sup>

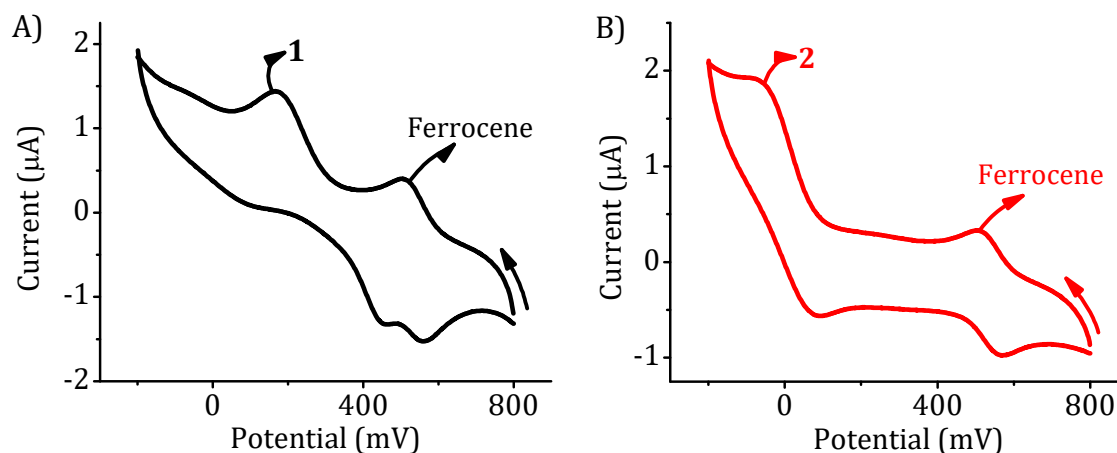


**Figure 4.1.** Cyclic voltammogram of the complexes A) **1** and B) **2** ( $10^{-3}$  M) in DMF (scan rate 1 V/s) in presence of ferrocene (1 mM) as an internal standard.

**Table 4.1.** Cyclic voltammetry measurements in DMF.<sup>a</sup>

Complexes	$E_{pa}/mV$	$E_{pc}/mV$	$E_{1/2}^b, mV$ ( $\Delta E_p^c, mV$ )	$^d n = i_{pa}/i_{pc}$
<b>1</b>	450	172	311 (278)	0.9
<b>2</b>	95	-73	11 (168)	0.3

<sup>a</sup>Measured in DMF for **1**, **2** with 0.1 M tetrabutyl ammonium hexafluorophosphate. <sup>b</sup> $E_{1/2}$  is calculated as average of anodic ( $E_{pa}$ ) and cathodic ( $E_{pc}$ ) peak potentials  $E_{1/2} = 1/2(E_{pa} + E_{pc})$ ; and <sup>c</sup> $\Delta E_p = E_{pa} - E_{pc}$  at scan rate 0.1 V/s. <sup>d</sup>Constant-potential coulometric data  $n = i_{pa}/i_{pc}$  calculated for  $1e^-$  transfer.

### 4.3.2. Single Crystal X-ray Analysis of the Ligand and the Complex **2**

In addition to the analytical and spectroscopic evidence, the ligand **3** and complex **2** were unambiguously characterized through single crystal X-ray structure analysis. The ORTEP view of **3** along with the atom numbering scheme is shown in Figure 4.2. The crystallographic data, selected bond distances and

angles are listed in Tables 4.2 and 4.3. The ligand, **3** crystallized in triclinic  $P1\bar{1}$ , along with three molecules of water in the asymmetric part of the unit cell. Interestingly, the benzimidazole rings formed a 'bowl-like' cavity and the naphthalimide moiety located within the aperture of the cavity, effectively making the system nonporous. Importantly, water occupied the intermolecular region and extended O–H $\cdots$ O (H $\cdots$ O, 2.76 Å) and O–H $\cdots$ N (H $\cdots$ N, 2.91 Å) hydrogen bonding with adjacent molecular units. Thus, each water molecule can be referred to as a two H-bond donor moiety and played a significant structure stabilizing role in the crystal lattice.

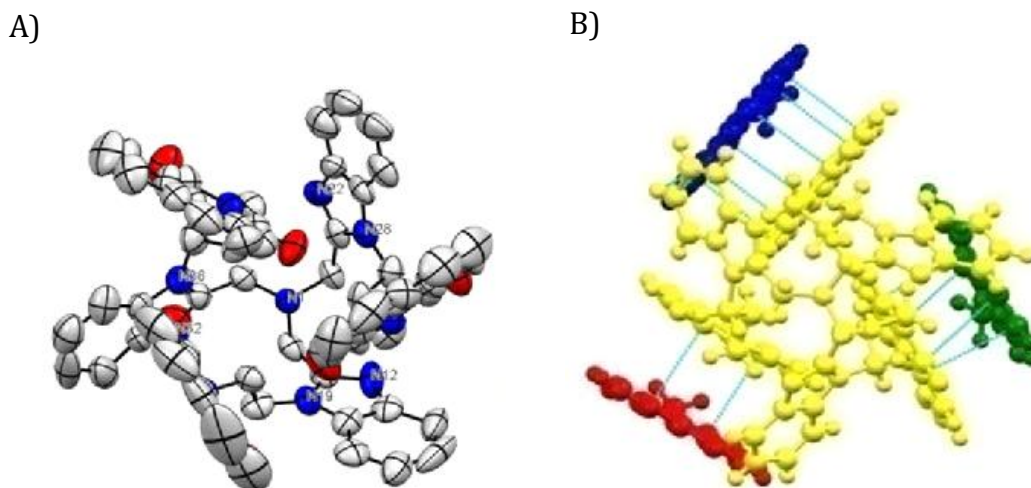


**Figure 4.2.** ORTEP view of A) the ligand (**3**) with ellipsoids at 50% probability level. (Solvent and hydrogen atoms have been omitted for clarity), B) Face-to-face stacking in **3** exhibited by the naphthalimide moiety. Three distinct molecular units are represented as green, red and blue.

Uniquely, the molecules of the ligand showed stacking ( $\pi$ - $\pi$ , average center-to-center distance between two adjacent benzimidazolyl groups was 4.04 Å) interactions involving both benzimidazolyl and naphthalimide moieties of the

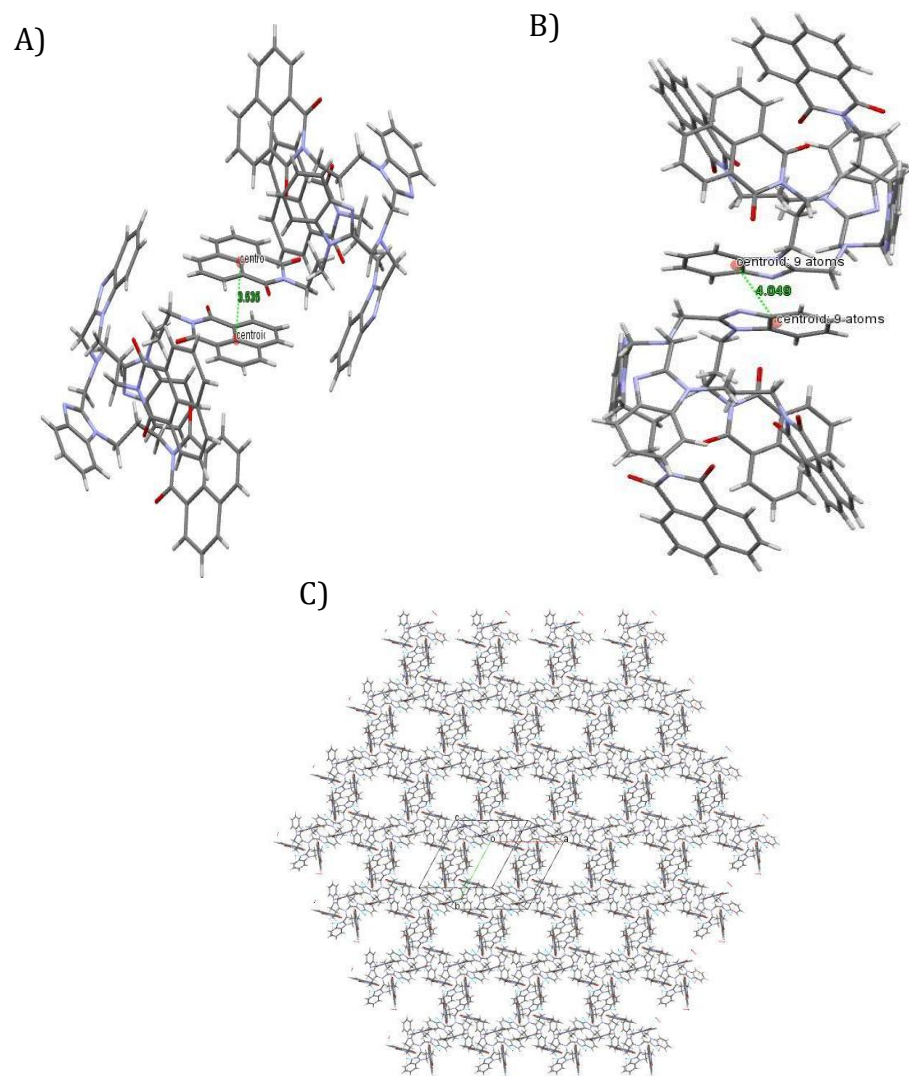


**Figure 4.3.** Unit cell structures of the ligand **3** showing intermolecular  $\pi$ - $\pi$  stacking interaction between two neighboring A) Naphthalimide B) Benzimidazolyl molecules and C) 3D network.

three benzimidazolyl groups available. Of these, two benzimidazolyl units were involved in  $\pi \cdots \pi$  interactions with the benzimidazolyl moieties of the two neighboring molecules of **3**. In contrast, all the three naphthalimide moieties were involved in face-to-face  $\pi \cdots \pi$  interactions with the three distinct molecular units (average center-to-center distances between the two adjacent naphthalimide groups were 4.04 Å and 3.54 Å, respectively)

(Figure 4.2). Thus, each molecule of the naphthalimide in **3** was in close contact with five different molecules, making the system sterically hindered. The images of the interactions exhibited by the benzimidazolyl and naphthalimide moieties are shown in Figure 4.3.

Similarly, the complex **2** was obtained by slow evaporation of a DMF solution and was crystallized in a triclinic fashion. The ORTEP plot of complex **2** along with the atom numbering schemes is shown in Figure 4.4. The asymmetric unit of complex **2** consisted of a discrete monomeric complex dication  $[\text{Cu}(\mathbf{3})(\text{H}_2\text{O})]^{2+}$ , two perchlorate anions, two DMF and four water molecules. The Cu(II) center is in a distorted trigonal bipyramidal coordination environment with an observed ' $\tau$ ' value of 0.96 (for reference,  $\tau = 1$  for an ideal trigonal bipyramid,  $\tau = 0$  for an ideal square pyramid according to the Addison/Reedijk geometric criterion).<sup>12</sup>

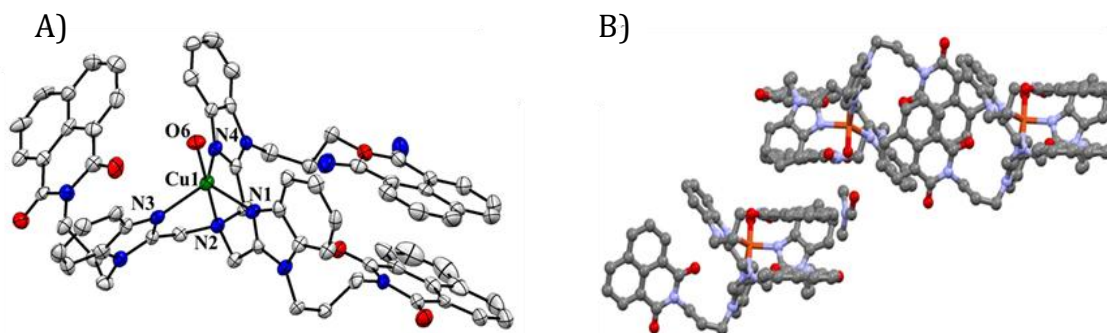


**Figure 4.4.** ORTEP view of A) the complex **2** with ellipsoids at 50% probability level. (Solvent, perchlorate ions and hydrogen atoms have been omitted for clarity) B) Different stacking modes of the naphthalimide moieties in complex **2**.

From the structural analysis, the bond angles in the equatorial and apical planes were found to be distorted to 109.11(17) (N5–Cu1–N3); 80.59(17) N2–Cu1–N4 and

98.32(16)° (O6–Cu1–N4) against the ideal trigonal angles of 120 and 90°. The tetradentate ligand, **3** was bonded to Cu(II) with the three benzimidazole nitrogen atoms (Cu–N<sub>bzim</sub>, 2.09(5), 2.03(4) and 2.11(5) Å), and was located at the equatorial plane, while the tertiary nitrogen atom (Cu–N<sub>am</sub>, 2.08(4) Å) and water (Cu–O<sub>H2O</sub>, 1.95(4) Å) occupied the apical positions. These bond distances Cu–N<sub>am</sub> (2.24 (15), 2.01(3) Å) and Cu–N<sub>bzim</sub> (1.97 Å) were found to be longer than those in the previous reports.<sup>13</sup>

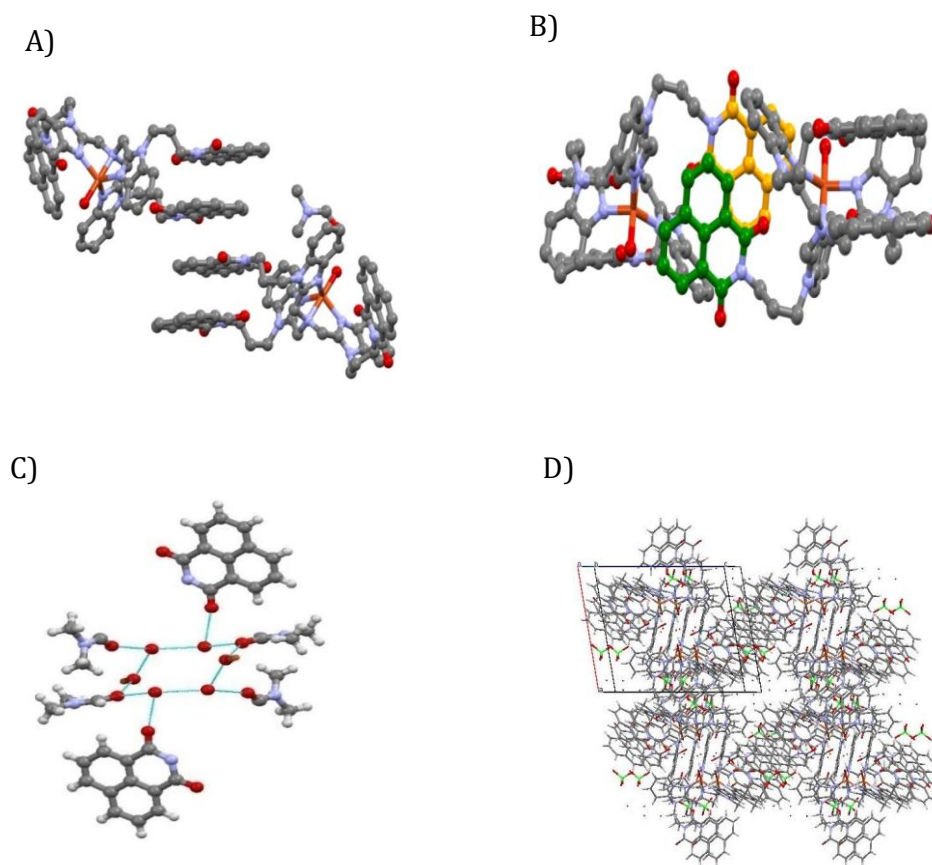


**Figure 4.5.** Unit cell parameters of the complex **2** showing A) Face-to-face stacking, B) Edge-to-edge stacking, C) The octamer hydrogen bonded network in the crystal, D) 3D network of Cu(II) complex along the b direction.

**Table 4.2.** Crystal data and structure refinement details for the ligand **3** and the complex **2**.

	<b>3</b> ·3H <sub>2</sub> O	<b>2</b> ·2DMF·4H <sub>2</sub> O
Formula weight (g mol <sup>-1</sup> )	1171.25	1615.91
Crystal system	Triclinic	Triclinic
Space group	<i>P</i> $\bar{1}$	<i>P</i> $\bar{1}$
<i>a</i> (Å)	15.68(2)	15.244(8)
<i>b</i> (Å)	16.44(2)	15.370(9)
<i>c</i> (Å)	17.69(2)	17.480(9)
$\alpha$ (°)	91.408(12)	82.582(8)
$\gamma$ (°)	115.658(13)	80.483(19)
$\beta$ (°)	117.999(12)	88.567(19)
<i>V</i> (Å <sup>3</sup> )	3477(9)	4005(4)
<i>Z</i>	2	2
Temperature /K	298(2)	123(2)
$\lambda$ (Å) (Mo- <i>K</i> $\alpha$ )	0.71073	0.71073
Crystal size (mm)	0.20x0.20x0.10	0.25x0.20x0.15
<i>F</i> (000)	1228	1682
Theta range for data collection	2.998-26.250	3.001-26.247
Data/restraints/parameters	13667/0/799	15656/0/ 1025
GOF on <i>F</i> <sup>2</sup>	0.707	1.024
<i>R</i> <sub>1</sub> [ <i>I</i> > 2 $\sigma$ ( <i>I</i> )]	0.0886	0.0941
<i>wR</i> <sub>2</sub> [ <i>I</i> > 2 $\sigma$ ( <i>I</i> )]	0.2216	0.2206



**Table 4.3.** Selected bond lengths (Å) and bond angles (deg) for the ligand **3** and the complex **2**.

	Bond Lengths (Å)		Bond Angles (deg)	
<b>3</b> ·3H <sub>2</sub> O	N22-C22	1.322(7)	C32-C31-N1	111.9(4)
	N32-C32	1.334(7)	C12-C11-N1	110.9(4)
	N12-C12	1.320(6)	C22-C21-N1	111.6(4)
	N1-C11	1.482(7)		
<b>2</b> ·2DMF·4H <sub>2</sub> O	Cu1-N2	2.076(4)	O6-Cu1-N4	98.32(16)
	Cu1-N5	2.093(5)	O6-Cu1-N2	178.73(18)
	Cu1-N4	2.028(4)	O6-Cu1-N3	100.02(16)
	Cu1-N3	2.109(5)	O6-Cu1-N5	101.33(18)
	Cu1-O6	1.950(4)	N2-Cu1-N5	79.82(18)
			N2-Cu1-N3	80.06(16)
			N2-Cu1-N4	80.59(17)
			N5-Cu1-N3	109.11(17)
			N4-Cu1-N3	121.91(18)
			N4-Cu1-N5	120.35(17)

In the complex **2**, the naphthalimide moieties exhibited distinct interaction characteristics with respect to its parent ligand. The coordination of copper(II) centre acts as an anchor, holding a rigid three-dimensional scaffold of the ligand (**3**) inducing a geometry to have effective intramolecular interactions between the two naphthalimide moieties. Furthermore, two of the naphthalimide moieties were locked in an intramolecular  $\pi\cdots\pi$  interaction (3.96 Å) (Figure 4.4B). These intramolecularly bound naphthalimide moieties interacted with similar dimer units from a neighboring

molecule to form a tetramer system.<sup>14</sup> The aforesaid intramolecular interactions were not observed in the ligand. The third naphthalimide moiety remained largely unbound, except for a weak edge-to-edge interaction (4.97 Å) with the neighboring molecule and could be an interacting point with biomolecules (vide infra). The 3D structure in the crystal was predominantly controlled by the perchlorate anions, together with DMF and lattice water, through O–H···O and C–H···O hydrogen bonds to form a cyclic O–H···O octamer motif consisting of two coordinated water, four lattice water and two DMF molecules (Figure 4.5). One can infer that the labyrinthine topology of the complex showed closed packing to be energetically demanding, forcing it to adopt a relatively open structure, wherein the void space was occupied by the hydrogen bonded guest moieties.

### 4.3.3. Photophysical Properties of the Ligand and Complexes

The absorption spectra of the ligand and the complexes showed a characteristic naphthalimide centered electronic spectral band in the region around 335 nm, which was attributed to  $\pi$ – $\pi^*$  transitions of the aromatic nitrogen donors.<sup>15</sup> In addition, complexes **1** and **2** displayed bands at ~450 nm ( $\epsilon = 4.7 \times 10^3 \text{ M}^{-1} \text{ cm}^{-1}$ ) and ~420 nm ( $\epsilon = 50 \text{ M}^{-1} \text{ cm}^{-1}$ ) attributed to ligand-to-metal charge transfer (LMCT) and  $(d\pi(\text{Cu})) \rightarrow$  ligand transitions, respectively.<sup>16</sup> The absorption and emission spectra of the ligand and the complexes are shown in Figure 4.6. Both the ligand **3** and complexes **1** and **2** showed characteristic emission of the naphthalimide chromophore  $\lambda_{\text{max}}$  at ~380 nm. In addition, an intense broad emission band  $\lambda_{\text{max}}$  was observed at 480 nm, which was attributed to the excimer of the naphthalimide chromophore.

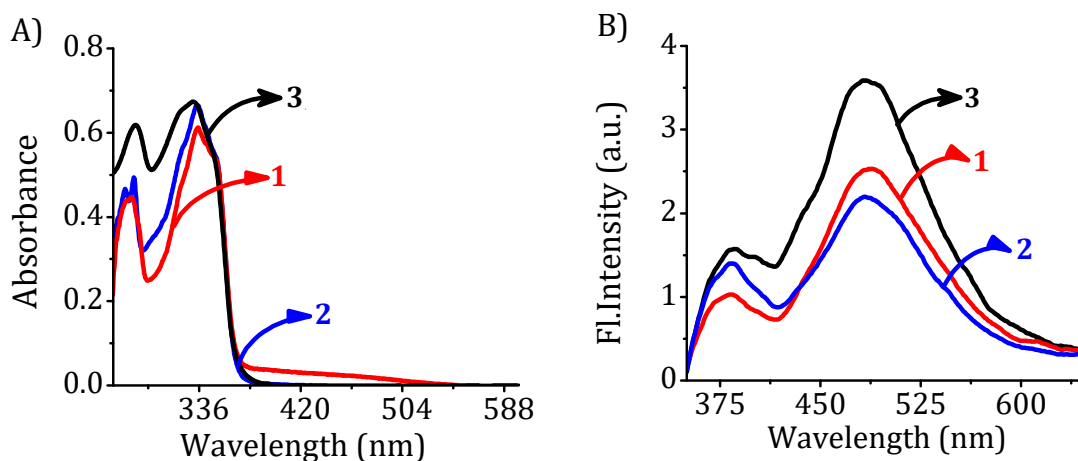


**Figure 4.6.** A) Absorption and B) emission spectra of the ligand **3** and complexes **1** and **2** ( $1.7 \times 10^{-5}$  M) in DMF. Excitation wavelength, 335 nm.

To understand the nature of the excimer formed in the ligand and the complexes, we have monitored concentration dependent emission changes. The excimer to monomer ratio ( $I_{480}/I_{380}$ ) was found to increase with the increase in concentration in the case of the ligand **3**, however; this ratio almost remained constant in the case of complexes **1** and **2**. These observations confirm the formation of inter and intramolecular excimers in the ligand and complexes, respectively. We have determined the fluorescence quantum yield ( $\Phi_F$ ) value of the ligand **3** and the complexes **1** and **2**, using quinine sulphate as a standard.<sup>17</sup> We observed  $\Phi_F = 0.70 \times 10^{-2}$  for the ligand, while complexes **1** and **2** showed quenched yields of  $0.61 \times 10^{-2}$  and  $0.58 \times 10^{-2}$ , respectively, due to the paramagnetic nature of the metal centre. The picosecond time-resolved fluorescence studies using 375 nm laser excitation indicated that all these systems exhibited a triexponential decay profile at  $\lambda_{em}$  480 nm with lifetime values of 6.62 (21%), 14.12 (72%), and 1.35 (8%) for **3**, 6.38 (23%), 14.36 (70%), and 1.37 (7%) for the complex **1** and 3.92 (49%), 1.10 (17%), and 13.47 (34%) for the complex **2**

(Figure 4.7). These lifetime values were attributed to the emissions from the monomer and different aggregated species present in solution as reported in the literature.<sup>6, 18</sup> The photophysical properties of these systems are summarized in Table 4.4.

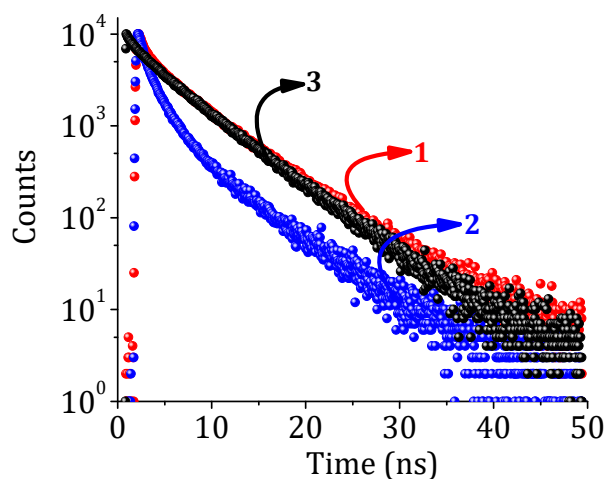


**Figure 4.7.** Lifetime profiles of the ligand **3** (10  $\mu\text{M}$ ) and the complexes **1** (10  $\mu\text{M}$ ) and **2** (10  $\mu\text{M}$ ) in DMF (at 480 nm).

**Table 4.4.** Photophysical properties of the ligand **3** and the complexes **1** and **2**.<sup>a</sup>

	$\lambda_{\text{ab}}$ , nm ( $\epsilon/\text{M}^{-1}\text{cm}^{-1}$ )	$\lambda_{\text{em}}$ , nm	$\tau$ , ns	$\phi_{\text{F}} \times 10^{-2}$
<b>3</b>	283 ( $3.6 \pm 1.2 \times 10^4$ )	380, 480	6.62 (21%)	0.70 $\pm$ 0.02
	331 ( $4.1 \pm 0.9 \times 10^4$ )		14.12 (72%)	
			1.35 (7%)	
<b>1</b>	282 ( $3.7 \pm 1.3 \times 10^4$ )	376, 480	6.38 (23%)	0.61 $\pm$ 0.01
	334 ( $4.3 \pm 1.1 \times 10^4$ )		14.36 (70%)	
	450 ( $4.7 \pm 1.2 \times 10^3$ )		1.37 (7%)	
<b>2</b>	280 ( $2.9 \pm 1.0 \times 10^4$ )	378, 480	3.92 (49%)	0.58 $\pm$ 0.02
	334 ( $4.0 \pm 1.3 \times 10^4$ )		1.10 (17%)	
	420 ( $50 \pm 1.1$ )		13.47 (34%)	

<sup>a</sup> The data are the average of more than three independent experiments, and the error is *ca.*  $\pm 5\%$ .

#### 4.3.4. DNA Binding Studies

To understand the biological affinity of the metal complexes **1** and **2**, we have investigated the binding affinity of these systems with ct-DNA with the aid of various photophysical as well as biophysical techniques. The addition of ct-DNA (0-10  $\mu\text{M}$ ) in small aliquots to 15% DMF-buffer (pH = 7.4) solution of the complex **1** (16.5  $\mu\text{M}$ ) resulted in a decrease in the absorption of the naphthalimide chromophore. For example, the absorption band at  $\sim 345$  nm exhibited *ca.* 38% hypochromism for the complex **1** with the addition of ct-DNA (Figure 4.8A). Similar observations were made with the complex **2**, which showed *ca.* 50% hypochromism at  $\sim 345$  nm (Figure 4.8B). The observation of hypochromicity in the absorption spectra indicates the affinity of naphthalimide moiety of the complexes **1** and **2** towards DNA. Similar experiments were carried out with the ligand **3**, wherein we observed negligible changes upon addition of ct-DNA, indicating its insignificant interactions with ct-DNA.

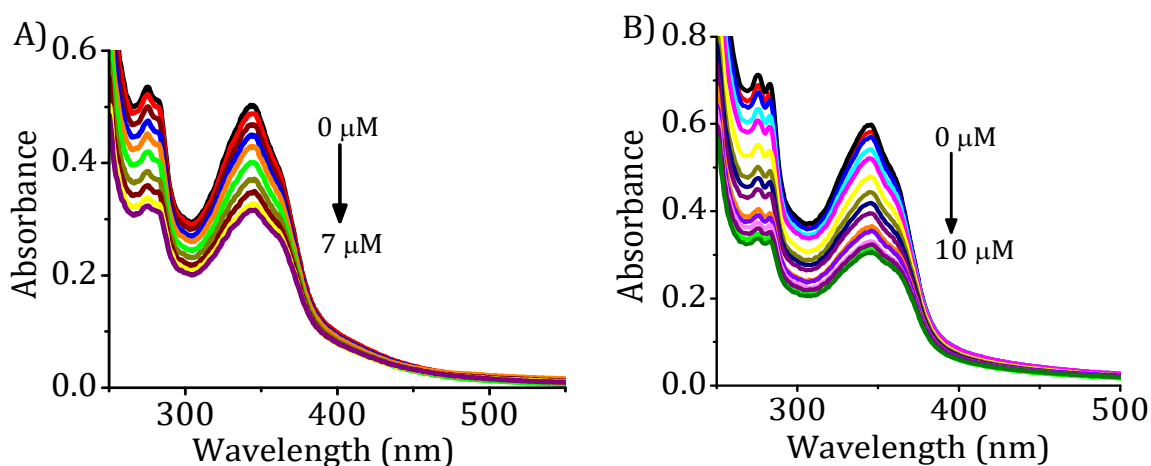


**Figure 4.8.** Changes in the absorption spectra of the complexes A) **1** (16.5  $\mu\text{M}$ ) and B) **2** (16.5  $\mu\text{M}$ ) with increasing concentration of ct-DNA in 15% DMF-phosphate buffer solution.

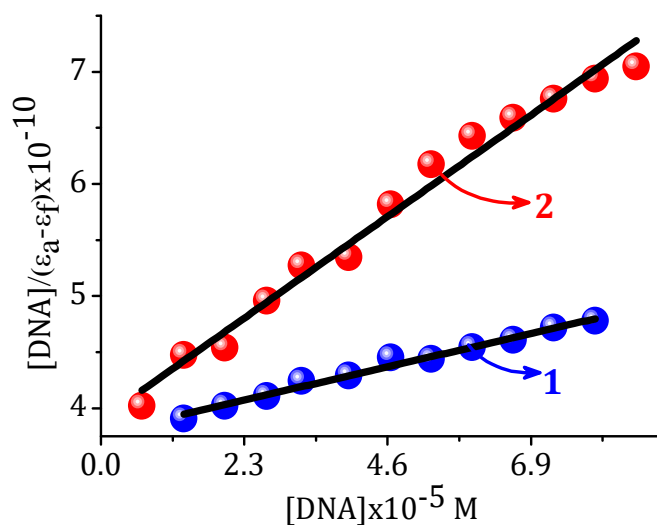


**Figure 4.9.** A) The plot of  $[DNA]/(\epsilon_a - \epsilon_f)$  vs  $[DNA]$  for the complexes **1** and **2**.

The intrinsic binding constant ( $K_{DNA}$ ) was calculated for the complexes **1** and **2** and the values are found to be  $0.34 \pm 0.7 \times 10^4$ , and  $1.01 \pm 1.1 \times 10^4 \text{ M}^{-1}$ , respectively (Figure 4.9). When compared to the reported Fe(III) and Cu(II) complexes without naphthalimide moieties ( $K_{DNA} = 10^4 \text{ M}^{-1}$ ),<sup>19</sup> the complexes having naphthalimide moiety ( $K_{DNA} = 10^5 \text{ M}^{-1}$ ) and the classical intercalator ( $K_{DNA} = 10^7 \text{ M}^{-1}$ ) showed high values of the association constant.<sup>6,20</sup> The fluorescence spectral measurements were also monitored with the increasing concentrations of ct-DNA ( $\lambda_{ex} = 345 \text{ nm}$ ). The complex **1** ( $16.5 \mu\text{M}$ ) showed negligible changes upon the addition of ct-DNA, whereas complex **2** ( $10 \mu\text{M}$ ) exhibited *ca.* 50% quenching at  $\lambda_{max} \sim 490 \text{ nm}$  upon adding  $8 \mu\text{M}$  of ct-DNA (Figure 4.10). The binding constant ( $K_{b, DNA}$ ) and binding site ( $n$ ) for the complex **2** were determined and the values are found to be  $1.1 \pm 0.9 \times 10^4 \text{ M}^{-1}$  and 0.85, respectively. These values are consistent with those obtained for the complex **2** through UV-Vis absorption spectral titrations.

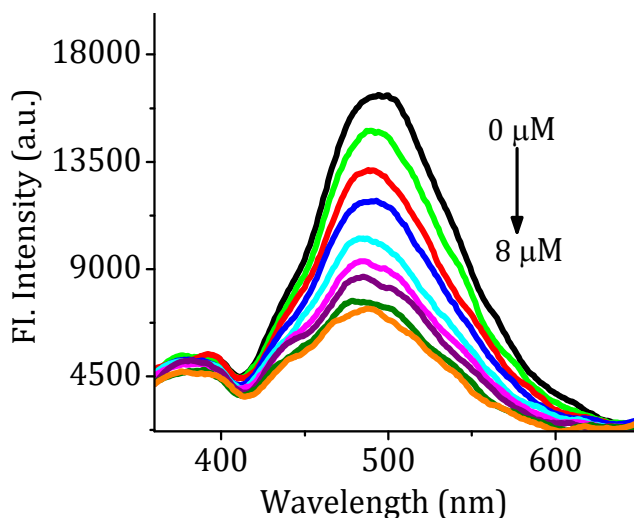


**Figure 4.10.** Emission spectra of the complex **2** (10  $\mu\text{M}$ ) with increasing concentration of ct-DNA. Excitation wavelength, 345 nm.

Furthermore to examine the binding mode of the complexes with ct-DNA, competitive ethidium bromide (EB) binding assay was employed. The addition of increasing concentrations of the complexes, for example, the complex **1** (0-10  $\mu\text{M}$ ) to ct-DNA (100  $\mu\text{M}$ ), previously treated with EB (50  $\mu\text{M}$ ), exhibited *ca.* 20% quenching at  $\lambda_{\text{max}} \sim 624$  nm with respect to the initial fluorescence intensity (Figure 4.11A). A similar trend was observed with the complex **2** (0-16  $\mu\text{M}$ ), wherein, we observed *ca.* 45% quenching in the fluorescence intensity (Figure 4.11B). In contrast, the fluorescence intensity of the DNA-EB complex showed negligible changes on addition of increasing concentrations of the ligand **3** (0-10  $\mu\text{M}$ ), which suggests that the ligand is found to be incompetent to displace EB from the DNA-EB complex. The values of Stern-Volmer constant were determined and are found to be *ca.*  $2.5 \times 10^4$ , for **1**;  $8.8 \times 10^4 \text{ M}^{-1}$ , for **2** (Figure 4.11C). These observations indicated the fact that the complexes **1** and **2**, moderately displace EB from the DNA-EB complex and are assumed to comprise groove

and/or electrostatic interactions with DNA.<sup>21</sup> The observation of lower values of  $K_{DNA}$  ( $0.11 \times 10^4 \text{ M}^{-1}$  for **1**; and  $0.76 \times 10^4 \text{ M}^{-1}$  for **2**) in DMF-buffer containing 100 mM NaCl, further confirms that the mode of interactions of these complexes with DNA could be due to the groove binding electrostatic interactions.

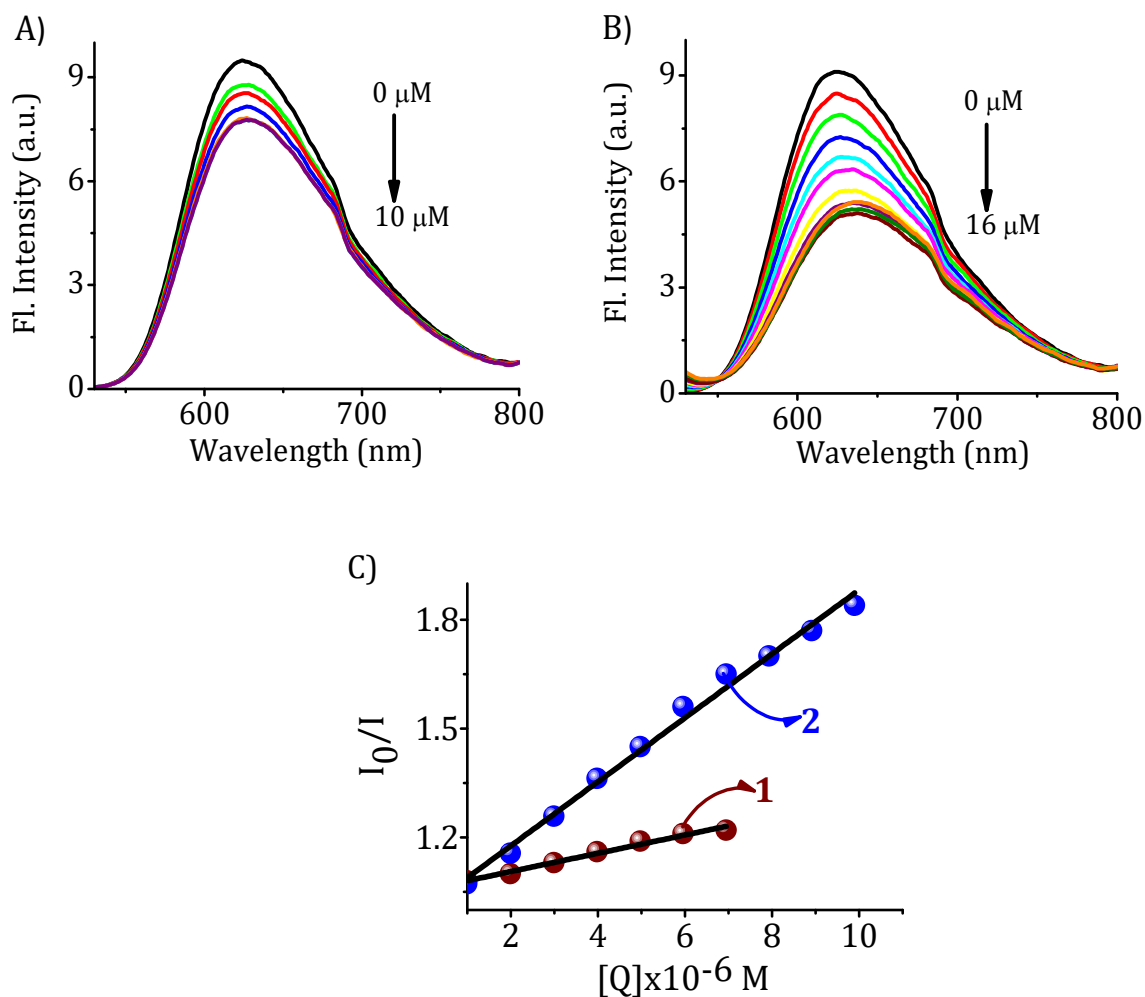


**Figure 4.11.** Fluorescence quenching curves of ct-DNA-bound ethidium bromide in presence of the complexes A) **1** (0-10  $\mu\text{M}$ ) and B) **2** (0-16  $\mu\text{M}$ ). C) The plot of  $I_0/I$  vs  $[Q]$  of the complexes **1** and **2**. Excitation wavelength, 510 nm.



The groove binding interactions of these complexes with ct-DNA were further established by thermal denaturation, viscosity and circular dichroism measurements. The oligonucleotide duplex containing DNA1: 5' CAC TGG CTT TTC GGT GCAT, and DNA2: 5' ATG CAC CGA AAA GCC AGTG (2  $\mu\text{M}$  each) showed thermal denaturation temperature ( $T_m$ ) of 50  $^{\circ}\text{C}$ . However, in the presence of the complexes (2.5 equivalents), we observed an increase in the melting temperature ( $T_m$ ) by *ca.* 2 and 3  $^{\circ}\text{C}$  for **1** and **2**, respectively (Figure 4.12A).

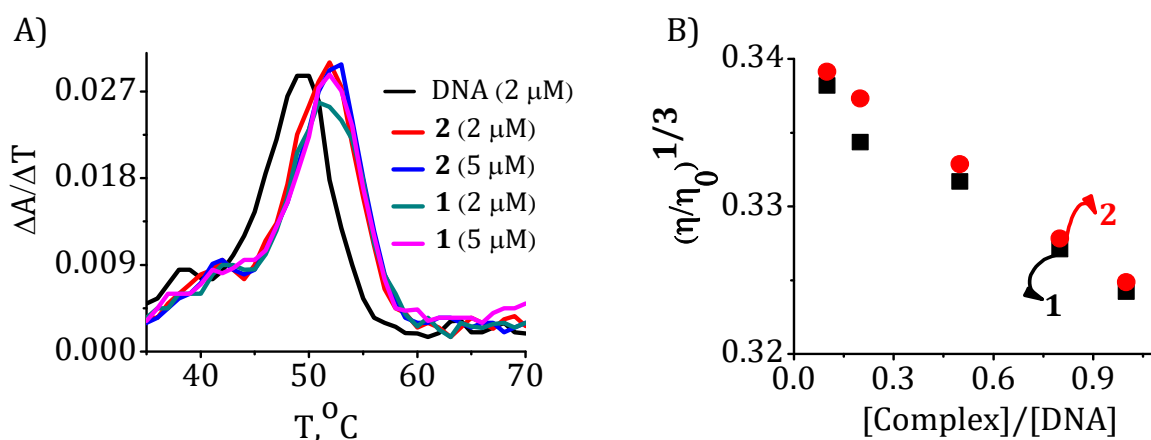


**Figure 4.12.** A) Thermal denaturation graph ( $T_m$ ) for the DNA duplex (DNA1/DNA2) (2  $\mu\text{M}$ ) in absence and presence of the complexes **1** and **2** (2, 5  $\mu\text{M}$  each) in 10 mM phosphate buffer. (DNA1: 5' CGT GCA TGC ACG GTAC-3', DNA2: 5' GTA CCG TGC AAT GTC CACG-3'). B) The plot of relative specific viscosity  $(\eta/\eta_0)^{1/3}$  vs [complex]/[DNA] ratio. ([DNA]: 100  $\mu\text{M}$ , [Complex]: 10-100  $\mu\text{M}$ ).

The increase in melting temperature suggests the fact that these systems stabilize the DNA duplex predominantly through the groove binding nature of the complexes as reported in the literature for similar systems.<sup>22</sup> Furthermore, the viscometric studies also have been carried out which showed a slight decrease in relative specific viscosity upon addition of complexes **1** and **2** (10–100  $\mu\text{M}$ ) to a solution of DNA (100  $\mu\text{M}$ ) in

DMF-phosphate buffer (Figure 4.12B). The viscosity results confirmed groove and/or surface-binding nature of the complexes.<sup>16,23</sup> The circular dichroism (CD) spectra of DNA (200  $\mu\text{M}$ ) in the presence of the complexes **1** and **2** (0–10  $\mu\text{M}$ ) showed a decrease in the ellipticity of both the positive and negative bands as compared to DNA (Figure 4.13). These results evidence the involvement of groove and/or surface binding and electrostatic interactions of complexes with DNA.

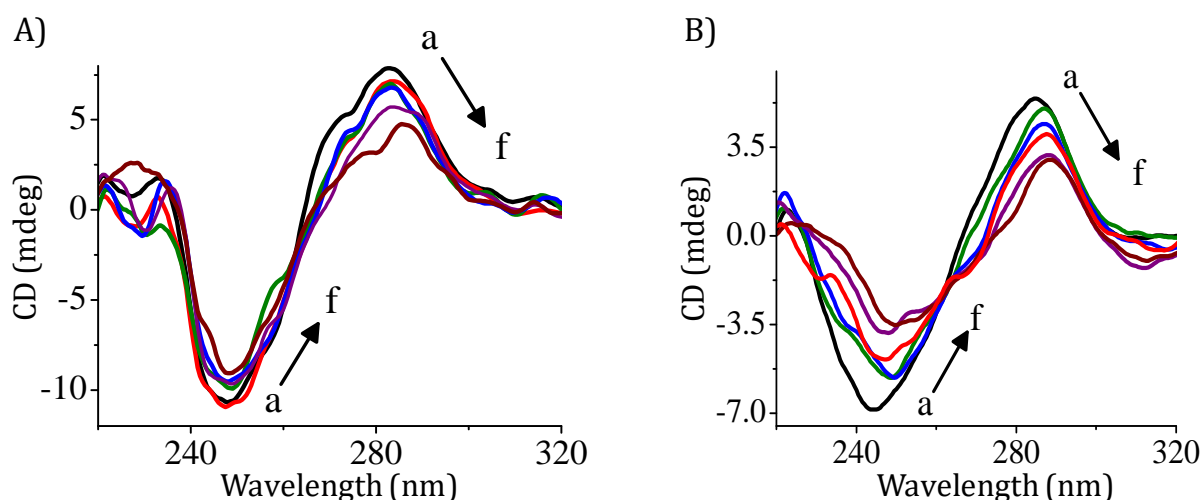


**Figure 4.13.** Circular dichroism spectra of DNA in the absence and presence of complexes A) **1** (0–10  $\mu\text{M}$ ) and B) **2** (0–10  $\mu\text{M}$ ) in DMF phosphate buffer (pH 7.4). [Complex]: a = 0; f = 10  $\mu\text{M}$ , [DNA] = 200  $\mu\text{M}$ .

The naphthalimide moieties in the ligand **3** showed negligible interactions with DNA probably due to the steric hindrance, while the complexes **1** and **2** exhibited efficient interactions through groove and involve the electrostatic mode with the sugar phosphate backbone of DNA. From these observations, it can be inferred that Cu(II) complex **2** exhibits higher binding propensity than the octahedral Fe(III) analogue **1** probably due to high charge on the copper(II) complex and their geometric difference.<sup>23</sup> However, the lower affinity of these complexes for DNA when compared to the reported

examples in the literature<sup>5</sup> could be correlated with the geometric constraints of naphthalimide moieties present in these systems. Based on solid state structure analysis, two of the naphthalimide moieties were engaged in stable intramolecular  $\pi$ - $\pi$  interactions. Though the solid state structure itself cannot be extrapolated to the solution based binding studies, it is rational to assume that robust intramolecular interactions could be effectively preserved in the solution state as well; intramolecular interactions are generally favored over intermolecular in the hierarchy of interactions.<sup>14</sup> Based on this assumption, it could be implied that the free naphthalimide moiety of the complexes **1** and **2** could be the benign interacting site with ct-DNA.

#### 4.3.5. Protein Interaction Studies

The interaction of the metallodrugs with proteins is important to understand their uptake, bio-distribution, overall toxicity, mechanism of action and shuttling of the complexes to cancer cells and hence we have explored the interaction of these complexes with BSA using various photophysical techniques. The spectrofluorimetric titration results of the complex **1** (16.6  $\mu$ M) with BSA (0-2  $\mu$ M) in DMF-phosphate buffer of pH = 7.4 ( $\lambda_{\text{ex}}$  = 345 nm) are shown in Figure 4.14A. Addition of increasing concentration of BSA (0-2  $\mu$ M) to the complex **1** (16.6  $\mu$ M) showed *ca.* 25% quenching in fluorescence intensity at  $\sim$ 490 nm along with a hypsochromic shift of 5-10 nm and an isoemissive point at  $\sim$ 445 nm. In similar titrations with the complex **2**, we observed *ca.* 48% quenching in fluorescence intensity at  $\sim$ 495 nm along with a hypsochromic shift of 5-10 nm. The observed changes in the fluorescence spectra of the complexes (**1** and **2**) and blue shift in emission maximum indicate that the active site of the protein is

in a hydrophobic environment.<sup>24</sup> The binding constants were calculated using a double-log plot (Figure 4.14B) and the values are found to be  $3.43 \pm 0.6 \times 10^4$  for **1** and  $8.12 \pm 0.8 \times 10^4 \text{ M}^{-1}$  for **2** and binding capacity ( $n$ ) varies from 0.96 for **1** to 1.04 for **2**.

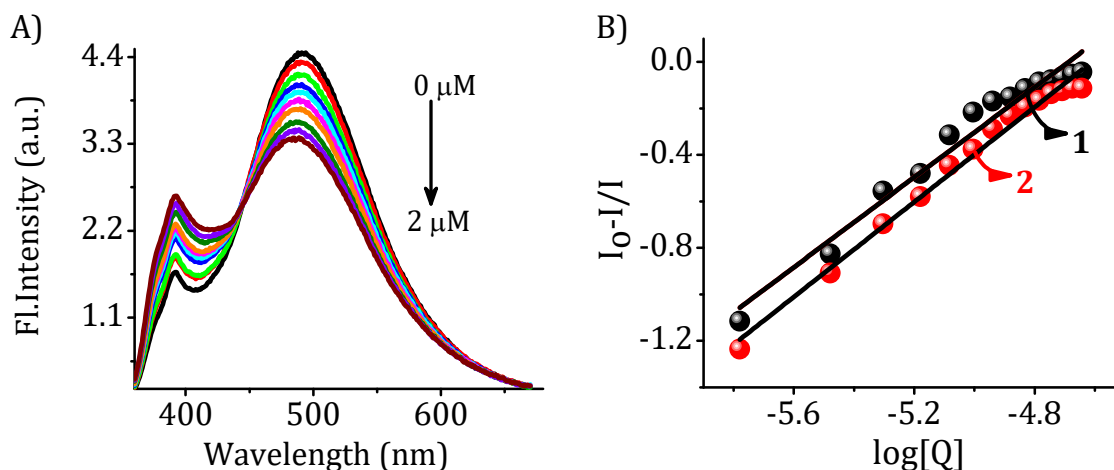


**Figure 4.14.** A) Fluorescence emission spectra of the complex **1** (16.6 μM) with increasing concentration of BSA (0-2 μM) in 10 mM DMF-phosphate buffer at pH 7.4 ;  $\lambda_{\text{ex}} = 345 \text{ nm}$  B) Double-log plots of the complexes **1** and **2** with BSA.

To determine the nature of protein binding affinity of the complexes, tryptophan emission quenching experiments were carried out with increasing concentration of the complexes in DMF-phosphate buffer at 27 °C. For example, addition of the complex **1** (0-18 μM) quenched the fluorescence emission of BSA up to *ca.* 90% at ~345 nm with a hypsochromic shift of 5-6 nm (Figure 4.15A). Similar observations were made with complex **2** (0-18 μM), which showed *ca.* 84% quenching at ~345 nm in the fluorescence intensity with a hypsochromic shift of 5-6 nm (Figure 4.15B). A decrease in the fluorescence intensity of BSA in complex **2** is accompanied with the appearance of a new band at ~480 nm, which is attributed to direct excitation of complex **2** and is confirmed by the excitation spectra of the complex **2** at 280 nm with increasing

concentration of BSA ( $2 \mu\text{M}$ ). The observed fluorescence quenching with a blue shift was attributed to the fact that the active site in the protein is buried in a hydrophobic environment.<sup>22</sup>

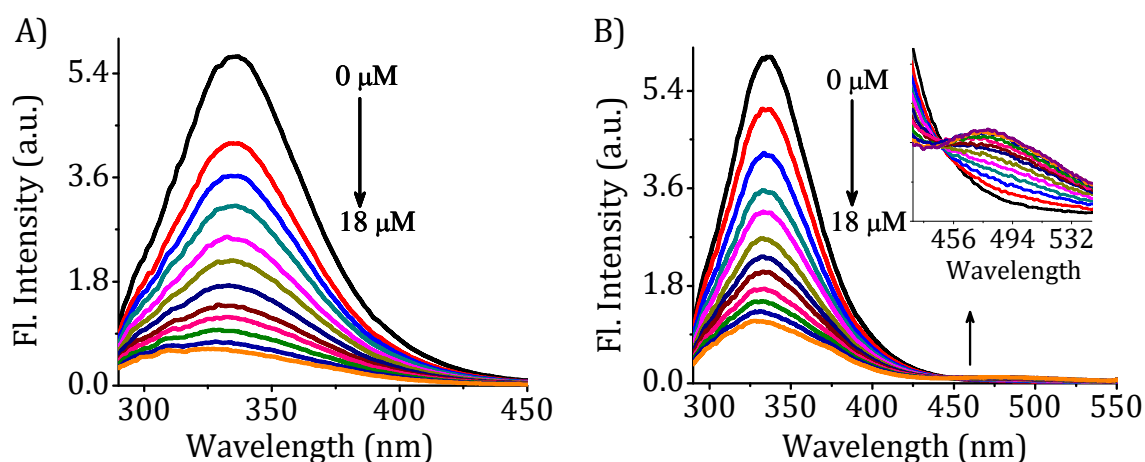


**Figure 4.15.** Emission spectra of BSA ( $2 \mu\text{M}$ ) with increasing concentration of the complexes A) **1** and B) **2** at  $27 \text{ }^\circ\text{C}$  in  $10 \text{ mM}$  DMF-phosphate buffer at  $\text{pH } 7.4$ ; Excitation wavelength,  $280 \text{ nm}$ . Inset of B) shows direct excitation of the complex **2**.

To understand the interaction of the complexes with BSA, Stern-Volmer constant values have been calculated at two different temperatures. The  $K_{SV, \text{BSA}}$  values are found to be  $4.25$  and  $3.84 \times 10^5 \text{ M}^{-1}$  for the complex **1** and  $1.70$  and  $1.53 \times 10^4 \text{ M}^{-1}$  for **2** at  $27 \text{ }^\circ\text{C}$  and  $37 \text{ }^\circ\text{C}$ , respectively (Figure 4.16A). Interestingly,  $K_{SV, \text{BSA}}$  values decreased with the increase in temperature and thereby confirmed the static quenching mechanism.<sup>25</sup> Furthermore, the bimolecular quenching constants ( $k_q$ ) were calculated and the values are found to be  $6.85 \pm 0.8 \times 10^{13} \text{ M}^{-1} \text{ s}^{-1}$  (for **1**) and  $2.74 \pm 0.9 \times 10^{13} \text{ M}^{-1} \text{ s}^{-1}$  (for **2**), at  $27 \text{ }^\circ\text{C}$  and  $6.19 \pm 1.1 \times 10^{13} \text{ M}^{-1} \text{ s}^{-1}$  (for **1**) and  $2.46 \pm 0.9 \times 10^{13} \text{ M}^{-1} \text{ s}^{-1}$  (for **2**), at  $37 \text{ }^\circ\text{C}$  (Figure 4.16B). These values evidence the involvement of the static quenching mechanism as reported in the literature.<sup>26</sup> The binding capacity values varied in the

range 1.05-1.10 (Table 4.5), which indicates that the interaction of **1** and **2** with BSA occurs through a single binding site.

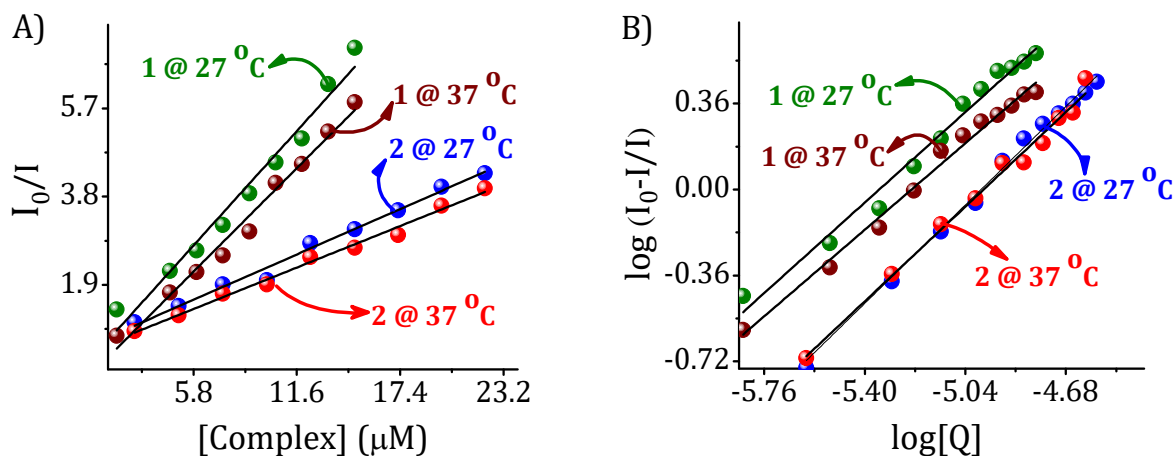


**Figure 4.16.** A) Stern–Volmer curves and B) Double-log plots of the complexes **1** and **2** with BSA at 27 °C and 37 °C.

Using the van't Hoff equation, the free energy change for BSA-complexes binding was determined. The observed values are found to be  $\Delta G = -32.31, -30.76 \text{ kJ mol}^{-1}$  for the complexes **1** and **2**, respectively. The negative values of  $\Delta G$  indicate a thermodynamically favorable binding process and also the negative values of  $\Delta H$  ( $-7.80$  (for **1**) and  $-8.11$  (for **2**)  $\text{kJ mol}^{-1}$ ) and positive values of  $\Delta S$  ( $0.082$  (for **1**) and  $0.073$  (for **2**)  $\text{kJ mol}^{-1} \text{ K}^{-1}$ ) confirm the involvement of electrostatic forces between the complexes and BSA protein (Table 4.5).<sup>27</sup> The results clearly demonstrate that the hydrophobic interactions play a major role in the interactions between the complexes **1** and **2** with BSA, but the involvement of electrostatic interactions could not be excluded completely because of  $\Delta G$  values which are derived from a large contribution of the T $\Delta S$  factor with little contribution of the  $\Delta H$  factor.

**Table 4.5.** Binding and relative thermodynamic parameters of BSA with the complexes **1** and **2**.

Si.No.	Temp (K)	Binding constant $K_b \times 10^5 (M^{-1})$	Number of binding site (n)	$\Delta H$ (kJ/mol)	$\Delta S$ (J/molK)	$\Delta G$ (kJ/mol)	R
<b>1</b>	300	4.1	1.05	-7.80	81.72	-32.31	0.981
	310	1.8	1.01			-33.13	0.988
<b>2</b>	300	5.0	1.14	-8.11	73.09	-30.03	0.995
	310	2.9	1.10			-30.76	0.989

R is the linear correlated coefficient

The synchronous fluorescence spectroscopy study was further employed to investigate the structural changes of BSA (2  $\mu M$ ) in presence of the complexes **1** and **2** (0-13  $\mu M$ ) (Figure 4.17).<sup>28</sup> The synchronous fluorescence spectra of BSA with varying concentrations of the complexes (0-13  $\mu M$ ) were acquired at  $\Delta\lambda$ , 15 nm and 60 nm in DMF-buffer (15%). At  $\Delta\lambda$ , 15 nm, addition of the complexes **1** and **2** to a solution of BSA resulted in a significant decrease of the fluorescence intensity at 300 nm of BSA up to *ca.* 74%. Similarly, at  $\Delta\lambda$  60 nm, the fluorescence intensity at 345 nm quenched up to *ca.* 86% accompanied by a slight red shift of *ca.* 2-3 nm.<sup>28</sup> The slight red shift in the emission maximum revealed that the interaction of the complexes with BSA affects the conformation of tryptophan residues.<sup>29</sup> However the microenvironment near the tyrosine residues did not alter throughout the binding process, suggesting the changes in the protein conformation and polarity of its surroundings.<sup>28</sup> These results suggest that the complexes **1** and **2** effectively bind with BSA and hence can have potential as anticancer agents.

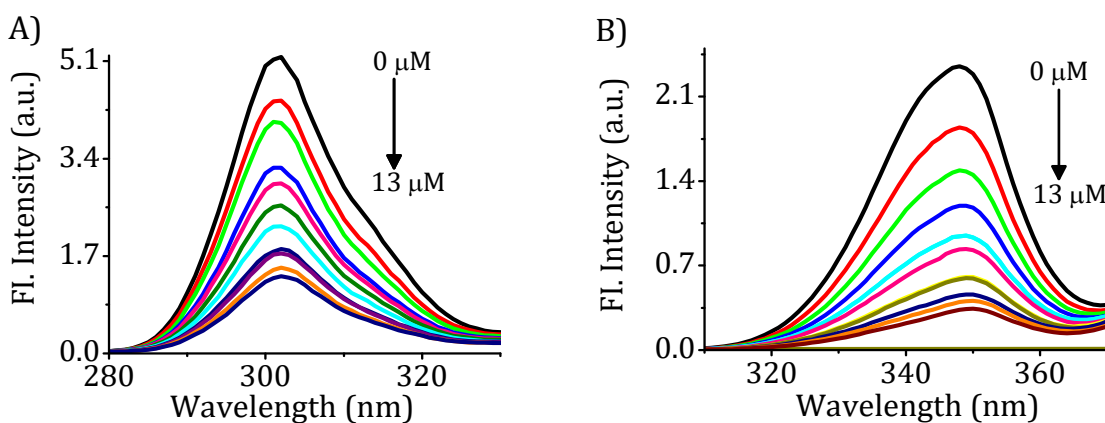


**Figure 4.17.** Synchronous spectra of BSA (2  $\mu\text{M}$ ) as a function of concentration of the complex **1** with wavelength difference of A)  $\Delta\lambda = 15$  nm and B)  $\Delta\lambda = 60$  nm in 10 mM DMF-phosphate buffer at pH 7.4.

#### 4.3.6. *In Vitro* Cytotoxicity and Fluorescent Staining Studies

We have investigated the *in vitro* cytotoxicity of the ligand and the complexes using the MTT assay against cervical carcinoma (HeLa) and normal human cardiac myoblasts (H9c2) cell lines. The ligand (**3**), the complexes (**1** and **2**) and free metal salts ( $\text{FeCl}_3$ ,  $\text{Cu}(\text{ClO}_4)_2 \cdot x\text{H}_2\text{O}$ ), were dissolved in DMSO, and blank samples containing the same volume of DMSO were taken as controls to identify the activity of the solvent. Experiments were carried out by exposing the cells to various concentrations of free metal salts, ligand (0-200  $\mu\text{M}$ ) and the complexes (0-100  $\mu\text{M}$ ). The inhibition in growth of cells in full medium was determined subsequently after extensive washing for 24 h. The MTT assay revealed that copper salts exerted very low cytotoxicity only at very high concentration (>150  $\mu\text{M}$ ), whereas iron salts showed negligible cytotoxicity in HeLa cells up to 200  $\mu\text{M}$  (Figure 4.18A). The ligand showed cytotoxicity with  $\text{IC}_{50} = 150$   $\mu\text{M}$  in HeLa cells, whereas it was found to be non-toxic to H9c2 cells up to 200  $\mu\text{M}$  concentration.



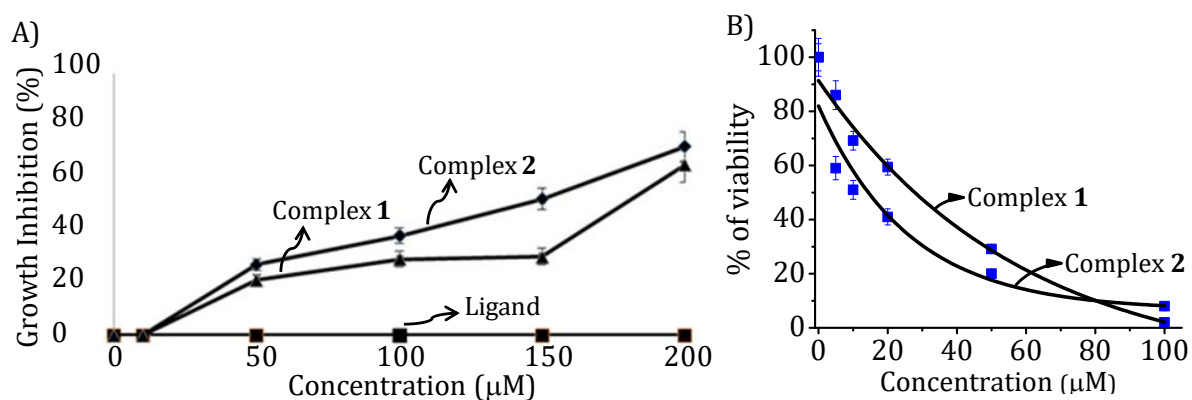


**Figure 4.18.** A) *In vitro* cytotoxicity assay with different concentrations of the ligand **3** and metal salts (0-200  $\mu\text{M}$ ) against the HeLa cell line (Data are mean%  $\pm$  SD of triplicate). B) Sigmoid fitted curves for the complexes **1** and **2** obtained by plotting cell viability against [Complex] through ORIGIN 8.5 software.

The bioactivity of the ligand was enhanced significantly upon coordination with redox-active biomimetic metal ions. These complexes exhibited  $\text{IC}_{50}$  values of  $32 \pm 0.19 \mu\text{M}$ , for **1** and  $10 \pm 0.21 \mu\text{M}$ , for **2**, against HeLa cells (sigmoid fitted curves shown in Figure 4.18B) show cell viability vs concentration). Figure 4.19 shows the percentage viability of cells treated with the complexes **1** and **2** against HeLa and H9c2 cells, respectively. Interestingly, the complex **2** displayed an excellent  $\text{IC}_{50}$  value of  $10 \pm 0.21 \mu\text{M}$ , indicating its high potency against HeLa cells.

The  $\text{IC}_{50}$  values obtained for **1** and **2** were much better than those reported for metal complexes  $[\text{Cu}(\text{L})(\text{THF})]$ , ( $\text{IC}_{50}$ :  $55 \mu\text{M}$ ),  $[\text{Cu}(\text{L})\text{Cl}]$  ( $\text{IC}_{50}$ :  $31.2 \mu\text{M}$ ), CuPDTP, CuADTP, CuBFDTP ( $\text{IC}_{50}$ :  $40\text{-}60 \mu\text{M}$ ),  $[\text{Fe}(\text{bpyag})(\text{anap})]^+$  and  $[\text{Fe}(\text{dpma})(\text{anap})]^+$  ( $\text{IC}_{50}$ :  $17\text{-}40 \mu\text{M}$ ) in similar cell lines.<sup>6,30</sup> The better cytotoxic activity of the two complexes under investigation compared to the free ligand and metal salts, corroborate the ability of the complexes to interact with both DNA and proteins through electrostatic and

hydrophobic interactions.<sup>30</sup> Both the complexes showed a low value of  $IC_{50}$  ( $\leq 10 \mu\text{M}$  for **1** and  $\leq 5 \mu\text{M}$  for **2**), when incubated for 48 h, indicating that the cell killing activity is time-dependent. The results demonstrated that the two complexes have a high potential to act as effective metal-based anticancer agents, as expected from the *in vitro* DNA/protein binding studies. *In vitro* activity of anticancer agents can also be correlated with lipophilicity and can be determined experimentally as well as theoretically. From the data, it is evident that the complex **1** ( $\log P=0.96$ ) is hydrophilic while the complex **2** ( $\log P=1.55$ ) is hydrophobic in nature. This hydrophobicity (for **2**) may contribute to an increased uptake of the complex by the cells, thereby enhancing its cytotoxicity.

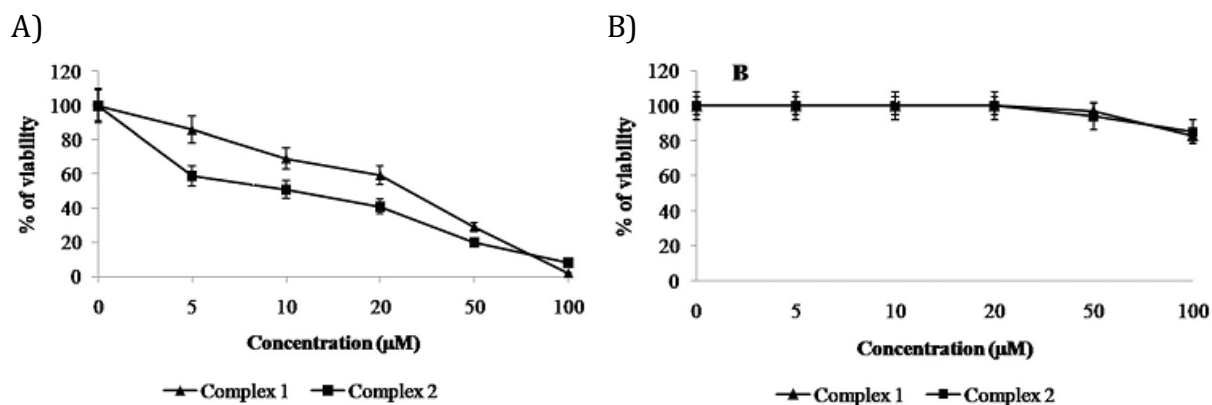


**Figure 4.19.** *In vitro* cytotoxicity assay of the complexes **1** and **2** in A) HeLa and B) H9c2 cell lines (Data are mean%  $\pm$  SD of triplicate).

The cytotoxic agents can cause cell death by several modes and among these apoptosis and necrosis are very prominent. The apoptosis or programmed cell death is characterized by cell shrinkage, blebbing of the plasma membrane and chromatin condensation.<sup>30,31</sup> To investigate the morphological changes and ability to induce cell

death by the complexes **1** and **2**, acridine orange/ethidium bromide (AO/EB) fluorescence staining was performed and the resulting images of the control and the treated HeLa cells are shown in Figure 4.20. Acridine orange penetrates into viable cells with intact DNA, through the plasma membrane and emits green fluorescence. The staining dye, EB emits red fluorescence in the cells with an altered cell membrane. In Figure 4.20B and C, red arrows show early apoptotic HeLa cells with membrane blebbing (in the case of **2**); however, the white arrows exhibit late apoptotic cells with EB intercalation into the nucleus because of membrane blebbing and leakage.

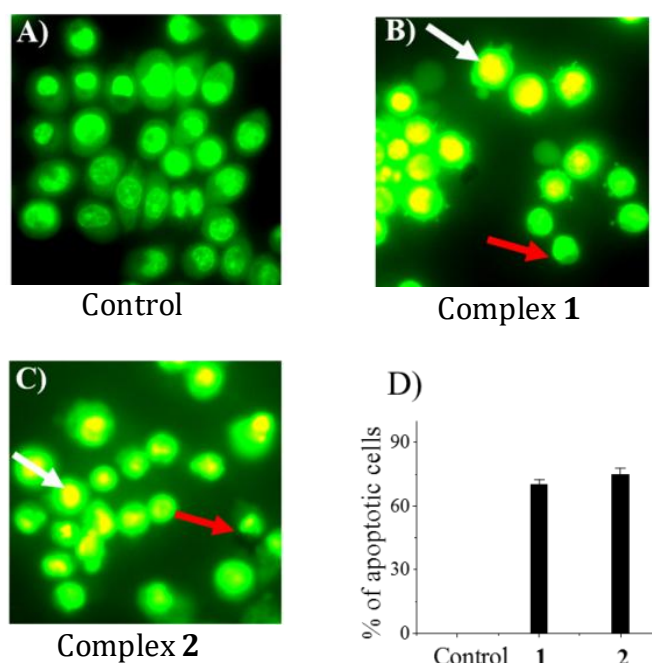


**Figure 4.20.** Fluorescence images of HeLa cells A) control HeLa cells B) HeLa cells treated with **1** (50  $\mu$ M) and C) HeLa cells treated with **2** (20  $\mu$ M), after staining with AO/EB. White and red arrows: Apoptotic and early apoptotic cells with blebbing. D) The graph shows manual count of apoptotic cells in percentage (Data are mean%  $\pm$  SD of duplicates).

From the data, it was clear that all cells exhibited typical characteristics of apoptotic cells like plasma membrane blebbing. However, there were no cells which were stained red. This indicates that the cell death occurred primarily through apoptosis. Both the complexes exhibited a higher percentage (70-78%) of apoptotic cell death (Figure 4.20D) due to the appended naphthalimide moiety in both the complexes, which enhanced the permeability of the complexes across the cell membrane and displayed enhanced cytotoxicity. The corresponding phase contrast images showed the disruption of the morphology of control cells from well spread and flattened pseudopodia shape (Figure 4.21B-C), which support the apoptotic mediated cell death. Interestingly, the complexes **1** and **2** were found to be non-toxic to normal H9c2 cells up to 100  $\mu\text{M}$  (Figure 4.21E-F).

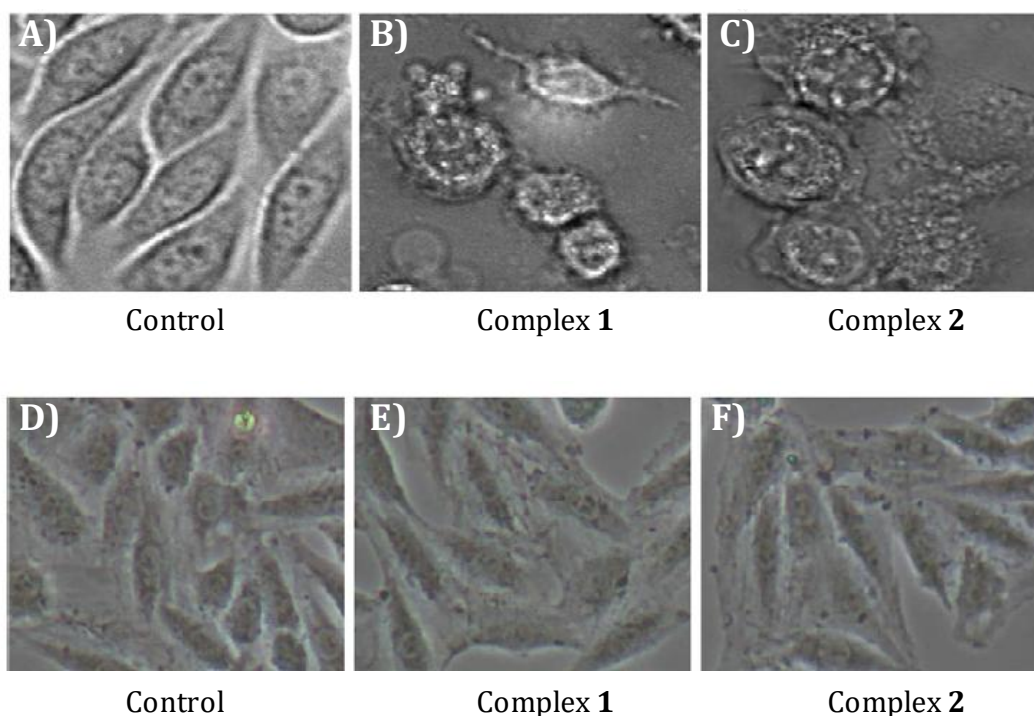


**Figure 4.21.** Phase contrast images of A, D) control (HeLa) and (H9c2) cells; B-C, E-F) after treatment of the complexes **1**(50  $\mu\text{M}$ ) and **2** (20  $\mu\text{M}$ ), respectively.

To understand the nuclear morphology and the nature of cell death mechanism, we have carried out DAPI (4',6-diamidino-2-phenylindole) staining with the complexes **1** and **2** and the resulting images of control and treated HeLa cells are shown in Figure 4.22 (bright field images shown in Figure 4.23). The control HeLa cells exhibited evenly stained nucleus with round and intact contours, whereas the treated cells showed significant fragmentation of the nucleus or condensed nuclei, which is the characteristic of apoptotic mediated cell death. These results are further supportive of the apoptotic mode of cell death by complexes **1** and **2**.

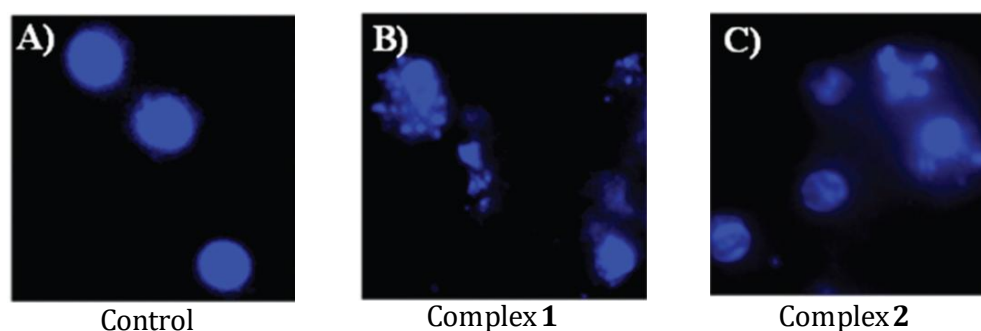


**Figure 4.22.** HeLa cells stained with DAPI and visualized under a fluorescence microscope A) control, B) **1** (20  $\mu\text{M}$ ) and C) **2** (20  $\mu\text{M}$ ).

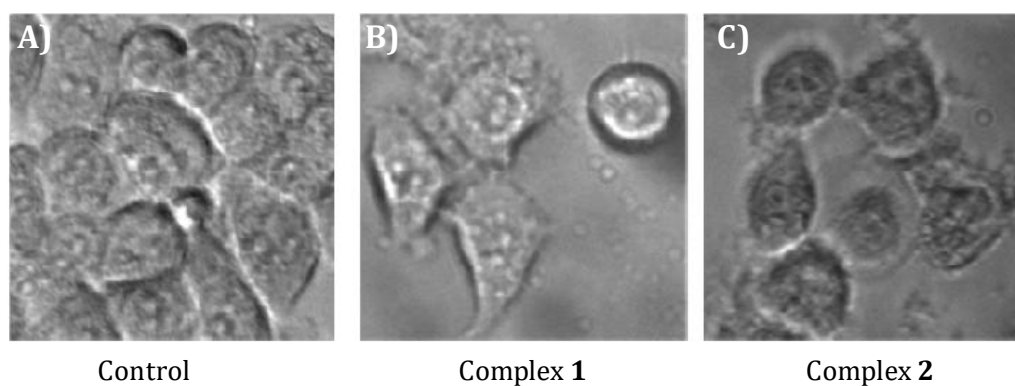


**Figure 4.23.** Bright-field images of A) control (HeLa) cells B) **1** (20  $\mu\text{M}$ ) and C) **2** (20  $\mu\text{M}$ ), respectively, after staining with DAPI.

### 4.3.7. Mechanism of Biological Activity

To further investigate the apoptotic cell death and to understand the mechanism of biological activity induced by the complexes **1** (15–30  $\mu\text{M}$ ) and **2** (5–10  $\mu\text{M}$ ) in HeLa cells, we carried out annexin V-FITC/PI studies through flow cytometric analysis. The double staining with annexin V fluorescein isothiocyanate (annexin V-FITC) and propidium iodide (PI), which is excluded from cells with intact membranes, permits discrimination between viable (annexin V<sup>-</sup>/PI<sup>-</sup>), early apoptotic (annexin V<sup>+</sup>/PI<sup>-</sup>), and late apoptotic/necrotic (annexin V<sup>+</sup>/PI<sup>+</sup>) cells.<sup>31</sup> The percentages of cell populations for the complexes **1** and **2** at various stages of apoptosis are exhibited in Figure 4.24. The lower left quadrant of each panel shows the viable cells, negative for both annexin V-FITC and PI.

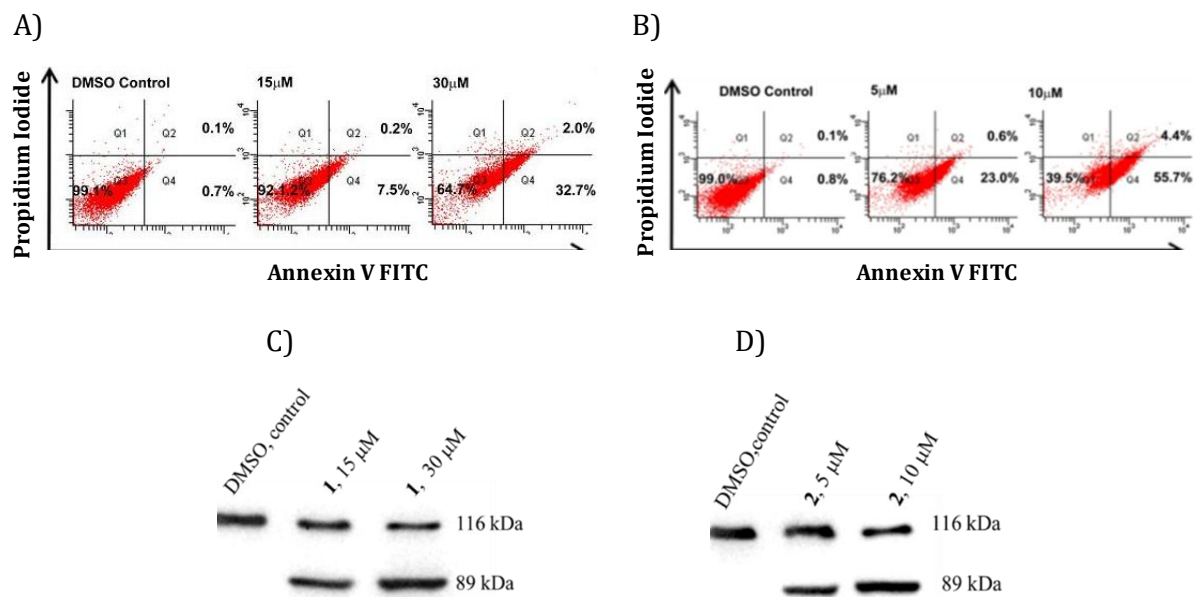


**Figure 4.24.** Flow cytometric analysis of HeLa cells treated with different concentrations (5–10  $\mu\text{M}$ ) of A) **1**, B) **2** for 24 h. C) and D) Immunoblot diagrams show PARP cleavage in HeLa cells treated with the complexes **1** (15–30  $\mu\text{M}$ ) and **2** (5–10  $\mu\text{M}$ ).

The lower right quadrants represent the apoptotic cells (annexin V-FITC+/PI-), while the upper right quadrants represent the late apoptotic/necrotic cells (annexin V-FITC+/PI+). The complex **2** was able to induce more than 50% of apoptotic death, whereas **1** produced ~37% of this type of cell death. The results indicated that both the complexes induced cell death largely by apoptosis. The ability of the compounds to induce apoptosis (**1** < **2**) was in agreement with the results of the MTT assay.

To further confirm apoptosis, we analyzed the poly(ADPribose) polymerase (PARP) cleavage, which is an indicator for apoptosis induction.<sup>30,31</sup> HeLa cells were incubated with different concentrations of the complexes **1** and **2** for 24 h and an immunoblot was performed to detect the PARP level. We observed the cleavage of PARP in the presence of both the complexes in a dose-dependent manner, the full-length 116 kDa peptide cleaved into 89 kDa (Figure 4.24C and D), whereas the control (0.1% DMSO) showed no PARP cleavage. The distinct molecular fragment of 89 kDa serves as a biochemical marker of cells undergoing apoptosis. These results indicated that both the complexes induce cell death in HeLa cells via apoptosis.

#### 4.4. Conclusions

In summary, we have synthesized and characterized a novel tripodal tetradentate ligand **3** and its iron(III) and copper(II) complexes **1** and **2**, respectively, having a rigid trichromophore (naphthalimide) that binds efficiently to DNA and proteins. Interestingly, the coordination with metal ions modulates the ligand orientation and induces intramolecular interaction between two naphthalimide moieties. The accessible naphthalimide chromophore interacts efficiently with ct-DNA and showed moderate

binding propensity for groove binding through electrostatic interactions. In addition, the protein interaction studies of the complexes **1** and **2** have resulted in high affinity for serum albumin. Synchronous spectral investigations revealed micro-environmental changes around the serum albumin in the presence of **1** and **2** due to the hydrophobic and electrostatic interactions. *In vitro* studies of the complexes (**1** and **2**) showed them to be non-toxic to normal H9c2 cell lines, whereas efficient cytotoxicity ( $32 \pm 0.19 \mu\text{M}$ ; for **1**, and  $10 \pm 0.21 \mu\text{M}$ ; for **2**) was shown for HeLa cells, and cell death was induced mainly through the apoptosis mechanism. The appended naphthalimide moiety enhanced the permeability of the complex across the cell membrane through hydrophobic interactions as revealed by the prominent morphological changes obtained by using AO/EB and DAPI staining methods. The apoptotic potential of both the complexes was confirmed by the annexin V apoptotic assay and PARP cleavage. These findings clearly indicate the importance of the complexation of the ligand **3** to biomimetic metal ions and their practical application as anticancer agents.

## 4.5. Experimental Section

### 4.5.1. General Techniques

The melting points were determined on a Mel-Temp II melting point apparatus.  $^1\text{H}$  and  $^{13}\text{C}$  NMR were recorded on a 500 MHz Bruker advanced DPX spectrometer. IR spectra were recorded on a Perkin Elmer Model 882 infrared spectrometer with KBr disks in the range  $4000\text{-}400 \text{ cm}^{-1}$ . MALDI-TOF MS analysis was performed with a Shimadzu Biotech Axima CFR plus instrument equipped with a nitrogen laser in the linear mode. The electronic absorption spectra and fluorescence spectra were recorded



on a Shimadzu UV-VIS-NIR scanning spectrophotometer and SPEX-Fluorolog F112X spectrofluorimeter. Quantum yields of fluorescence were measured by equation 4.1 using optically dilute solutions (quinine sulphate solution is used as standard). Fluorescence lifetimes were measured using IBH picoseconds time correlated single photon counting system. The fluorescence decay profiles were deconvoluted using IBH data station software V2.1 and minimizing the  $\chi^2$  values of the fit to  $1 \pm 0.1$ . Magnetic susceptibilities were determined at 296 K with Vibrating Sample Magnetometer model 155, using nickel as a standard. Solution state magnetic moment was determined at room temperature using the Evans method. Diamagnetic corrections were carried out with Pascal's increments. Molar conductivities were determined in DMF at  $10^{-3}$  M at 25 °C with a Systronics 304 conductometer. Cyclic voltammetry measurements were carried out using a CV-50W electroanalyzer in DMF using platinum wire as auxiliary electrode, glassy-carbon as working electrode. The potentials were referenced to the standard Ag/AgCl electrode and ferrocene (0.53 V,  $E_{1/2}$ ) was used as an internal standard.

#### 4.5.2. Materials and Methods

Anhydrous  $\text{FeCl}_3$  and  $\text{Cu}(\text{ClO}_4)_2 \cdot 6\text{H}_2\text{O}$  were purchased from Aldrich and S. D. Fine Chemicals, India and used without further purification. Tris(2-benzimidazolylmethyl)amine, and 2-(3-bromopropyl)-benzo[de]isoquinoline-1,3-dione was prepared by reported procedures.<sup>32</sup> Calf thymus DNA (CT-DNA), BSA, ethidium bromide (EB) and oligonucleotides (DNA1; 5' CAC TGG CTT TTC GGT GCAT, DNA2: 5'

ATG CAC CGA AAA GCC AGTG were purchased from Sigma. All the solvents were dried prior to use.

### 4.5.3. Synthesis of the Ligand and the Complexes

**4.5.3.1. Synthesis of the Ligand 3.** A mixture of tris(2-benzimidazolylmethyl)amine (0.20 g, 0.49 mM) and  $K_2CO_3$  (4.9 mM) in dry dimethylformamide was stirred for 0.5 h under a nitrogen atmosphere. After 0.5 h, 2-(3-bromo-propyl)-benzo[de]isoquinoline-1,3-dione (0.50 g, 1.57 mM) was added and the reaction mixture was stirred at room temperature for 12 h. The yellow mixture was poured into 100 mL water and yellow precipitate was filtrated out and washed with water, small amount of methanol and diethyl ether and dried in vacuo. This crude product was recrystallized from chloroform-methanol (1:1) to give the block shaped white crystals. Yield: (73%, 0.40 g, 0.36 mM). mp 168-170 °C, ESI-MS: Ligand displays a peak at  $m/z$  1119.43 (calcd  $m/z$  1119.23);  $^1H$  NMR (500 MHz,  $DMSO-d_6$ )  $\delta$  8.26-8.31 (m, 12H), 7.36-7.38 (d, 3H), 7.48-7.49 (d, 3H), 7.70-7.73 (t, 6H), 6.86-6.96 (m, 6H), 4.39 (s, 6H), 4.18-4.21 (t, 6H), 3.68-3.71 (t, 6H), 1.73-1.77 (q, 6H);  $^{13}C$  NMR (500 MHz,  $CDCl_3$ )  $\delta$  28.1, 37.4, 41.6, 50.4, 109.8, 119.7, 121.9, 122.7, 126.8, 127.9, 131.1, 131.4, 133.8, 135.2, 142.3, 150.9, 163.6; UV-visible [DMF,  $\lambda_{max}/nm$  ( $\epsilon/M^{-1}cm^{-1}$ ): 283 (35,660), 331 (40,530). IR data ( $\nu_{max}/cm^{-1}$ ): 1699, (C=O), 1590, (C=N), 1465, 1442, 1346, 1238, 780; Elemental Anal. Calcd for  $C_{69}H_{54}N_{10}O_6$ (%): C, 74.05; H, 4.86; N, 12.51. Found: C, 74.34; H, 4.88; N, 12.23.

**4.5.3.2. Synthesis of the Complex 1.** A methanolic solution (5 mL) of anhydrous iron(III) chloride (0.08 g, 0.48 mM) was added to a solution of **3** (0.54 g, 0.48 mM) in

dichloromethane (5 mL) with constant stirring. After 1 hour stirring, orange colour precipitate obtained which was filtered off and dried in vacuo. Yield: (80%, 0.50 g, 0.39 mM). Selected IR data ( $\nu_{\max}/\text{cm}^{-1}$ ): 1698, 1656, (C=O), 1583, (C=N), 1441, 1340, 1239, 780; UV-visible [DMF,  $\lambda_{\max}/\text{nm}$  ( $\epsilon/\text{M}^{-1}\text{cm}^{-1}$ ): 282 (37,000), 334 (43,000), 450 (4740);  $\mu_{\text{eff}}$  (296 K): 5.88 BM;  $\Lambda\text{M}$  (in DMF):  $58 \Omega^{-1}\text{cm}^2\text{mol}^{-1}$ ; MALDI-TOF: 1210.55; Elemental Anal. Calcd for  $\text{C}_{70}\text{H}_{58}\text{N}_{10}\text{FeCl}_3\text{O}_6$  (%): C, 64.80; H, 4.51; N, 10.80. Found: C, 65.12; H, 4.78; N, 11.02.

**4.5.3.3. Synthesis of the Complex 2.** A methanolic solution (5 mL) of  $\text{Cu}(\text{ClO}_4)_2 \cdot 6\text{H}_2\text{O}$  (0.185 g, 0.50 mM) was added to a solution of **3** (0.56 g, 0.50 mM) in dichloromethane (5 mL) with constant stirring. After 2 h stirring, light green color precipitate obtained which was filtered off and dried in vacuo. The crude product was recrystallized from dimethylformamide to give block shaped green crystals. Yield: (75%, 0.53 g, 0.38 mM). IR data ( $\nu_{\max}/\text{cm}^{-1}$ ): 1698, 1656, (C=O), 1582,  $\nu(\text{C}=\text{N})$ , 1442, 1351, 1235, 1102, 780, 623; UV-visible [DMF,  $\lambda_{\max}/\text{nm}$  ( $\epsilon/\text{M}^{-1}\text{cm}^{-1}$ ): 280 (29,578), 334 (40,060), 420 (50);  $\mu_{\text{eff}}$  (296 K): 1.71 BM;  $\Lambda\text{M}$  (in DMF):  $130 \Omega^{-1}\text{cm}^2\text{mol}^{-1}$ ; MALDI-TOF: 1183.97; Elemental Anal. Calcd for  $\text{C}_{69}\text{H}_{56}\text{N}_{10}\text{CuCl}_2\text{O}_{15}$  (%): C, 59.21; H, 4.03; N, 10.01. Found: C, 59.51; H, 4.31; N, 10.28.

#### 4.5.4. X-ray Crystallography

Single crystals of **3**·3H<sub>2</sub>O and **2**·2DMF·4H<sub>2</sub>O were obtained from a CH<sub>2</sub>Cl<sub>2</sub>- CH<sub>3</sub>OH mixture and DMF, respectively. The data sets for the single-crystal X-ray studies for **3**·3H<sub>2</sub>O and **2**·2DMF·4H<sub>2</sub>O were collected with Mo K $\alpha$  ( $\lambda = 0.71073 \text{ \AA}$ ) radiation on a RIGAKU diffractometer. All the calculations were performed using SHELXTL.

#### 4.5.5. DNA Binding Experiments

The DNA binding experiments were performed in 10 mM phosphate buffer (pH 7.4) (2mM NaCl) using DMF-buffer (15%) solution. A solution of calf thymus DNA (CT-DNA) was sonicated for 2 h and filtered through a 0.45  $\mu\text{M}$  millipore filter. The concentration of ct-DNA was determined from the absorption intensity at 260 nm with  $\epsilon$  value of 6600  $\text{M}^{-1}\text{cm}^{-1}$ .<sup>33</sup> Absorption titration experiments were made using different concentration of CTDNA, while keeping the complex concentration constant. Samples were equilibrated at room temperature for 5 min before recording each spectrum. Fluorescence emission spectra of the DNA-EB system were determined with DNA pre-treated with ethidium bromide (EB) at a ratio of  $[\text{DNA}]/[\text{EB}] = 2$  for 30 min in 15% DMF- $\text{H}_2\text{O}$ . Subsequently, varying concentrations of **1** and **2** (0-10  $\mu\text{M}$ ) were gradually dispensed into the cuvette, incubated for 5 min at room temperature. The fluorescence emission spectra of the samples were recorded from 530 to 800 nm by using  $\lambda_{\text{ex}}$  at 510 nm. DNA melting experiments were carried out by monitoring the absorption intensity of oligonucleotides (DNA1: 5' CGT GCA TGC ACG GTAC-3', DNA2: 5' GTA CCG TGC AAT GTC CACG-3') (2  $\mu\text{M}$ ) at 260 nm at various temperatures, both in the absence and presence of **1** and **2** (2-5  $\mu\text{M}$ ).  $\Delta T_m$  values were calculated by determining the midpoints of melting curves from the first-order derivatives. Viscometric titrations were performed using LAUDA DLK10 automated viscometer, thermostatted at 25  $^\circ\text{C}$  in a constant temperature bath. The concentration of ct-DNA was 100  $\mu\text{M}$ , and the flow times were measured with an automated timer. Each sample was measured 3 times and an average flow time was calculated. Data were presented as  $(\eta/\eta_0)^{1/3}$  versus

[complex]/[DNA], ( $\eta$ ,  $\eta_0$ : Specific viscosities of DNA in presence and absence of complexes, respectively).<sup>34</sup>

#### 4.5.6. Protein Binding Studies

Spectrofluorimetric titrations of the complexes **1** and **2** (0-16  $\mu\text{M}$ ) in DMF-buffer (15%) solution at pH 7.4 ( $\lambda_{\text{ex}} = 345 \text{ nm}$ ) was also performed with increasing concentration of BSA. Quenching of the fluorescence emission of tryptophan residues of BSA was done using **1** and **2** as quenchers. To solutions of BSA in phosphate buffer at pH 7.4, increments of quenchers were added and the emission signals at  $\sim 344 \text{ nm}$  ( $\lambda_{\text{ex}}$  at 280 nm) were recorded after each addition of the quenchers at the corresponding temperature (27  $^{\circ}\text{C}$  and 37  $^{\circ}\text{C}$ ). Conformational changes were studied using synchronous fluorescence measurements. Synchronous fluorescence spectral studies were performed at  $\Delta\lambda = 15 \text{ nm}$  and 60 nm using similar concentration of BSA.

#### 4.5.7. Cytotoxicity Studies Using MTT Assay

MTT assay was done to measure the effect of ligand and metal complexes on the growth inhibition of human cervical cancer (HeLa) cells and H9c2 cell lines.<sup>35</sup> Cells were treated with different concentrations of ligand and complexes for 24 h and the percentage of growth inhibition was calculated as follows,

$$\% \text{ of growth inhibition} = [1 - \text{absorbance of treated cells} / \text{absorbance of untreated cells}] \times 100$$

#### **4.5.8. Morphological Analysis**

The morphological alterations in confluent monolayers of HeLa cells treated with or without metal complexes for 24 h and observed the transmitted light images to see the morphological alterations. (Magnification-40X)

#### **4.5.9. Acridine Orange/Ethidium Bromide (AO/EB) Staining**

HeLa cells were treated with or without metal complexes for 24 h were washed with PBS and trypsinised. 25  $\mu$ l of cell suspension ( $1 \times 10^4$  cells/mL) were incubated with 1  $\mu$ l of acridine orange/ethidium bromide (one part each of 100  $\mu$ g/mL of acridine orange and 100  $\mu$ g/mL of ethidium bromide in PBS) just prior to microscopy.<sup>36</sup> A 10  $\mu$ l of gently mixed suspension was placed on a microscope slide covered with glass slips and examined under fluorescent microscope (BD) connected to a digital imaging system.

#### **4.5.10. DAPI Staining**

DAPI staining<sup>37</sup> was done to study the nuclear fragmentation  $1 \times 10^4$ /mL HeLa cells in the exponential growing phase were treated with 20  $\mu$ M and 50  $\mu$ M concentrations of both iron and copper complexes for 24 h. After treatment, cells were stained with DAPI (10 $\mu$ g/mL) for 10 min, washed with PBS twice and images were taken using a Live Cells Imager (BD pathway TM Bioimage System, BD Biosciences).

#### **4.5.11. Flow Cytometric Annexin V Apoptotic Studies**

Approximately  $10^6$  HeLa cells were seeded on 100 mm dishes and incubated for 24 h at 37 °C under 5% CO<sub>2</sub>. Cells were incubated with 5 and 10  $\mu$ M of complex **2** as well as with 15 and 30  $\mu$ M of the complex **1** for 24 h. In this experiment, 0.1% DMSO was

taken as control. Cells were stained with FITC-labeled Annexin using Annexin V-FITC apoptosis detection kit (Sigma Aldrich) according to the manufacturer's instruction, and a flow cytometric analysis was then carried out using FACS Aria (BD, USA).

#### 4.5.12. Immunoblot Analysis

Approximately  $10^6$  HeLa cells were seeded on 100 mm dishes and incubated for 24 h at 37 °C under 5% CO<sub>2</sub>. Cells were incubated with 5 and 10 μM of complex **2** as well as with 15 and 30 μM of the complex **1** for 24 h. In this experiment 0.1% DMSO was taken as control. Cells were then lysed, and the total protein content was measured using Bradford's reagent. Then 75 mg of total protein was loaded for SDS-PAGE, and immunoblotting was carried out using PARP antibody (cell signaling), and horseradish peroxidase-conjugated secondary antibodies (Santa Cruz) were used, followed by detection using enhanced chemiluminescence (ECL) method.

#### 4.5.13. Lipophilicity

To quantify the lipophilicity of the ligand and complexes, water-octanol partition coefficients (P) were measured using the shake-flask method.<sup>38</sup>

#### 4.5.14. Equations Employed

The quantum yields of fluorescence were calculated using (quinine sulphate ( $\Phi_f = 0.54$ ) in 0.1 N H<sub>2</sub>SO<sub>4</sub> as standard) the equation 4.1,

$$\Phi_u = \frac{A_s F_u n_u^2}{A_u F_s n_s^2} \Phi_s \quad \text{----- (eq 4.1)}$$

wherein,  $A_s$  and  $A_u$  are the absorbance of standard and unknown, respectively.  $F_s$  and  $F_u$  are the areas of fluorescence peaks of the standard and unknown and  $n_s$  and  $n_u$  are the

refractive indices of the solvents used for the standard and unknown, respectively.  $\Phi_s$  and  $\Phi_u$  are the fluorescence quantum yields of the standard and unknown compound.

The intrinsic binding constants ( $K_{DNA}$ ) were calculated by using by the equation 4.2,<sup>39</sup>

$$[DNA]/(\varepsilon_a - \varepsilon_f) = [DNA]/(\varepsilon_b - \varepsilon_f) + 1/K_{DNA}(\varepsilon_b - \varepsilon_f) \quad \text{----- (eq 4.2)}$$

wherein, [DNA] is the concentration of CT-DNA in base pairs. The apparent absorption coefficient  $\varepsilon_a$  was obtained by calculating  $A_{obsd}/[\text{complex}]$ . The terms  $\varepsilon_f$  and  $\varepsilon_b$  correspond to the extinction coefficient of free (unbound) and fully bound complexes, respectively. A plot of  $[DNA]/(\varepsilon_a - \varepsilon_f)$  vs [DNA] gives  $K_{DNA}$  as the ratio of slope  $[1/(\varepsilon_b - \varepsilon_f)]$  to intercept  $[1/K_{DNA}(\varepsilon_b - \varepsilon_f)]$ . When a small molecules bind to a DNA or protein to a set of equivalent sites, the number of sites  $n$  can be obtained from the following equation 4.3,<sup>40</sup>

$$\log \frac{(I_0 - I)}{I} = \log K_b + n \log [Q] \quad \text{----- (eq 4.3)}$$

wherein,  $K_b = K_{b,DNA}$  and  $K_{b,BSA}$  is the binding constant of the complex with DNA/BSA and  $n$  is the number of binding sites per DNA/BSA molecule and [Q] is the total concentration of the quencher. The number of binding sites ( $n$ ) and binding constant  $K_b$  have been calculated from linear fitting plots of  $\log(I_0 - I)/I$  vs  $\log [Q]$  at different temperatures (300, 310 K).

The quenching parameter can be analyzed according to the Stern-Volmer equation 4.4,<sup>41</sup>

$$I_0/I = 1 + K_{SV} [Q] \quad \text{----- (eq 4.4)}$$



wherein,  $I_0$  and  $I$  are the fluorescence intensities of the CT DNA in the absence and presence of complexes, respectively.  $K_{SV}$  is the Stern–Volmer dynamic quenching constant and  $[Q]$  is the total concentration of the quencher. From Stern–Volmer plot of  $I_0/I$  versus  $[Q]$ , the quenching constants ( $K_{SV}$ ) were obtained from the slope. The bimolecular quenching constant ( $k_q$ ) was evaluated from  $k_q = K_{SV}/\tau_0$ , wherein  $K_{SV}$  and  $\tau_0$  are Stern–Volmer quenching constant and average life time ( $\tau_0=10^{-8}$  s) of BSA in the absence of quencher.<sup>12</sup> The values of  $\Delta H$  and  $\Delta S$  can be estimated from the following van't Hoff equation 4.5,

$$\ln K_T = -\frac{H}{RT} + \frac{\Delta S}{R} \quad \text{-----(eq 4.5)}$$

The free energy changes ( $\Delta G$ ) at different temperatures can be calculated from the following equation 4.6,

$$\Delta G = \Delta H - T\Delta S = -RT \ln K \quad \text{-----(eq 4.6)}$$

## 4.6. References

1. (a) Du, Y. H.; Huang, J.; Weng, X. C.; Zhou, X. *Curr. Med. Chem. Anti-Cancer Agents* **2010**, *17*, 173. (b) Orvig, C.; Abrams, M. J. *Chem. Rev.* **1999**, *99*, 2201.
2. (a) Thompson, K. H.; Chris, O. *Science* **2003**, *300*, 936. (b) Song, H.; Kaiser, J. T.; Barton, J. K. *Nat. Chem.* **2012**, *4*, 615. (c) Zeglis, B. M.; Pierre, V. C.; Barton, J. K. *Chem. Commun.* **2007**, 4565.
3. (a) Ohndorf, U. M.; Rould, M. A.; He, Q.; Pabo, C. O.; Lippard, S. J. *Nature* **1999**, *399*, 708. (b) Gasser, G.; Ott, I.; Metzler-Nolte, N. *J. Med. Chem.* **2011**, *54*, 3. (c) Dhar, S.;

- Lippard, S. J. *Bioinorg. Med. Chem.*, Enzo Alessio, Ed. Wiley-VCH Verlag GmbH & Co. KGaA, Weinheim, Germany, **2011**, 79.
4. (a) Liu, Y.; Li, K.; Wei, S.-C.; Pan, M.; Su, C.-Y. *Cryst. Eng. Comm.* **2011**, *13*, 4564. (b) Panja, A. *Inorg. Chem. Commun.* **2013**, *32*, 42.
5. (a) Banerjee, S.; Veale, E. B.; Phelan, C. M.; Murphy, S. A.; Tocci, G. M.; Gillespie, L. J.; Frimannsson, D. O.; Kelly, J. M.; Gunnlaugsson, T. *Chem. Soc. Rev.* **2013**, *42*, 1601. (b) Bran M. F.; Ramos, A. *Curr. Med. Chem. Anti-Cancer Agents* **2001**, *1*, 237. (c) Waring, M. J.; Gonzalez, A.; Jimenez, A.; Vazquez, D. *Nucleic Acids Res.* **1979**, *7*, 217.
6. (a) Banerjee, S.; Kitchen, J. A.; Bright, S. A.; O'Brien, J. E.; Williams, J. D. C.; Kelly, M.; Gunnlaugsson, T. *Chem. Commun.* **2013**, *49*, 8522. (b) Basu, U.; Khan, I.; Hussain, A.; Gole, B.; Kondaiah, P.; Chakravarty, A. R. *Inorg. Chem.* **2014**, *53*, 2152. (c) Li, Q.; Browne, W. R.; Roelfes, G. *Inorg. Chem.* **2010**, *49*, 11009. (d) Basu, U.; Khan, I.; Hussain, A.; Kondaiah, P.; Chakravarty, A. R. *Angew. Chem. Int. Ed.* **2012**, *51*, 2658. (e) Dyke, M. M. V.; Dervan, P. B. *Science* **1984**, *225*, 1122.
7. (a) Michael, R.; Duff, J.; Kumar, C. V. *Metallomics* **2009**, *1*, 518. (b) Zhang, Y.-Z.; Zhou, B.; Liu, Y.-X.; Zhou, C.-X.; Ding, X.-L.; Liu, Y. *J. Fluoresc.* **2008**, *18*, 109.
8. Hossain, S. U.; Sengupta, S.; Bhattacharya, S. *Bioorg. Med. Chem.* **2005**, *13*, 5750.
9. Geary, W. J. *Coord. Chem. Rev.* **1971**, *7*, 81.
10. (a) Piguet, C. *J. Chem. Educ.* **1997**, *74*, 815. (b) Sur, S. K. *J. Magn. Reson.* **1989**, *82*, 169. (c) Evans, D. F. *J. Chem. Soc.* **1959**, 2003.

11. (a) Gupta, S.; Maheshwari, M. K. *Chem. Sci. Trans.* **2013**, *2*, 927. (b) Bencini A.; Gatteschi, D. *Inorg. Chem.* **1977**, *16*, 1994.
12. Addison, A. W.; Rao, T. N.; Reedijk, J.; Rijn, J. V.; Verschoor, G. C. *J. Chem. Soc. Dalton Trans.* **1984**, *7*, 1349.
13. (a) Panja, A.; Goswami, S.; Shaikh, N.; Roy, P.; Manassero, M.; Butcher, R. J.; Banerjee, P. *Polyhedron* **2005**, *24*, 2921. (b) Wu, H.; Li, Y.; Gao, Y. *Acta. Crystallogr. Sect. E* **2004**, *60*, 277. (c) Su, C. Y.; Kang, B. S.; Wen, T. B.; Tong, Y. X.; Yang, X. P.; Zhang, C.; Liu, H. Q.; Sun, J. *Polyhedron* **1999**, *18*, 1577.
14. Etter, M. C. *Acc. Chem. Res.* **1990**, *23*, 120.
15. (a) Kucheryavy, P.; Li, G.; Vyas, S.; Hadad, C.; Glusac, K. D. *J. Phys. Chem. A* **2009**, *113*, 6453. (b) Barros, T. C.; Filho, P. B.; Toscano, V. G.; Politi, M. J. *J. Photochem. Photobiol.* **1995**, *89*, 141. (c) Shankar, B. H.; Ramaiah, D. *J. Phys. Chem. B* **2011**, *115*, 13292.
16. (a) Rajendiran, V.; Karthik, R.; Palaniandavar, M.; Evans, H. S.; Periasamurthy, V. S.; Akbarsha, M. A.; Srinag, B. S.; Krishnamurty, H. *Inorg. Chem.* **2007**, *46*, 8208. (b) Li, M. J.; Lan, T. Y.; Cao, X.-H.; Yang, H.-H.; Shi, Y.; Yi, C.; Chen, G.-N. *Dalton Trans.* **2014**, *43*, 2789.
17. Viji, M.; Nair, A. K.; Nandajan, P. C.; Ramaiah, D. *RSC Adv.* **2014**, *4*, 47982.
18. Plyusnin, V. F.; Kupryakov, A. S.; Grivin, V. P.; Shelton, A. H.; Sazanovich, I. V.; Meijer, A. J.; Weinstein, J. A.; Ward, M. D. *Photochem. Photobiol. Sci.* **2013**, *12*, 1666.

19. (a) Banerjee, S.; Kitchen, J. A.; Bright, S. A.; O'Brien, J. E.; Clive Williams, D.; Kelly, J. M.; Gunnlaugsson, T. *Chem. Commun.* **2013**, *49*, 8522. (b) Roy, S.; Saha, S.; Majumdar, R.; Dighe, R. R.; Chakravarty, A. R. *Inorg. Chem.* **2009**, *48*, 9501.
20. (a) Ghosh, K.; Tyagi, N.; Kumar, P.; Singh, U. P. *Inorg. Chim. Acta* **2014**, *412*, 20. (b) Liu, C.; Zhou, J.; Li, Q.; Wang, L.; Liao, Z.; Xu, H. *J. Inorg. Biochem.* **1999**, *75*, 233. (c) Cory, M.; McKee, D. D.; Kagan, J.; Miller, J. A. *J. Am. Chem. Soc.* **1985**, *107*, 2528.
21. (a) Barron, G. A.; Bermano, G.; Gordon, A.; Lin, P. K. T. *Eur. J. Med. Chem.* **2010**, *45*, 1430. (b) Pages, B. J.; Li, F.; Wormell, P.; Ang, D. L.; Clegg, J. K.; Kepert, C. J.; Spare, L. K.; Danchaiwijit, S.; Aldrich-Wright, J. R. *Dalton Trans.* **2014**, *43*, 15566.
22. (a) Kuruvilla, E.; Joseph, J.; Ramaiah, D. *J. Phys. Chem. B* **2005**, *109*, 21997. (b) Neelakandan, P. P.; Ramaiah, D. *Angew. Chem. Int. Ed.* **2008**, *47*, 8407. (c) Zhao, X.-L.; Li, Z.-S.; Zheng, Z.-B.; Zhang, A.-G.; Wang, K.-Z. *Dalton Trans.* **2013**, *42*, 5764.
23. (a) Wu, J.-Z.; Yuanand, L.; Wu, J.-F. *J. Inorg. Biochem.* **2005**, *99*, 2211. (b) Talib, J.; Harman, D. G.; Dillon, C. T.; Wright, J. A.; Becka, J. L.; Ralph, S. F. *Dalton Trans.* **2009**, 504. (c) Ihmels, H.; Mattay, J.; May, F.; Thomasa, L. *Org. Biomol. Chem.* **2013**, *11*, 5184. (d) Barone, G.; Terenzi, A.; Lauria, A.; Almerico, A. M.; Leal, J. M.; Busto, N.; Garcíac, B. *Coord. Chem. Rev.* **2013**, *257*, 2848.
24. (a) Mallick, A.; Chandra, S.; Maiti, S.; Chattopadhyay, N. *Biophys. Chem.* **2004**, *112*, 9. (b) Jisha, V. S.; Arun, K. T.; Hariharan, M.; Ramaiah, D. *J. Am. Chem. Soc.* **2006**, *128*, 6024.
25. Eftink, M. R.; Ghiron, C. A. *J. Phys. Chem.* **1976**, *80*, 486.

26. Zhao, X.; Liu, R.; Chi, Z.; Teng, Y.; Qin, P. *J. Phys. Chem. B* **2010**, *114*, 5625.
27. (a) Ross, P. D.; Subramanian, S. *Biochemistry* **1981**, *20*, 3096. (b) Jisha, V. S.; Arun, K. T.; Hariharan, M.; Ramaiah, D. *J. Phys. Chem. B* **2010**, *114*, 5912.
28. (a) Cui, F. L.; Wang, J. L.; Cui, Y. R.; Li, J. P. *Anal. Chim. Acta* **2006**, *571*, 175. (b) Ibrahim, N.; Ibrahim, H.; Kim, S.; Nallet, J. P.; Nepveu, F. *Biomacromolecules* **2010**, *11*, 3341.
29. (a) Ramachandran, E.; Raja, D. S.; Bhuvanesh, N.S. P.; Natarajan, K. *Dalton Trans.* **2012**, *41*, 13308. (b) Samari, F.; Hemmateenejad, B.; Shamsipur, M.; Rashidi, M.; Samouei, H. *Inorg. Chem.* **2012**, *51*, 3454.
30. (a) Devi, D. G.; Cibin, T. R.; Ramaiah, D.; Abraham, A. J. *Photochem. Photobiol. B: Biology* **2008**, *92*, 153. (b) Liu, H.; Sadler, P. J. *Acc. Chem. Res.* **2011**, *44*, 349. (c) Thomas, A. P.; Babu, P. S. S.; Nair, S. A.; Ramakrisnan, S.; Ramaiah, D.; Chandrashekar, T. K.; Srinivasan, A.; Pillai, M. R. *J. Med. Chem.* **2012**, *55*, 5110. (d) Berthet, N.; Martel-Frchet, V.; Michel, F.; Philouze, C.; Hamman, S.; Ronot, X.; Thomas, F. *Dalton Trans.* **2013**, *42*, 8468.
31. (a) Karunakaran, S. C.; Babu, P. S. S.; Madhuri, B.; Marydasan, B.; Paul, A. K.; Nair, A. S.; Rao, K. S.; Srinivasan, A.; Chandrashekar, T. K.; Rao, C. M.; Pillai, R.; Ramaiah, D. *ACS Chem. Biol.* **2013**, *8*, 127 (b) González-Álvarez, M.; Pascual-Álvarez, A.; Agudo, L. C.; Castiñeiras, A.; Liu-González, M.; Borrás, J.; Alzuet-Piña, G. *Dalton Trans.* **2013**, *42*, 10244.
32. Hossain, S. U.; Sengupta, S.; Bhattacharya, S. *Bioorg. Med. Chem.* **2005**, *13*, 5750.

33. Reichman M. E.; Rice, S. A.; Thomas, C. A.; Doty, P. *J. Am. Chem. Soc.* **1954**, *76*, 3047.
34. (a) Cohen, G.; Eisenberg, H. *Biopolymers* **1966**, *4*, 429. (b) Scudiero, D. A.; Shoemaker, R. H.; Paull, K. D.; Monks, A.; Tierney, S.; Nofziger, T. H.; Currens, M. J.; Seniff, D.; Boyd, M. R. *Cancer Res.* **1988**, *48*, 4827.
35. Zhang, J. H.; Yu, J.; Li, W. X.; Cheng, C. P. *Chin. J. Physiol.* **1998**, *41*, 121.
36. Tanious, F. A.; Veal, J. M.; Buczak, H.; Ratmeyer, L. S.; Wilson, W. D. *Biochemistry* **1992**, *31*, 3103.
37. Wolf, A.; Shimer, G. H.; Meehan, T. *Biochemistry* **1987**, *26*, 6392.
38. Gratton, E.; Silva, N.; Mei, G.; Rosato, N.; Savini, I.; Finazzi-Agro, A. *Int. J. Quantum. Chem.* **1992**, *42*, 1479.
39. Saric, M. M.; Mornar, A.; Crnjevic, T. B.; Jasprica, I. *Croatica Chem. Acta* **2004**, *1-2*, 367.
40. Lee, M.; Rhodes, A. L.; Wyatt, M. D.; Forrow, S.; Hartley, J. A. *Biochemistry* **1993**, *32*, 4237.
41. Divsalar, A.; Bagheri, M. J.; Saboury, A. A.; Mansoori-Torshizi, H.; Amani, M. *J. Phys. Chem. B* **2009**, *113*, 14035.

## LIST OF PUBLICATIONS

1. Fluorescent Chemodosimeter Based on *NHC* Complex for Selective Recognition of Cyanide Ions in Aqueous Medium, **Viji, M.**; Nair, A. K.; Nandajan, P. C.; Ramaiah, D. *RSC Adv.* **2014**, *4*, 47982- 47986.
2. Enhancement in intramolecular interactions and in vitro biological activity of a tripodal tetradentate system upon complexation, Tyagi, N.; **Viji, M.**; Karunakaran, S. C.; Varughese, S.; Ganesan, S.; Priya, S.; Babu, P. S. S.; Nair, A. S.; Ramaiah, D. *Dalton Trans.* **2015**, *44*, 15591-15601.
3. Aryl Appended Half-Sandwich Ruthenium(II)-*NHC* Complexes: Synthesis, Characterization and Catalytic Applications, **Viji, M.**; Tyagi, N.; Ramaiah, D. *Inorg. Chem.* **2017**, 00, 000 (Under Review).
4. Synthesis of Efficient and Air-Stable Ruthenophane Systems and Study of their Applications in Catalysis, **Viji, M.**; Tyagi, N.; Ramaiah, D. *J. Phys. Org. Chem.* **2017**, 00, 000 (Under Review).
5. *In Vitro* and *In Vivo* Demonstration of Necrotic Mediated Photodynamic Activity in Human Ovarian Cancer Cells Through a Novel Chlorine, Betsy, M.; Madhuri, B.; **Viji, M.**; Karunakaran, S. C.; Jose, J.; Cherukommu, S.; Chandrashekar, T. K.; Rao, K. S.; Rao, Ch M.; Ramaiah, D. *ACS Chem. Biol.* **2017** (Communicated).
6.  $\mu$ -Oxo-Bridge Iron Complexes: Synthesis, Characterization and Application in Transfer Hydrogenation of Ketones, Tyagi, N.; **Viji, M.**; Ramaiah, D. **2017** (Under Preparation).

## PAPERS PRESENTED IN CONFERENCES

1. *NHC* Based Fluorescent Chemodosimeter for Selective Recognition of Cyanide Ions in Aqueous Medium, **M. Viji**, A. K. Nair, P. C. Nandajan, and D. Ramaiah, A Poster Presented at 17<sup>th</sup> CRSI National Symposium in Chemistry, CSIR-NCL, Pune, India, **2015**, February 06-08.
2. Photomorphogenesis of  $\gamma$ -globulin: Effect on Sequential Ordering and Knock Out of Gold Nanoparticles Array, D. T. Jayaram, B. H. Shankar, **M. Viji**, and D. Ramaiah, A Poster Presented at 8th Mid-Year CRSI National Symposium in Chemistry, CSIR-NEIST, Jorhat, Assam, India, **2014**, July 10-12.

